Late Transition Metal Complexes of NHC-Based Macrocycles

by

Rhiann Erica Andrew

A thesis submitted in partial fulfilment of the requirements for the degree of Doctor of Philosophy in Chemistry

University of Warwick, Department of Chemistry

July 2016

Table of Contents

ACKNOWLEDGEMENTS

Extensive thanks, of course, go to my supervisor Dr. Adrian Chaplin for his patient guidance and support, all the more remarkable given his extensive experience, knowledge and enthusiasm. I struggled to keep up sometimes, but I hope we got there in the end! Additional thanks to Adrian and the University of Warwick for securing and providing funding for my thoroughly enjoyable time at Warwick.

Thanks are owed to Dr. Ivan Prokes and Rob Perry for their help with NMR spectroscopy, and to Phil Aston for mass spectrometry analysis and advice. A huge thank you to Peter Brindley, a magician with glass, for all the custom projects and patient repairs. I am endlessly grateful for the support from Dr. Jo Geden and Dr. Penny Turner, who helped me find my feet at Warwick and were always happy to help.

I'd like to thank all the Chaplin group members, both past and present, in more detail than would fit on this page. I will continue to miss the quietly magnificent Simone, the not-so-quiet but equally entertaining Thibault and the boundless enthusiasm of 'tía' Lucero; all of whom were goldmines of experience and advice. The same goes for current members Rich and Matt who have been excellent colleagues and happy to talk through anything from columns to cricket, trituration to tech. To the 'newbies' Caroline, Jack and Baptiste, it genuinely feels like you've always been here, and I wish you lots of fun and all the best of luck. Finally, Ruth, despite your frankly terrifying obsession with Eurovision, you have been an excellent friend, personal secretary, cake provider, social hub… in short, my 'Lighthouse' (rocks are over-rated) over the past 3-4 years and I can't thank you enough, you are truly 'Made of Stars'.

Outside of 'The Bubble', I owe a debt of gratitude to my family and friends, not only for putting up with me through all of this, but in all things. You've told me I'm insane so many times I almost feel the need to prove it, and in doing so I've achieved things I never expected, thank you.

DECLARATION OF COLLABORATIVE AND PUBLISHED WORK

This thesis is submitted to the University of Warwick in support of my application for the degree of Doctor of Philosophy. It has been composed by myself and has not been submitted in any previous application for any degree.

The work presented (including data generated and data analysis) was carried out by the author except in the cases outlined below:

- Crystallographic analysis of all compounds, for which solid-state structures are described, was conducted by Dr. Adrian B. Chaplin, Associate Professor, University of Warwick. The lineshape analysis and simulation of VT NMR spectra of complex **3a** and subsequent Eyring analysis (**Chapter 2**) was also conducted by Dr. Chaplin.
- Synthesis of nickel(II) chloride complex **8** (**Chapter 2**), which was conducted by Caroline M. Storey, PhD student, University of Warwick.
- The computational investigation of the dynamics of rhodium(I) carbonyl complexes, (**Chapter 3**), which was conducted by Dr. C. André Ohlin, Monash University.
- Synthesis of rhodium(I) biscarbonyl complex **18** (**Chapter 3**), which was conducted by Dominic W. Ferdani, MChem student, University of Warwick.

Parts of this thesis have been published by the author:

1. Andrew, R. E.; Chaplin, A. B. Synthesis, structure and dynamics of NHC-based palladium macrocycles. *Dalton Trans.* **2014**, *43*, 1413 – 1423.
2. Andrew, R. E.; Chaplin, A. B. Synthesis and reactivity of NHC-based rhodium macrocycles. *Inorg. Chem.* **2015**, *54*, 312 - 322.
3. Andrew, R. E.; Ferdani, D. W.; Ohlin, C. A.; Chaplin, A. B. Coordination Induced Atropisomerism in an NHC-based Rhodium Macrocycle. *Organometallics* **2015**, *53*, 913 – 917.
4. Andrew, R. E.; González-Sebastián, L.; Chaplin, A. B. NHC-based pincer ligands: Carbenes with a bite. *Dalton Trans.* **2016**, *45*, 1299 – 1305.
5. Andrew, R. E.; Storey, C. M.; Chaplin, A.B. Well-defined coinage metal transfer agents for the synthesis of NHC-based nickel, rhodium and palladium macrocycles. *Dalton Trans.* **2016**, *45*, 8937-8944

ABSTRACT

N-heterocyclic carbene (NHC) ligands are an important and diverse ligand class, conferring stability and enabling reaction control of coordinated metal centres. Pincer ligand architectures bearing such donors are an increasingly prevalent design motif, combining the strong donor characteristics of carbenes with the favourable thermal stability possible with a *mer*-tridentate geometry. Macrocyclic variants of NHC-based pincers are of interest as they may impart further stability and reaction control, in addition to serving as potential building blocks for the construction of interlocked, supramolecular systems.

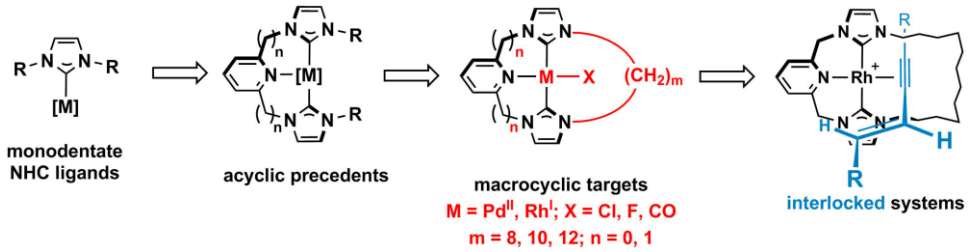

Enabling study of the reactivity and structural properties of late transition metal complexes of macrocyclic CNC pincer ligands, the coordination chemistry of a series of pro-ligands of varying ring size (n = 1; m = 8, 10, 12) has been explored. Investigation of the dynamics and structures of palladium(II) halide complexes identified an optimal ring size, which was subsequently employed in the preparation of rhodium-based derivatives (n = 0, 1; m = 12) *via* two converging synthetic routes. The organometallic chemistry, dynamic behaviour and structures of the resulting rhodium complexes are described. Through investigation of terminal alkyne coupling reactions using a macrocyclic rhodium ethylene complex, potential for the preparation of novel supramolecular assemblies was explored. As a result, a series of complexes bearing mechanically entrapped enynes were isolated and fully characterised in solution and the solid-state.

ABBREVIATIONS

acac	Acetyl Acetone
Ar	Aryl
Ar^F	3,5-Bis(trifluoromethyl)phenyl
br	broad
Bz	Benzyl
ca.	circa
CAAC	Cyclic (alkyl)(amino)carbenes
calc.	calculated
CCDC	Cambridge Crystallographic Data Centre
COD	Cyclooctadiene
COSY	Correlation Spectroscopy
DCC	N,N'-Dicyclohexylcarbodiimide
DFT	Density Functional Theory
DiFB	1,2-Difluorobenzene
DIPP	2,6-Di(isopropyl)phenyl
DME	Dimethoxyethane
DMF	Dimethyl Formamide
EDTA	Ethylenediaminetetraacetic Acid
ESI-HRMS	Electrospray Ionisation – High Resolution Mass Spectrometry
ESI-LRMS	Electrospray Ionisation – Low Resolution Mass Spectrometry
equiv.	equivalents
fwhm	full width at half maximum
HOBT	1-hydroxy-benzotriazole
IR	Infra-Red
KHMDS	Potassium hexamethyldisilamide
Mes	2,4,6-Tri(methyl)phenyl
MLCT	Metal to Ligand Charge Transfer
NBE	Norbornadiene
NHC	*N*-Heterocyclic Carbene
NMP	*N*-methyl-2-pyrrolidone
NMR	Nuclear Magnetic Resonance
NOESY	Nuclear Overhauser Effect Spectroscopy
ppm	parts per million

TBE	*tert*-butyl ethylene
TEP	Tolman Electronic Parameter
THF	Tetrahydrofuran
tmed	*N*,*N*,*N*',*N*'-tetramethylethylenediamine
TOF	Turnover frequency
TON	Turnover number
UV-vis	UltraViolet-Visible
VT	Variable Temperature
XRD	X-Ray Diffraction

CHAPTER 1. INTRODUCTION

1.1 NHC Ligands

1.1.1 Overview

Defined as a carbenic centre within a nitrogen-containing heterocyclic system, *N*-Heterocyclic carbenes (NHCs) are an important and diverse ligand class (**Fig. 1.1**), conferring stability and enabling reaction control of coordinated metal centres.[1-4] Since Arduengo's seminal report of a stable imidazolium-derived NHC **A1**,[5] the vast majority of progress in the field has concerned imidazolylidenes and their saturated counterparts as monodentate ligands.[6]

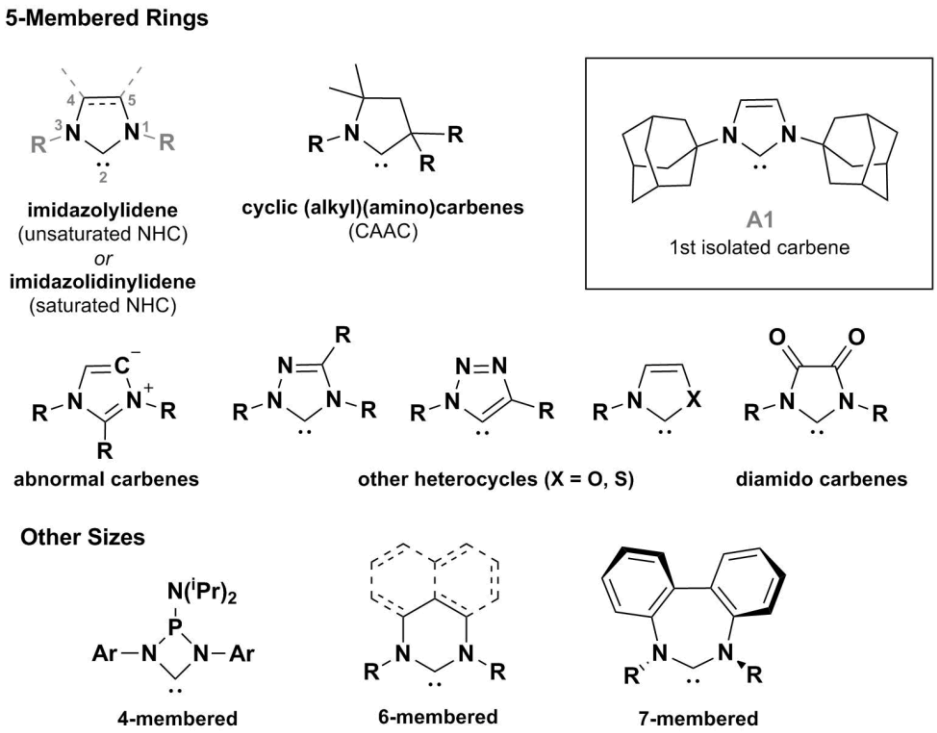

Fig. 1.1: *Common NHCs.*

Modification of ring-size and substitution pattern can tune electronic and steric properties of the carbene.[7] Unlike substituents of traditionally-employed phosphines, the *N*-substituents of NHC ligands are directed towards the coordination sphere of a metal (**Fig. 1.2**).[8] The resulting steric crowding of the metal centre can be quantified using percentage buried-volume (% V_{bur}) calculations.[9-11] Variation of the *N*-substituents during synthesis of the imidazolium precursor to an NHC is generally straightforward, enabling the formation of a diverse library of NHC ligands and complexes thereof. Such modularity has in turn driven study of the substituent-dependence of the electronic and steric parameters of metal-NHC complexes.[6,12-16]

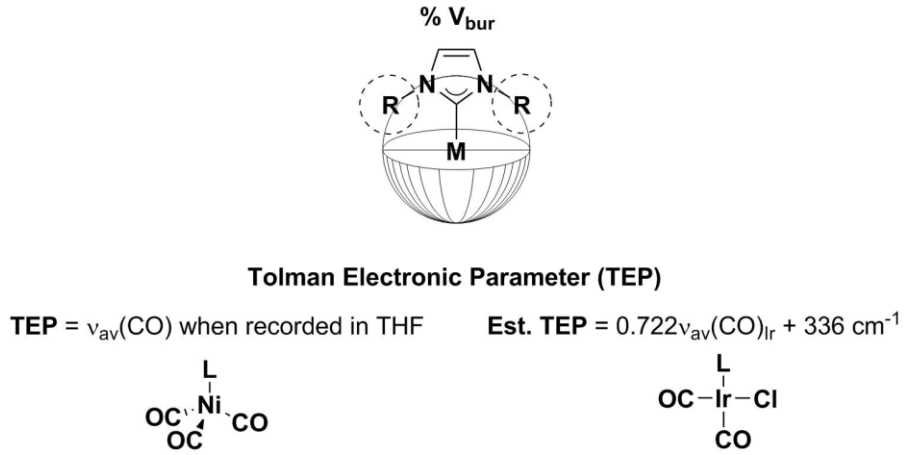

Fig. 1.2: *Quantification of steric and electronic parameters of NHC ligands.*

It is widely accepted that NHC ligands (particularly imidazolylidine variants) are stronger σ-donors than typical alkyl-phosphine counterparts and display little π-accepting ability.[12,14] Electronic properties of NHC and phosphine ligands are typically quantified using the Tolman Electronic Parameter (TEP). This is the A_1 symmetric ν(CO) stretching frequency of carbonyl ligands on a tris-carbonyl Ni complex of the ligand under investigation (*i.e.* 'L' in $[Ni(CO)_3L]$, **Fig. 1.2**).[9,14,17] However, safety concerns have recently emerged regarding the preparation of $[Ni(CO)_3L]$ complexes, and they have proved difficult to synthesise when using sterically hindered NHC ligands, which prefer to form $[Ni(CO)_2(NHC)]$ complexes.[9] Instead, Crabtree and co-workers have compared ν(CO) stretches of $[Ir(CO)_2(NHC)Cl]$ with existing NHC and PPh_3 TEP values, and report relationships such as **Est. TEP** (**Fig 1.2**).[18,19] Using this strategy, TEP values can be determined for ligands in instances when synthesis of $[Ni(CO)_3L]$ is problematic.

Gusev has estimated the TEP of over 70 $[Ni(CO)_3(NHC)]$ complexes using DFT calculations, producing values in good agreement with the experimental data available.[8] By either method, TEP values generally indicate greater σ-donor strength of NHC ligands in comparison with phosphines and much of the success of NHCs has been attributed to their higher σ-donating ability than that of analogous phosphine complexes.[2,20,21] NHC-based complexes have also demonstrated greater thermal stability than related phosphines,[22] as well as stabilisation of electron deficient metal centres.[9]

Nevertheless, π back-donation has been investigated in some systems, with two modes identified; the out-of-plane π_1 and in-plane π_2 shown in **Fig. 1.3**.[23,24] DFT calculations indicate that the degree of π character in the metal-to-ligand interactions is small in comparison with the σ-donor contribution.[13,16,24-26]

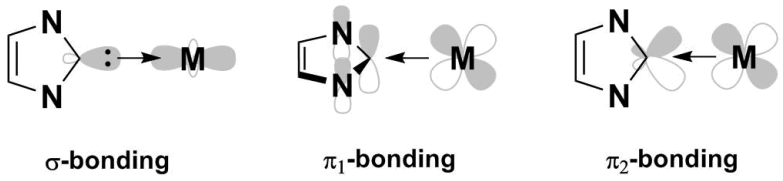

Fig. 1.3: *Bonding regimes in NHC-to-metal interactions.*

Experimentally, comparison of the respective ^{77}Se and ^{31}P shifts of selenium and phosphenium adducts of NHCs reveals particularly strong π-accepting character in CAACs and diamido carbenes, while shifts for saturated and 6-membered NHCs indicate less π-accepting ability (**Fig. 1.4**).[12,27-30]

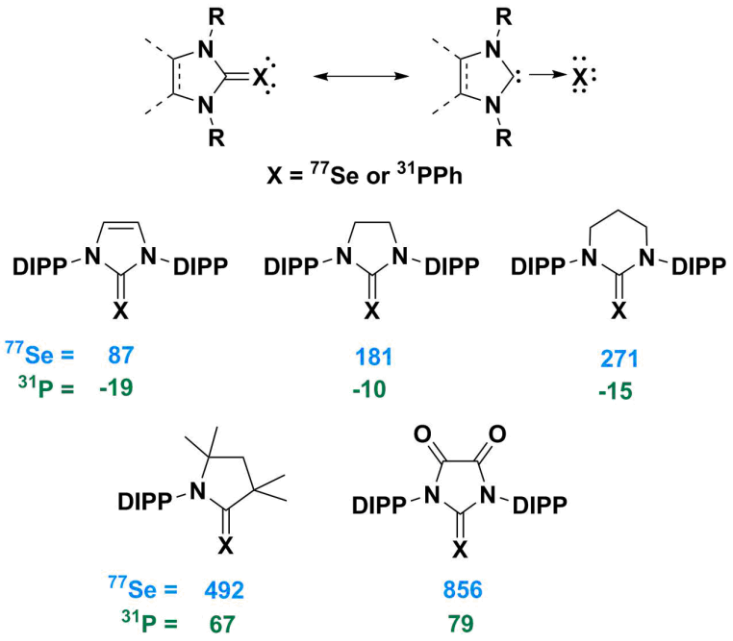

Fig. 1.4: *Selenium and phosphenium adducts of NHCs.*

Following the first reported use of an NHC in catalysis,[31] numerous other catalytic applications have supported their versatility; the ubiquitous example being the 2nd Generation Grubbs catalyst (**A2**, **Fig. 1.5**) and later derivatives.[2,32] Other informative examples include the recent report of an NHC-stabilised Au(III) species **A3** active in Michael additions,[33] and air and moisture-stable ruthenium-benzimidazolin-2-ylidene catalysts effective in the *N*-alkylation of amines with alcohols (**A4**).[34] Additionally, an array of copper and palladium NHC-complexes have been used in 'click' chemistry, hydrosilyations and C-C couplings, most notably the PEPPSI catalyst **A5**.[35-37]

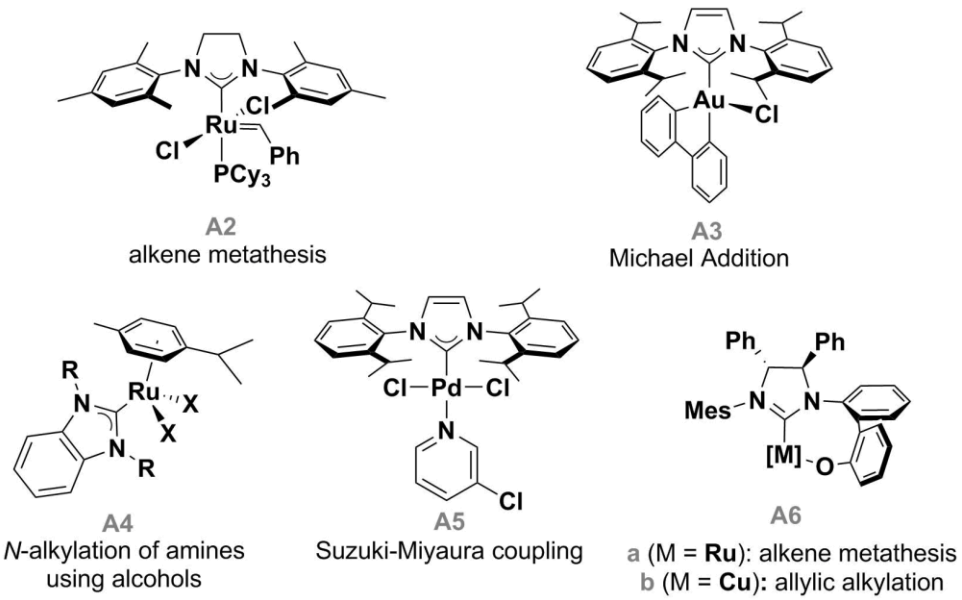

Fig. 1.5: *Catalysts incorporating monodentate NHC ligands.*

1.1.2 Synthesis and Complexation of NHC Pro-Ligands

Common routes to NHC pro-ligands (shown in blue) are depicted in **Scheme 1.1**. Bis-alkylation of an imidazole derivative, to afford an imidazolium salt, is by far the most prevalent, but ring-closing of α,β-di-keto/amino alkanes is a popular alternative.[6] Such ring-closing methodologies are particularly useful when asymmetric substitution ($R^1 \neq R^2$),[38] backbone substitution and/or saturation are desired.[39] This stepwise methodology is used effectively to prepare **A6** (**Fig. 1.5**), which is used in enantioselective alkene metathesis (**A6a**) and allylic alkylation reactions (**A6b**).[38] Additionally, 6 and 7-membered rings can be accessed *via* reaction with a C-H source such as $HC(OEt)_3$,[40,41] or by the formadimine reaction pioneered by Dervisi and Cavell.[42]

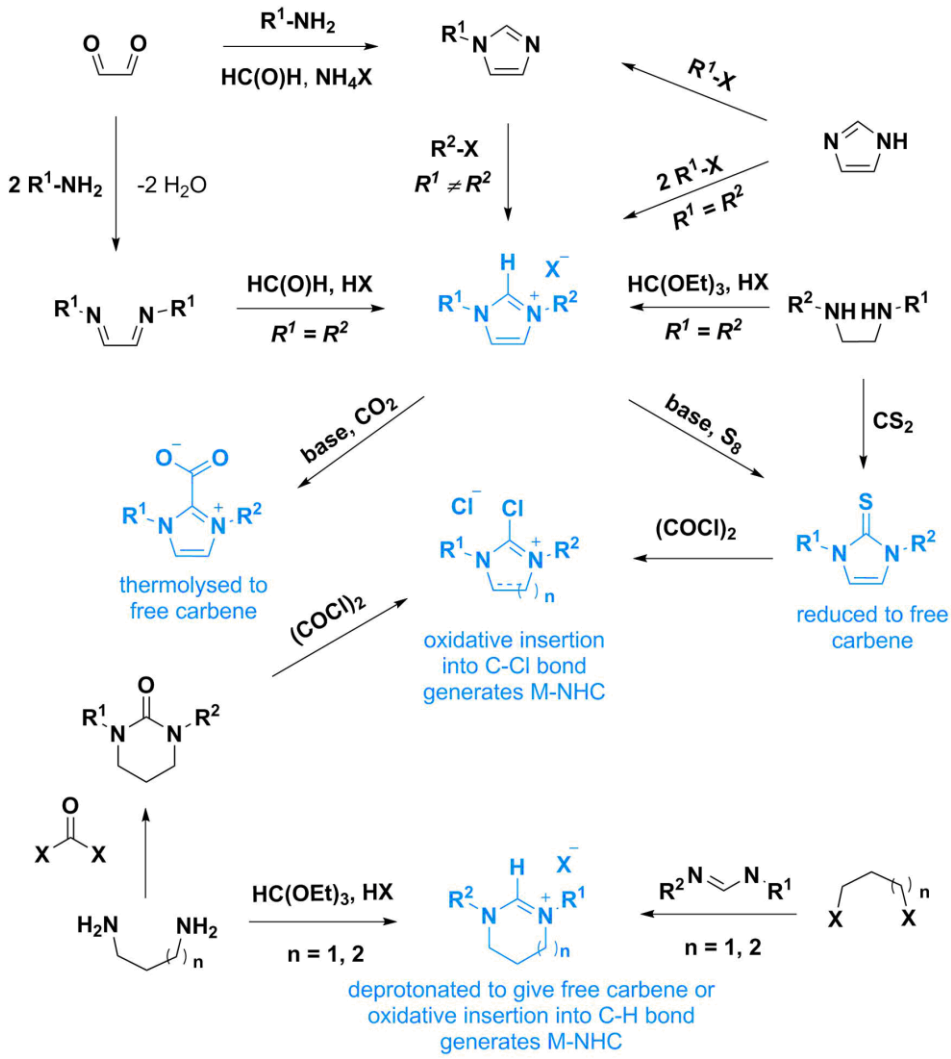

Scheme 1.1: *Synthesis of monodentate NHC pro-ligands.*

Avoiding difficulties encountered in purification of imidazolium salts, which can be hygroscopic, the CO_2, thione and chloride adducts in **Scheme 1.1** are also viable NHC pro-ligands. CO_2 and thione adducts may be accessed *via* trapping of the *in-situ* generated free carbene with CO_2 gas or elemental sulphur, respectively.[43,44] The C=S bond may also be formed in the ring-closing reaction of diamino ethanes with CS_2,[39] or by alkylation of thioureas.[45] Once obtained these protected NHC ligands are stable and isolable, enabling further purification before deprotection to afford the free carbene. Thermolysis of the NHC-CO_2 bond is employed *in-situ* in the preparation of **A7** (**Scheme 1.2**),[43] while reduction of a series of thione adducts with potassium metal enables isolation of the free carbenes before coordination to rhodium in racemic complexes **A8**.[46] Alternatively, reaction of oxalyl chloride with carbon-chalcogen double bonds of imidazolium precursors affords chloro-imidazolium salts. Fürstner and co-workers have shown that oxidative addition into the C-Cl bonds may be used to access Pd(II) and Ni(II) complexes (*i.e.* **A9**).[39]

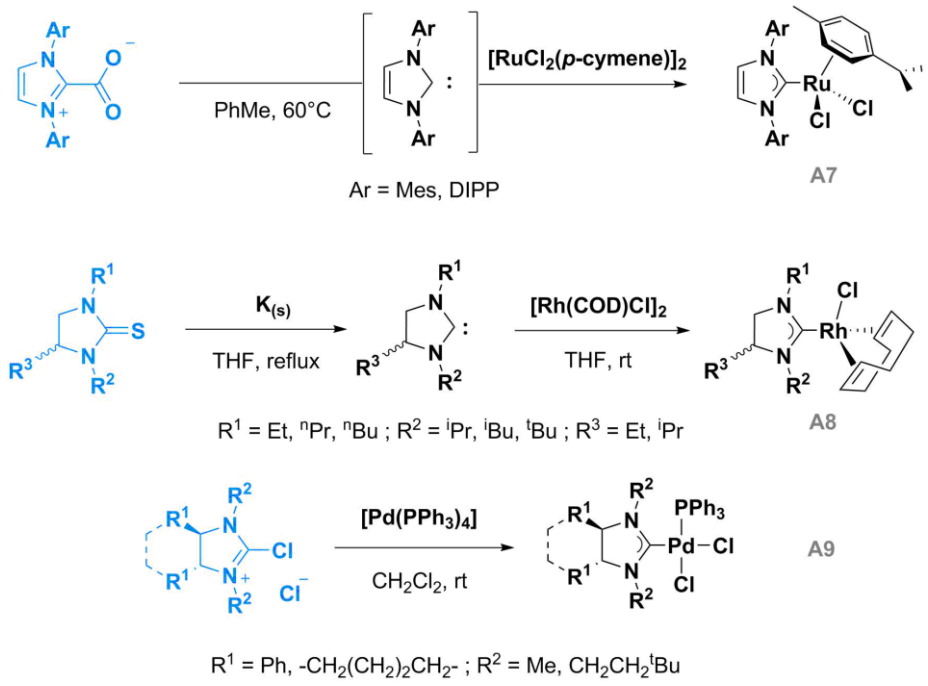

Scheme 1.2: *Use of protected NHC ligands.*

For the majority of NHC complexes, the free carbene is accessed *in-situ via* deprotonation of an imidazolium salt in the presence of a metal precursor (**Scheme 1.3**).[2,6,47,48] Isolation of free-carbenes is often inhibited by their innate air and moisture sensitivity, but a number of examples – such as **A1** and **A10** – are known and can be directly employed in complexation reactions (**isolated carbene** route).[49] Alternatively, the free carbene may be generated *in-situ* before addition of the metal, as demonstrated by Thieuleux and co-workers in their synthesis of a silica-supported metathesis catalyst, **A12** (**M + B**$^-$ route).[50]

Avoiding issues associated with sensitive intermediates and poor functional group tolerance, 'accessible syntheses' – as per Nelson's insightful review[7] – have been employed in the formation of many metal complexes. Here, weak bases such as triethylamine[51] and K_2CO_3 (**M + B** route, **A13**)[52] are employed to promote metallation while maintaining a low concentration of free carbene. Palladium NHCs are often accessed *via* such steady-state reactions with weak bases and the formation of **A14** by Sarkar is an elegant demonstration of the use of [$Pd(OAc)_2$] as a bifunctional base and metal-precursor (**M(B)$_2$** route).[53] Coinage metals, particularly Ag[25] and Cu,[10] form weaker bonds with NHCs than many other transition metals, yet can be more readily isolated than free carbenes. These properties make them useful carbene-transfer reagents for the subsequent formation of Au, Pd, Rh and Ir complexes (**M$_2$O** route).[9,54]

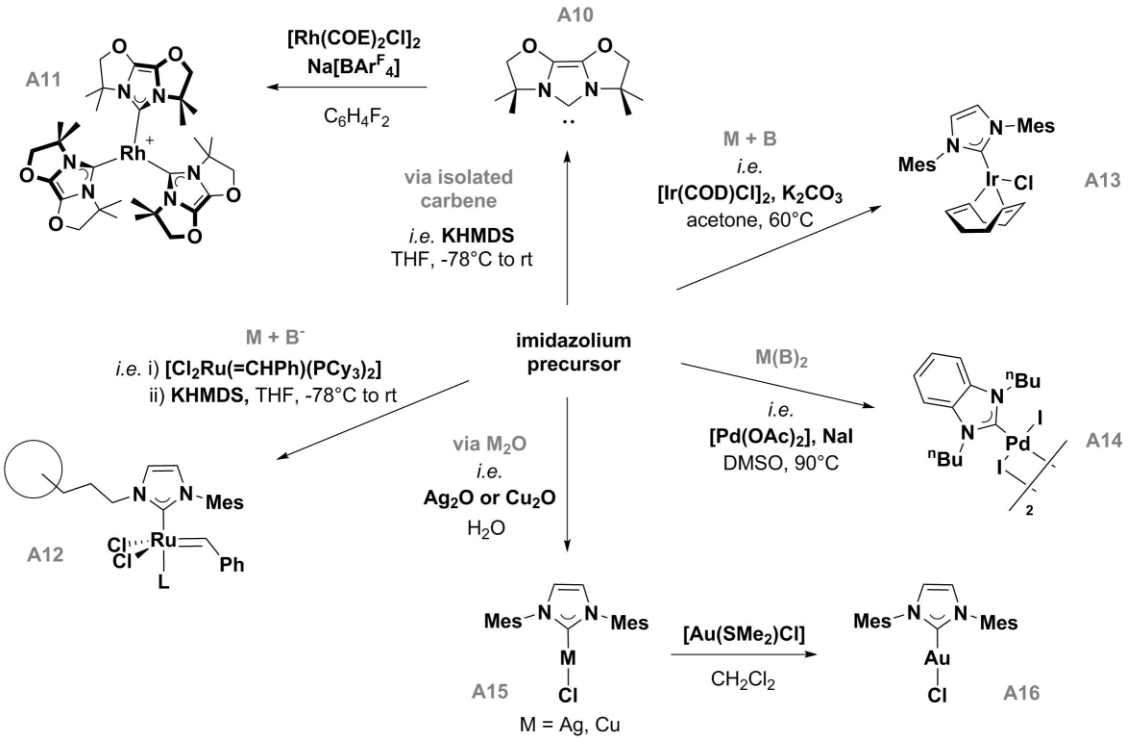

Scheme 1.3: *Complexation routes to monodentate NHC complexes from imidazolium salts.*

1.1.3 Deactivation Modes for NHC Complexes

The strong metal-NHC bond generally results in more stable complexes than the equivalent phosphines,[55] but a few established modes of deactivation are worth noting. Migratory-insertion of metal-substituents into the metal-carbene bond in M(NHC)R systems (where R = H, alkyl, aryl) results in reductive elimination of imidazolium salts from nickel and palladium centres (**A17**, **Scheme 1.4**).[56] When 6-membered amido-carbenes are employed with Group 12 metals, migration occurs with retention of the metal-carbon connection (**A18**). Further elimination of methane and cadmium metal is observed in **A18b** to afford the NHC-olefin **A19**.[57]

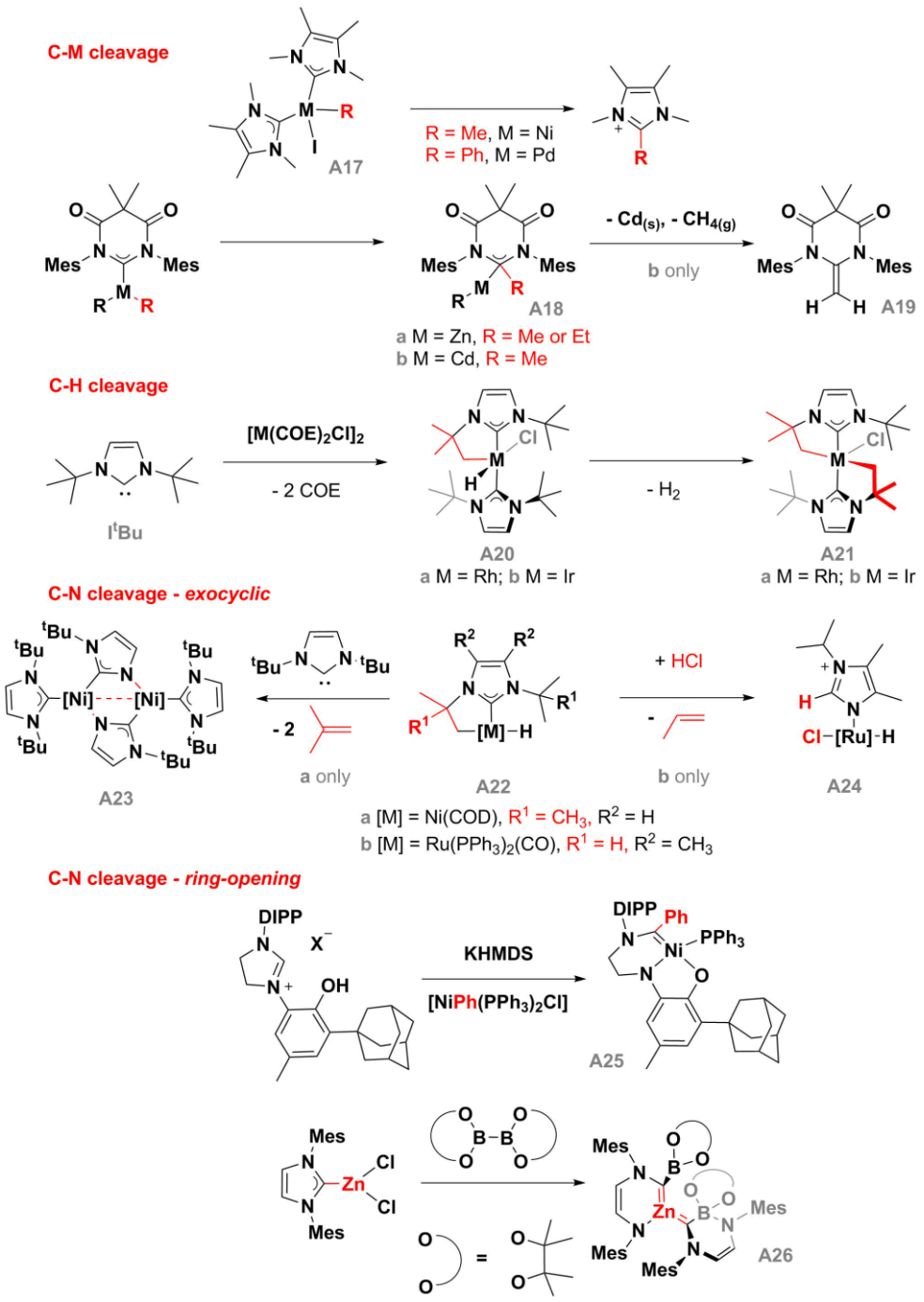

Scheme 1.4: *Representative decomposition routes of NHCs.*

Alternatively, the metal can insert into bonds of the ligand. Cyclometallation of *N*-substituents has been reported in a range of systems, particularly those utilising *tert*-butyl groups. C-H bond activation is observed on reaction of free carbene **I^{t}Bu** with Ir and Rh precursors to afford **A20**, which may undergo a second activation (**A21**, **Scheme 1.4**).[58]

Cyclometallated *N*-alkyl NHCs **A22** also undergo a second activation, but into the *exocyclic* C-N bonds to enable the *N*-coordination mode shown in **A23** and **A24**.[59-61] Insertion into internal C-N bonds can also occur, resulting in ring-opening of the NHC.[62] By this pathway, Grubbs *et al*

obtained 6-membered cyclometallated ring **A25**, the product of insertion into an *endocyclic* C-N bond.[63] The authors suggest that the insertion is instigated by migration of the phenyl ligand (in red) onto the carbene, and have shown that replacement of this functionality with a more hindered mesityl group enables isolation of the previously expected alkoxy-NHC complex.

C-N bond cleavage has also been observed in a zinc-boryl system, when attempts at trapping a reaction intermediate in the borylation of alkyl halides (catalysed by a Zn-IMes complex) induced the formation of crystallographically characterised **A26**.[64] This unusual structure is the product of double insertion of zinc and boron into the C-N bonds of two NHCs, forming a trigonal planar zinc centre stabilised intramolecularly by a borate anion.

1.2 NHC-Based Pincers[a]

1.2.1 Overview

Meridonal, tridentate 'pincer' ligands are widely used in organometallic chemistry and catalysis, conferring thermal stability and tunable reaction control.[65] Bisphosphine-based 'PEP' pincers (where the central donor E is commonly C^-, N^- or N) are archetypal examples.[66,67] PEP complexes of transition metals have proved to be robust and highly active catalysts for hydrogenation of C=X bonds (X = C, O, N) as well as dehydrogenation of C-X bonds (X = O, N, **A27**),[68] dehydrogenation and aromatisation of alkanes (**A28**)[69] and C-C coupling reactions (**A29**).[70]

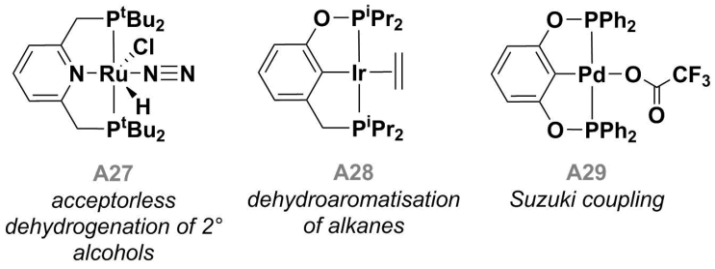

Fig. 1.6: *PEP-type catalysts.*

Building on the success of PEP-type pincers, analogues bearing terminal NHC donors have been developed. 'CEC' pincers, where 'C' denotes a carbenic centre and E = C^-, N^- or N, constitute a burgeoning ligand class and represent the majority of NHC-based pincer ligands reported. Other variants have received attention, particularly those containing central NHC donors (*e.g.* **A30 – A33**, **Fig. 1.7**).[71-75]

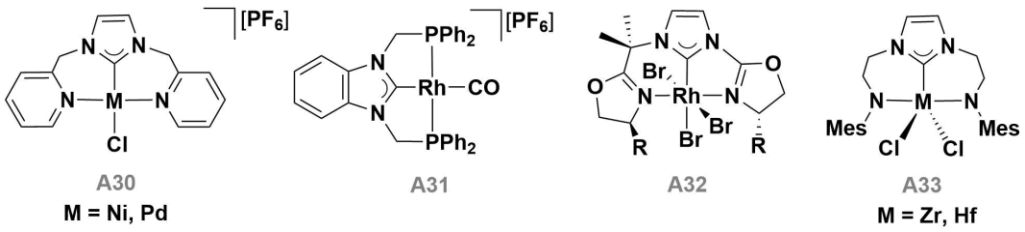

Fig. 1.7: *Non CEC-type NHC-based pincers.*

Imidazolylidene-derived **Type I** and **Type II** ligands (**Fig. 1.8**) were the first examples of CEC-pincers and remain heavily investigated, featuring in 84 % of publications and accounting for 78 % of solid-state structures (from a survey of 179 articles referring to the synthesis, study or application of CEC-type structures up until September 2015). **Type I** and **Type II** systems are

[a] Parts of this section have been published in a recent review: Andrew, R. E.; Gonzalez-Sebastian, L.; Chaplin, A. B. *Dalton Trans.* **2016**, *45*, 1299-1305.

differentiated by use of methylene spacers between the NHCs and the central aromatic donor. Consequently the sub-classes can be specified as C-E-C^{R} and C^E^C^{R} pincers, for **Type I** and **Type II** respectively, with R denoting the *N*-substituent. As well as being potentially reactive functionalities,[76,77] the methylene spacers in **Type II** complexes induce a conformational twist into the backbone. As a result, the *trans* NHC donors have an orthogonal relationship and the complex has overall C_2 symmetry; as opposed to C_{2v} symmetry observed for **Type I** systems. This twist produces two atropisomers that are often dynamic in solution; a process which has been investigated extensively by Crabtree and co-workers and is also reported herein (**Chapter 3**).[78-80]

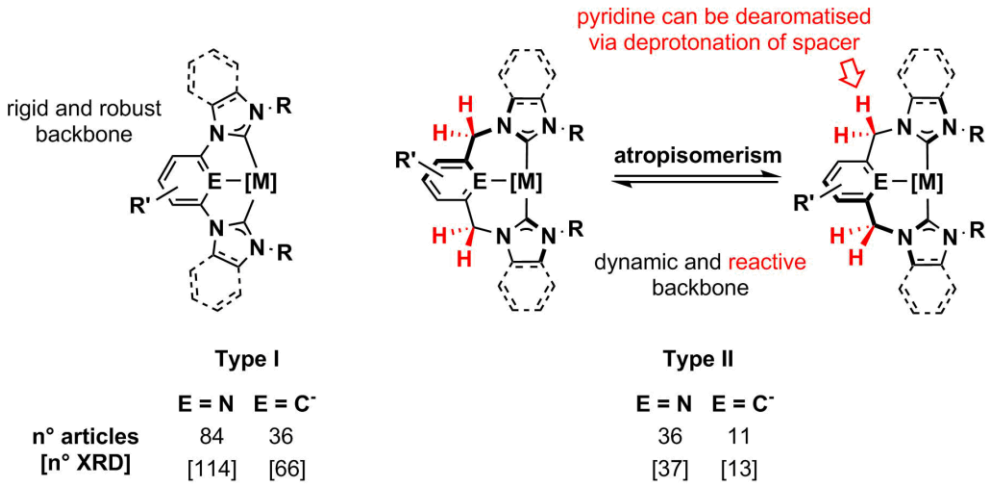

Fig. 1.8: *General structures and properties of* ***Type I*** *and* ***Type II*** *complexes with tabulated counts of associated articles and crystal structures.*

Modification of **Type I** and **Type II** structures has afforded a diverse range of NHC-based pincers, representative examples of which are given in **Fig. 1.9**. Substitution of the central heterocycle group for other N-based donors, both anionic and neutral, enables tuning of the electronic properties of the metal as well as introduction of further functionality. For example, amido-bridged **A34** demonstrates facile oxidative addition to the rhodium centre as a result of greater electronic density provided by the anionic ligand.[81] Alternatively, the incorporation of an amino-pyrazine tether into **A35** enables solid phase support without detrimental effect on its catalytic function in Heck and Suzuki couplings.[82]

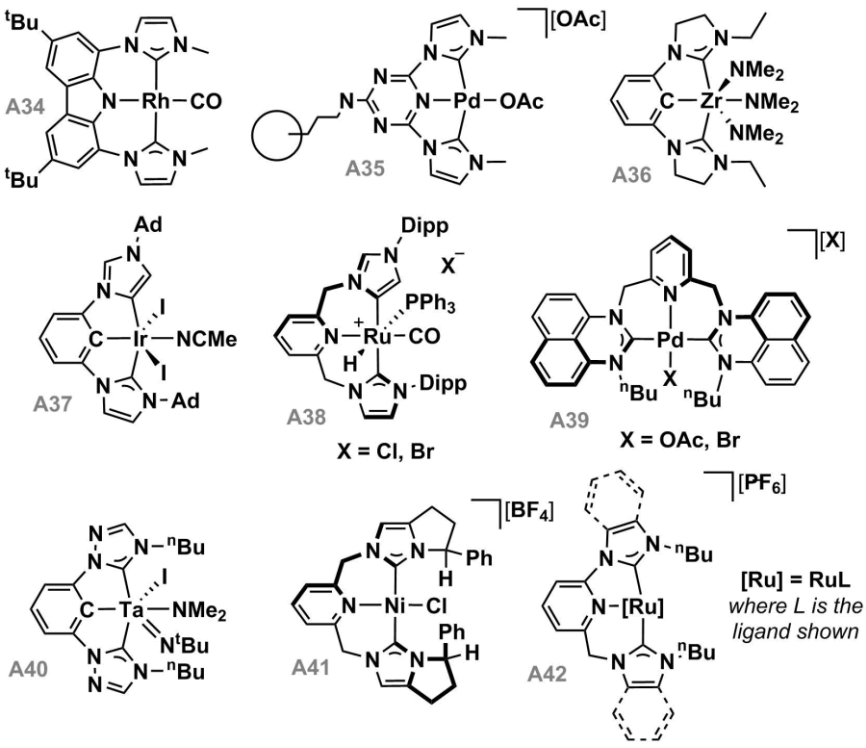

Fig. 1.9: *Examples of CEC pincers.*

CEC pincers with saturated (**A36**),[83] abnormal (**A37**[84] and **A38**[76]), 6-membered (**A39**)[85] and triazole-based (**A40**)[86] NHCs have also been described, broadening the scope of electronic and structural properties of the ligand class. Chiral nickel complex **A41** uses imidazolylidene-derived donors, but its fused cyclopentyl rings effectively stop the atropisomerism process of the **Type II** backbone, opening up a promising avenue for asymmetric catalysis.[87] Bearing only one methylene spacer, Ru-complexes **A42** represent a rare combination of **Type I** and **Type II** structures.[88]

1.2.2 Synthesis of NHC-Based Pincers

CEC pro-ligands are generally synthesised *via* direct adaptation of procedures employed for monodentate imidazolium salts. For example, double alkylation of bis(bromo)- or bis(bromomethyl)-aryls and pyridyls is a typical route to **Type I** and **Type II** ligands, respectively (**Scheme 1.5**). Formation of pyridyl-centred pro-ligands [**C-N-C**$^{\mathbf{DIPP}}$].2HX (X = Br, I) requires forcing condtions (solvent-free melt, 190°C, 7 days) due to the high-energy S_NAr substitution, while synthesis of lutidine, xylyl and bromo-aryl centred pro-ligands [**C^E^C**$^{\mathbf{Me}}$].2HBr (E = N, C-H, C-Br) proceeds within 12 h. Reflecting the scarcity of saturated NHC-pincer ligands, ring-closing methodology is less common but is used to access the saturated C-C-C pincer precursor to zirconium complex **A36**.

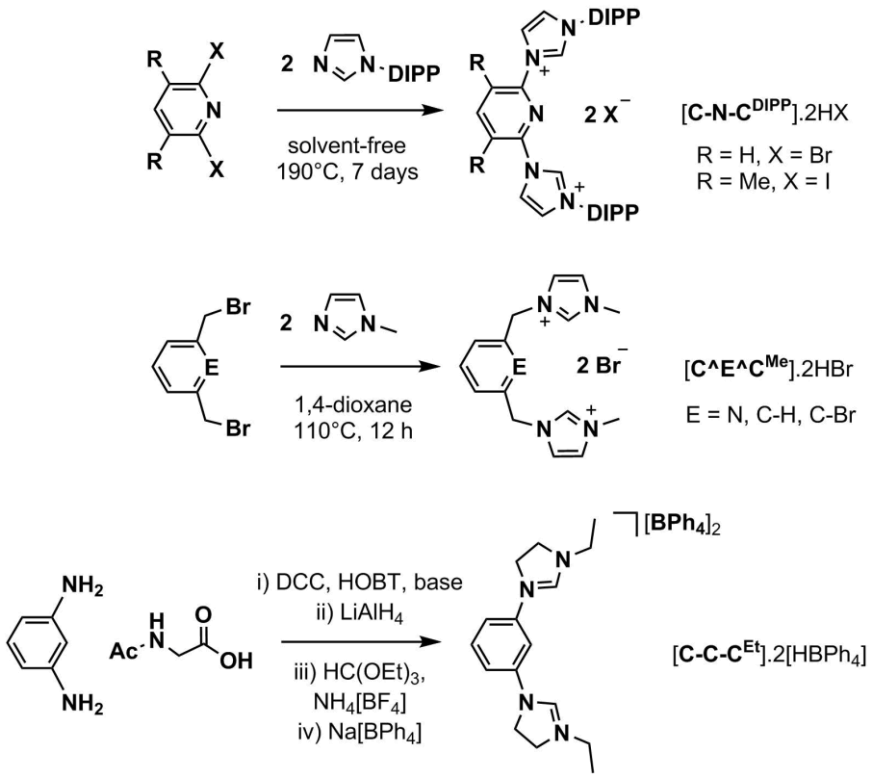

Scheme 1.5: *Example syntheses of NHC-pincer pro-ligands.*

As shown in **Scheme 1.6**, pincer pro-ligands are typically metallated using equivalent deprotonation procedures to those for monodentate NHC donors (*vide supra*). Isolation of the free-carbenes is inhibited by their innate air and moisture sensitivity, and a recent search of the literature identified only 10 examples. Of these, eight utilise a rigid **Type I** architecture and the two systems that yielded crystals suitable for XRD share the protective steric bulk of DIPP substituents on the distal imidazolyl nitrogens (*c.f.* **A43**, **isolated carbene** route from [**C-N-C^{DIPP}**].2HBr, **Scheme 1.6**).[89]

Instead, deprotonation is often conducted *in-situ*, as demonstrated by the one-pot platination of bis-aryl amide **A45** (**M + B$^-$** route),[90] but the formation of multi-nuclear complexes or clusters may also occur.[91] For example, attempts at synthesising a rhodium **Type I** complex *via* an 'accessible synthesis' using weak external base Et_3N with $[Rh(COD)Cl]_2$ are frustrated by the generation of bimetallic complex **A46**.[91] Refluxing the reaction mixture in aerated MeCN does afford rhodium pincer **A47a**, but also results in oxidation at the metal centre. Similarly, reaction of the same pro-ligand with $[Ru(COD)Cl_2]_n$ and Et_3N in refluxing EtOH gives ruthenium pincer **A47b**, formed in low yield *via* decarbonylation of the solvent.[48] Despite such shortcomings, accessible syntheses still represent a popular route to NHC-based pincer complexes, with both external bases (*e.g.* Et_3N) and internal bases (*e.g.* $[Pd(OAc)_2]$ and $[Fe(HMDS)_2]$; **A48** and **A49** respectively, **M(B)$_2$** route) regularly employed.[80,92]

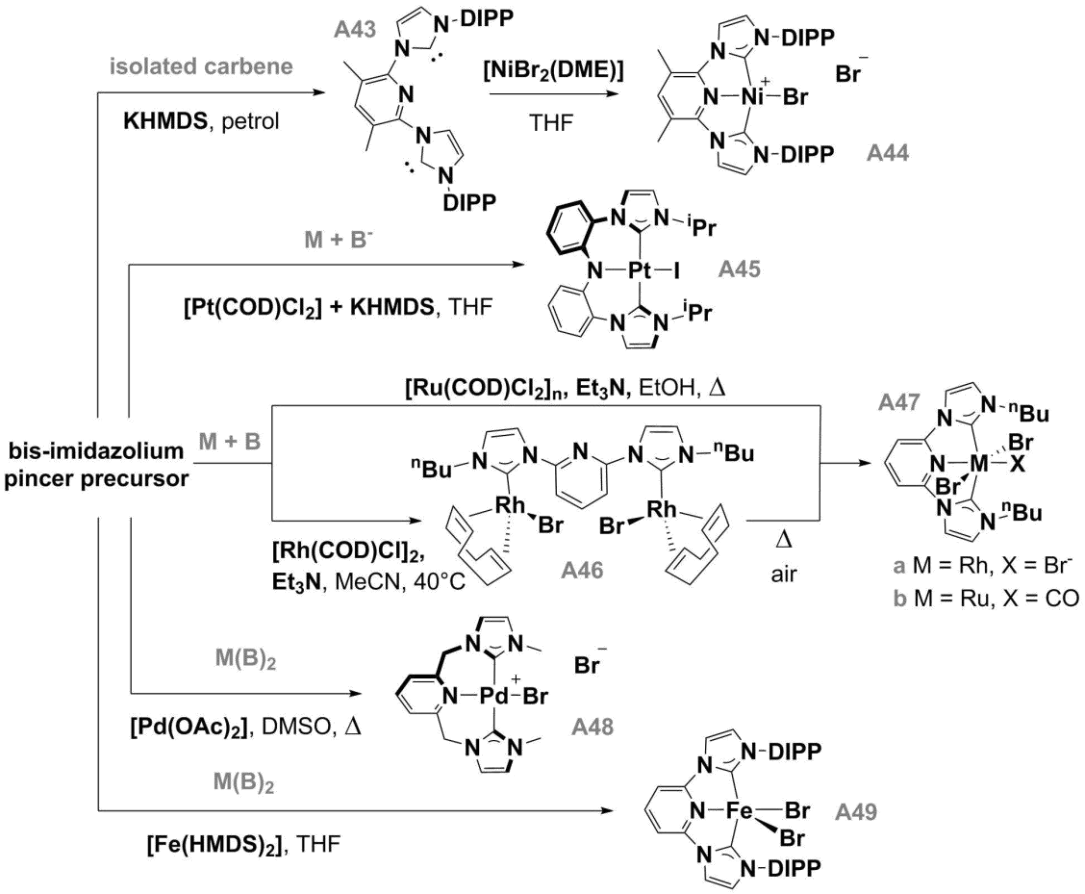

Scheme 1.6: *Base-directed metallation routes to CEC pincers.*

Removing the requirement for an external base, coinage metal complexes (either isolated or *in-situ*) are desirable carbene-transfer reagents. Ag_2O has been used to good effect in the synthesis of a series of bridged and unbridged [Pd(CNC^R)X] complexes (*i.e.* R = Me; X = halide, Me; **A50**) and, while the *in-situ* transmetallation procedure is highly effective,[93-95] a number of **Type II** silver intermediates have been isolated and used independently (**Scheme 1.7**).[95-97] As illustrated by **A51**, in the absence of strongly coordinating counter-ions (*i.e.* halides), these silver complexes are often dimeric in structure. In more constrained systems (discussed in **Section 1.4** and **Chapter 2**, **Section 2.3.1**), dynamic processes involving fragmentation into mononuclear species can be observed, implying facile cleavage of the Ag-NHC bond and demonstrating their suitability for carbene transfer to other transition metals.[96-98]

In addition, transmetallation methodology is also used in the preparation of CCC complexes. For example, reaction of silver transfer agent **A52** with a highly reactive Ir(I)-ethylene precursor (produced *in-situ*) proceeded to give **A53** after oxidative addition of the central C-Br bond (**Scheme 1.7**).[99] Transmetallation from copper transfer agents has not been previously used to obtain CEC pincer complexes, but is described herein (**Chapter 2**, **Section 2.3.2**).

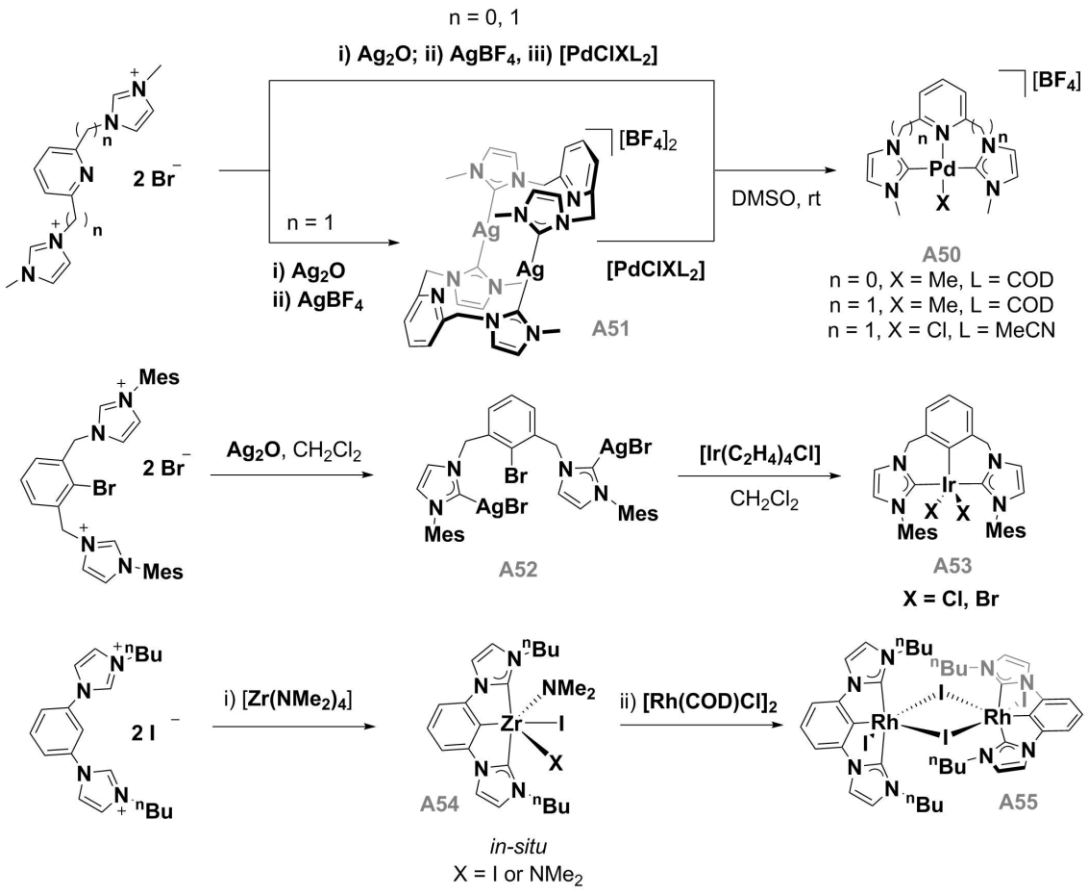

Scheme 1.7: *Transmetallation routes to NHC-pincers.*

Installing a reactive functionality on the central aryl ring, such as C-Br in **A52**,[100] is a common modification of the ligand when a central aryl donor is required. Xylyl precursors require an additional deprotonation or oxidative addition of the central C-H bond, which is not always compatible with the desired metal fragment. Accessing CCC-complexes using traditional deprotonation methods often requires strong bases, and/or high temperatures to complete the pincer architecture after initial carbene-coordination.[101-103] In sterically hindered structures such forcing conditions may favour the formation of abnormally-coordinated products, such as the mixed Ir(CCC) pincer **A37** (**Fig. 1.9**, *vide supra*) described by Zuo for catalytic transfer hydrogenation.[84] Alternatively, $[Zr(NMe_2)_4]$ has been introduced as a versatile carbene transfer reagent in these systems, and has enabled access to C-C-C complexes of rhodium (**A55**, **Scheme 1.7**),[104] iridium,[105] and platinum.[106]

The formation of abnormal carbenes is not restricted to CCC-based structures, and the mixed normal/abnormal Ru(C^N^C) pincer **A38** (**Fig. 1.9**, *vide supra*) was observed by Pidko *et al* when PPh_3 was employed as an ancillary ligand. When LiBr is present in the reaction mixture **A56** is instead produced (**Scheme 1.8**).[76]

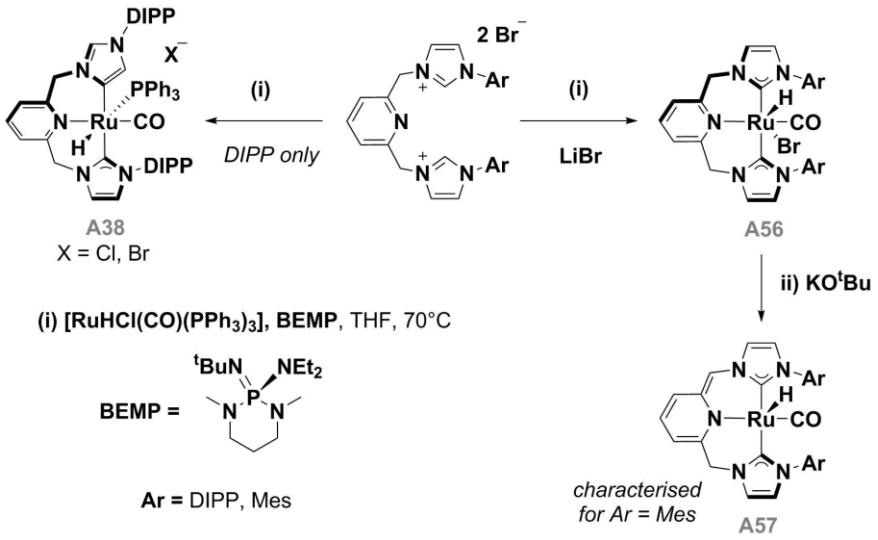

Scheme 1.8: *Formation of Ru(C^N^C) and dearomatisation to afford Ru(C*N^C) complexes.*

Comparable with Ru(P^N^P) systems championed by Milstein and co-workers (*i.e.* **A27**, **Fig. 1.6**),[67,107-110] Ru(C^N^C) complexes have demonstrated similar reactivity with strong bases, forming dearomatised pincers such as **A57** (notated as Ru(C*N^C), see **Scheme 1.8**), which have been shown to activate hydrogen, nitriles and CO_2.[76,111,112] Under basic reaction conditions, **A38** and **A56** are potent catalysts, outperforming phosphine-based P^N^P pincer complexes in ester hydrogenation reactions.[76] Such examples demonstrate the versatility of the **Type II** motif and its potential to match or better the application of P^E^P-based counterparts in organometallic catalysis.

1.2.3 Applications of NHC-Based Pincers

Continuing the comparison of PEP and CEC-pincers, Ir(C-C-C) complexes, such as **A58** (**Fig. 1.10**), promote catalytic transfer dehydrogenation of alkanes. Turnover numbers are low (10 after 24 h using NBE as acceptor, 1 when TBE is used) and catalysts are less robust than corresponding Ir(PCP) complexes.[103] Remarkably, when dehydrogenation of cyclooctane is conducted under acceptorless conditions, **A58** demonstrates greater conversion and high initial activity (TON 103 after 22 h; TOF *ca*. 12 h^{-1} at 150°C) more akin to that of the phosphine analogues, although catalyst decomposition is observed after 24 h.[100] Selective C-H bond activation and borylation of aryls has also been reported for **A58**, with yields generally ≤ 60 % at 2 mol % loading (TON 30 after 24 h). Near-quantitative conversion was achieved in the same time-frame for a bis-CF_3 aryl, indicating a preference for electron-deficient systems.[103]

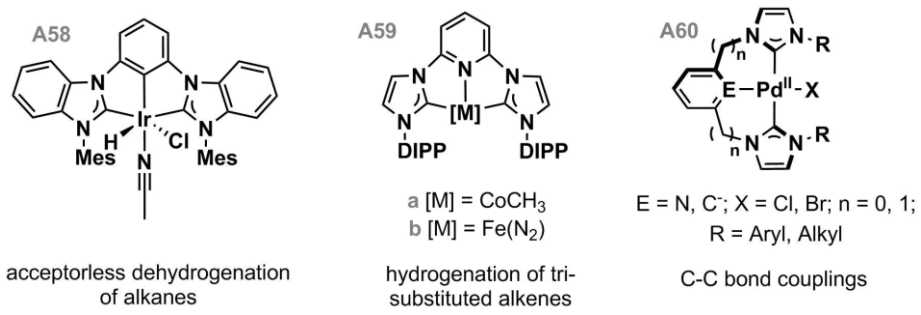

Fig. 1.10: *Applications of NHC-based pincers.*

The reverse reaction, hydrogenation of alkenes, is catalysed by Fe- and Co-CNC^{DIPP} complexes **A59**, with both highly active for tri-substituted and sterically hindered alkenes.[113,114] The cobalt complex **A59a** is the more active, showing complete conversion of *trans*-methylstilbene after 5 h at 5 mol % loading.[114] Additionally, NHC-based pincer complexes have been employed in catalyic hydrosilylation,[115-118] hydroamination[105,119-124] and hydrovinylation[125] reactions.

Reflecting the early success of Pd(CEC^{R}) complexes (general formula **A60**, **Fig. 1.10**) in Heck and Suzuki couplings,[93,126] the application of NHC-based pincers in C-C bond coupling reactions has seen extensive investigation. Ni(CEC) complexes have been employed in Suzuki-Miyaura and Kumada couplings,[127-134] while CNC complexes of early transition metals Ti, V and Cr have proved active in ethylene dimerisation and polymerisation reactions.[135-137]

NHC-based pincers have also been investigated for their photophysical properties and photochemical applications. Bearing structural resemblance to terpyridine (terpy) ligands, planar **Type I** pincers are particularly prevalent in this field,[106,138-141] with ruthenium complexes (**A61**, **A62**; **Fig 1.11**)[142-145] demonstrating microsecond ^{3}MLCT excited-state lifetimes, which are up to four orders of magnitude longer than those of bis(terpy) analogues. Notably, while a **Type II** congener of **A62** is non-emissive,[146] aforementioned complexes **A42** (**Fig. 1.9**), which bear two asymmetric meridonal pincers, demonstrate comparable ^{3}MLCT excited-state lifetimes of 0.2 – 8.7 μs.[88]

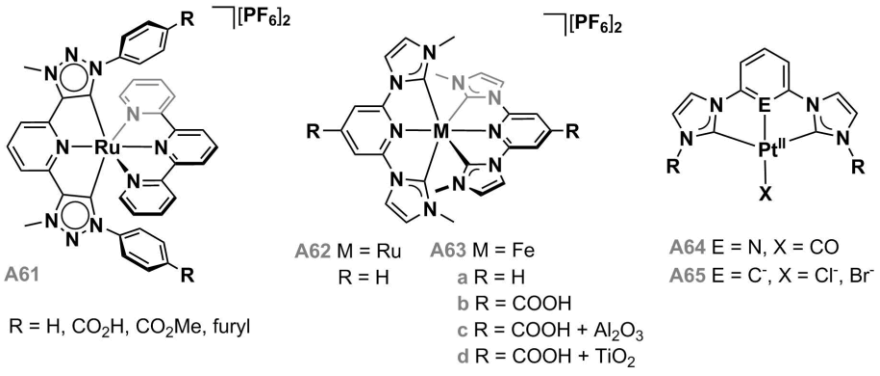

Fig. 1.11: *NHC-based pincers with photochemical application.*

Remarkable, picosecond, lifetimes have been reported for iron complexes **A63**, which may be immobilised onto solid substrates *via* interaction with a pendant carboxylic acid.[141,147-149] Al_2O_3-immobilised **A63c** has the longest reported ^{3}MLCT excited-state lifetime (37 ps) for a mononuclear Fe complex, while **A63d**, on TiO_2, shows photosensitisation.

The photophysical properties of **Type I** Pt^{II} complexes are tunable by the nature of the central donor and overall charge, with dicationic **A64** demonstrating vapochromic behaviour while Pt(C-C-C) pincers are blue-light emitters both in solution and in the solid-state (E = C^-, **A65**).[150,151]

1.2.4 Deactivation Modes of NHC-Based Pincers

With high temperatures employed in many desired catalytic applications, the potential ability of NHC-based pincer ligands to confer thermal stability is a strong motivation for their application and further development. However, as in monodentate systems (*vide supra*), the metal-NHC bonds of **Type I** and **Type II** pincers can be susceptible to decomposition. In palladium and nickel CNC pincers, the exact nature (and rate) of decomposition is sensitive to the identity of the *N*-substituents and the metal. While alkyl-substituted $[Pd(C\hat{}N\hat{}C^R)Me]^+$ and $[Pd(C\text{-}N\text{-}C^R)Me]^+$ complexes (R = Me, ^{t}Bu; **A66**, **Scheme 1.9**) undergo concerted reductive elimination of a C2-Me imidazolium salt at high temperature,[94] attempts at synthesising $[Pd(C\text{-}N\text{-}C^{DIPP})Me]^+$ systems resulted in methyl-migration to form palladium-bound carbanion **A67**.[152] No further decomposition is observed for **A67**, but when the same reaction is conducted with $[Ni(Me)_2(tmed)]$, migration of a methyl-group onto the C2 carbon is accompanied by ring-opening to afford **A68**.[89] The exact mechanism of this process is not known, but is postulated to go *via* a nickel analogue of **A67**, followed by base-catalysed rearrangement.

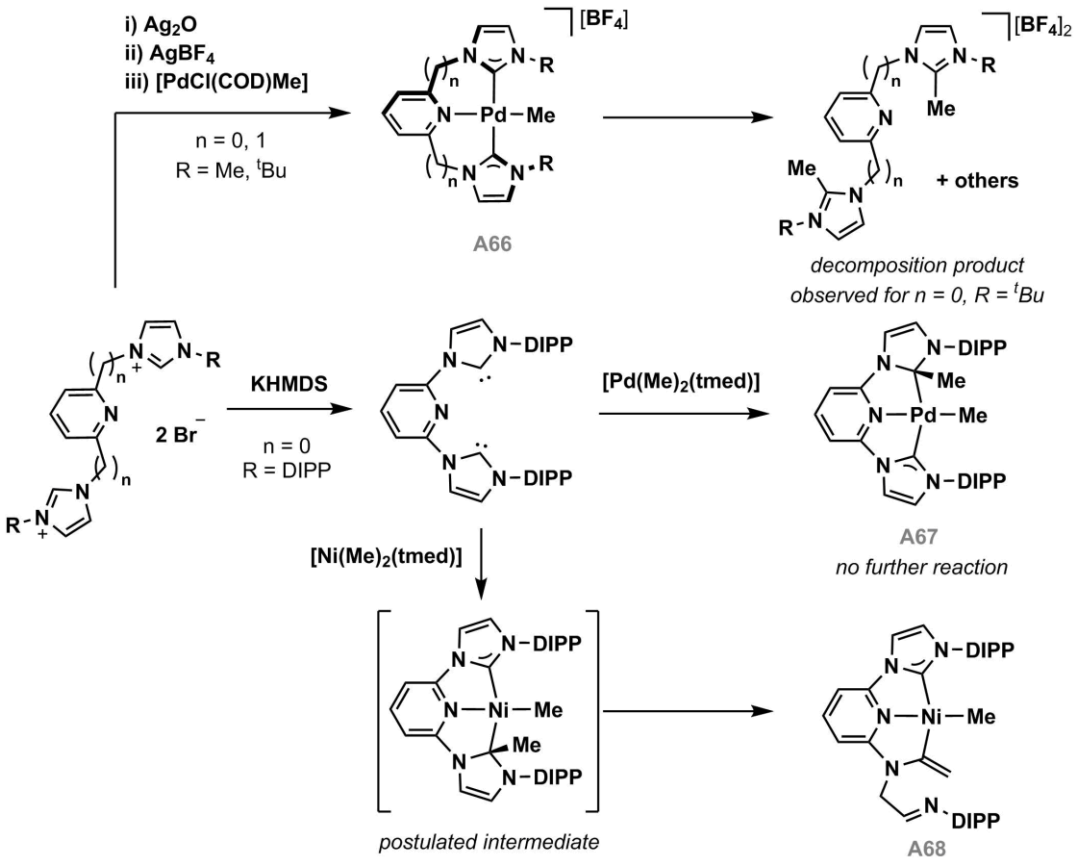

Scheme 1.9: *Known decomposition pathways of CNC pincers.*

1.3 Macrocyclic Ligands

1.3.1 Overview

Macrocyclic ligands have long been investigated for their ability to encapsulate metal ions, demonstrating large binding constants and high thermal stability through a combination of the chelate effect and the pre-organisation of donor atoms.[153,154] Excellent size selectivity can be achieved for species that fit comfortably inside such rings, with mis-matched ions (too large, too small) exerting extra conformational strain on the macrocycle on binding.[154] This property has driven the application of macrocyclic ligands in ion-extraction/exchange materials and in a range of biomedical fields, such as MRI contrast agents (able to bind and transport paramagnetic metals), fluorescent ion-sensors for assays and radiopharmaceuticals (stabilising and transporting radioactive isotopes to target tissue).[155,156] Crown ethers (*e.g.* **18-crown-6**, **Fig. 1.12**) and aza-macrocycles (*e.g.* **cyclen** and **cyclam**) are highly versatile ligand classes, with variations in ring-size and substitution pattern facilitating employment in all of the above applications.

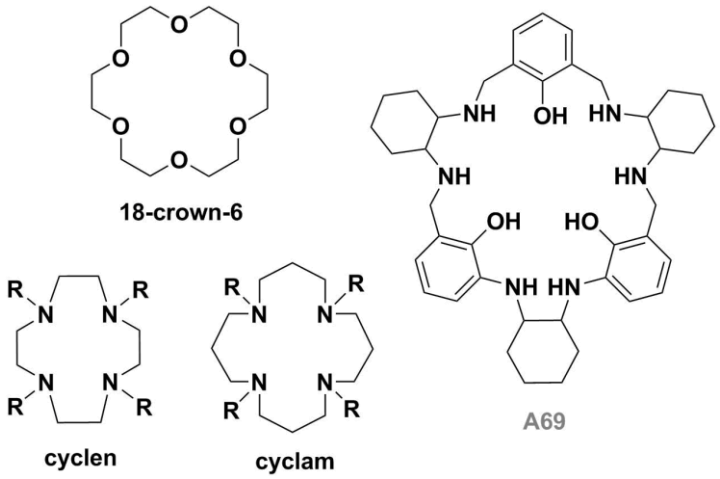

Fig. 1.12: *Common crown ethers and aza-macrocycles and ligand* ***A69****.*

Comparisons to the ability of enzymes to selectively bind and manipulate ions or molecules are often made.[157] For example, macrocyclic ligand **A69** has been shown to bind zinc and mixed zinc-copper clusters in an analogous fashion to the active site of P1 nuclease.[158] Furthermore, these clusters are stable in aqueous solutions and are active in the hydrolysis of calf thymus DNA, demonstrating an ability to mimic the enzyme's biological function, structure and thermal stability.

1.3.2 Applications of Macrocyclic Complexes of Late Transition Metals

Incorporation of transition metals into macrocyclic architectures, and study of the resulting coordination complexes, has led to development of structural and chemical behaviour not observed in acyclic systems (**Fig. 1.13**). Macrocycles **A70**, for example, enable formation of bimetallic assemblies on reaction with $[Rh(CO)_2Cl]_2$ that place the two cationic rhodium centres in close proximity.[159,160] Mononuclear poly-ethylene glycol and cryptand variants of this ligand enable the complimentary binding of water (**A71**) and Lewis acids (**A72**), respectively, expressing the potential non-innocence of such macrocyclic structures and the ability to overcome coulombic repulsion in polycationic systems.[160,161]

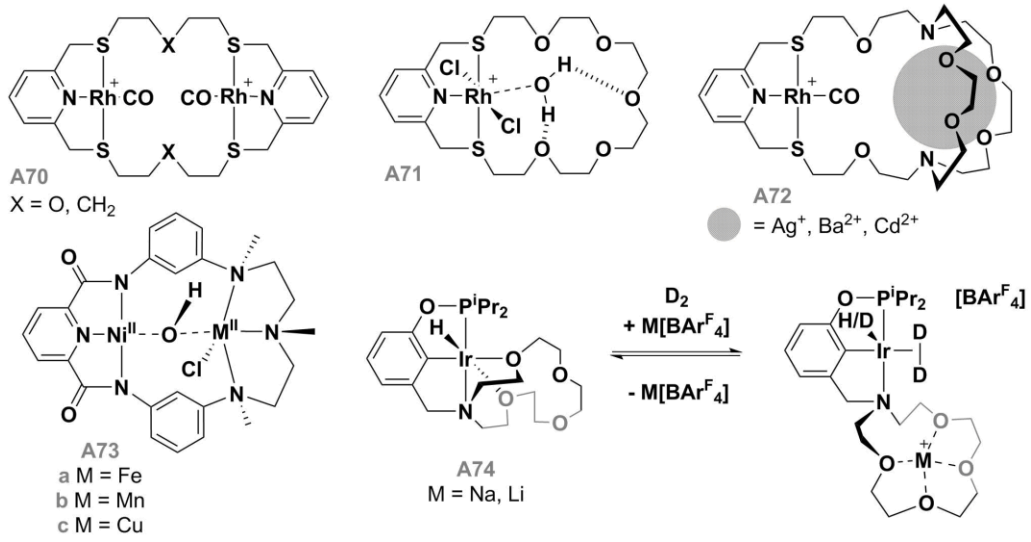

Fig. 1.13: *Pincer-complexes incorporating secondary macrocyclic binding sites.*

The secondary binding pocket in Ni-OH complexes **A73** allows formation of bimetallic assemblies and μ^2-binding of hydroxide between nickel and Fe, Cu or Mn centres.[162] Iron-bound **A73a** mimics a catalytically active site of carbon monoxide dehydrogenase, and CO_2 bridged bimetallic macrocycles have also been reported.[163] Ir-PCN pincer **A74** bears a pendant aza-crown macrocycle, through which it may bind an auxillary alkali metal. In the absence of a cation source, the macrocycle coordinates to the metal centre, inhibiting H-D exchange on Ir.[164] Addition of Na^+ or Li^+ (as $M[BAr^F_4]$) induces rate enhancements of up to 250x, while subsequent addition of a chloride source results in a return to the inhibited coordination mode. Although not encompassing the metal coordination sphere, the macrocycle of complex **A74** hence acts as a gate, controlling the reactivity of the iridium centre under certain conditions.[165]

Macrocyclic ligands have also been used to place two catalytically active metal centres in close-proximity, enabling cooperative behaviour and resulting in higher activity or selectivity

than mononuclear congeners. Such was found for bimetallic Cu^{I}-Cu^{I} assembly **A75** (**Fig. 1.14**), which affords greater enantioselectivity (69 % *ee*) than its acyclic monometallic equivalent (19 % *ee*; **A76**) for the oxidative coupling of 2-naphthol.[166] Bimetallic Fe^{II}-Fe^{II} or Co^{II}-Co^{II} complexes **A77** also demonstrate higher activity in ethylene polymerisation reactions when both coordination sites are occupied.[167]

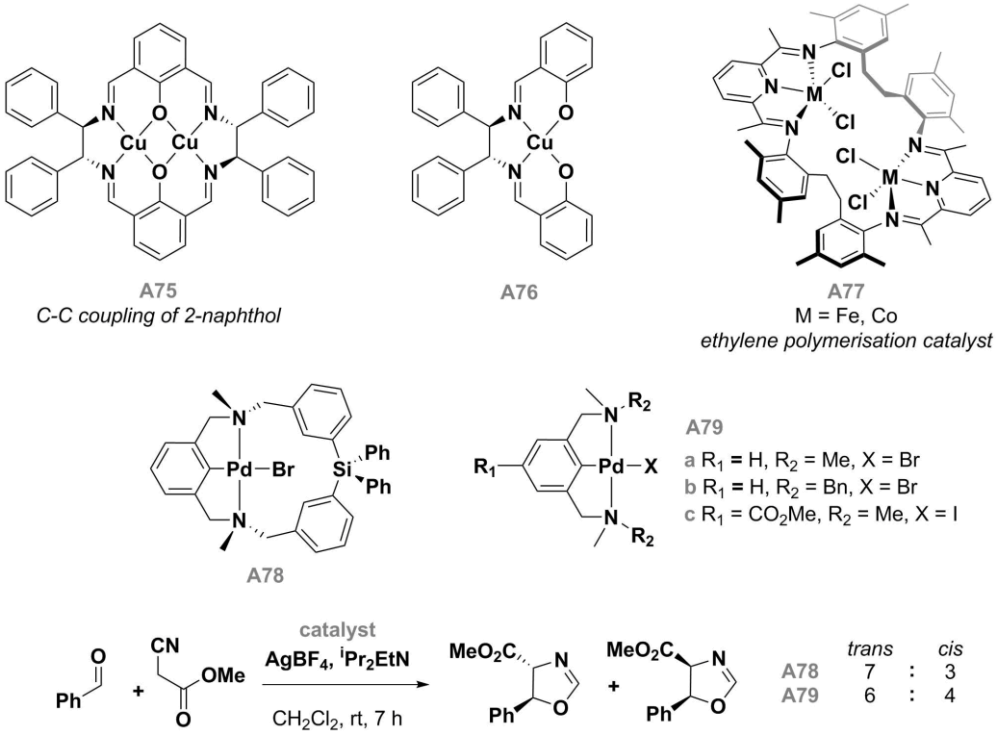

Fig. 1.14: *Catalytic applications of macrocyclic pincer complexes.*

Enhanced reaction control may also be achieved by monometallic macrocyclic systems such as **A78**. While showing comparable activity to acyclic analogues (89 % conversion *vs* 83 %, 40 % and 99 % for **A79a**, **A79b** and **A79c**, respectively), an increase in selectivity for the *trans* diastereoisomer is observed when **A78** is employed in asymmetric aldol condensations (7 : 3 *trans*/*cis* ratio *c.f.* consistently 6 : 4 for acyclic **A79a-c**).[168]

1.3.3 Applications of Macrocyclic Complexes in the Construction of Interlocked Systems

In addition to enforcing reaction control *via* transient encapsulation of reactive functionalities within a ring, macrocycles may be employed in the mechanical entrapment of non-coordinated components to afford a permanently-interlocked assembly. The simplest examples of such interlocked architectures are 2-component [2]rotaxanes and [2]catenanes (**Fig**. **1.15**). In each case the macrocycle and the central component have no connecting covalent bonds and are capable of independent movement. Induction and control of this movement by external stimuli such as temperature, ion concentration, pH, photochemical input and electrochemical

potential have been shown for a range of systems and such findings have driven recent explorations into their application as molecular machines.[169]

Fig. 1.15: *General structures of [2]rotaxanes and [2]catenanes.*

Starting with macrocycle **A80**, Sauvage demonstrated the first use of a transition metal (copper) as a template for formation of a catenated complex (**A81**, **Scheme 1.10**). Coordination of an acyclic phenanthroline unit to the preformed copper-macrocycle positions the phenol termini above and below the existing ligand. This orientation favours ring-closing alkylation of the subsequently added tether, as opposed to oligomerisation, and **A81** is afforded in 42 % yield from **A80**.[170] Complex **A81** is air-stable and was shown to be electrochemically resistant to demetallation, but the copper ion may be abstracted with KCN to give the free catenane **A82**.[171]

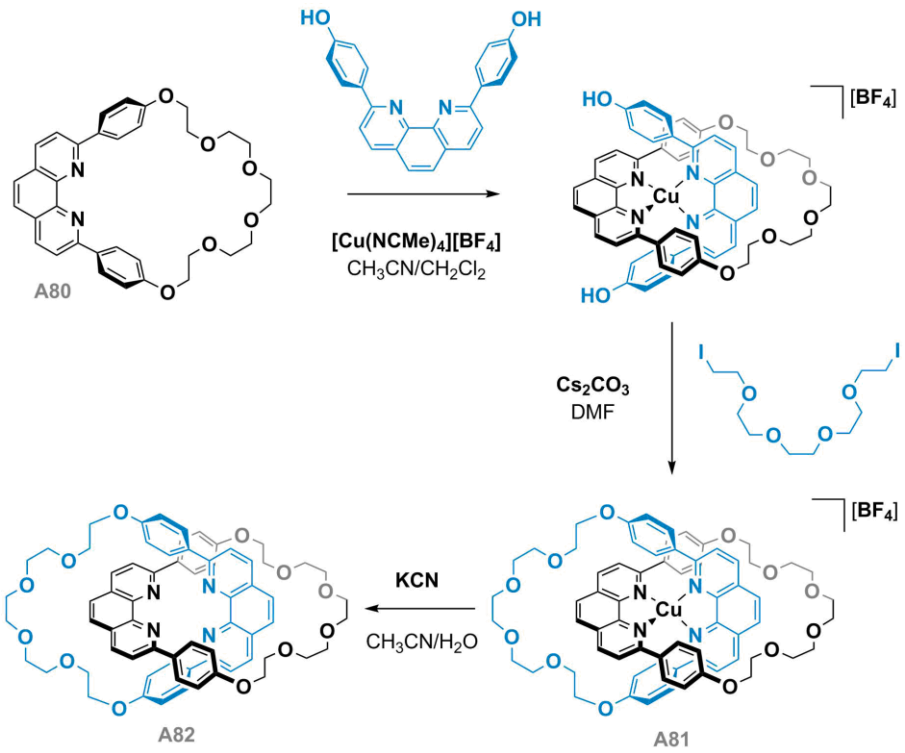

Scheme 1.10: *Synthesis of [2]catenane* ***A82****.*

Template synthesis is an established route to macrocyclic structures and more complex supramolecular architectures, with coordination of a metal centre favouring the macrocyclic or interlocked product over oligomeric mixtures.[172-174] As exemplified by copper in the formation

of **A82**, the template may serve a purely structural role (*passive-metal template synthesis* – the metal-ligand coordination complex favours a ring-closing reaction by pre-orientation of the active components, or provides a charged centre that repels other charged monomers),[175] but can also participate directly in the ring-closing reaction (*active-metal template synthesis*).[176] Particularly elegant examples of the latter include catalytic sp^3-sp^3 coupling of bromo-alkanes through a pybox-containing macrocycle to afford [2]rotaxane **A83** (**Scheme 1.11**).[177] The active catalyst for the coupling reaction is a transient adduct of the macrocycle and nickel, and its discovery led to the development of acyclic variants for the catalytic homo-coupling of a range of bromo-alkanes.

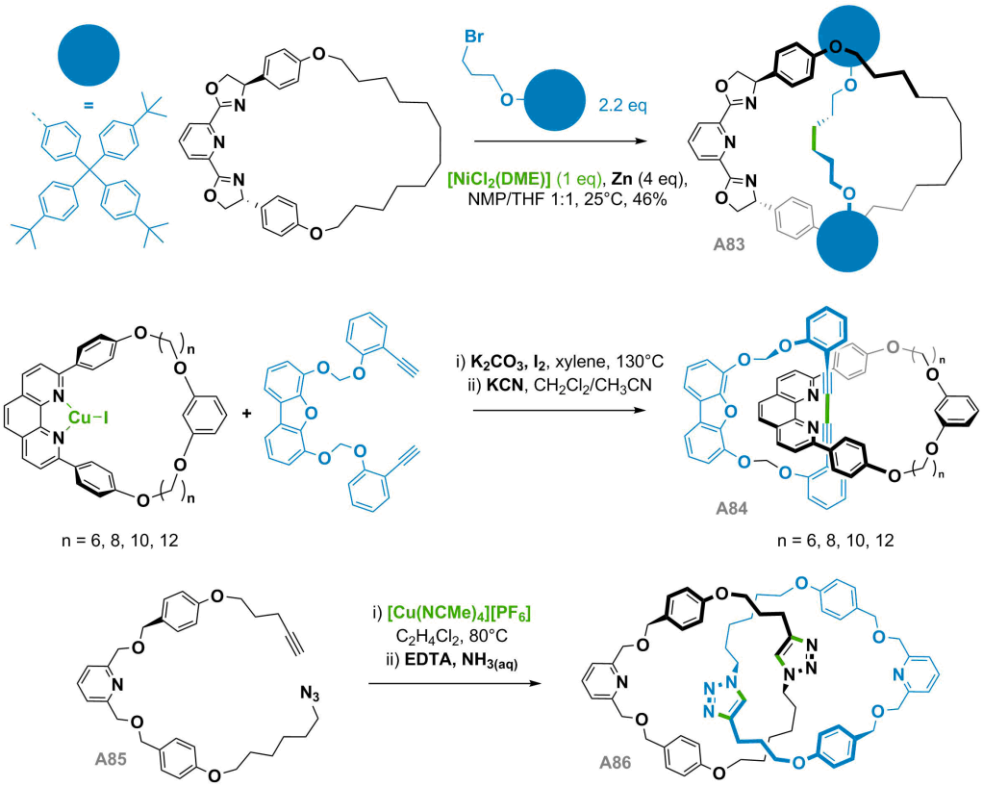

Scheme 1.11: *Active-metal templated syntheses of [2]rotaxanes.*

Using variants of macrocycle **A80**, Saito *et al* generated [2]catenanes **A84** *via* Glaser-coupling of terminal alkynes in up to 64 % yield (n = 6).[178] The efficiency of these reactions was dependent on ring-size, with larger rings limited to *ca*. 30 % yield. Bypassing isolation of a macrocyclic coordination complex, Leigh and co-workers employed acyclic alkyne-azide **A85** in a 'double-click' reaction to generate **A86** with remarkable selectivity and 46 % yield.[179] To explain this selectivity, over monomeric and oligomeric assemblies, the authors propose that the second, catenate-forming, 'click' is promoted by coordination of the alkyne to a second copper ion, bound to the triazole of the first-formed macrocycle. By this mechanism, both active and passive metal templation are employed to favour catenane formation.

1.4 NHC-Based Macrocyclic Pincer Ligands

While a range of alkyl and aryl-based *N*-substituents have been explored for NHC-based pincer ligands, their function is generally limited to modification of steric bulk around the metal centre. Tethering of these positions to the same linkage in a ring-closing reaction would enable the formation of NHC-based macrocycles; potentially combining the favourable properties of NHC-pincers (tridentate binding, strong σ-donor ability) with those of macrocyclic ligands (steric confinement, potential for supramolecular architectures and reaction control).

A limited number of NHC-based macrocyclic pro-ligands have been reported, with few shown to coordinate metals in a meridonal fashion. Mimicking the rigid, tetradentate structure of porphyrins and predominantly investigated for their electrochemical properties,[180] a range of transition metal complexes of related bis(NHC) and tetra(NHC) ligands have been prepared (**A87**, **A88** and **A89**, **Fig. 1.16**).[175,180-183] Notably, the cobalt chloride **A87b** is active in the photochemical activation of water to generate hydrogen.[181]

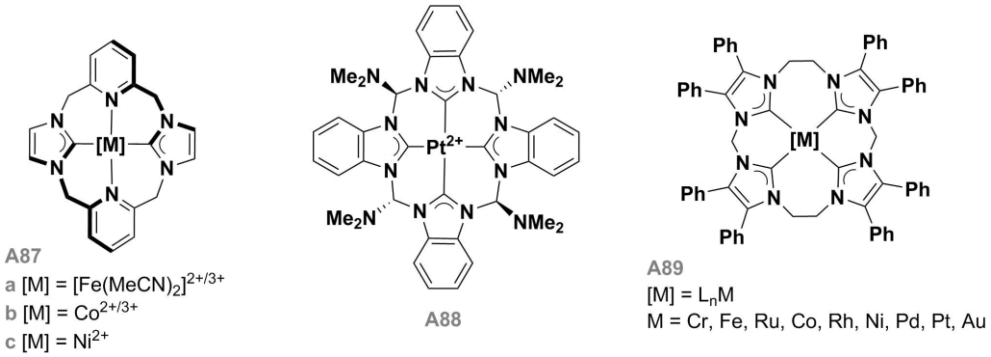

Fig. 1.16: *Macrocyclic complexes containing NHCs.*

Ligands **A90-A93** more closely resemble the pincers detailed in **Section 1.2**, with **Type I** and **Type II** backbones present. However, no pincer complexes of these have been reported. Investigations have instead centred on the formation of multinuclear cages and metallocycles with silver and gold.[96,97,184,185]

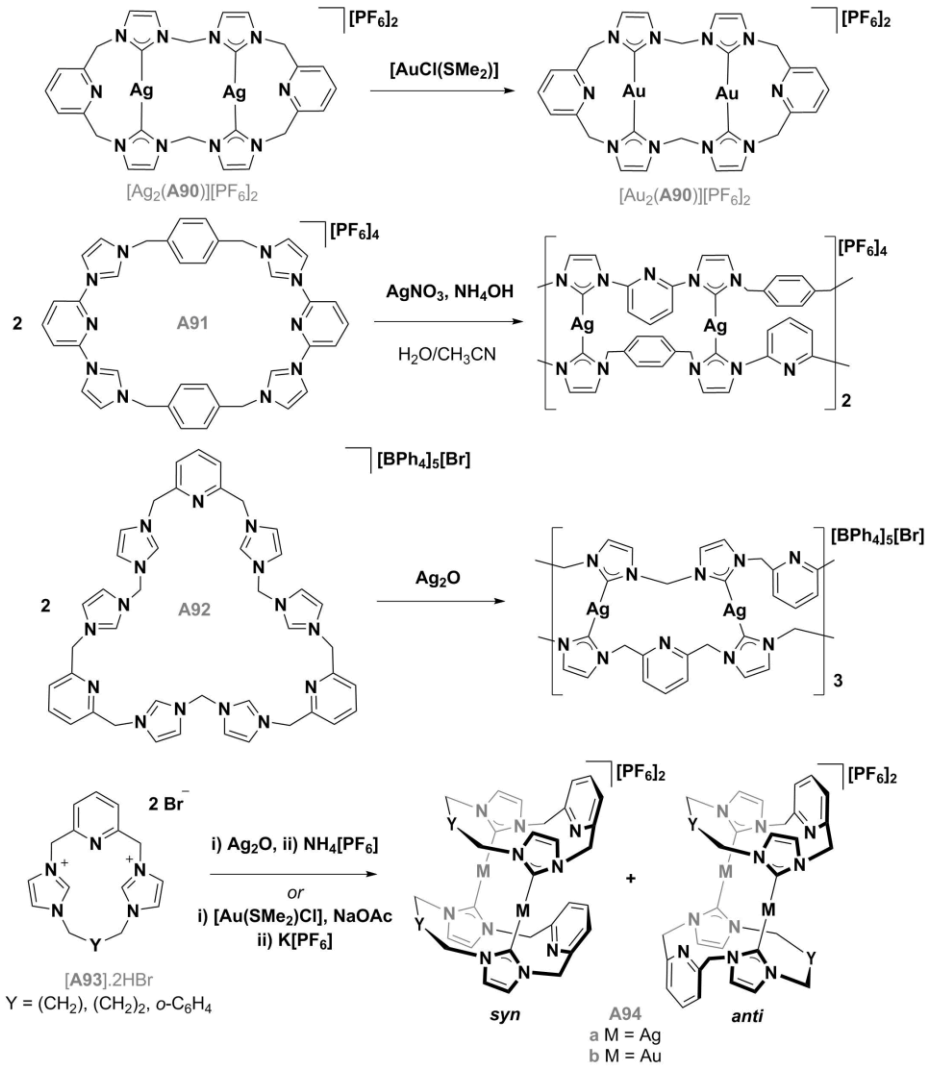

Scheme 1.12: *Synthesis of* ***Type I*** *and* ***Type II*** *NHC-based macrocyclic complexes.*

As observed by the groups of Hahn and Biffis, reaction of ligands **A93** with Ag_2O or [$AuCl(SMe_2)$] affords dicationic dimers **A94** with *syn* and *anti*-conformations (**Scheme 1.12**), which – in the case of **A94a** – interconvert in solution at room temperature.[96,97,186] Absence of this process in **A94b** implicates cleavage of the weaker Ag-NHC bond during interconversion.

Palladation or platination of **A93** using [$Pd(OAc)_2$], [$Pd(acac)_2$] or [$Pt(acac)_2$] affords the respective palladium and platinum dibromides **A95** and **A96** (**Scheme 1.13**).[97,186] Characterisation using NMR spectroscopy, alongside crystallographic analysis (of **A95b** and **A96a**), confirm that only the NHCs of these small and conformationally-restricted macrocycles are bound and in a *cis*-fashion. The ring appears unable to accommodate *trans*-coordination of the NHCs or coordination of the pyridine. Larger rings (28 – 38 atoms) are able to bind palladium in a tridentate mode, as shown by palladium halide complexes **A97**[187] and **A98**[188] (**Scheme 1.13**), the latter of which is accessed using a mercury salt as a transmetallation reagent.

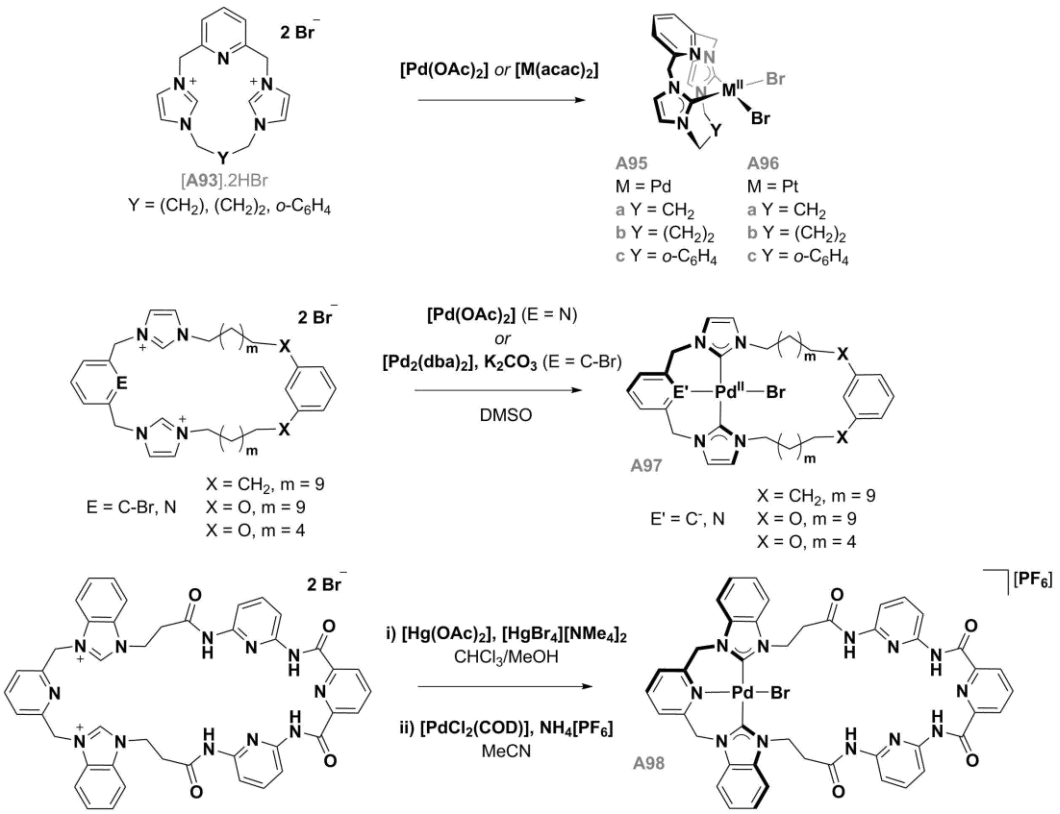

Scheme 1.13: *Syntheses of NHC-based pincer complexes of palladium directly from imidazolium salts.*

Macrocycles **A95**, **A97** and **A98** have been investigated for application in Pd-catalysed C-C coupling reactions. Small macrocycles **A95** are active in Sonagashira couplings with yields of 65 – 83 % obtained for the reaction between bromo acetophenone and phenylacetylene (1 mol %, 1 h, 100°C), comparable with acyclic Pd(CNC) pincers.[186] However, no clear advantage over acyclic precedents was found and the high temperatures required for significant reaction rates also result in more rapid loss of activity, indicative of catalyst decomposition.

While **A98** is ineffective in the Heck coupling of bromobenzene and styrene,[188] complexes **A97** are active in both the Heck coupling of butyl-acrylate and iodotoluene (down to 2 mol % loading), and the homo-coupling of phenylacetylenes (10 mol % loading).[187] Good yields are obtained for the Heck reaction, and the lutidine-centred macrocycles (**E = N**) generally outperform the xylene-based complexes under comparable conditions. As with **A95**, conversions are lower at higher temperatures, suggesting catalyst degradation. For the homo-coupling of phenyl acetylene, the xylene-based complexes (**E = C**$^-$) demonstrate greater conversion at higher temperatures, outperforming the lutidine variants. In summary, while macrocycles **A95** and **A97** are significantly inferior to established palladium systems, they do demonstrate some activity and macrocyclisation does not completely inhibit their function.

1.5 Aims and Objectives

The aim of this project is to prepare and study late transition metal complexes of macrocyclic CNC pincer ligands (**Scheme 1.14**). In order to investigate the structural effects of the macrocycle in the absence of other donor-based interactions, macrocycles of minimal functionalisation and varying ring size will be targeted, requiring expansion of the current synthetic methodology. The structure, dynamic behaviour and reactivity of these systems will be investigated, and comparisons made with acyclic congeners and literature precedents. Finally, the capacity of these macrocyclic complexes and their derivatives to form stable interlocked assemblies *via* through-ring coupling reactions will be explored, enabling investigation of reaction mechanisms.

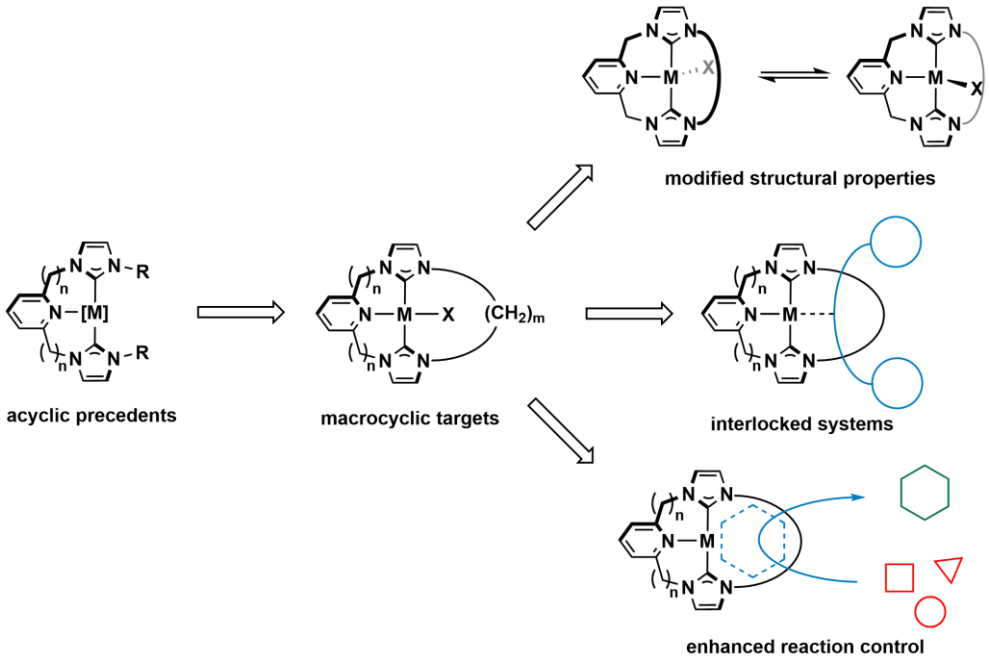

Scheme 1.14: *Schematic of aims and objectives.*

1.6 References

(1) Fevre, M.; Pinaud, J.; Gnanou, Y.; Vignolle, J.; Taton, D. *Chem. Soc. Rev.* **2013**, *42*, 2142-2172.
(2) Glorius, F. In *N-Heterocyclic Carbenes in Transition Metal Catalysis*; Springer Berlin Heidelberg: 2007; Vol. 21, p 1-20.
(3) Segarra, C.; Mas-Marzá, E.; Mata, J. A.; Peris, E. *Organometallics* **2012**, *31*, 5169-5176.
(4) Aznarez, F.; Sanz Miguel, P. J.; Tan, T. T. Y.; Hahn, F. E. *Organometallics* **2016**, *35*, 410-419.
(5) Arduengo, A. J.; Harlow, R. L.; Kline, M. *J. Am. Chem. Soc.* **1991**, *113*, 361-363.
(6) Herrmann, W. A. *Angew. Chem. Int. Ed.* **2002**, *41*, 1290-1309.
(7) Nelson, D. J. *Eur. J. Inorg. Chem.* **2015**, *2015*, 2012-2027.
(8) Gusev, D. G. *Organometallics* **2009**, *28*, 6458-6461.
(9) Scott, N. M.; Nolan, S. P. *Eur. J. Inorg. Chem.* **2005**, *2005*, 1815-1828.
(10) Furst, M. R. L.; Cazin, C. S. J. *Chem. Commun.* **2010**, *46*, 6924-6925.
(11) Poater, A.; Cosenza, B.; Correa, A.; Giudice, S.; Ragone, F.; Scarano, V.; Cavallo, L. *Eur. J. Inorg. Chem.* **2009**, *2009*, 1759-1766.
(12) Liske, A.; Verlinden, K.; Buhl, H.; Schaper, K.; Ganter, C. *Organometallics* **2013**, *32*, 5269-5272.
(13) Alcarazo, M.; Stork, T.; Anoop, A.; Thiel, W.; Fürstner, A. *Angew. Chem. Int. Ed.* **2010**, *49*, 2542-2546.
(14) Nelson, D. J.; Nolan, S. P. *Chem. Soc. Rev.* **2013**, *42*, 6723-6753.
(15) de Frémont, P.; Marion, N.; Nolan, S. P. *Coord. Chem. Rev.* **2009**, *253*, 862-892.
(16) Marchione, D.; Belpassi, L.; Bistoni, G.; Macchioni, A.; Tarantelli, F.; Zuccaccia, D. *Organometallics* **2014**, *33*, 4200-4208.
(17) Dorta, R.; Stevens, E. D.; Scott, N. M.; Costabile, C.; Cavallo, L.; Hoff, C. D.; Nolan, S. P. *J. Am. Chem. Soc.* **2005**, *127*, 2485-2495.
(18) Chianese, A. R.; Kovacevic, A.; Zeglis, B. M.; Faller, J. W.; Crabtree, R. H. *Organometallics* **2004**, *23*, 2461-2468.
(19) Chianese, A. R.; Li, X.; Janzen, M. C.; Faller, J. W.; Crabtree, R. H. *Organometallics* **2003**, *22*, 1663-1667.
(20) Ohki, Y.; Aoyagi, K.; Seino, H. *Organometallics* **2015**, *34*, 3414-3420.
(21) Lee, M.-T.; Hu, C.-H. *Organometallics* **2004**, *23*, 976-983.
(22) Khalili Najafabadi, B.; Corrigan, J. F. *Dalton Trans.* **2015**, *44*, 14235-14241.
(23) Radius, U.; Bickelhaupt, F. M. *Coord. Chem. Rev.* **2009**, *253*, 678-686.
(24) Luy, J.-N.; Hauser, S. A.; Chaplin, A. B.; Tonner, R. *Organometallics* **2015**, *34*, 5099-5112.
(25) de Frémont, P.; Scott, N. M.; Stevens, E. D.; Nolan, S. P. *Organometallics* **2005**, *24*, 2411-2418.
(26) Azzopardi, K. M.; Bistoni, G.; Ciancaleoni, G.; Tarantelli, F.; Zuccaccia, D.; Belpassi, L. *Dalton Trans.* **2015**, *44*, 13999-14007.
(27) Back, O.; Henry-Ellinger, M.; Martin, C. D.; Martin, D.; Bertrand, G. *Angew. Chem. Int. Ed.* **2013**, *52*, 2939-2943.
(28) Rodrigues, R. R.; Dorsey, C. L.; Arceneaux, C. A.; Hudnall, T. W. *Chem. Commun.* **2014**, *50*, 162-164.
(29) Paul, U. S. D.; Sieck, C.; Haehnel, M.; Hammond, K.; Marder, T. B.; Radius, U. *Chem. Eur. J.* **2016**,*22*, 11005-11014.
(30) Tretiakov, M.; Shermolovich, Y. G.; Singh, A. P.; Samuel, P. P.; Roesky, H. W.; Niepotter, B.; Visscher, A.; Stalke, D. *Dalton Trans.* **2013**, *42*, 12940-12946.
(31) Herrmann, W. A.; Elison, M.; Fischer, J.; Köcher, C.; Artus, G. R. J. *Angew. Chem. Int. Ed.* **1995**, *34*, 2371-2374.
(32) Hartung, J.; Dornan, P. K.; Grubbs, R. H. *J. Am. Chem. Soc.* **2014**, *136*, 13029-13037.
(33) Wu, C.-Y.; Horibe, T.; Jacobsen, C. B.; Toste, F. D. *Nature* **2015**, *517*, 449-454.

(34) Shan, S. P.; Xiaoke, X.; Gnanaprakasam, B.; Dang, T. T.; Ramalingam, B.; Huynh, H. V.; Seayad, A. M. *RSC Advances* **2015**, *5*, 4434-4442.
(35) Diez-Gonzalez, S.; Escudero-Adan, E. C.; Benet-Buchholz, J.; Stevens, E. D.; Slawin, A. M. Z.; Nolan, S. P. *Dalton Trans.* **2010**, *39*, 7595-7606.
(36) Teci, M.; Brenner, E.; Matt, D.; Toupet, L. *Eur. J. Inorg. Chem.* **2013**, *2013*, 2841-2848.
(37) O'Brien, C. J.; Kantchev, E. A. B.; Valente, C.; Hadei, N.; Chass, G. A.; Lough, A.; Hopkinson, A. C.; Organ, M. G. *Chem. Eur. J.* **2006**, *12*, 4743-4748.
(38) Van Veldhuizen, J. J.; Campbell, J. E.; Giudici, R. E.; Hoveyda, A. H. *J. Am. Chem. Soc.* **2005**, *127*, 6877-6882.
(39) Kremzow, D.; Seidel, G.; Lehmann, C. W.; Fürstner, A. *Chem. Eur. J.* **2005**, *11*, 1833-1853.
(40) Mayr, M.; Wurst, K.; Ongania, K.-H.; Buchmeiser, M. R. *Chem. Eur. J.* **2004**, *10*, 1256-1266.
(41) Scarborough, C. C.; Grady, M. J. W.; Guzei, I. A.; Gandhi, B. A.; Bunel, E. E.; Stahl, S. S. *Angew. Chem. Int. Ed.* **2005**, *44*, 5269-5272.
(42) Binobaid, A.; Iglesias, M.; Beetstra, D. J.; Kariuki, B.; Dervisi, A.; Fallis, I. A.; Cavell, K. J. *Dalton Trans.* **2009**, 7099-7112.
(43) Tudose, A.; Demonceau, A.; Delaude, L. *J. Organomet. Chem.* **2006**, *691*, 5356-5365.
(44) Tapu, D.; McCarty, Z.; Hutchinson, L.; Ghattas, C.; Chowdhury, M.; Salerno, J.; VanDerveer, D. *J. Organomet. Chem.* **2014**, *749*, 134-141.
(45) Nelyubina, Y. V.; Gazieva, G. A.; Baranov, V. V.; Belyakov, P. A.; Chizhov, A. O.; Lyssenko, K. A.; Kravchenko, A. N. *Russ. Chem. Bull.* **2009**, *58*, 1353-1360.
(46) Hahn, F. E.; Le Van, D.; Paas, M.; Frohlich, R. *Dalton Trans.* **2006**, 860-864.
(47) Peris, E.; Crabtree, R. H. *Coord. Chem. Rev.* **2004**, *248*, 2239-2246.
(48) Poyatos, M.; Mata, J. A.; Falomir, E.; Crabtree, R. H.; Peris, E. *Organometallics* **2003**, *22*, 1110-1114.
(49) Chaplin, A. B. *Organometallics* **2014**, *33*, 624-626.
(50) Karamé, I.; Boualleg, M.; Camus, J.-M.; Maishal, T. K.; Alauzun, J.; Basset, J.-M.; Copéret, C.; Corriu, R. J. P.; Jeanneau, E.; Mehdi, A.; Reyé, C.; Veyre, L.; Thieuleux, C. *Chem. Eur. J.* **2009**, *15*, 11820-11823.
(51) Chianese, A. R.; Bremer, P. T.; Wong, C.; Reynes, R. J. *Organometallics* **2009**, *28*, 5244-5252.
(52) Savka, R.; Plenio, H. *Dalton Trans.* **2015**, *44*, 891-893.
(53) Hohloch, S.; Deibel, N.; Schweinfurth, D.; Frey, W.; Sarkar, B. *Eur. J. Inorg. Chem.* **2014**, *2014*, 2131-2139.
(54) Citadelle, C. A.; Nouy, E. L.; Bisaro, F.; Slawin, A. M. Z.; Cazin, C. S. J. *Dalton Trans.* **2010**, *39*, 4489-4491.
(55) Trnka, T. M.; Grubbs, R. H. *Acc. Chem. Res.* **2001**, *34*, 18-29.
(56) McGuinness, D. S.; Cavell, K. J.; Skelton, B. W.; White, A. H. *Organometallics* **1999**, *18*, 1596-1605.
(57) Collins, L. R.; Hierlmeier, G.; Mahon, M. F.; Riddlestone, I. M.; Whittlesey, M. K. *Chem. Eur. J.* **2015**, *21*, 3215-3218.
(58) Scott, N. M.; Dorta, R.; Stevens, E. D.; Correa, A.; Cavallo, L.; Nolan, S. P. *J. Am. Chem. Soc.* **2005**, *127*, 3516-3526.
(59) Häller, L. J. L.; Page, M. J.; Erhardt, S.; Macgregor, S. A.; Mahon, M. F.; Naser, M. A.; Vélez, A.; Whittlesey, M. K. *J. Am. Chem. Soc.* **2010**, *132*, 18408-18416.
(60) Burling, S.; Mahon, M. F.; Powell, R. E.; Whittlesey, M. K.; Williams, J. M. J. *J. Am. Chem. Soc.* **2006**, *128*, 13702-13703.
(61) Caddick, S.; Cloke, F. G. N.; Hitchcock, P. B.; de K. Lewis, A. K. *Angew. Chem. Int. Ed.* **2004**, *43*, 5824-5827.
(62) Dutton, J. L.; Wilson, D. J.; Iversen, K. J. *Dalton Trans.* **2014**, *43*, 12820-12823.
(63) Waltman, A. W.; Ritter, T.; Grubbs, R. H. *Organometallics* **2006**, *25*, 4238-4239.

(64) Bose, S. K.; Fucke, K.; Liu, L.; Steel, P. G.; Marder, T. B. *Angew. Chem. Int. Ed.* **2014**, *53*, 1799-1803.
(65) Albrecht, M.; Lindner, M. M. *Dalton Trans.* **2011**, *40*, 8733-8744.
(66) Selander, N.; J. Szabó, K. *Chem. Rev.* **2011**, *111*, 2048-2076.
(67) Gunanathan, C.; Milstein, D. *Chem. Rev.* **2014**, *114*, 12024-12087.
(68) Zhang, J.; Gandelman, M.; Shimon, L. J. W.; Rozenberg, H.; Milstein, D. *Organometallics* **2004**, *23*, 4026-4033.
(69) Ahuja, R.; Punji, B.; Findlater, M.; Supplee, C.; Schinski, W.; Brookhart, M.; Goldman, A. S. *Nat. Chem.* **2011**, *3*, 167-171.
(70) Bedford, R. B.; Draper, S. M.; Noelle Scully, P.; Welch, S. L. *New J. Chem.* **2000**, *24*, 745-747.
(71) Pugh, D.; Danopoulos, A. A. *Coord. Chem. Rev.* **2007**, *251*, 610-641.
(72) Chen, C.; Qiu, H.; Chen, W. *J. Organomet. Chem.* **2012**, *696*, 4166-4172.
(73) Plikhta, A.; Pöthig, A.; Herdtweck, E.; Rieger, B. *Inorg. Chem.* **2015**, *54*, 9517-9528.
(74) Schneider, N.; César, V.; Bellemin-Laponnaz, S.; Gade, L. H. *Organometallics* **2005**, *24*, 4886-4888.
(75) Spencer, L. P.; Fryzuk, M. D. *J. Organomet. Chem.* **2005**, *690*, 5788-5803.
(76) Filonenko, G. A.; Cosimi, E.; Lefort, L.; Conley, M. P.; Copéret, C.; Lutz, M.; Hensen, E. J. M.; Pidko, E. A. *ACS Catal.* **2014**, *4*, 2667-2671.
(77) del Pozo, C.; Iglesias, M.; Sánchez, F. l. *Organometallics* **2011**, *30*, 2180-2188.
(78) Miecznikowski, J. R.; Grundemann, S.; Albrecht, M.; Megret, C.; Clot, E.; Faller, J. W.; Eisenstein, O.; Crabtree, R. H. *Dalton Trans.* **2003**, 831-838.
(79) Hahn, F. E.; Jahnke, M. C.; Pape, T. *Organometallics* **2007**, *26*, 150-154.
(80) Gründemann, S.; Albrecht, M.; Loch, J. A.; Faller, J. W.; Crabtree, R. H. *Organometallics* **2001**, *20*, 5485-5488.
(81) Moser, M.; Wucher, B.; Kunz, D.; Rominger, F. *Organometallics* **2007**, *26*, 1024-1030.
(82) Ghotbinejad, M.; Khosropour, A. R.; Mohammadpoor-Baltork, I.; Moghadam, M.; Tangestaninejad, S.; Mirkhani, V. *J. Mol. Catal. A: Chem.* **2014**, *385*, 78-84.
(83) Rubio, R. J.; Andavan, G. T. S.; Bauer, E. B.; Hollis, T. K.; Cho, J.; Tham, F. S.; Donnadieu, B. *J. Organomet. Chem.* **2005**, *690*, 5353-5364.
(84) Zuo, W.; Braunstein, P. *Organometallics* **2012**, *31*, 2606-2615.
(85) Tu, T.; Malineni, J.; Bao, X.; Doetz, K. H. *Adv. Synth. Catal.* **2009**, *351*, 1029-1034.
(86) Helgert, T. R.; Hollis, T. K.; Oliver, A. G.; Valle, H. U.; Wu, Y.; Webster, C. E. *Organometallics* **2014**, *33*, 952-958.
(87) Yoshida, K.; Horiuchi, S.; Takeichi, T.; Shida, H.; Imamoto, T.; Yanagisawa, A. *Org. Lett.* **2010**, *12*, 1764-1767.
(88) Naziruddin, A. R.; Kuo, C.-L.; Lin, W.-J.; Lo, W.-H.; Lee, C.-S.; Sun, B.-J.; Chang, A. H. H.; Hwang, W.-S. *Organometallics* **2014**, *33*, 2575-2582.
(89) Pugh, D.; Boyle, A.; Danopoulos, A. A. *Dalton Trans.* **2008**, 1087-1094.
(90) Cross, W. B.; Daly, C. G.; Ackerman, R. L.; George, I. R.; Singh, K. *Dalton Trans.* **2011**, *40*, 495-505.
(91) Poyatos, M.; Mas-Marzá, E.; Mata, José A.; Sanaú, M.; Peris, E. *Eur. J. Inorg. Chem.* **2003**, *2003*, 1215-1221.
(92) Danopoulos, A. A.; Tsoureas, N.; Wright, J. A.; Light, M. E. *Organometallics* **2004**, *23*, 166-168.
(93) Nielsen, D. J.; Cavell, K. J.; Skelton, B. W.; White, A. H. *Inorg. Chim. Acta* **2002**, *327*, 116-125.
(94) Nielsen, D. J.; Magill, A. M.; Yates, B. F.; Cavell, K. J.; Skelton, B. W.; White, A. H. *Chem. Commun.* **2002**, 2500-2501.
(95) Nielsen, D. J.; Cavell, K. J.; Skelton, B. W.; White, A. H. *Inorg. Chim. Acta* **2006**, *359*, 1855-1869.

(96) Biffis, A.; Cipani, M.; Tubaro, C.; Basato, M.; Costante, M.; Bressan, E.; Venzo, A.; Graiff, C. *New J. Chem.* **2013**, *37*, 4176-4184.
(97) Radloff, C.; Gong, H.-Y.; Schulte to Brinke, C.; Pape, T.; Lynch, V. M.; Sessler, J. L.; Hahn, F. E. *Chem. Eur. J.* **2010**, *16*, 13077-13081.
(98) Morgan, B. P.; Galdamez, G. A.; Gilliard, J. R. J.; Smith, R. C. *Dalton Trans.* **2009**, 2020-2028.
(99) Schultz, K. M.; Goldberg, K. I.; Gusev, D. G.; Heinekey, D. M. *Organometallics* **2011**, *30*, 1429-1437.
(100) Chianese, A. R.; Drance, M. J.; Jensen, K. H.; McCollom, S. P.; Yusufova, N.; Shaner, S. E.; Shopov, D. Y.; Tendler, J. A. *Organometallics* **2014**, *33*, 457-464.
(101) Liu, X.; Braunstein, P. *Inorg. Chem.* **2013**, *52*, 7367-7369.
(102) Naziruddin, A. R.; Huang, Z.-J.; Lai, W.-C.; Lin, W.-J.; Hwang, W.-S. *Dalton Trans.* **2013**, *42*, 13161-13171.
(103) Chianese, A. R.; Mo, A.; Lampland, N. L.; Swartz, R. L.; Bremer, P. T. *Organometallics* **2010**, *29*, 3019-3026.
(104) Rubio, R. J.; Andavan, G. T. S.; Bauer, E. B.; Hollis, T. K.; Cho, J.; Tham, F. S.; Donnadieu, B. *J. Organomet. Chem.* **2005**, *690*, 5353-5364.
(105) Bauer, E. B.; Andavan, G. T. S.; Hollis, T. K.; Rubio, R. J.; Cho, J.; Kuchenbeiser, G. R.; Helgert, T. R.; Letko, C. S.; Tham, F. S. *Org. Lett.* **2008**, *10*, 1175-1178.
(106) Zhang, X.; Wright, A. M.; DeYonker, N. J.; Hollis, T. K.; Hammer, N. I.; Webster, C. E.; Valente, E. J. *Organometallics* **2012**, *31*, 1664-1672.
(107) Gunanathan, C.; Milstein, D. *Acc. Chem. Res.* **2011**, *44*, 588-602.
(108) Gunanathan, C.; Milstein, D. *Science* **2013**, *341*, 1229712.
(109) Hahn, C.; Spiegler, M.; Herdtweck, E.; Taube, R. *Eur. J. Inorg. Chem.* **1999**, *1999*, 435-440.
(110) Zhang, J.; Leitus, G.; Ben-David, Y.; Milstein, D. *Angew. Chem. Int. Ed.* **2006**, *45*, 1113-1115.
(111) Filonenko, G. A.; Smykowski, D.; Szyja, B. M.; Li, G.; Szczygiel, J.; Hensen, E. J. M.; Pidko, E. A. *ACS Catal.* **2015**, *5*, 1145-1154.
(112) Filonenko, G. A.; Aguila, M. J. B.; Schulpen, E. N.; van Putten, R.; Wiecko, J.; Müller, C.; Lefort, L.; Hensen, E. J. M.; Pidko, E. A. *J. Am. Chem. Soc.* **2015**, *137*, 7620-7623.
(113) Yu, R. P.; Darmon, J. M.; Hoyt, J. M.; Margulieux, G. W.; Turner, Z. R.; Chirik, P. J. *ACS Catal.* **2012**, *2*, 1760-1764.
(114) Yu, R. P.; Darmon, J. M.; Milsmann, C.; Margulieux, G. W.; Stieber, S. C. E.; DeBeer, S.; Chirik, P. J. *J. Am. Chem. Soc.* **2013**, *135*, 13168-13184.
(115) Pugh, D.; Wells, N. J.; Evans, D. J.; Danopoulos, A. A. *Dalton Trans.* **2009**, 7189-7195.
(116) Poyatos, M.; Mas-Marza, E.; Mata, J. A.; Sanau, M.; Peris, E. *Eur. J. Inorg. Chem.* **2003**, *2003*, 1215-1221.
(117) Andavan, G. T. S.; Bauer, E. B.; Letko, C. S.; Hollis, T. K.; Tham, F. S. *J. Organomet. Chem.* **2005**, *690*, 5938-5947.
(118) Krueger, A.; Albrecht, M. *Chem. Eur. J.* **2012**, *18*, 652-658.
(119) Houghton, J.; Dyson, G.; Douthwaite, R. E.; Whitwood, A. C.; Kariuki, B. M. *Dalton Trans.* **2007**, 3065-3073.
(120) Cho, J.; Hollis, T. K.; Helgert, T. R.; Valente, E. J. *Chem. Commun.* **2008**, 5001-5003.
(121) Cho, J.; Hollis, T. K.; Valente, E. J.; Trate, J. M. *J. Organomet. Chem.* **2010**, *696*, 373-377.
(122) Helgert, T. R.; Hollis, T. K.; Valente, E. J. *Organometallics* **2012**, *31*, 3002-3009.
(123) Clark, W. D.; Cho, J.; Valle, H. U.; Hollis, T. K.; Valente, E. J. *J. Organomet. Chem.* **2014**, *751*, 534-540.
(124) Cao, P.; Cabrera, J.; Padilla, R.; Serra, D.; Rominger, F.; Limbach, M. *Organometallics* **2012**, *31*, 921-929.
(125) Serra, D.; Cao, P.; Cabrera, J.; Padilla, R.; Rominger, F.; Limbach, M. *Organometallics* **2011**, *30*, 1885-1895.
(126) Peris, E.; Loch, J. A.; Mata, J.; Crabtree, R. H. *Chem. Commun.* **2001**, 201-202.

(127) Inamoto, K.; Kuroda, J.-i.; Sakamoto, T.; Hiroya, K. *Synthesis* **2007**, 2853-2861.
(128) Inamoto, K.; Kuroda, J.-i.; Kwon, E.; Hiroya, K.; Doi, T. *J. Organomet. Chem.* **2009**, *694*, 389-396.
(129) Inamoto, K.; Kuroda, J.-i.; Hiroya, K.; Noda, Y.; Watanabe, M.; Sakamoto, T. *Organometallics* **2006**, *25*, 3095-3098.
(130) Tu, T.; Mao, H.; Herbert, C.; Xu, M.; Doetz, K. H. *Chem. Commun.* **2010**, *46*, 7796-7798.
(131) Xu, M.; Li, X.; Sun, Z.; Tu, T. *Chem. Commun.* **2013**, *49*, 11539-11541.
(132) MaGee, K. D. M.; Travers, G.; Skelton, B. W.; Massi, M.; Payne, A. D.; Brown, D. H. *Aust. J. Chem.* **2012**, *65*, 823-833.
(133) Brown, D. H.; Skelton, B. W. *Dalton Trans.* **2011**, *40*, 8849-8858.
(134) Kuroda, J.-i.; Inamoto, K.; Hiroya, K.; Doi, T. *Eur. J. Org. Chem.* **2009**, *2009*, 2251-2261.
(135) McGuinness, D. S.; Suttil, J. A.; Gardiner, M. G.; Davies, N. W. *Organometallics* **2008**, *27*, 4238-4247.
(136) McGuinness, D. S.; Gibson, V. C.; Steed, J. W. *Organometallics* **2004**, *23*, 6288-6292.
(137) McGuinness, D. S.; Gibson, V. C.; Wass, D. F.; Steed, J. W. *J. Am. Chem. Soc.* **2003**, *125*, 12716-12717.
(138) Wong, C.-Y.; Lai, L.-M.; Pat, P.-K.; Chung, L.-H. *Organometallics* **2010**, *29*, 2533-2539.
(139) Zhang, Y.-M.; Shao, J.-Y.; Yao, C.-J.; Zhong, Y.-W. *Dalton Trans.* **2012**, *41*, 9280-9282.
(140) Chung, L.-H.; Cho, K.-S.; England, J.; Chan, S.-C.; Wieghardt, K.; Wong, C.-Y. *Inorg. Chem.* **2013**, *52*, 9885-9896.
(141) Duchanois, T.; Etienne, T.; Beley, M.; Assfeld, X.; Perpete, E. A.; Monari, A.; Gros, P. C. *Eur. J. Inorg. Chem.* **2014**, *2014*, 3747-3753.
(142) Schulze, B.; Escudero, D.; Friebe, C.; Siebert, R.; Görls, H.; Köhn, U.; Altuntas, E.; Baumgaertel, A.; Hager, M. D.; Winter, A.; Dietzek, B.; Popp, J.; González, L.; Schubert, U. S. *Chem. Eur. J.* **2011**, *17*, 5494-5498.
(143) Brown, D. G.; Sanguantrakun, N.; Schulze, B.; Schubert, U. S.; Berlinguette, C. P. *J. Am. Chem. Soc.* **2012**, *134*, 12354-12357.
(144) Brown, D. G.; Schauer, P. A.; Borau-Garcia, J.; Fancy, B. R.; Berlinguette, C. P. *J. Am. Chem. Soc.* **2013**, *135*, 1692-1695.
(145) Sinn, S.; Schulze, B.; Friebe, C.; Brown, D. G.; Jäger, M.; Altuntaş, E.; Kübel, J.; Guntner, O.; Berlinguette, C. P.; Dietzek, B.; Schubert, U. S. *Inorg. Chem.* **2014**, *53*, 2083-2095.
(146) Muhavini Wawire, C.; Jouvenot, D.; Loiseau, F.; Baudin, P.; Liatard, S.; Njenga, L.; Kamau, G. N.; Casida, M. E. *J. Photochem. Photobiol., A* **2013**, *276*, 8-15.
(147) Liu, Y.; Harlang, T.; Canton, S. E.; Chabera, P.; Suarez-Alcantara, K.; Fleckhaus, A.; Vithanage, D. A.; Goeransson, E.; Corani, A.; Lomoth, R.; Sundstroem, V.; Waernmark, K. *Chem. Commun.* **2013**, *49*, 6412-6414.
(148) Duchanois, T.; Etienne, T.; Cebrian, C.; Liu, L.; Monari, A.; Beley, M.; Assfeld, X.; Haacke, S.; Gros, P. C. *Eur. J. Inorg. Chem.* **2015**, *2015*, 2469-2477.
(149) Harlang, T. C. B.; Liu, Y.; Gordivska, O.; Fredin, L. A.; Ponseca Jr, C. S.; Huang, P.; Chábera, P.; Kjaer, K. S.; Mateos, H.; Uhlig, J.; Lomoth, R.; Wallenberg, R.; Styring, S.; Persson, P.; Sundström, V.; Wärnmark, K. *Nat. Chem.* **2015**, *7*, 883-889.
(150) Lee, C.-S.; Zhuang, R. R.; Sabiah, S.; Wang, J.-C.; Hwang, W.-S.; Lin, I. J. B. *Organometallics* **2011**, *30*, 3897-3900.
(151) Zhang, X.; Wright, A. M.; DeYonker, N. J.; Hollis, T. K.; Hammer, N. I.; Webster, C. E.; Valente, E. J. *Organometallics* **2012**, *31*, 1664-1672.
(152) Danopoulos, A. A.; Tsoureas, N.; Green, J. C.; Hursthouse, M. B. *Chem. Commun.* **2003**, 756-757.
(153) Hancock, R. D.; Martell, A. E. *Chem. Rev.* **1989**, *89*, 1875-1914.
(154) Comba, P. *Coord. Chem. Rev.* **1999**, *185–186*, 81-98.
(155) Mewis, R. E.; Archibald, S. J. *Coord. Chem. Rev.* **2010**, *254*, 1686-1712.
(156) Alexander, V. *Chem. Rev.* **1995**, *95*, 273-342.
(157) Lindoy, L. F.; Park, K.-M.; Lee, S. S. *Chem. Soc. Rev.* **2013**, *42*, 1713-1727.

(158) Korupoju, S. R.; Mangayarkarasi, N.; Zacharias, P. S.; Mizuthani, J.; Nishihara, H. *Inorg. Chem.* **2002**, *41*, 4099-4101.
(159) Parker, D.; Lehn, J.-M.; Rimmer, J. *J. Chem. Soc., Dalton Trans.* **1985**, 1517-1521.
(160) Helps, I. M.; Matthes, K. E.; Parker, D.; Ferguson, G. *J. Chem. Soc., Dalton Trans.* **1989**, 915-920.
(161) Carroy, A.; Lehn, J.-M. *J. Chem. Soc., Chem. Commun.* **1986**, 1232-1234.
(162) Zhang, X.; Huang, D.; Chen, Y.-S.; Holm, R. H. *Inorg. Chem.* **2012**, *51*, 11017-11029.
(163) Huang, D.; Holm, R. H. *J. Am. Chem. Soc.* **2010**, *132*, 4693-4701.
(164) Kita, M. R.; Miller, A. J. M. *J. Am. Chem. Soc.* **2014**, *136*, 14519-14529.
(165) Grajeda, J.; Kita, M. R.; Gregor, L. C.; White, P. S.; Miller, A. J. M. *Organometallics* **2016**, *35*, 306-316.
(166) Gao, J.; Reibenspies, J. H.; Martell, A. E. *Angew. Chem. Int. Ed.* **2003**, *42*, 6008-6012.
(167) Takeuchi, D.; Takano, S.; Takeuchi, Y.; Osakada, K. *Organometallics* **2014**, *33*, 5316-5323.
(168) Rodríguez, G.; Lutz, M.; Spek, A. L.; van Koten, G. *Chem. Eur. J.* **2002**, *8*, 45-57.
(169) Balzani, V.; Credi, A.; Raymo, F. M.; Stoddart, J. F. *Angew. Chem. Int. Ed.* **2000**, *39*, 3348-3391.
(170) Dietrich-Buchecker, C. O.; Sauvage, J. P.; Kintzinger, J. P. *Tetrahedron Lett.* **1983**, *24*, 5095-5098.
(171) Dietrich-Buchecker, C.; Sauvage, J.-P. *Tetrahedron* **1990**, *46*, 503-512.
(172) Ruwwe, J.; Martín-Alvarez, J. M.; Horn, C. R.; Bauer, E. B.; Szafert, S.; Lis, T.; Hampel, F.; Cagle, P. C.; Gladysz, J. A. *Chem. Eur. J.* **2001**, *7*, 3931-3950.
(173) Ayme, J.-F.; Beves, J. E.; Campbell, C. J.; Leigh, D. A. *Chem. Soc. Rev.* **2012**, *42*, 1700-1712.
(174) Siegel, J. S. *Science* **2012**, *338*, 752-753.
(175) Hahn, F. E.; Langenhahn, V.; Lügger, T.; Pape, T.; Le Van, D. *Angew. Chem. Int. Ed.* **2005**, *44*, 3759-3763.
(176) Hoekman, S.; Kitching, M. O.; Leigh, D. A.; Papmeyer, M.; Roke, D. *J. Am. Chem. Soc.* **2015**, *137*, 7656-7659.
(177) Goldup, S. M.; Leigh, D. A.; McBurney, R. T.; McGonigal, P. R.; Plant, A. *Chem. Sci.* **2010**, *1*, 383-386.
(178) Sato, Y.; Yamasaki, R.; Saito, S. *Angew. Chem. Int. Ed.* **2009**, *48*, 504-507.
(179) Goldup, S. M.; Leigh, D. A.; Long, T.; McGonigal, P. R.; Symes, M. D.; Wu, J. *J. Am. Chem. Soc.* **2009**, *131*, 15924-15929.
(180) Klawitter, I.; Anneser, M. R.; Dechert, S.; Meyer, S.; Demeshko, S.; Haslinger, S.; Poethig, A.; Kuehn, F. E.; Meyer, F. *Organometallics* **2015**, *34*, 2819-2825.
(181) Kawano, K.; Yamauchi, K.; Sakai, K. *Chem. Commun.* **2014**, *50*, 9872-9875.
(182) Baker, M. V.; Skelton, B. W.; White, A. H.; Williams, C. C. *Organometallics* **2002**, *21*, 2674-2678.
(183) Lu, Z.; Cramer, S. A.; Jenkins, D. M. *Chem. Sci.* **2012**, *3*, 3081-3087.
(184) Edwards, P. G.; Hahn, F. E. *Dalton Trans.* **2011**, *40*, 10278-10288.
(185) Hahn, F. E.; Radloff, C.; Pape, T.; Hepp, A. *Chem. Eur. J.* **2008**, *14*, 10900-10904.
(186) Biffis, A.; Cipani, M.; Bressan, E.; Tubaro, C.; Graiff, C.; Venzo, A. *Organometallics* **2014**, *33*, 2182-2188.
(187) Watarai, N.; Kawasaki, H.; Azumaya, I.; Yamasaki, R.; Saito, S. *Heterocycles* **2009**, *79*, 531-548.
(188) Meyer, K.; Dalebrook, A. F.; Wright, L. J. *Dalton Trans.* **2012**, *41*, 14059-14067.

CHAPTER 2. SYNTHESIS AND OPTIMISATION OF MACROCYCLE SIZE

This chapter describes the synthesis and study of NHC-based macrocyclic complexes of the form shown in **Fig. 2.1**. Synthetic methodology for accessing the necessary pro-ligands and their subsequent complexation to palladium is detailed. Following studies of the structural and dynamic properties of these species, the dodecamethylene spaced macrocycle (n = 12) is shown to be optimal for encapsulation of palladium and an ancillary ligand. Finally, methods of transmetallation to d^8 transition metals were explored using silver and copper coordination complexes of this macrocycle.

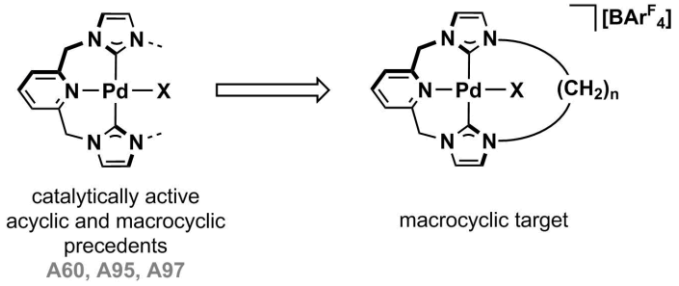

Fig. 2.1: *Target macrocyclic palladium complexes. X = Cl, F; n = 8, 10, 12.*

Publications resulting from work described in this chapter:

1. Andrew, R. E.; Chaplin, A. B. *Dalton Trans.* **2014**, *43*, 1413-1423.
2. Andrew, R. E.; Storey, C. M.; Chaplin, A. B. *Dalton Trans.* **2016**, *45*, 8937-8944

2.1 Pro-Ligand Synthesis

Adapting the methodology established for smaller macrocycles **A93** (**Chapter 1**, **Scheme 1.12**),[1] synthesis of macrocyclic pro-ligands containing octa-, deca- and dodecamethylene spacers was achieved by reaction between 2,6-bis(bromomethyl)pyridine and the corresponding bis-imidazoles (**1a-c**, obtained from bis-alkylation of dibromoalkanes)[2,3] to afford [**2a-c**].2HBr in moderate yields (19-23 %, **Scheme 2.1**). Despite precautions to limit oligomerisation of the starting materials, including high dilution and simultaneous dropwise addition of both reagents into hot solvent, recrystallisation was necessary to obtain the pro-ligands [**2**].2HBr analytically pure as hygroscopic white solids, which were subsequently stored and handled under an inert atmosphere.

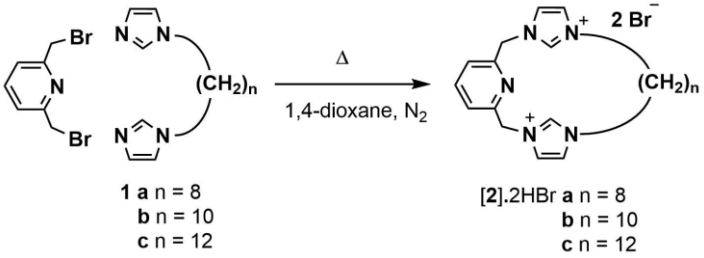

Scheme 2.1: *Synthesis of pro-ligands [**2**].2HBr.*

The new dibromide salts were fully characterised by NMR spectroscopy, mass spectrometry and elemental analysis. All three compounds display apparent C_{2v} symmetry by ^{1}H and ^{13}C NMR spectroscopy, with singlet signals for the acidic imidazolium proton in the range δ 10.5 – 10.9 and the corresponding ^{13}C signals between δ 137.6 and 138.5. ESI-HRMS spectra contain dominant dication peaks, $[M]^{2+}$ = 175.6207 (calc. 175.6206) *m/z*; 189.6361 (calc. 189.6362) *m/z* and 203.6521 (calc. 203.6519) *m/z*, with the expected half-integer isotope patterns, helping to corroborate their macrocyclic nature. Additionally, single crystals were obtained from the recrystallisation of decamethylene-spaced [**2b**].2HBr, aiding verification of its structure (**Fig. 2.2**).

Encouragingly, [**2b**].2HBr conforms roughly to one plane, suggesting a degree of flexibility not observed with the aforementioned smaller ring sizes of [**A93**].2HBr. Crystallographic analysis of the butylene-spaced pro-ligand (Y = $(CH_2)_2$, **Chapter 1**, **Scheme 1.12**) indicated a puckered ring, whereby the heterocyclic moieties are accommodated by folding of the alkyl chain. This results in a more restricted pro-ligand where the charged imidazolium rings are held closer together than in [**2b**].2HBr (C7···C11 = 4.110(4) Å, [**A93**].2HBr; *c.f.* 4.504(9) Å, [**2b**].2HBr). Although crystal packing effects cannot be ruled out in this case, such restricted space within the macrocycle presumably contributes to the inability of the ligand to coordinate palladium in the

tridentate fashion observed for acyclic congeners.[1] Hence, a less distorted ligand conformation may be indicative of a greater facility for metal complexation.

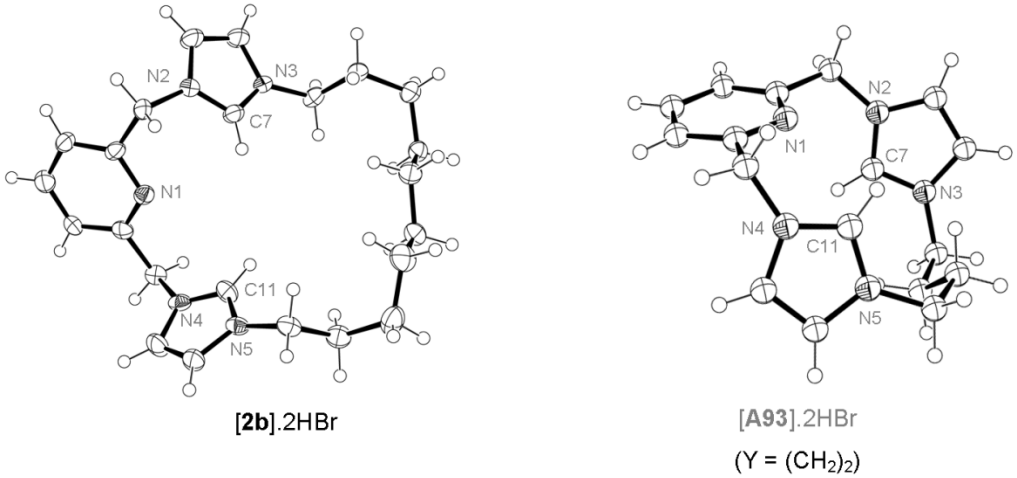

Fig. 2.2: *ORTEP representations of [**2b**].2HBr and [**A93**].2HBr for comparison.[1] Thermal ellipsoids at 50 % and counter anions omitted for clarity. Structure shown for [**2b**].2HBr is one of two independent molecules (Z' = 2).*

2.2 Palladium Halide Complexes

2.2.1 Synthesis and Characterisation of Palladium Chloride Complexes 3

Pro-ligands [**2**].2HBr were metallated at room temperature using a one-pot deprotonation-transmetallation procedure, similar to those employed by Cavell, Danopoulos and Youngs.[4-7] In particular, a variation of this method was used to access [Pd(C^N^C^{Me})Cl][BF_4], **A99**, the simplest acyclic congener of the target complexes.[7] Formation of the silver transfer agent *in-situ* using Ag_2O and Na[BAr^F_4] followed by addition of [$PdCl_2(NCPh)_2$] afforded air and moisture stable [Pd(**2**)Cl][BAr^F_4], **3**, after purification on silica (**Scheme 2.2**). Moderate yields of 31 %, 55 % and 58 % were obtained after recrystallisation for **3a** (n = 8), **3b** (n = 10) and **3c** (n = 12), respectively. Use of palladium(II) precursor [$PdCl_2(NCMe)_2$] provided near equivalent yields of **3**, but substitution of the counter-ion for $[BF_4]^-$ was detrimental to the yield and purity, as was the addition of Na[BAr^F_4] at a later stage in the reaction.

The weakly-coordinating $[BAr^F_4]^-$ anion was elected to mitigate effects of outer-sphere anion coordination,[8] which have been observed in acyclic systems,[9] and appears to aid solubility of the silver transfer agent in the reaction mixture (*vide infra*). Similarly, **3** demonstrate high solubility in a range of organic solvents, including Et_2O, $CHCl_3$ and MeCN.

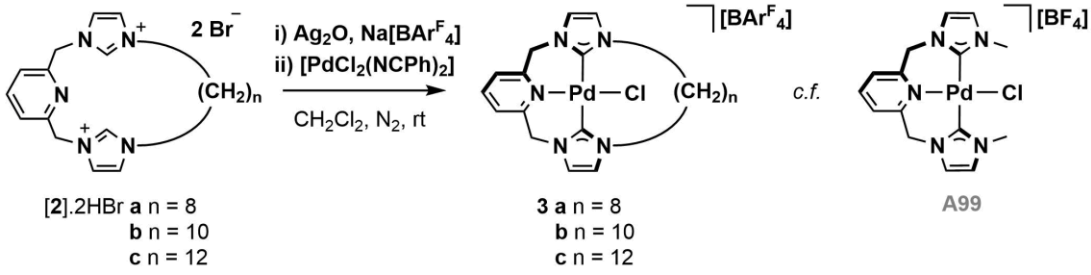

Scheme 2.2: *Synthesis of palladium chloride complexes **3**.*

Macrocyclic complexes **3** exhibit strong parent cation signals in their high-resolution mass spectra, with the $[M]^+$ ions at 490.0993 (calc. 490.0989) *m/z*, 518.1308 (calc. 518.1303) *m/z* and 546.1616 (calc. 546.1617) *m/z* displaying the expected isotope patterns. In all cases, elemental analyses are in good agreement with the general formula [Pd(**2**)Cl][BAr^F_4].

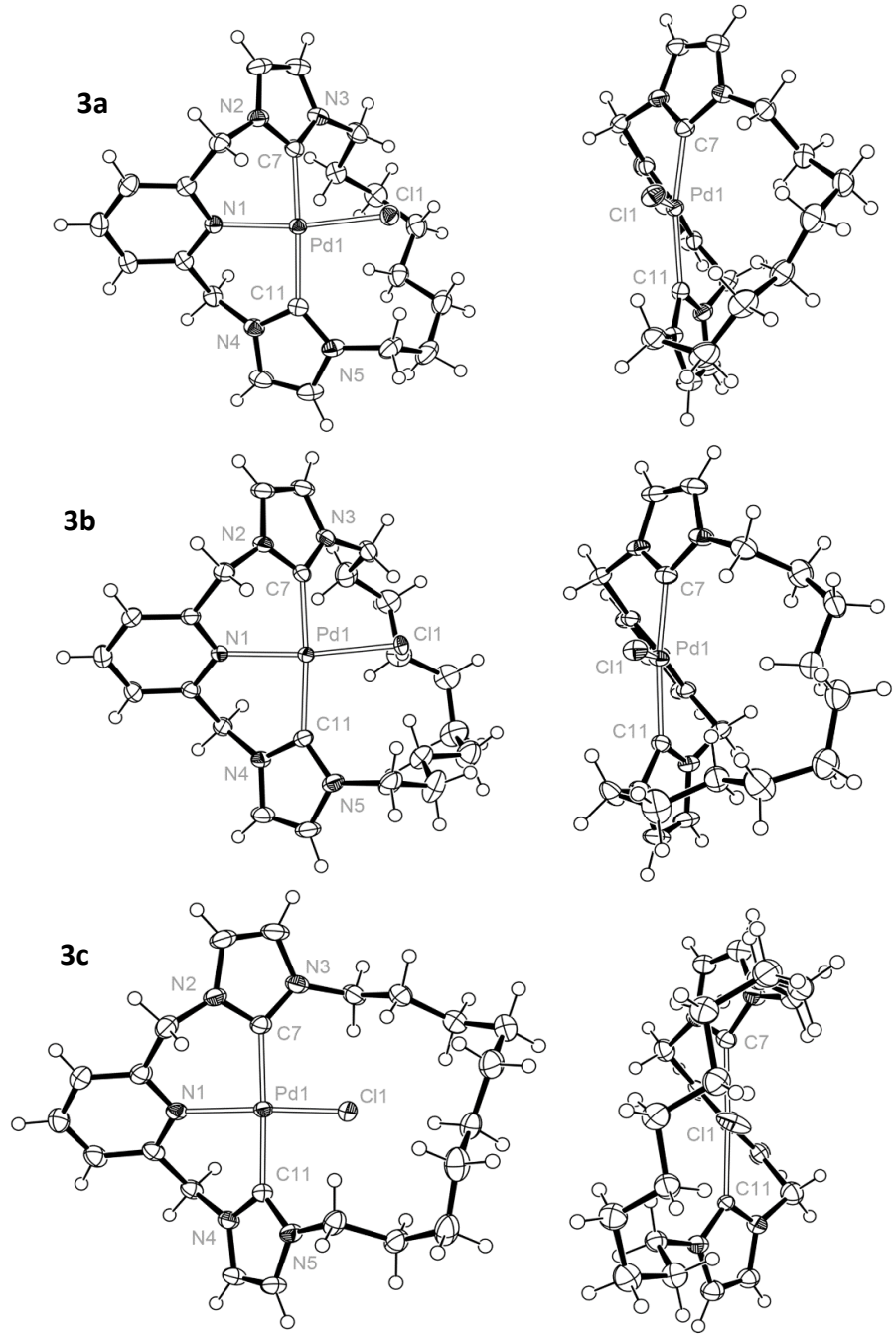

Fig. 2.3: *ORTEP representations of the crystal structures of **3a-c** with thermal ellipsoids at 50 % probability. Solvent molecules and $[BAr^{F}_{4}]^{-}$ counter anions omitted for clarity.*

Table 2.1: *Selected solid-state metrics and $^{13}C\{^{1}H\}$ NMR data for **3a-c** and **A99**, for comparison.*

	3a	**3b**	**3c**	***A99***
δ_{NCN}	162.4	163.3	164.5	*164.4*
Pd-N /Å	2.087(2)	2.080(2)	2.077(10)	*2.068(1)*
Pd-Cl /Å	2.3051(5)	2.3217(5)	2.287(4)	*2.2978(5)*
Pd-C_{NCN} / Å	1.983(2), 2.073(2)	2.004(2), 2.078(2)	2.056(13), 2.036(12)	*2.026(2), 2.029(2)*
N-Pd-Cl /°	163.39(4)	166.29(5)	176.2(3)	*178.19(3)*
C_{NCN}-Pd-C_{NCN} /°	168.82(7)	171.93(8)	172.8(6)	*176.60(7)*

The solid-state structures of **3** have all been determined by single crystal XRD (**Fig. 2.3**). Each complex is four-coordinate square planar with **2** functioning as meridional donors. Metal-to-

pincer-ligand bond lengths are consistent with those of acyclic precedents (r_{PdN} *ca*. 2.1 Å; r_{PdCl} *ca*. 2.3 Å; r_{PdC} *ca*. 2.0 Å)[4,7,10,11] but the degree to which each complex adopts ideal square planar geometry has a strong dependence on the length of the alkyl spacer.

Smaller macrocycles (**2a**, n = 8; **2b**, n = 10) afford distorted metal centres due to their inability to encircle the chloride ligand. In order to sufficiently bind the metal in a meridonal fashion, the alkyl chains of these smaller macrocycles are displaced to one side and both the C_{NCN}-Pd-C_{NCN} and N-Pd-Cl connections are puckered out of the plane (N1-Pd1-Cl1 = 163.39(4)° for **3a**, 166.29(5)° for **3b**; C7-Pd1-C11 = 168.82(7)° for **3a**, 171.93(8)° for **3b**). Such distortions from planarity in palladium(II) complexes are relatively rare; near-linear bond angles are reported for **A99**[7] and angles approaching 180° are still observed for acyclic Pd(C^N^C) complexes with bulky aryl substituents on the *N*-termini.[11]

Extreme contractions of N-Pd-Cl bond angles have been observed in complexes where rigid ligand components are pointing directly into the coordination sphere, *i.e.* the Me-substituents in planar thiazole-based NNN complex **A100** reported by Bröring and Kleeberg (153.04(8)°, **Fig. 2.4**),[12] and the *para*-phenyl component of benziporphyrin species **A101** (150.0(1)°).[13] Although possessing a large degree of flexibility (*vide infra*), it would appear that the alkyl chains of the macrocycles exert sufficient steric hindrance on the chloride ligand to induce a similar structural distortion.

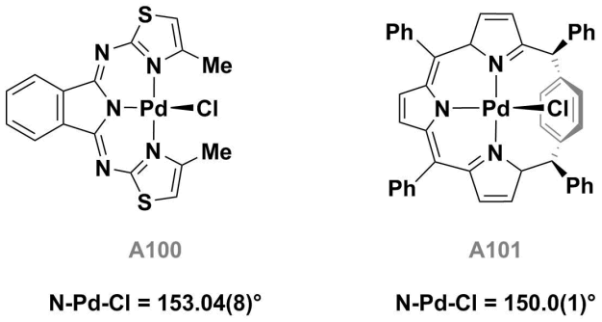

Fig. 2.4: *Pincer complexes of palladium with contracted N-Pd-Cl bond angles.*

In contrast with **2a** and **2b**, the larger ring of **2c** is better able to accommodate the ancillary ligand, and the complex has near-ideal square planar geometry (N1-Pd1-Cl1 = 176.2(3)°; C7-Pd1-C11 = 172.8(6)°) as well as a 'box-like' arrangement of the dodecamethylene linker, in which three sections of the alkyl chain adopt the classic staggered-conformation.

In solution, metallation of the pre-carbenic carbons of [**2**].2HBr to afford **3** is accompanied by a shift to higher frequency of *ca.* 25 ppm in the $^{13}C\{^1H\}$ NMR spectra ($CDCl_3$), resulting in singlets at around 163 ppm, similar to acyclic $[Pd(C^N^C^{Me})Cl]^+$ **A99** (δ 164).[4] Contrary to the observed distortion in the solid-state, but in-keeping with acyclic precedents, each complex displays C_2

symmetry in solution NMR spectra (CD_2Cl_2, 500 MHz, 298 K) with the methylene bridge protons diastereotopic. Separation of the corresponding doublets increases with spacer length ($\Delta\delta$ = 0.27 (**3a**, n = 8), 0.51 (**3b**, n = 10) and 0.60 (**3c**, n = 12)) and no broadening of these signals was observed on heating to 308 K.

Atropisomerisation *via* rearrangement of the pincer backbone conformation is indicated in [Pd(C^E^C^R)X]Y complexes (**A60**, **Fig. 2.5**) by coalescence of the diastereotopic methylene bridge protons, enabling investigation of this dynamic process by ^{1}H NMR spectroscopy.[9,14] Atropisomerism may be induced thermally or by coordination of an outer-sphere ion (*i.e.* Y) when lutidine is the central donor, to give intermediate **A102**. The mechanisms of these processes, and variants thereof, are discussed in greater detail in **Chapter 3**. Here it is sufficient to say that the absence of observable atropisomerism, up to 308 K, in **3** is consistent with the weakly coordinating nature of the [BAr$^F_4$]$^-$ counter anion, precluding formation of an intermediate such as **A102**.

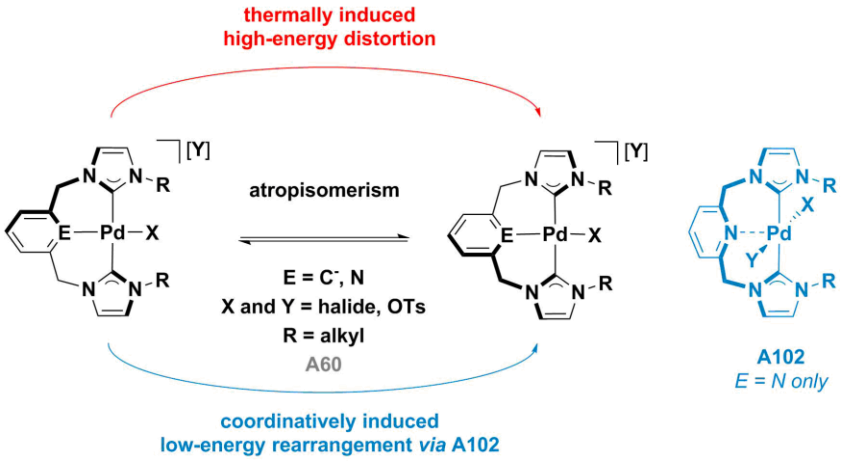

Fig. 2.5: *Atropisomerisation of acyclic **A60**.*

Cooling of the octa- and deca-methylene spaced complexes **3a** and **3b** from 298 to 185 K resulted in loss of C_2 symmetry. The decoalescence is most pronounced for complex **3a** and an asymmetric C_1 conformation, consistent with its crystal structure, was observed at low temperature (**Fig. 2.6**). Hence, the time-averaged C_2 symmetry observed at room temperature is consistent with interconversion between enantiomeric C_1 conformations, wherein the methylene linker is displaced to one side or the other. At 185 K, the previously equivalent *meta*-protons of the pyridine are represented by two doublets of doublets (b and b', **Fig. 2.6**), and four inequivalent doublets ($^3J_{HH}$ = 1.3 Hz) are observed for the imidazolylidene protons (c, c', d and d'). Using the latter resonances, it was possible to simulate and measure the rate of their exchange as they move between slow (185 K) and fast (298 K) exchange limits. Eyring analysis of the temperature dependence of these values afforded an activation barrier ($\Delta G^{\ddagger}_{298\ K}$) of 45 ± 9 kJ mol^{-1} ($\Delta H^{\ddagger}$ = 43 ± 4 kJ mol^{-1}, $\Delta S^{\ddagger}$ = - 7 ± 17 J mol^{-1} K^{-1}). These values are consistent

with estimations using the coalescence temperatures (T_c) and slow-exchange separations ($\Delta\nu$) of similarly paired signals in the spectra (**Eq. 2.1**),[15] which affords $\Delta G^{\ddagger}_{est}$ = 43.7, 45.1 and 46.4 kJ mol^{-1} for exchange of the *meta*-substituted protons of the pyridine and both *N*-methylene groups, respectively.

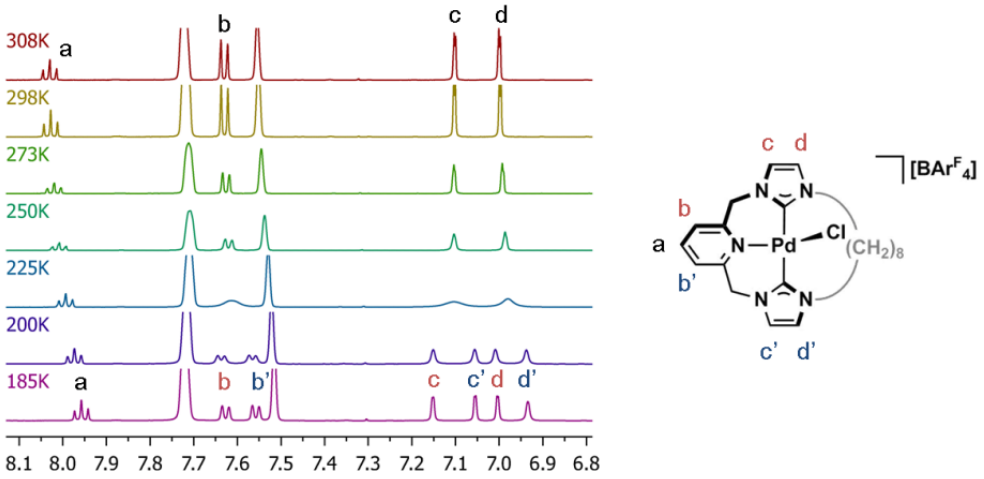

Fig. 2.6: *VT ^{1}H NMR spectra of **3a** depicting exchange of inequivalent protons of the pincer ligand. Protons x and x' in the C_1 structure are indicated for illustrative purposes only; the signals have not been unambiguously assigned.*

$$\Delta G^{\ddagger}_{est} = aT_c[9.972 + \log(T_c/\Delta\nu)] \quad \text{kJ mol}^{-1}$$

Eq. 2.1: *Where $a = 1.914 \times 10^{-2}$ kJ·mol^{-1}·T^{-1}, T_c is the coalescence temperature in Kelvin and $\Delta\nu$ is the peak separation (Hz) at the slow exchange limit.*

With a larger macrocyclic cavity and greater flexibility, the dodecamethylene-spaced **3c** has apparent C_2 symmetry across a wide temperature range; spectra remain unchanged from 200 – 298 K. Representing an intermediate regime, the majority of signals of **3b** are at coalescence at 185 K, but the slow exchange limit is not fully reached. Using **Eq 2.1** and an assumed $\Delta\nu$ of 62 Hz (that shown for c and c' in **3a**), the barrier was estimated at $\Delta G^{\ddagger}_{est}$ = 37 kJ mol^{-1}. This barrier to interconversion is significantly lower than that of complex **3a**, as expected from the reduced distortion observed in the solid-state structure of **3b**.

2.2.2 Synthesis and Characterisation of Palladium Fluoride Complexes 4

To further investigate the dynamic properties of complexes of **2**, palladium adducts with smaller ancillary ligands were targeted. Treatment of **3** with excess AgF in acetonitrile afforded palladium(II) fluoride complexes **4** in good to moderate yields (45 – 88 %) after filtration (**Scheme 2.3**).

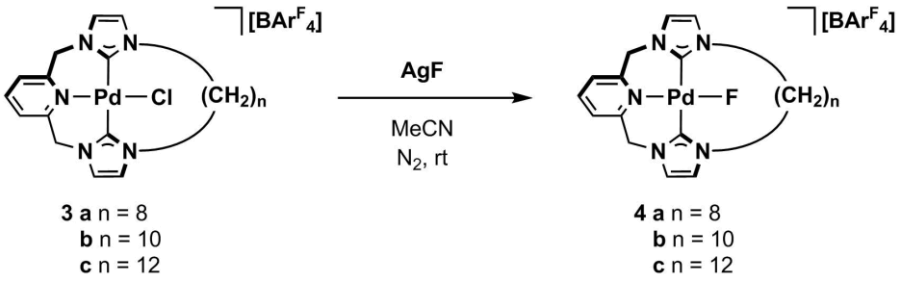

3 **a** n = 8
b n = 10
c n = 12

4 **a** n = 8
b n = 10
c n = 12

Scheme 2.3: *Synthesis of palladium fluoride complexes* ***4****.*

In contrast to chlorides **3**, fluorides **4** are markedly moisture-sensitive and readily decomposed on silica and in solution. Facile loss of the fluoride ligand is apparent by ESI-HRMS and only solvent adducts of [Pd(**2**)]$^{2+}$ were observed. Nevertheless, elemental analyses are in good agreement with the general formula [Pd(**2**)F][BAr$^F_4$]. ^{19}F NMR spectroscopy also provides clear evidence of the formation of **4,** with the fluoride ligands characterised by unusually low frequency signals at *ca.* -400 ppm. Although at the extreme end of the range of reported shifts for Pd-F complexes, such high shielding has precedent in a Pd(PNP)F complex reported by Ozerov *et al*, where the halide appears at -414 ppm.[16] Room temperature ^{1}H and ^{13}C{^{1}H} NMR spectra are generally similar to those of the chloride complexes, with resonances for the carbene carbons observed at 165 ppm (*c.f.* 163 ppm for **3**).

While the room temperature ^{1}H NMR spectra of **4b** and **4c** display apparent C_2 symmetry, enhanced dynamic behaviour and C_{2v} symmetry is observed for **4a** at 298 K – indicating both atropisomerism of the pincer backbone and dynamic movement of the alkyl chain. Cooling to 185 K resulted in decoalescence of both the imidazoylidene and the methylene signals in **4a**, but the slow exchange limit was not reached. Envisaging an atropisomerisation process proceeding by either outer-sphere coordination of excess F$^-$, or facile dissociation of F$^-$ in solution, analysis of the ^{1}H and ^{19}F{^{1}H} NMR spectra of **4a** in the presence of excess F$^-$ ([^{n}Bu$_4$NF].1.5(H$_2$O)) was attempted. Rapid degradation of the sample was observed by NMR spectroscopy, with disappearance of the ^{19}F NMR signal at -392.1 ppm and production of multiple species in the ^{1}H NMR spectrum. As previously noted, **4** are water-sensitive and in the absence of readily available anhydrous, non-coordinating sources of F$^-$,[17] further study of the dynamic properties of **4a** was not pursued.

Broad resonances are also observed for the *N*-CH$_2$ protons of the decamethylene chain in low temperature ^{1}H NMR spectra of **4b**, consistent with the exchange process detailed for its chloride analogue **3b**. Signals for the imidazoylidene backbone and methylene bridge protons remain reasonably sharp and indicate a lower barrier to interconversion, which is estimated using the diastereotopic *N*-C<u>H$_2$</u>CH$_2$ signals (employing **Eq. 2.1** and $\Delta\nu$ of 600 Hz from **3b**) at $\Delta G^{\ddagger}_{est}$ ≤ 37 kJ mol^{-1}. These observations indicate that reduction in the size of the ancillary

ligand results in lower activation barriers for the exchange of C_1 enantiomeric conformations, which further corroborates a mechanism involving movement of the methylene linker from one side of the metal coordination plane to the other. Consistent with the greater flexibility of the dodecamethylene spaced system, no change is observed in the ^{1}H NMR spectra of **4c** between 200 and 298 K.

Interestingly, long-range $^{2h}J_{FC}$ coupling is visible for the *N*-substituted and central carbons of the linker in **4a** to the tune of 13.6 and 6.4 Hz, respectively, at 298 K (**Fig. 2.7**). Consistent with the larger macrocyclic cavities employed, no coupling is observed for the central carbons of complexes **4b** and **4c**, and a reduced coupling of 6.3 Hz was measured for the terminal carbons of both linkers. The $^{2h}J_{FC}$ values found are consistent with C-H···F interactions reported in the literature,[18] however, no $^{1h}J_{FH}$-coupling is evident in the ^{1}H or ^{19}F NMR spectra. At 298 K, the relevant peaks of the proton spectra are sufficiently broadened (by fluxional processes and multiple inequivalent neighbours) to disguise the expected 1-2 Hz $^{1h}J_{FH}$-coupling. Similarly, H···F interactions could not be conclusively identified from the low temperature ^{1}H spectra.

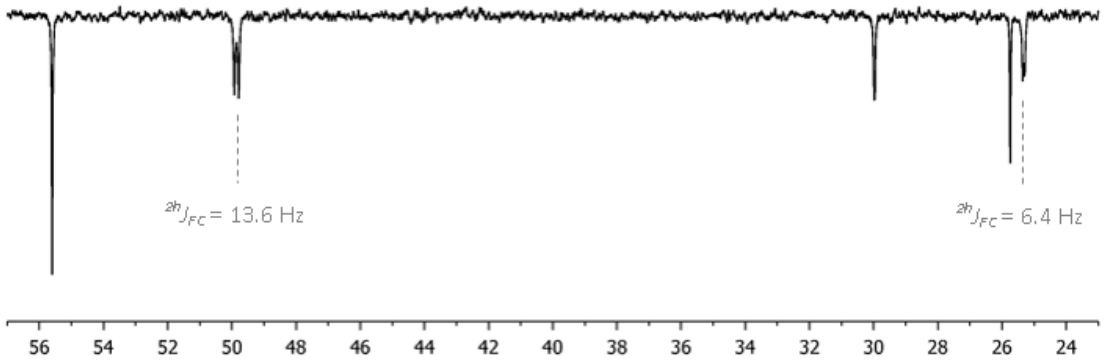

Fig. 2.7: *Alkyl region of $^{13}C\{^{1}H\}$ NMR spectrum of **4a** showing long range $^{2h}J_{FC}$ coupling ($CDCl_3$, 101 MHz, 298 K).*

Crystals suitable for XRD were obtained for **4a** and **4b** by slow diffusion of pentane into chloroform solutions. The coordination geometries of the octa- and deca-methylene spaced fluorides resemble those of **3b** (n = 10) and **3c** (n = 12) respectively, with the macrocycles **2a** and, particularly, **2b** experiencing reduced interaction with the smaller ancillary ligand. Like **3b**, **4a** has the alkyl chain significantly displaced to one side and a N-Pd-F bond angle of 171.12(8)° (*c.f.* N-Pd-Cl = 171.93(8)° (**3b**) and 168.82(7)° (**3a**)).

Supporting the observation of $^{2h}J_{FC}$ coupling, interatomic distances between the fluoride and protons of the terminal and central methylene groups of the alkyl spacer are between 2-3.5 Å, within the accepted hydrogen bonding range (sum of Van der Waals radii is 2.67 Å). Similar distances are observed for the terminal methylene protons in **4b** but the central portion of the linker is further removed from the halide. Crystals of **4c** could not be grown and this complex notably decomposes in chloroform solution to reform **3c**. However, retention of C_2 symmetry

from 298 – 185 K would suggest uninhibited movement of the spacer lateral to the coordination plane, as indicated for **3c**.

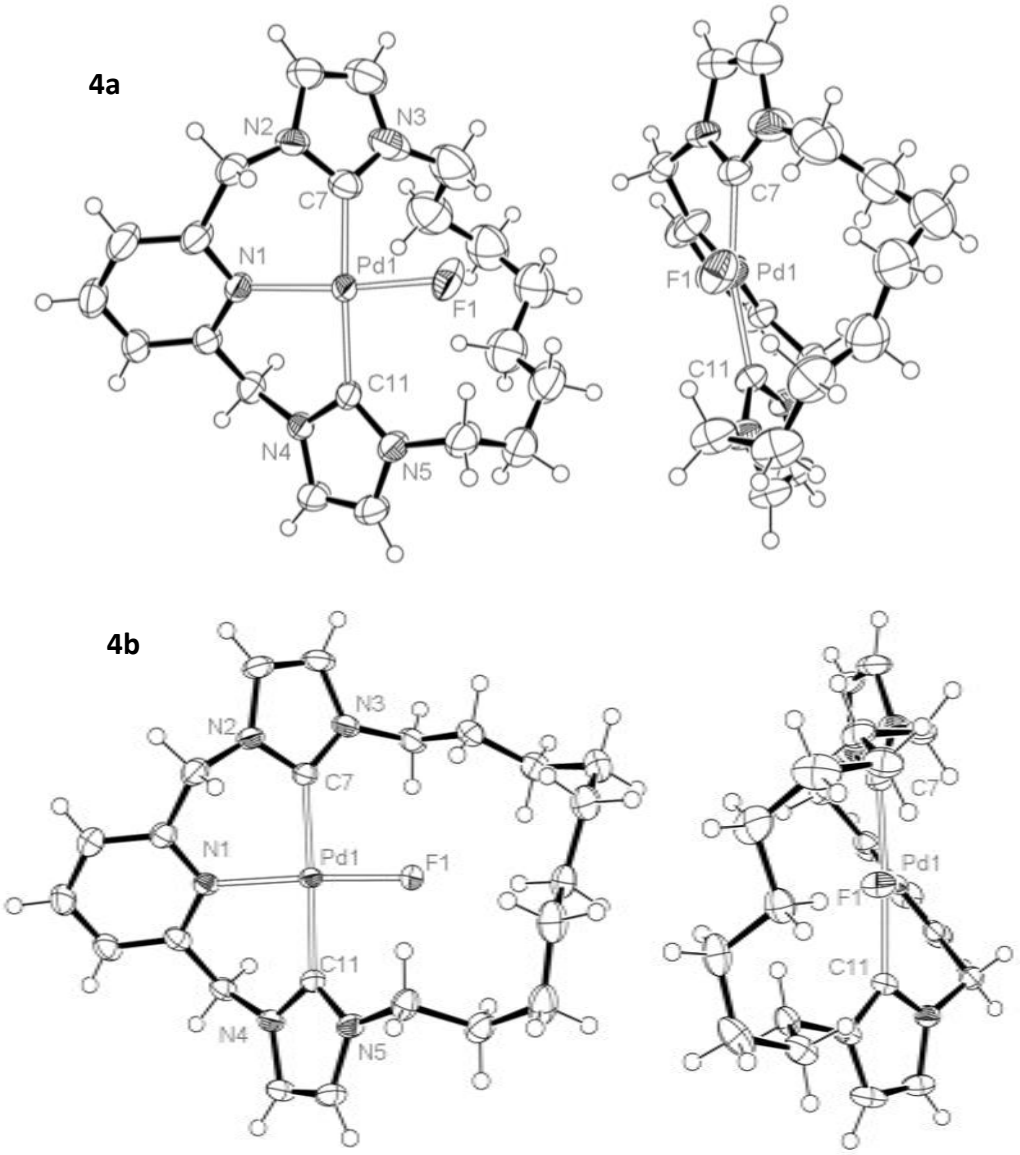

Fig. 2.8: *ORTEP representations of **4a** (**top**) and **4b** (**bottom**). Thermal ellipsoids at 50 % probability. $[BAr^{F}{}_{4}]^{-}$ counter anions, solvent and minor disordered components omitted for clarity. Structure shown for **4a** is one of two independent molecules (Z' = 2).*

Table 2.2: *Selected solid-state metrics and $^{13}C\{^{1}H\}$ and $^{19}F\{^{1}H\}$ NMR data for complexes **4a-c**.*

	4a	**4b**	**4c**
δ_{NCN} /ppm	164.8	165.0	164.7
δ_{F} /ppm	-392.08	-399.89	-399.91
Pd-N /Å	2.043(1)	2.035(2)	-
Pd-F /Å	2.011(2)	1.9588(13)	-
Pd-C_{NCN} /Å	2.008(3), 2.035(3)	2.018(2), 1.999(2)	-
N-Pd-F /°	171.12(8)	175.77(7)	-
C_{NCN}-Pd-C_{NCN} /°	170.3(1)	175.66(10)	-

2.2.3 Further Reactivity of Palladium Chloride Complexes 3

In order to further investigate the coordination chemistry of the palladium macrocycles, and the potential for binding hydrocarbon ligands through the ring, abstraction of chloride from **3** in the presence of an alkyne was attempted. Although both **3b** and **3c** undergo transmetallation with AgF, no reaction was apparent by ^{1}H NMR spectroscopy on stirring either complex in CH_2Cl_2 with an excess of Na[BAr^F_4] and 2-butyne for 48 hours. Potential explanations are that 2-butyne may not be sufficiently strong a donor, or the sodium cation not electrophilic enough to promote dissociation of the chloride ligand from an already cationic complex. In accordance with the latter, a mixture of **3c** and Na[BAr^F_4] showed no change in its ^{1}H NMR spectrum after 36 hours. Addition of Ag[BF_4] to this mixture and sonication resulted in the precipitation of metallic particulates and a complicated ^{1}H NMR spectrum was obtained. ^{19}F{^{1}H} NMR spectra also contained multiple signals around δ -60, rather than those expected for [BAr^F_4]$^-$ and [BF_4]$^-$. Both observations suggested decomposition involving the counter anions had taken place.

Acyclic and macrocyclic Pd(C^E^C) type complexes (such as **A103**, **Scheme 2.4**) have been reported to be effective catalysis for a range of reactions, particularly Mizoroki-Heck C-C couplings (**Section 1.2.3**).[19-21] Macrocyclic ligands have potential for enforcing a specific approach and coordination geometry of incoming reagents, thereby inducing selectivity. Bearing the largest macrocycle and most able to allow coordination of substituents to the metal centre, **3c** was selected for evaluation as a catalyst for the Mizoroki-Heck coupling of bromobenzene and styrene.

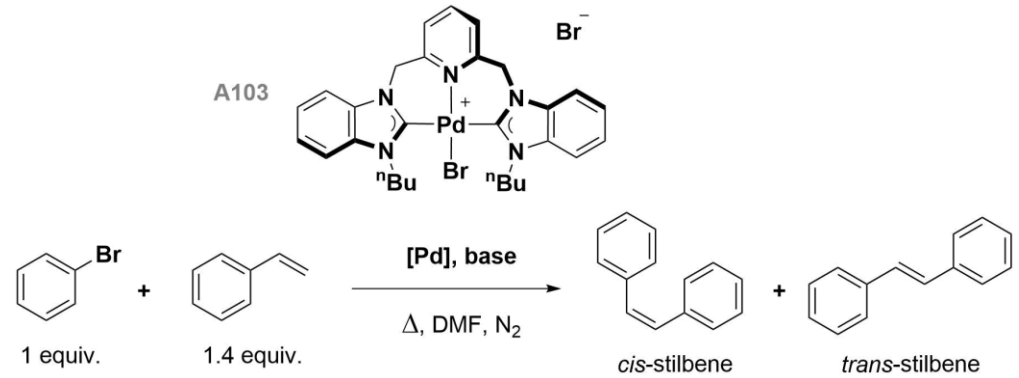

Scheme 2.4: *Mizoroki-Heck coupling of bromobenzene and styrene.*

Table 2.3: *Comparison of **3c** vs **A103** in Mizoroki-Heck C-C coupling.*

[Pd]	Loading	Base	Temperature	Time	Selectivity (cis:trans)	Yield
A103	*0.3 mol %*	*Na_2CO_3*	*115°C*	*24 h*	*1 : 16.8*	*83 %*
3c	5 mol %	NaOAc	150°C	20 h	0 : 1	50 %
3c + Hg	5 mol %	NaOAc	150°C	20 h	-	0 %

Heating bromobenzene with a slight excess of NaOAc and styrene at 150°C for 20 h in the presence of **3c** (5 mol %) resulted in low-yielding but selective conversion to *trans*-stilbene, thus demonstrating greater selectivity than that observed by Hahn and co-workers for **A103** (albeit at a lower catalyst loading and temperature). However, repeating the experiment in the presence of mercury – an established procedure for the inhibition of heterogeneous catalysis[22,23] – resulted in no catalytic turnover. This, along with darkening of the reaction mixture during catalysis, is indicative of the production of catalytically active heterogeneous palladium species *via* decomposition of the complex under the reaction conditions.

2.3 Transmetallation Reactions

While the use of *in-situ* generated silver transfer agents is straightforward and afforded palladium complexes **3** in satisfactory yields, purification on silica was required to remove impurities and the resulting general procedure may not be amenable to the isolation of more reactive, air and moisture-sensitive complexes. Isolation of a well-defined silver(I) complex of **2c** was targeted in order to gain better insight into its *in-situ* role and to facilitate selective preparation of **3c** along with other late transition metal complexes of **2c**. To further explore the scope of transmetallation methodology, copper adducts of **2c** were also targeted and investigated for their application as transfer agents.

Despite copper-based transmetallation methodology being well established (*i.e.* **A15** (M = Cu) and **A16**, **Scheme 1.3**, **Chapter 1**),[24,25] examples of NHC-based pincer complexes of copper are limited,[26] and their use as transmetallation reagents even more rare. Reported complexes of bis(NHC) pro-ligands include mononuclear **A104**, **A105** and **A107** (**Fig. 2.9**)[27-29] and multinuclear adducts **A106** and **A108**,[26,30] wherein the ligand does not necessarily coordinate as a meridonal pincer. None of these well-defined complexes have been used as transfer agents (although a silver-based analogue of **A108** is used to obtain both a Pd(CNC) complex and a dinuclear gold adduct). Instead, a trinuclear NHC-bridged Cu(I) cluster **A109** has been shown to undergo transmetallation, affording Pd(II) and Ni(II) pincer complexes (**A30**, **Fig. 2.9**, also shown in **Fig. 1.7**, **Chapter 1**).[31]

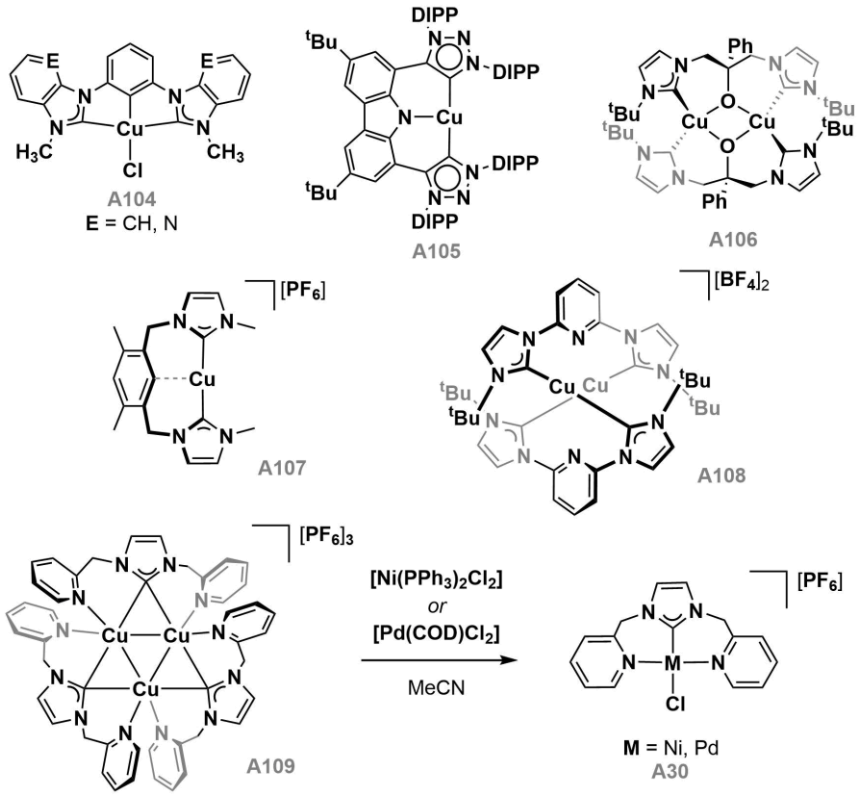

Fig. 2.9: *Copper complexes of NHC-based pincer ligands.*

2.3.1 Synthesis and Characterisation of Silver and Copper-based Transfer Agents

*2.3.1.1 Synthesis and Characterisation of Silver Transfer Agent **5***

Using a slight modification of the procedure for its *in-situ* generation, the silver NHC-macrocycle **5** was obtained from [**2c**].2HBr as a white powder in 82 % yield (**Scheme 2.5**).

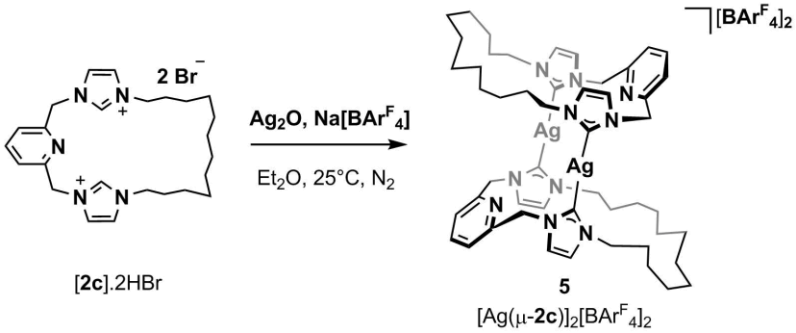

***Scheme 2.5** Synthesis of silver(I) complex **5**.*

Complex **5** is highly soluble in a range of solvents (*e.g.* CH_2Cl_2, Et_2O, $CHCl_3$, MeCN) and crystals suitable for XRD were obtained from an Et_2O-pentane layer, enabling structural elucidation of **5** in the solid-state as a dinuclear complex $[Ag(\mu\text{-}\mathbf{2c})]_2[BAr^F{}_4]_2$ (**Fig. 2.10**). Multinuclear silver NHC complexes of this type are common in the literature and di-, tri-, tetra- and even hexanuclear Ag and Au arrangements have been characterised (see **Scheme 1.12**, **Chapter 1**).[32-35]

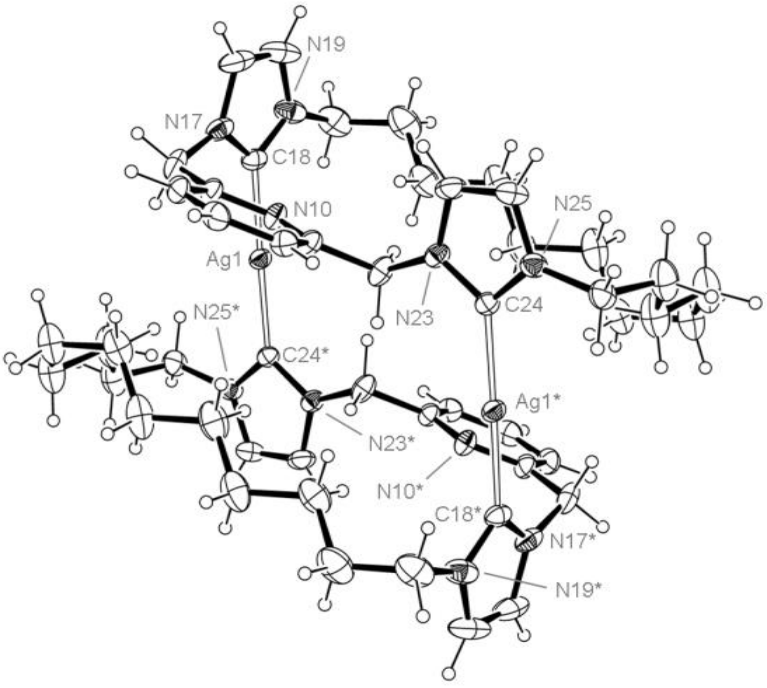

***Fig. 2.10:** ORTEP representation of **5**. Thermal ellipsoids drawn at 30 % probability, minor disordered components and $[BAr^F{}_4]^-$ counter anions omitted for clarity. The starred atoms are generated by the symmetry operation 2-x,1-y,1-z. Selected bond lengths (Å) and angles (°): Ag1-C18, 2.077(3); Ag1-C24*, 2.080(3); Ag1···Ag1*, 7.2732(6); C24-Ag1-C18*, 178.99(13); N25-C24-C18*-N19*, 100.2(4); N23-C24-C18*-N17*, 89.3(4).*

Connecting the macrocyclic C^N^C ligands of **5**, the C_{NCN}-Ag-C_{NCN} bond angles are near linear (178.99(13)°), with Ag-C_{NCN} bond lengths of 2.057(6) and 2.054(6) Å. While these metrics are comparable with related acyclic (**A110**, **A111**)[29,36] and cyclic examples (**A112**),[1,37,38] the NHC donors do not adopt the co-planar arrangement observed in such precedents and instead are arranged orthogonally (N25-C24-C18*-N19* = 100.2(4)°; N23-C24-C18*-N17* = 89.3(4)). This twist is accompanied by an unusually large Ag···Ag separation of 7.2732(6) Å (*c.f.* 3.7171(5), **A110**; 3.538(2), **A112** [E = N, Y = (CH_2)] and 4.6636(7) Å, **A112** [E = N, Y = $(CH_2)_2$]). These features are presumably necessary to accommodate the large aliphatic spacer in a geometry that places the maximum number of methylene groups in a staggered conformation.

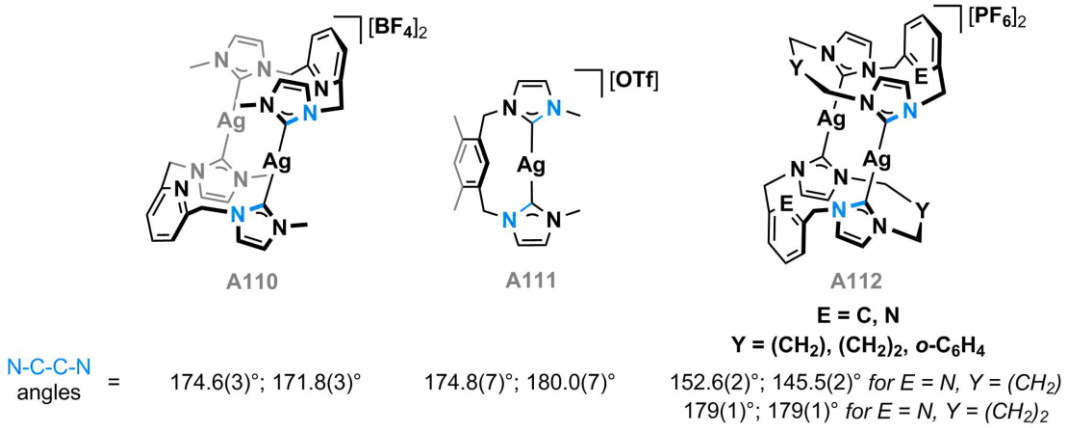

Fig. 2.11: *Preceding Ag-bridged omplexes of C^E^C ligands.*

In solution, integration of signals in the ^{1}H NMR spectrum of **5** at 298 K confirms the 1 : 1 ratio of ligand to counter anion, which is also supported by microanalysis data (effective formula [Ag(**2c**)]$_n$[BAr$^F{}_4$]$_n$). However, **5** exhibits C_{2v} symmetry on the NMR timescale (CD_2Cl_2, 500 MHz) and broad signals pertaining to the pincer backbone indicate dynamic processes. The observation of high symmetry with respect to the solid-state *pseudo*-C_i structure suggests facile fragmentation in solution into the monomeric fragment [Ag(**2c**)]$^+$, which is also the major signal observed in ESI-HRMS spectra at 512.1927 *m/z* (calc. 512.1938) with the expected integer-spaced isotope pattern. The related monomeric copper adduct [Cu(**2c**)]$^+$, is also observed in solution (*vide infra*).

Decoalescence of the previously broad ^{1}H signals of **5** on cooling from 298 to 250 K results in an equilibrium mixture of three major compounds; one of C_{2v} symmetry and two of apparent C_s symmetry (1 : 0.5 : 1). These species are tentatively assigned as monomeric [Ag(**2c**)]$^+$, and the dimeric structures *syn*-[Ag(μ-**2c**)]$_2{}^{2+}$ and *anti*-[Ag(μ-**2c**)]$_2{}^{2+}$, respectively. Further cooling to 200 K results in a shift in the equilibrium toward the species assigned to *anti*-[Ag(μ-**2c**)]$_2{}^{2+}$ (*ca.* 60 %), which is consistent with the *pseudo*-C_i symmetric structure observed in the solid-state being *enthalpically* favoured in solution at lower temperatures. The broadened room

temperature spectra are therefore indicative of the monomeric state being *entropically* favoured, as expected for a fragmentation process.

Signals pertaining to the backbone are also broadened in the $^{13}C\{^{1}H\}$ NMR spectrum at 298 K, particularly for the imidazolylidene moieties. The carbene resonance is not observed at this temperature, but its position at 181 ppm can be inferred using 2D heteronuclear correlation spectra and is consistent with those of **A110** and **A112** (181 and 180 – 185 ppm, respectively). Three carbene signals are observed in the $^{13}C\{^{1}H\}$ NMR spectrum on cooling to 200 K, consistent with the presence of three species in slow exchange.

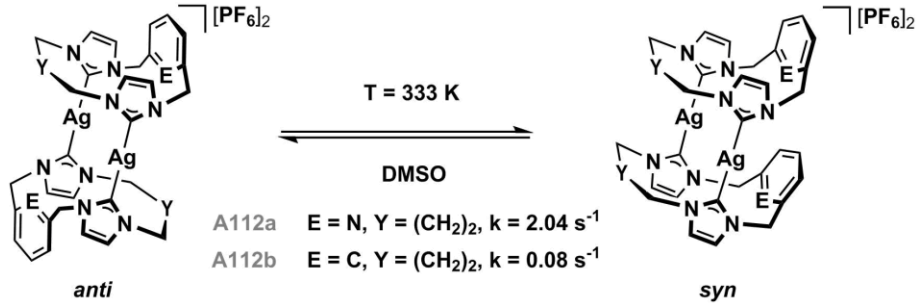

Fig. 2.12: *Isomerisation between anti and syn conformations of* ***A112a*** *and* ***A112b****.*

Assignment of the three components of the low temperature NMR spectra of **5** was aided by comparison with smaller macrocyclic pincers **A112**, which equilibrate between *syn*- and *anti*-isomers in solution (**Fig. 2.12**).[1,38] In these more constrained systems, the isomers of both silver(I) and gold(I) complexes (**Scheme 1.12**, **Chapter 1**) are distinguishable in solution by NMR spectroscopy and can be separated by recrystallisation. Isomerically pure solutions of *syn*-**A112a** undergo rapid equilibration, providing a mix of *syn* and *anti*-isomers identical to that obtained prior to recrystallisation.[38] A mechanism that accounts for the facile interconversion of *syn* and *anti*-isomers has not yet been definitively elucidated; however, the absence of this process in related Au-systems indicates that Ag-NHC bond cleavage is involved. Additionally, the authors note that a non-pyridyl linked bis-NHC (**A112b**) converts at a reduced rate compared to its pyridyl analogue, suggesting that coordination by the pyridine moiety also plays a role. Various equilibria between Ag-NHC binding modes have been identified elsewhere in the literature, albeit mostly in the presence of coordinating counter-ions.[39]

The solution-based dynamics of **5** ultimately demonstrate facile Ag–NHC bond cleavage under conditions relevant to its use as a transfer agent.

*2.3.1.2 Synthesis and Characterisation of Copper Adducts of **2c**; **6** and **7***

Initial attempts to synthesise a cationic copper adduct of **2c** *via* a one-step deprotonation and metallation in the presence of $Na[BAr^{F}_{4}]$ were unsuccessful. However, a stepwise process

involving copper bromide complex **6** (obtained in 76 % yield) enabled isolation of **7** (59 % yield from **6**, 45 % overall) as shown in **Scheme 2.6**. Differing only in the counter anions present, the complexes have very similar ^{1}H and $^{13}C\{^{1}H\}$ NMR spectra (CD_2Cl_2, 400 MHz). Both sets of spectra exhibit sharp signals with apparent C_{2v} symmetry consistent with formation of mononuclear $[Cu(\mathbf{2c})]^+$ fragments in solution. Along with the appearance of signals pertaining to $[BAr^F_4]^-$, key differences moving from **6** to **7** include a smaller separation between the imidazolylidene ^{1}H signals ($\Delta\delta$ = 0.08 (**7**) *vs* 0.24 (**6**)), and a small downfield shift in the carbenic carbon resonance (δ 180.3 (**7**) *vs* 178.7 (**6**)). These changes are consistent with the expected difference in ion-pairing in the two systems in CD_2Cl_2 solution.

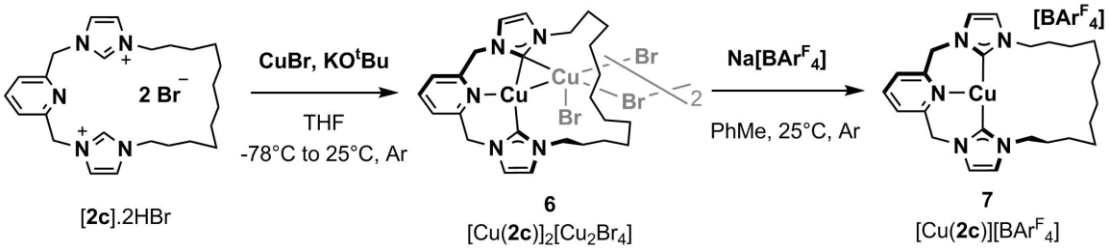

Scheme 2.6: *Synthesis of copper complexes **6** and **7**.*

The solid-state structures of **6** and **7** have far more to distinguish them. Complex **7** is represented in **Fig. 2.13** by one of two unique cations from the unit cell (Z' = 2), which illustrates adoption of a T-shaped geometry; C_{NCN}-Cu-N = 91.9(1)° and 90.5(1)°, C_{NCN}-Cu-C_{NCN} = 176.37(13)°. These bond metrics are in good agreement with those reported for **A105**, although the anionic nature of the component CNC pincer ligand leads to a shorter Cu–N bond length (2.017(2) Å for **A105** *vs* 2.233(3) Å for **7**). The macrocycle **2c** binds copper with the NHC moieties twisted orthogonally out of the coordination plane, resulting in near C_2 symmetry. The observed C_{2v} symmetry in solution is most likely a result of rapid atropisomerism of the pincer backbone, unhindered in the absence of an ancillary ligand and further enabled by relatively weak Cu-NHC bonds.

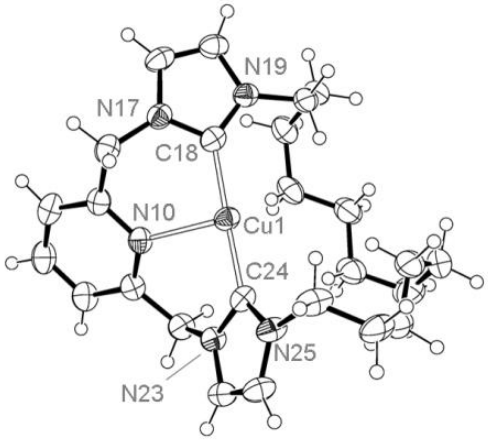

Fig. 2.13: *ORTEP representation of **7**. Thermal ellipsoids at 50 %, only one of two unique cations shown (Z' = 2) with $[BAr^F{}_4]^-$ counter anions omitted for clarity. Selected bond lengths (Å) and angles (°): Cu1-N10, 2.233(3); Cu1-C18, 1.905(3); Cu1-C24, 1.906(3); C18-Cu1-C24, 176.37(13).*

Despite its apparent similarity to **7** in solution, **6** (**Fig. 2.14**) is a dimer in the solid-state, consisting of two [Cu(**2c**)]$^+$ units bridged by a $[Cu_2Br_4]^{2-}$ dianion. Each [Cu(**2c**)]$^+$ unit features a copper atom coordinated in a near T-shape fashion (C_{NCN}-Cu-C_{NCN} = 167.92(11)°) and C_{NCN}-Cu bonds that are longer than those observed in **7** (see **Table 2.4**). The distortion from ideal geometry results from a μ^2-bridging interaction of one of the NHC donors with both pincer-ligated Cu1 and $[Cu_2Br_4]^{2-}$ dianion-based Cu2 (Cu1-C24-Cu2 = 76.95(9)°)), which in turn promotes a short cuprophilic bond of 2.5209(5) Å.

Table 2.4*: Selected solid-state metrics and $^{13}C\{^1H\}$ NMR data for **5 - 7**.*

	5 (**M = Ag**)	**6** (**M = Cu**)	**7** (**M = Cu**)
δ_{NCN}	181[a]	178.7	180.3
M-N /Å	-	2.246(2)	2.233(3)
M-C_{NCN} /Å	2.057(6), 2.045(6)	1.925(3), 1.980(3)[b], 2.070(3)[c]	1.905(3), 1.906(3)
C_{NCN}-M-C_{NCN} /°	179.0(1)	167.92(11)	176.37(13)
Cu-C_{NCN}-Cu /°	-	76.95(9)	-

[a] Obtained from 2D heteronuclear correlation spectra. [b] Cu1-C24. [c] Cu2-C24.

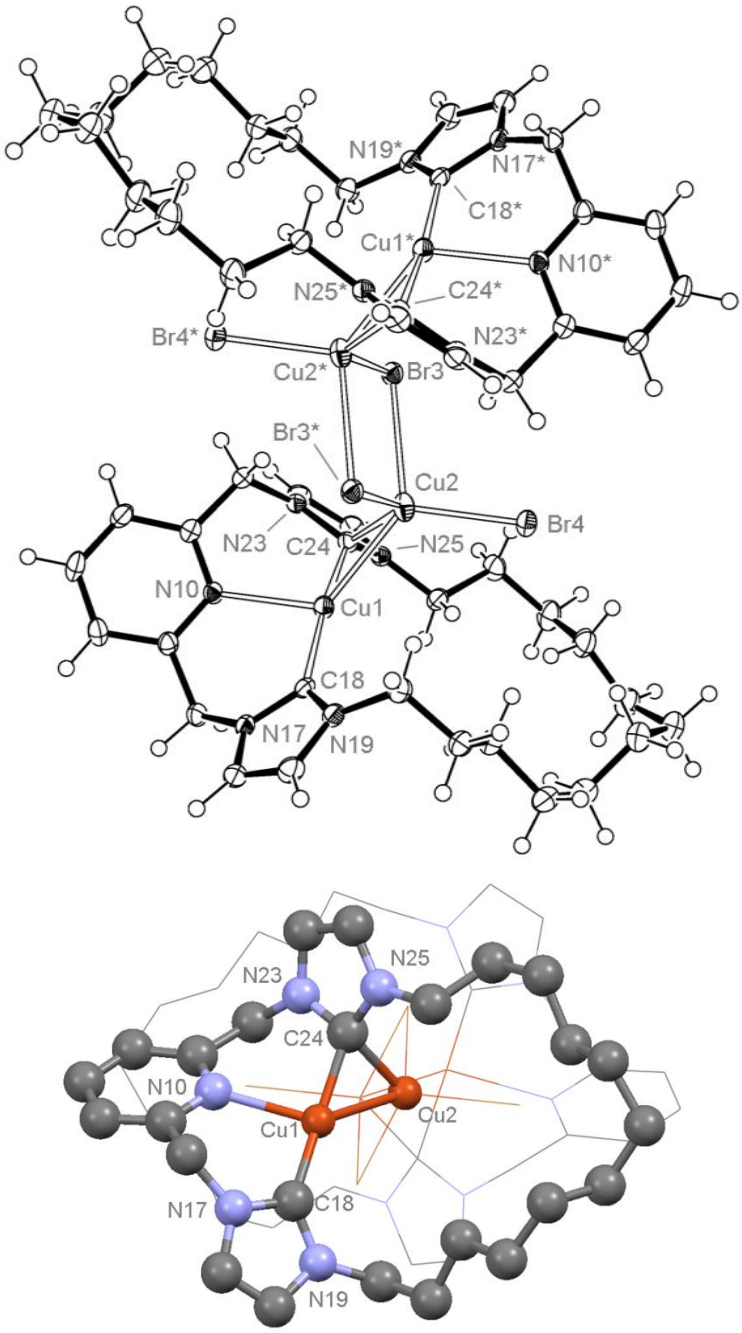

Fig. 2.14: (Top) *ORTEP representation of solid-state structure of* ***6****. Thermal ellipsoids at 30 % probability.* ***(Bottom)*** *Ball-and-stick/wireframe representation of the dimer displaying classical and bridging NHC interactions; hydrogen atoms omitted for clarity. The starred atoms are generated by the symmetry operation 1 – x, 1 – y, 1 – z. Selected bond lengths (Å) and angles (°): Cu1-Cu2, 2.5209(5); Cu1-N10, 2.246(2); Cu1-C18, 1.925(3); Cu1-C24, 1.980(3); Cu2-Br3, 2.4583(4); Cu2-Br3*, 2.7728(5); Cu2-Br4, 2.4149(4); Cu2-C24, 2.070(3); Cu2-Br3-Cu2*, 83.794(15); Br3-Cu2-Br3*, 96.206(15); Cu1-Cu2-C24, 49.92(7); C18-Cu1-C24, 167.92(11).*

A number of crystallographically characterised silver and copper complexes containing μ^2-binding NHCs have been reported.[31,40] Perhaps the most striking examples are M_3L_3 (M = Ag, Cu) trinuclear complexes such as **A109** (**Fig. 2.9**)[41] and those studied by Catalano and co-workers.[42] As discussed above, the dimeric nature of **6** is not retained in solution, with C_{2v} symmetry observed by ^{1}H and ^{13}C NMR spectroscopy and appearance of the carbenic carbons as a singlet at 180 ppm. This resonance is at higher frequency than those reported for the

aforementioned trinuclear imidazolylidene systems (167 – 169 ppm), which retain μ^2-bridging interactions in solution.[31,41-43] The bridged dimer observed for **6** would appear to be an artefact of the solid-state with facile fragmentation in solution to afford mononuclear $[Cu(\mathbf{2c})]^+$.

2.3.2 Application of 5 and 7 in Transmetallation Reactions

Small scale transmetallation reactions, conducted in CD_2Cl_2 and monitored by ^1H NMR spectroscopy, were used to assess the application of **5** and **7** as transfer agents for production of Pd, Rh and Ni complexes (**Scheme 2.7**).

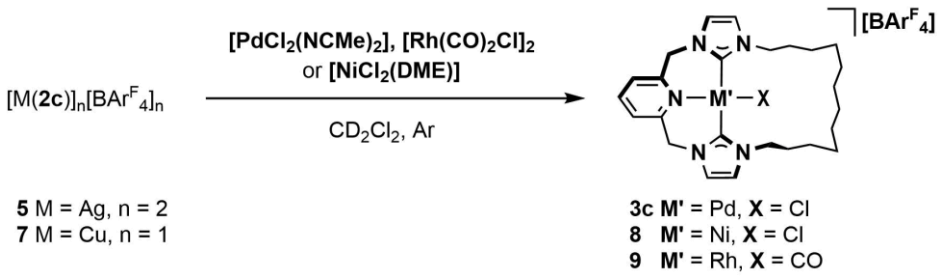

Scheme 2.7: *Small scale (0.08 mmol in 0.5 mL solvent) transmetallation reactions using **5** or **7**.*

Table 2.5: *Transmetallation reactions of **5** and **7**.*

Precursor	Reagent	Time (h)	Temp. (°C)	Product	NMR yield
$[PdCl_2(NCMe)_2]$	**5**	0.5	20	**3c**	73%
$[PdCl_2(NCMe)_2]$	**7**	0.5	20	**3c**	23%
$[NiCl_2(DME)]$	**5**	20	20	**8**	22%[a]
$[NiCl_2(DME)]$	**5**	20	40	**8**	76%
$[NiCl_2(DME)]$	**7**	20	20	**8**	86%[a]
$[NiCl_2(DME)]$	**7**	5	40	**8**	90%
$[Rh(CO)_2Cl]_2$	**5**	0.5	20	**9**	72%
$[Rh(CO)_2Cl]_2$	**7**	0.5	20	**9**	98%

[a] Incomplete conversion.

For comparison with the *in-situ* transmetallation procedure employed for palladium complexes **3**, initial investigations focused on reaction of $[PdCl_2(NCMe)_2]$ with **5** and **7**. Suspensions of $[PdCl_2(NCMe)_2]$ and the appropriate coinage metal complex in CD_2Cl_2 required sonication to aid solubilisation of the palladium precursor, proceeding to give yellow (**5**) or brown (**7**) mixtures. After 30 minutes no signals pertaining to the starting materials were observed by ^1H NMR spectroscopy. For silver adduct **5**, a spectrum containing **3c** as the major product was recorded. Using the relative integration of the *ortho*-protons of Ar^F (δ 7.72, 8H) to the imidazolylidene signals (δ 7.14 and 6.96, both 2H), the yield of **3c** was determined to be 73 %. Transmetallation using **7** was less successful, with only 23 % of **3c** present under the same reaction conditions. In combination with the facile synthesis of **5** (82 %), the high NMR yield of **3c** from **5** (73 %) promised a higher overall yield of **3c** from [**2c**].2HBr than that obtained in the

one-pot reaction (58 %, *vide supra*). To substantiate this, the reaction mixture was eluted through a silica plug in air and concentrated to afford **3c** as a white solid in *ca.* 75 % yield; corresponding to an overall yield from [**2c**].2HBr of 63 % and representing a marginal improvement over the *in-situ* method.

Encouraged by this result, preparation of the nickel congener [Ni(**2c**)Cl][BAr^F_4] **8** was targeted by reaction of the transfer agents with [$NiCl_2$(DME)]. Suspension of this nickel(II) precursor with either **5** or **7** in CD_2Cl_2 resulted in the very slow formation of **8** in both cases, but particularly when **5** was employed. After periodic sonication and 20 hours at room temperature the NMR yields of **8** were calculated to be 22 and 86 % for **5** and **7**, respectively, using integration of an isolated pyCH_2 signal against the *ortho*-protons of Ar^F. Incomplete conversion was apparent by the presence of signals pertaining to starting material in both spectra, but no additional products were observed. The reactions were subsequently repeated at 40°C to promote complete conversion, affording **8** in 76 and 90 % yield from **5** (20 h) and **7** (5 h), respectively. Filtration through an alumina plug in air afforded pure **8** in *ca.* 27 % yield in both cases. A similarly low yield of 29 % was obtained when **5** was generated and employed *in-situ* on a larger scale.[44] As such, preparation of **8** *via* transmetallation from the isolated silver transfer agent poses no significant advantage over the one-pot procedure.

Transfer of **2c** to nickel is marked by adoption of C_2 symmetry by ^{1}H NMR spectroscopy, with diagnostic diastereotopic methylene bridge protons at 6.30 ppm and 5.14 ppm ($^2J_{HH}$ = 15.0 Hz) bearing close resemblance to those of **3c**, **A41**[45] and **A113**[46] ($^2J_{HH}$ = 15.0 – 15.8 Hz, **Section 2.2.1** and **Fig. 2.15**). Shifted upfield with respect to the silver and copper reagents (*ca.* 180 ppm), the carbene $^{13}C\{^1H\}$ signal is located at 162.1 ppm (CD_2Cl_2), within the range of those found for **3** and **4** (160-165 ppm, $CDCl_3$). Elemental analysis of **8** is consistent with the formula [Ni(**2c**)Cl][BAr^F_4] and high resolution ESI-HRMS shows a parent ion at 498.1929 *m/z* (calc. 498.1929) with the expected isotopic distribution.

The solid-state structure of **8** obtained by single-crystal XRD closely resembles that of **3c**, with macrocycle **2c** adopting a box-like conformation.[47] Reflecting the smaller atomic radius of nickel, shorter distances are observed for the metal-pincer (*ca.* 0.15 Å smaller) and for metal-chloride bonds (r_{NiCl} = 2.145(2) Å *c.f.* 2.287(4) for r_{PdCl} in **3c**). Additionally, the coordination plane is closer to ideal square planar geometry than in **3c**, with angles between *trans*-substituents tending more towards 180° (**Table 2.6**). Structural metrics are also highly comparable with **A41** and **A113** (r_{NiCl} = *ca.* 2.15 Å).[45,46] The close agreement of key metrics of **8** with **A113** (Ar = Mes) suggests that the alkyl spacer has negligible effect on the coordination geometry.

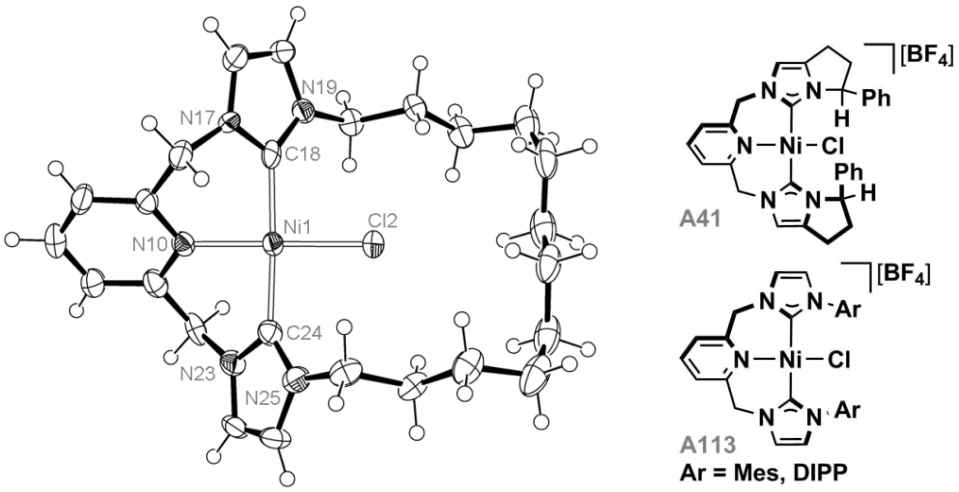

Fig. 2.15: *ORTEP representation of **8** alongside ChemDraw structures of Ni(C^N^C)Cl precedents. Thermal ellipsoids at 50 % probability and $[BAr^F{}_4]^-$ counter anion omitted for clarity.*

Table 2.6: *Selected bond lengths and angles for **8** and **A113** (Ar = Mes).*

	Ni-Cl /Å	**Ni-N** /Å	**Ni-C_{NCN}** /Å	**N-Ni-Cl** /°	**C_{NCN}-Ni-C_{NCN}** /°
8	2.145(2)	1.928(5)	1.898(6), 1.916(6)	179.06(15)	176.6(3)
A113	*2.1581(11)*	*1.921(3)*	*1.891(3), 1.910(4)*	*170.31(10)*	*173.42(16)*

Of particular interest to this project are rhodium-based macrocycles, for which ready access to square-planar Rh^{I} and octahedral Rh^{III} complexes may enable investigation of the effect of the macrocycle on both reactivity and structural features (see **Chapter 3**). Hence, the preparation of [Rh(**2c**)(CO)][$BAr^F{}_4$] **9** was targeted. Mixtures of **5** or **7** with $[Rh(CO)_2Cl]_2$ form yellow suspensions immediately on dissolution in CD_2Cl_2 and total consumption of starting material was evident in ^{1}H NMR spectra within 30 minutes. The resulting species has apparent C_{2v} symmetry with equivalent methylene bridge protons assigned to a broad singlet at 5.24 ppm. Integration of the product imidazolylidene signals (δ 7.14 and 7.01, 2H, $^3J_{HH}$ = 1.8 Hz) against the *ortho*-protons of the Ar^F counter anion was used to determine the conversion.

Transmetallation from **5** affords an impure mixture to which the C_{2v} symmetric species contributes 72 %. The analogous reaction with **7** however proceeds cleanly and purity was assessed to be 98 %. The rhodium adduct was found to be air and moisture sensitive and required purification using a short silica plug under an atmosphere of nitrogen. Analysis of the concentrated eluent (82 % isolated yield from **7**) was conducted using ^{1}H NMR spectroscopy in CD_2Cl_2. Contrary to the C_{2v} symmetry observed during the reaction, isolated samples of **9** demonstrate C_2 symmetry, with diastereotopic methylene bridge protons at 5.46 ppm and 5.04 ppm ($^2J_{HH}$ = 14.8 Hz). These signals are significantly broader than those of **3c** and **8**, indicating – along with the disparity between *in-situ* and isolated samples – facile atropisomerism of the pincer backbone. This process is presumed to result from residual

carbon monoxide in the reaction mixture and is discussed in greater detail in **Chapter 3** (**Section 3.2**), along with the spectral and structural properties of **9**.

Although transmetallation from **7** afforded pure **9** in 82 % yield after silica purification, the greater number of steps required to obtain **7** from [**2c**].2HBr (35 % overall yield) diminishes the utility of this method. Instead, **9** is most efficiently prepared on a large scale *via* a one-pot procedure utilising *in-situ* generation of **5**. After silica purification, this procedure affords **9** in 52 % isolated yield from pro-ligand [**2c**].2HBr. With a range of acyclic rhodium carbonyl CNC and PNP complexes as precedents,[48,49] this *in-situ* transmetallation methodology provides a facile means by which to investigate the effect of a macrocyclic ligand (*i.e.* **2c**) on the structural and chemical behaviour of **9**.

Together, the transmetallation reactions to afford palladium (**3c**), nickel (**8**) and rhodium (**9**) adducts of ligand **2c** indicate that the silver complex **5** (either *in-situ* or isolated) is an effective carbene transfer agent for the preparation of late transition metal complexes. Additional precursors were also screened. Products of the reactions between $[Rh(C_2H_4)_2Cl]_2$ and **5** or **7** proved unstable under the conditions employed above, but later work under an ethylene atmosphere resulted in the successful formation of a rhodium-ethylene complex from **5** (**Chapter 4**). Unfortunately, third row metal precursors $[IrCl(CO)_2(toluidine)]$, $[IrCl(COD)]_2$, $[PtCl_2(COD)]$ and $[PtCl_2(NCMe)_2]$ gave intractable mixtures.

2.4 Experimental Procedures and Selected Data

2.4.1 Experimental Procedure

General considerations. Manipulations were performed under an inert atmosphere, using Schlenk (nitrogen, argon) and glove box (argon) techniques unless otherwise stated. Glassware was oven dried and flamed under vacuum prior to use. Anhydrous solvents (<0.005 % H_2O) were purchased from ACROS or Aldrich and used as supplied: MeCN, CH_2Cl_2, $CHCl_3$, THF, 1,4-dioxane, pentane and Et_2O. CD_2Cl_2 and C_6D_6 were dried over CaH_2 and sodium metal respectively prior to vacuum-distillation, and stored under an atmosphere of argon. $CDCl_3$ (for NMR characterisation of **4**) was dried over 3 Å molecular sieves, vacuum-distilled and stored over sieves. CuBr was purchased from Aldrich and purified using a literature procedure with sodium sulphite as reductant.[50,51] $Na[BAr^F_4]$[8] and $[Rh(CO)_2Cl]_2$[52] were synthesised using literature procedures. All other reagents are commercial products and were used without further purification. NMR spectra were recorded on Bruker DPX-300, DPX-400, AV-400, DRX-500 and AV-600 spectrometers at 298 K unless otherwise stated. Chemical shifts are quoted in ppm and coupling constants in Hz. ESI-HRMS were recorded on a Bruker MaXis mass spectrometer. Microanalyses were performed at the London Metropolitan University by Stephen Boyer.

*2.4.1.1 Preparation of Bis-imidazoles **1***

General Procedure. To a stirred solution of imidazole (2.00 g, 29.3 mmol) in THF (100 mL) at 0°C, NaH (60 % wt suspension in mineral oil, 1.29 g, 32.3 mmol) was added portion-wise over 5 minutes followed by dibromoalkane (14.7 mmol; neat or in 50 mL THF). The resulting mixture was refluxed for 5 hours to give an off-white suspension. The reaction mixture was cooled to room temperature, removed from inert atmosphere, quenched with H_2O and extracted with EtOAc (3 x 50 mL). The combined organic extracts were washed with H_2O, dried over Na_2SO_4 and concentrated *in vacuo* to give the crude product. Sonication in Et_2O (**1a**, **1c**) or EtOAc/Et_2O (**1b**) and cooling to -10°C afforded the pure products as white crystalline solids.

1a: Yield: 2.85 g (79 %).

^{1}H NMR (400 MHz, $CDCl_3$) δ 7.40 (s, 2H), 7.00 (s, 2H), 6.84 (s, 2H), 3.86 (t, $^3J_{HH}$ = 7.2, 4H), 1.70 (app. quint, *J* = 7, 4H), 1.23 (br, 8H). **^{13}C{^{1}H} NMR** (101 MHz, $CDCl_3$) δ 137.0, 129.4, 118.8, 46.9, 31.0, 28.9, 26.4. **ESI-HRMS** (CH_3CN, 180°C, 3 kV) positive ion: 247.1914 *m/z*, $[M + H]^+$ (calc. 247.1917). **Elemental Analysis** Calc. for $C_{14}H_{22}N_4$ (246.35 $gmol^{-1}$): C, 68.26; H, 9.00; N, 22.74. Found: C, 68.12; H, 8.91; N, 22.62.

1b: Yield (with $0.5H_2O$): 2.15 g (52 %).

^{1}H NMR (400 MHz, $CDCl_3$) δ 7.46 (s, 2H), 7.05 (s, 2H), 6.90 (s, 2H), 3.92 (t, $^3J_{HH}$ = 7.0, 4H), 1.86 (s, 1H, H_2O), 1.76 (app. quint, *J* = 7, 4H), 1.30 – 1.17 (m, 12H). **^{13}C{^{1}H} NMR** (101 MHz, $CDCl_3$) δ 137.2, 129.5, 118.9, 47.2, 31.2, 29.4, 29.2, 26.7. **ESI-HRMS** (CH_3CN, 180°C, 3 kV) positive ion: 275.2225 *m/z*, $[M + H]^+$ (calc. 275.2230). **Elemental Analysis** Calc. for $C_{16}H_{26}N_4.0.5(H_2O)$ (with $0.5(H_2O)$ 283.41 [without 274.40] $gmol^{-1}$): C, 67.81; H, 9.60; N, 19.77.

1c: Yield (with 1.5 H_2O): 3.90 g (81 %).

^{1}H NMR (400 MHz, $CDCl_3$) δ 7.42 (s, 2H), 7.00 (s, 2H), 6.86 (s, 2H), 3.88 (t, $^3J_{HH}$ = 7.1, 4H), 2.69 (s, 3H, H_2O), 1.74 (app. quint, *J* = 7, 4H), 1.21 – 1.31 (m, 16H).**^{13}C{^{1}H} NMR** (101 MHz, $CDCl_3$) δ 137.1, 129.3, 118.8, 47.1, 31.1, 29.5, 29.4, 29.1, 26.6. **ESI-HRMS** (CH_3CN, 180°C, 3 kV) positive ion: 303.2547 *m/z*, $[M + H]^+$ (calc. 303.2543). **Elemental Analysis** Calc. for $C_{18}H_{90}N_4.1.5(H_2O)$ (329.48 $gmol^{-1}$): C, 65.62; H, 10.10; N, 17.01. Found: C, 65.41; H, 9.86; N, 17.01

*2.4.1.2 Preparation of Pro-ligands [**2**].2HBr*

General Procedure. To refluxing 1,4-dioxane (150 mL), equimolar solutions of 2,6-bis(bromomethyl)pyridine and bis-imidazole **1** in 1,4-dioxane (*ca*. 0.075 M, dried over 3 Å molecular sieves) were simultaneously added dropwise over 30 minutes. The resulting reaction mixture was refluxed for 16 hours, cooled to approx. 50°C and the solvent removed *in vacuo*. The resulting off-white residue was extracted with MeCN (*ca*. 200 mL) with vigorous stirring. The MeCN solution was filtered, concentrated and excess Et_2O added to precipitate the product. The product was isolated by filtration and washed with excess Et_2O.

[**2a**].2HBr: following the general procedure using 2,6-bis(bromomethyl)pyridine (0.79 g, 2.98 mmol) and **1a** (0.73 g, 2.98 mmol), the product was obtained as an off-white foam. Yield: 0.47 g (31 %).

^{1}H NMR (400 MHz, CD_2Cl_2) δ 10.55 (app. t, *J* = 2, 2H), 8.00 (app. t, *J* = 2, 2H), 7.82 (dd, $^3J_{HH}$ = 8.4, 7.0, 1H), 7.72 (app. d, *J* = 8, 2H), 7.40 (app. t, *J* = 2, 2H), 5.82 (s, 4H), 4.42 (t, $^3J_{HH}$ = 6.4, 4H), 1.88 (app. quint, *J* = 7, 4H), 1.32–1.41 (m, 4H), 1.18–1.28 (m, 4H). **^{13}C{^{1}H} NMR** (101 MHz, CD_2Cl_2) δ 153.6, 139.5, 137.9, 124.6, 124.4, 122.1, 54.2, 50.1, 29.6, 27.5, 24.7. **ESI-HRMS** (CH_2Cl_2, 180 °C, 3 kV) positive ion: 175.6207 *m/z*, $[M]^{2+}$ (calc. 175.6206). **Elemental Analysis** Calc. for $C_{21}H_{29}N_5Br_2{\cdot}1.4(H_2O)$ (536.52 [511.30] g mol^{-1}): C, 47.01; H, 5.97; N, 13.05. Found: C, 47.17; H, 5.45; N, 13.01.

[**2b**].2HBr: following the general procedure using 2,6-bis(bromomethyl)pyridine (1.00 g, 3.77 mmol) and **1b** (1.03 g, 3.77 mmol), the product was obtained as a white crystalline solid. Yield: 0.71 g (35 %).

^{1}H NMR (400 MHz, CD_2Cl_2) δ 10.80 (app. t, *J* = 2, 2H), 7.94 (app. t, *J* = 2, 2H), 7.82 (dd, $^{3}J_{HH}$ = 8.1, 7.3, 1H), 7.69 (app. d, *J* = 8, 2H), 7.23 (app. t, *J* = 2, 2H), 5.82 (s, 4H), 4.42 (t, $^{3}J_{HH}$ = 7.1, 4H), 1.96 (app. quint, *J* = 7, 4H), 1.37–1.46 (m, 8H), 1.30–1.35 (m, 4H). **^{13}C{^{1}H} NMR** (101 MHz, CD_2Cl_2) δ 153.7, 139.6, 138.5, 124.4, 123.8, 121.9, 54.0, 50.5, 29.6, 27.9, 27.4, 25.0. **ESI-HRMS** (CH_2Cl_2, 180 °C, 3 kV) positive ion: 189.6361 *m*/*z*, $[M]^{2+}$ (calc. 189.6362). **Elemental Analysis** Calc. for $C_{23}H_{33}N_5Br_2$ (539.35 g mol^{-1}): C, 51.22; H, 6.17; N, 12.98. Found: C, 51.08; H, 6.08; N, 12.89.

[**2c**].2HBr: following the general procedure using 2,6-bis(bromomethyl)pyridine (1.08 g, 4.08 mmol) and **1c** (1.23 g, 4.08 mmol), the product was obtained a white crystalline solid. Yield: 0.90 g (39 %).

^{1}H NMR (400 MHz, CD_2Cl_2) δ 10.84 (br, 2H), 8.17 (app. t, *J* = 2, 2H), 7.69–7.78 (m, 3H), 7.37 (app. t, *J* = 2, 2H), 5.78 (s, 4H), 4.42 (t, $^{3}J_{HH}$ = 7.0, 4H), 1.93 (app. quint, *J* = 7, 2H), 1.22–1.41 (m, 16H). **^{13}C{^{1}H} NMR** (101 MHz, CD_2Cl_2) δ 153.8, 139.4, 138.4, 124.3, 123.9, 122.0, 53.9, 50.2, 30.0, 28.1 (2C), 27.9, 25.3. **ESI-HRMS** (CH_2Cl_2, 180 °C, 3 kV) positive ion: 203.6521 *m*/*z*, $[M]^{2+}$ (calc. 203.6519). **Elemental Analysis** Calc. for $C_{25}H_{37}N_5Br_2$ (567.40 g mol^{-1}): C, 52.92; H, 6.57; N, 12.34. Found: C, 52.82; H, 6.53; N, 12.17.

*2.4.1.3 Preparation of Palladium Chloride Complexes **3***

General Procedure. A mixture of [**2**].2HBr (1 equiv.), Ag_2O (1 equiv.) and Na[BAr^F_4] (1.1 equiv.) in CH_2Cl_2 (3 mL) were stirred in the absence of light for 16 hours. A solution of $[PdCl_2(NCPh)_2]$ (1 equiv.) in CH_2Cl_2 (*ca*. 3 mL) was added and the suspension stirred for a further 5 hours. The solution was filtered and the filtrate reduced to dryness *in vacuo* to afford the crude product. Purification was achieved by passing through a silica pad using CH_2Cl_2 eluent.

[Pd(**2a**)Cl][BAr^F_4] (**3a**): following the general procedure using [**2a**].2HBr (0.060 g, 0.117 mmol) and subsequent recrystallisation from $CHCl_3$–pentane, the product was obtained as pale-yellow crystalline solid. Yield: 0.049 g (31 %).

^{1}H NMR (400 MHz, $CDCl_3$) δ 7.71 (t, $^{3}J_{HH}$ = 7.7, 1H, py), 7.66–7.71 (m, 8H, Ar^F), 7.49 (br, 4H, Ar^F), 7.38 (d, $^{3}J_{HH}$ = 7.7, 2H, py), 6.94 (d, $^{3}J_{HH}$ = 1.9, 2H, imid), 6.90 (d, $^{3}J_{HH}$ = 1.9, 2H, imid), 5.39–5.51 (m, 2H, *N*-CH_2), 5.34 (d, $^{2}J_{HH}$ = 15.3, 2H, pyCH_2), 5.08 (d, $^{2}J_{HH}$ = 15.3, 2H, pyCH_2), 3.80 (dt, $^{2}J_{HH}$ = 13.3, $^{3}J_{HH}$ = 6.6, 2H, *N*-CH_2), 2.79 (br, 2H, CH_2), 1.98–2.14 (m, 2H, CH_2), 1.72–1.86 (m, 2H, CH_2), 1.60–1.72 (m, 2H, CH_2), 1.41–1.54 (m, 2H, CH_2), 1.12–1.25 (m, 2H, CH_2). **^{13}C{^{1}H} NMR** (101 MHz, $CDCl_3$) δ 162.4 (s, Pd-C), 161.8 (q, $^{1}J_{CB}$ = 50, Ar^F), 154.7 (s, py), 141.7 (s, py), 134.9 (s, Ar^F), 129.1 (qq, $^{2}J_{FC}$ = 32, $^{3}J_{CB}$ = 3, Ar^F), 125.7 (s, py), 124.6 (q, $^{1}J_{FC}$ = 273, Ar^F), 123.7 (s, imid), 120.4 (s, imid), 117.7 (quint, $^{3}J_{FC}$ = 4, Ar^F), 56.2 (s, py*C*H_2), 50.0 (s, *N*-*C*H_2), 31.1 (s, CH_2), 26.6 (s, CH_2), 26.5

(s, CH_2). **ESI-HRMS** (CH_3CN, 180 °C, 3 kV) positive ion: 490.0993 *m*/*z*, $[M]^+$ (calc. 490.0989). **Elemental Analysis** Calc. for $C_{53}H_{39}BClF_{24}N_5Pd$ (1354.56 g mol^{-1}): C, 46.99; H, 2.90; N, 5.17. Found: C, 46.92; H, 2.87; N, 5.15.

[Pd(**2b**)Cl][BAr^F_4] (**3b**): following the general procedure using [**2b**].2HBr (0.064 g, 0.110 mmol) and subsequent recrystallisation from $CHCl_3$–pentane, the product was obtained as pale-yellow hexagonal platelets. Yield: 0.094 g (55 %).

^{1}H NMR (400 MHz, $CDCl_3$) δ 7.66–7.71 (m, 8H, Ar^F), 7.64 (t, $^3J_{HH}$ = 7.4, 1H, py), 7.49 (br, 4H, Ar^F), 7.35 (d, $^3J_{HH}$ = 7.4, 2H, py), 6.97 (d, $^3J_{HH}$ = 1.7, 2H, imid), 6.87 (d, $^3J_{HH}$ = 1.7, 2H, imid), 5.57 (d, $^2J_{HH}$ = 15.3, 2H, pyCH_2), 4.98 (d, $^2J_{HH}$ = 15.3, 2H, pyCH_2), 4.59–4.73 (m, 2H, *N*-CH_2), 4.33–4.46 (m, 2H, *N*-CH_2), 2.30–2.43 (m, 2H, CH_2), 1.77–1.92 (m, 2H, CH_2), 1.57–1.70 (m, 2H, CH_2), 1.08–1.48 (m, 10H, CH_2). **^{13}C{^{1}H} NMR** (101 MHz, $CDCl_3$) δ 163.3 (s, Pd-C), 161.8 (q, $^1J_{CB}$ = 50, Ar^F), 155.0 (s, py), 141.6 (s, py), 134.9 (s, Ar^F), 129.1 (qq, $^2J_{FC}$ = 32, $^3J_{CB}$ = 3, Ar^F), 125.3 (s, py), 124.6 (q, $^1J_{FC}$ = 273, Ar^F), 123.2 (s, imid), 120.4 (s, imid), 117.7 (quint, $^3J_{FC}$ = 4, Ar^F), 56.0 (s, pyCH_2), 49.9 (s, *N*-CH_2), 30.3 (s, CH_2), 27.8 (s, CH_2), 27.4 (s, CH_2), 25.5 (s, CH_2). **ESI-HRMS** (CH_3CN, 180 °C, 3 kV) positive ion: 518.1308 *m*/*z*, $[M]^+$ (calc. 518.1303). **Elemental Analysis** Calc. for $C_{55}H_{43}BClF_{24}N_5Pd$ (1382.61 g mol^{-1}): C, 47.78; H, 3.13; N, 5.07. Found: C, 47.85; H, 3.11; N, 5.07.

[Pd(**2c**)Cl][BAr^F_4] (**3c**): following the general procedure using [**2c**].2HBr (0.100 g, 0.176 mmol) and subsequent recrystallisation from Et_2O–hexane, the product was obtained as a white crystalline solid. Yield: 0.151 g (58 %).

^{1}H NMR (400 MHz, $CDCl_3$) δ 7.66–7.70 (m, 8H, Ar^F), 7.58 (t, $^3J_{HH}$ = 7.6, 1H, py), 7.48 (br, 4H, Ar^F), 7.32 (d, $^3J_{HH}$ = 7.6, 2H, py), 7.02 (d, $^3J_{HH}$ = 1.7, 2H, imid), 6.89 (d, $^3J_{HH}$ = 1.7, 2H, imid), 5.63 (d, $^2J_{HH}$ = 15.0, 2H, pyCH_2), 4.97 (d, $^2J_{HH}$ = 15.0, 2H, pyCH_2), 4.72 (td, $^2J_{HH}$ = 12.4, $^3J_{HH}$ = 3.6, 2H, *N*-CH_2), 3.75 (td, $^2J_{HH}$ = 12.4, $^3J_{HH}$ = 5.7, 2H, *N*-CH_2), 2.09–2.22 (m, 2H, CH_2), 1.64–1.77 (m, 2H, CH_2), 1.31–1.57 (m, 14H, CH_2), 1.08–1.20 (m, 2H, CH_2). **^{13}C{^{1}H} NMR** (101 MHz, $CDCl_3$) δ 164.5 (s, Pd-C), 161.8 (q, $^1J_{CB}$ = 50, Ar^F), 154.8 (s, py), 141.5 (s, py), 134.9 (s, Ar^F), 129.1 (qq, $^2J_{FC}$ = 32, $^3J_{CB}$ = 3, Ar^F), 125.4 (s, py), 124.6 (q, $^1J_{FC}$ = 273, Ar^F), 122.4 (s, imid), 121.0 (s, imid), 117.7 (quint, $^3J_{FC}$ = 4, Ar^F), 55.7 (s, pyCH_2), 51.6 (s, *N*-CH_2), 31.0 (s, CH_2), 28.3 (s, CH_2), 27.1 (s, CH_2), 27.0 (s, CH_2), 23.2 (s, CH_2). **ESI-HRMS** (CH_3CN, 180 °C, 3 kV) positive ion: 546.1616 *m*/*z*, $[M]^+$ (calc. 546.1617). **Elemental Analysis** Calc. for $C_{57}H_{47}BClF_{24}N_5Pd$ (1410.66 g mol^{-1}); C, 48.53; H, 3.36; N, 4.96. Found: C, 48.41; H, 3.29; N, 4.98.

*2.4.1.4 Preparation of Palladium Fluoride Complexes **4***

General procedure. To a solution of AgF in MeCN (3 mL) was added a solution of **3** in MeCN (2 mL). The resulting suspension was stirred in the dark at room temperature for 1–3 hours. The solvent was removed *in vacuo* and the product extracted with $CHCl_3$ through celite (Pasteur pipette, 3 cm).

[Pd(**2a**)F][BAr^F_4] (**4a**): following the general procedure using AgF (0.023 g, 0.181 mmol) and **3a** (0.050 g, 0.037 mmol) – stirred for 1 hour, the product was obtained as an off-white solid. Yield: 0.030 g (61 %).

^{1}H NMR (400 MHz, $CDCl_3$) δ 7.67–7.72 (m, 9H, py + Ar^F), 7.49 (br, 4H, Ar^F), 7.35 (d, $^3J_{HH}$ = 7.8, 2H, py), 6.95 (d, $^3J_{HH}$ = 1.8, 2H, imid), 6.90 (d, $^3J_{HH}$ = 1.8, 2H, imid), 5.23 (s, 4H, pyCH_2), 4.31 (app. t, J_{HH} = 7, 4H, *N*-CH_2), 2.04–2.15 (m, 4H, CH_2), 1.42–1.53 (s, 8H, CH_2). **^{19}F NMR** (377 MHz, $CDCl_3$) δ −62.38 (s, Ar^F), −392.08 (s, Pd-F). **^{13}C{^{1}H} NMR** (101 MHz, $CDCl_3$) δ 164.8 (s, Pd-C), 161.8 (q, $^1J_{CB}$ = 50, Ar^F), 155.4 (s, py), 141.2 (s, py), 134.9 (s, Ar^F), 129.1 (qq, $^2J_{FC}$ = 32, $^3J_{CB}$ = 3, Ar^F), 126.2 (s, py), 124.6 (q, $^1J_{FC}$ = 273, Ar^F), 123.2 (s, imid), 119.7 (s, imid), 117.7 (quint, $^3J_{FC}$ = 4, Ar^F), 55.8 (s, pyCH_2), 50.0 (d, $^{2h}J_{FC}$ = 14, *N*-CH_2), 30.2 (s, CH_2), 26.0 (s, CH_2), 25.5 (d, $^{2h}J_{FC}$ = 6, CH_2). **ESI-HRMS** (CH_2Cl_2, 180 °C, 3 kV) positive ion: 500.1283 *m*/*z* (100 %), $[M - F + HCOO]^+$ (calc. 500.1278); 456.1377 *m*/*z* (35 %), $[M - F + H]^+$ (calc. 456.1382). **Elemental Analysis** Calc. for $C_{53}H_{39}BF_{25}N_5Pd{\cdot}0.5(CHCl_3)$ (1397.79 [1338.10] g mol^{-1}): C, 45.97; H, 2.85; N, 5.01. Found: C, 45.77; H, 2.86; N, 4.93.

[Pd(**2b**)F][BAr^F_4] (**4b**): following the general procedure using AgF (0.019 g, 0.150 mmol) and **3b** (0.056 g, 0.041 mmol) – stirred for 3 hours, the product was obtained as a white solid. Yield: 0.049 g (88 %).

^{1}H NMR (400 MHz, $CDCl_3$) δ 7.67–7.71 (m, 8H, Ar^F), 7.66 (t, $^3J_{HH}$ = 7.8, 1H, py), 7.49 (br, 4H, Ar^F), 7.35 (d, $^3J_{HH}$ = 7.8, 2H, py), 6.98 (d, $^3J_{HH}$ = 1.8, 2H, imid), 6.90 (d, $^3J_{HH}$ = 1.8, 2H, imid), 5.60 (d, $^2J_{HH}$ = 15.2, 2H, pyCH_2), 4.97 (d, $^2J_{HH}$ = 15.2, 2H, pyCH_2), 4.66 (td, $^2J_{HH}$ = 12.5, $^3J_{HH}$ = 3.9, 2H, *N*-CH_2), 3.71 (td, $^2J_{HH}$ = 12.5, $^3J_{HH}$ = 5, 2H, *N*-CH_2), 2.00–2.15 (m, 2H, CH_2), 1.34–1.81 (m, 12H, CH_2), 0.97–1.12 (m, 2H, CH_2). **^{19}F NMR** (377 MHz, $CDCl_3$) δ −62.38 (s, Ar^F), −399.89 (s, Pd-F). **^{13}C{^{1}H} NMR** (101 MHz, $CDCl_3$) δ 165.0 (s, Pd-C), 161.8 (q, $^1J_{CB}$ = 50, Ar^F), 155.6 (s, py), 141.2 (s, py), 134.9 (s, Ar^F), 129.1 (qq, $^2J_{FC}$ = 32, $^3J_{CB}$ = 3, Ar^F), 126.0 (s, py), 124.6 (q, $^1J_{FC}$ = 273, Ar^F), 122.3 (s, imid), 120.3 (s, imid), 117.7 (quint, $^3J_{FC}$ = 4, Ar^F), 55.6 (s, pyCH_2), 50.6 (d, $^{2h}J_{FC}$ = 6, *N*-CH_2), 30.4 (s, CH_2), 27.0 (s, CH_2), 25.6 (s, CH_2), 24.5 (s, CH_2). **ESI-HRMS** (CH_2Cl_2, 180 °C, 3 kV) positive ion: 542.1762 *m*/*z* (100 %), $[M - F + CH_3COO]^+$ (calc. 542.1747); 528.1604 *m*/*z* (10 %), [M – F +

HCOO]$^+$ (calc. 528.1591). **Elemental Analysis** Calc. for $C_{55}H_{43}BF_{25}N_5Pd$ (1366.15 g mol^{-1}): C, 48.35; H, 3.17; N, 5.13. Found: C, 48.45; H, 3.11; N, 5.17.

[Pd(**2c**)F][BAr$^F_4$] (**4c**): following the general procedure using AgF (0.022 g, 0.173 mmol) and **3c** (0.050 g, 0.035 mmol) – stirred for 1 hour, the product was obtained as an oil that was washed with pentane and dried to give a white foam. Yield: 0.022 g (45 %).

^{1}H NMR (400 MHz, $CDCl_3$) δ 7.64–7.72 (m, 8H, Ar^F), 7.56 (t, $^3J_{HH}$ = 7.7, 1H, py), 7.48 (br, 4H, Ar^F), 7.29 (d, $^3J_{HH}$ = 7.7, 2H, py), 7.01 (d, $^3J_{HH}$ = 1.9, 2H, imid), 6.92 (d, $^3J_{HH}$ = 1.9, 2H, imid), 5.67 (d, $^2J_{HH}$ = 15.1, 2H, pyCH_2), 4.94 (d, $^2J_{HH}$ = 15.1, 2H, pyCH_2), 4.75 (dt, $^2J_{HH}$ = 12.1, $^3J_{HH}$ = 5.2, 2H, *N*-CH_2), 3.83 (dt, $^2J_{HH}$ = 11.8, $^3J_{HH}$ = 5.2, 2H, *N*-CH_2), 1.73–1.97 (m, 4H, CH_2), 1.15–1.53 (m, 16H, CH_2). **^{19}F NMR** (377 MHz, $CDCl_3$) δ −62.39 (s, Ar^F), −399.91 (s, Pd-F). **^{13}C{^{1}H} NMR** (101 MHz, $CDCl_3$) δ 164.7 (s, Pd-C), 161.9 (q, $^1J_{CB}$ = 50, Ar^F), 155.8 (s, py), 141.3 (s, py), 134.9 (s, Ar^F), 129.1 (qq, $^2J_{FC}$ = 32, $^3J_{CB}$ = 3, Ar^F), 125.8 (s, py), 124.6 (q, $^1J_{FC}$ = 273, Ar^F), 121.7 (s, imid), 120.6 (s, imid), 117.6 (quint, $^3J_{FC}$ = 4, Ar^F), 55.6 (s, pyCH_2), 50.0 (d, $^{2h}J_{FC}$ = 6, *N*-CH_2), 31.0 (s, CH_2), 27.4 (s, CH_2), 27.3 (s, CH_2), 27.2 (s, CH_2), 24.4 (s, CH_2). **ESI-HRMS** (CH_2Cl_2, 180 °C, 3 kV) positive ion: 570.2068 *m/z* (100 %), [M – F + CH_3COO]$^+$ (calc. 570.2060); 556.1902 *m/z* (5 %), [M – F + HCOO]$^+$ (calc. 556.1903). **Elemental Analysis** Calc. for $C_{57}H_{47}BF_{25}N_5Pd$ (1394.21 g mol^{-1}): C, 49.10; H, 3.40; N, 5.02. Found: C, 49.10; H, 3.28; N, 5.13.

2.4.1.5 Preparation of Transmetallation Reagents

[Ag(**2c**)]$_2$[BAr$^F_4$]$_2$ (**5**): A mixture of [**2c**].2HBr (100 mg, 0.1762 mmol), Ag_2O (42 mg, 0.1812 mmol) and Na[BAr$^F_4$] (170 mg, 0.1918 mmol) in Et_2O (5 mL) was stirred in the absence of light for 48 h. The resulting grey suspension was filtered through a celite plug (pipette, 3 cm) under a flow of N_2 and concentrated to a white foam. The product was extracted in hot $CHCl_3$ through a celite plug (pipette, 3 cm) and precipitated by addition of excess pentane with sonication. Washing with pentane afforded the product as a white powder, which was stored in an argon-filled glove box in the absence of light. Yield: 200 mg (82 %). Crystals suitable for XRD were grown from an ether-pentane layer under nitrogen.

^{1}H NMR (400 MHz, CD_2Cl_2) δ 7.82 (br, 1H, py), 7.70 – 7.75 (m, 8 H, Ar^F), 7.56 (s, 4H, Ar^F), 7.42 (br, 2H, py), 7.17 (br, 2H, imid), 7.05 (s, 2H, imid), 5.25 (br, 4H, pyCH_2), 4.06 (app. t, *J* = 7, 4H, *N*-CH_2), 1.79 (app. quint, *J* = 7, 4H, CH_2) 1.15 – 1.35 (m, 16 H, CH_2). **^{13}C{^{1}H} NMR** (101 MHz, CD_2Cl_2) *carbene not identified* δ 162.3 (q, $^1J_{CB}$ = 50, Ar^F), 155.1 (s, py), 140.5 (br, py), 135.4 (s, Ar^F), 129.4 (qq, $^2J_{FC}$ = 32, $^3J_{CB}$ = 3, Ar^F), 125.3 (q, $^1J_{FC}$ = 273, Ar^F), 125.0 (br, py), 124.1 (br, imid), 120.2 (br, imid), 118.0 (quint, $^3J_{FC}$ = 4, Ar^F), 57.1 (s, pyCH_2), 53.8 (m, $CHDCl_2$ + *N*-CH_2), 31.4 (s, CH_2), 27.5 (s, CH_2), 27.4 (s, CH_2), 26.5 (s, CH_2), 25.8 (s, CH_2). **ESI-HRMS** (CH_3CN, 180 °C, 3 kV) positive

ion: 512.1927 *m/z*, $[M]^+$ (calc. 512.1938). **Elemental Analysis** Calc. for $C_{57}H_{47}AgBF_{24}N_5$ (1376.68 g mol^{-1}): C, 49.73; H, 3.44; N, 5.09. Found: C, 46.08; H, 3.23; N, 4.58. (calc. for $C_{57}H_{47}AgBF_{24}N_5.CHCl_3$ (1496.05 g mol^{-1}): C, 46.28; H, 3.22; N, 4.64.)

[Cu(**2c**)]$_2$[Cu_2Br_4] (**6**): A mixture of [**2c**].2HBr (200 mg, 0.3525 mmol) and CuBr (152 mg, 1.0574 mmol) in THF (7 mL) under argon was cooled to -78°C before addition of a saturated THF solution of KO^tBu (100 mg, 0.8813 mmol) via cannula to afford an orange suspension. The reaction vessel was allowed to come to room temperature then sealed and sonicated to produce a yellow suspension which was stirred for a further 30 h before filtration. Addition of excess pentane to the filtrate and removal of solvent by filtration afforded the product as an air and moisture-sensitive yellow powder. Yield: 147 mg (76 %). Crystals suitable for XRD were grown from a CD_2Cl_2-pentane layer.

^{1}H NMR (400 MHz, CD_2Cl_2) δ 7.78 (t, $^3J_{HH}$ = 7.7, 1H, py), 7.39 (d, $^3J_{HH}$ = 7.7, 2H, py), 7.22 (d, $^3J_{HH}$ = 1.7, 2H, imid), 6.98 (d, $^3J_{HH}$ = 1.7, 2H, imid), 5.37 (br, 4H, pyCH_2), 4.17 (t, $^3J_{HH}$ = 6.8, 4H, *N*-CH_2), 1.78-1.88 (m, 4H, CH_2), 1.14-1.34 (m, 16H, CH_2). **^{13}C{^{1}H} NMR** (101 MHz, CD_2Cl_2) δ 178.7 (s, carbene), 155.5 (s, py), 139.4 (s, py), 123.2 (s, py), 122.5 (s, imid), 120.8 (s, imid), 56.3 (s, pyCH_2), 52.1 (s, *N*-CH_2), 31.2 (s, CH_2), 28.1 (s, CH_2), 27.8 (s, CH_2), 25.8 (s, CH_2). **ESI-HRMS** (CH_3CN, 180 °C, 3 kV) positive ion: 468.2185 *m/z*, $[M]^+$ (calc. 468.2183). **Elemental Analysis** Calc. for $C_{50}H_{70}Br_4Cu_4N_{10}$ (1384.96 g mol^{-1}): C, 43.36; H, 5.09; N, 10.11. Found: C, 43.28; H, 4.97; N, 9.99.

[Cu(**2c**)][BAr^F_4] (**7**): A mixture of **6** (53 mg, 0.0383 mmol) and Na[BAr^F_4] (90 mg, 0.1016 mmol) were sonicated in toluene (3 mL) then stirred at room temperature for 2 days before filtration. The filtrate was concentrated to dryness before solubilisation in THF and addition of excess of pentane to precipitate the yellow microcrystalline product as an adduct with THF, **7**.0.5(THF). Yield: 62 mg, (61 %). Crystals suitable for XRD were grown from a THF-pentane layer.

^{1}H NMR (400 MHz, CD_2Cl_2) δ 7.83 (t, $^3J_{HH}$ = 7.8, 1H, py), 7.73 (br, 8H, Ar^F), 7.56 (br, 4H, Ar^F), 7.42 (d, $^3J_{HH}$ = 7.8, 2H, py), 7.10 (d, $^3J_{HH}$ = 1.2, 2H, imid), 7.02 (d, $^3J_{HH}$ = 1.2, 2H, imid), 5.19 (br, 4H, pyCH_2), 4.20 (t, $^3J_{HH}$ = 7.6 , 4H, *N*-CH_2), 1.78 – 1.93 (m, 4H, CH_2), 1.25 – 1.48 (m, 16 H, CH_2). **^{13}C{^{1}H} NMR** (101 MHz, CD_2Cl_2) δ 180.3 (s, carbene), 162.3 (q, $^1J_{CB}$ = 50, Ar^F) 153.8 (s, py), 140.2 (s, py), 135.4 (s, Ar^F), 129.5 (qq, $^2J_{FC}$ = 32, $^3J_{CB}$ = 3, Ar^F), 125.2 (q, $^1J_{FC}$ = 271, Ar^F), 124.1 (s, py), 123.2 (s, imid), 119.6 (s, imid), 118.1 (quint, $^3J_{FC}$ = 4, Ar^F), 54.9 (s, pyCH_2), 52.9 (s, *N*-CH_2), 34.7 (s, CH_2), 31.4 (s, CH_2), 27.2 (s, CH_2), 27.1 (s, CH_2), 25.8 (s, CH_2), 25.6 (s, CH_2), 22.9 (s, CH_2). **ESI-HRMS** (CH_3CN, 180 °C, 3 kV) positive ion: 468.2185 *m/z*, $[M]^+$ (calc. 468.2183). **Elemental Analysis** Calc. for $C_{57}H_{47}BCuF_{24}N_5$ (1332.33 g mol^{-1}): C, 51.38; H, 3.56; N, 5.26. Found: C, 51.48; H, 3.47; N, 5.34.

2.4.1.6 Transmetallation Experiments

General Procedure for Transmetallation Reactions: In an argon-filled glove box, a J. Young's NMR tube was charged with approx. 0.008 mol of transmetallation reagent **5** or **7** and a slight excess (per metal atom) of metal precursor before addition of 0.5 mL of CD_2Cl_2. The reaction was monitored by ^{1}H NMR spectroscopy for the specified time. When total consumption of the starting material was observed, the sample was filtered through a silica or alumina plug, washing with CH_2Cl_2. The filtrate was concentrated, weighed and its purity assessed by ^{1}H NMR.

Generation of [Pd(2c)Cl][BAr$^F_4$] (3c) from isolated 5 or 7: Use of 1.1 equiv. (0.0088 mmol) of $[Pd(NCMe)_2Cl_2]$ with **5** or **7** achieved total consumption of the starting materials in 0.5 h. Reaction with **6** afforded an intractable mixture. The mixture generated from **5** was exposed to air and passed through a short Si plug, washing with CH_2Cl_2. The filtrate was concentrated to afford **3c** as a white solid. Yield: 9 mg (78 %). ^{1}H NMR ($CDCl_3$) spectrum consistent with that previously described.

Generation of [Ni(2c)Cl][BAr$^F_4$] (8) from isolated 5 or 7: Use of 1.4 equiv. (0.0112 mmol) of $[NiCl_2(DME)]$ with **5** or **7** (0.008 mmol) was conducted at 25°C or 40°C respectively and monitored by NMR spectroscopy. On completion of heated reactions, the sample was passed through a short alumina plug, washing with CH_2Cl_2. The filtrate was concentrated to afford **8** as a yellow solid. Yield: 5.6 mg (26 %) from **5**; 5.9 mg (27 %) from **7**.

^{1}H NMR ($CDCl_3$, 300 MHz) δ 7.66 – 7.70 (m, 8 H, Ar^F), 7.48 (br, 4H, Ar^F), 7.41 (t, $^3J_{HH}$ = 7.7, 1H, py), 7.16 (d, $^3J_{HH}$ = 7.7, 2H, py), 7.00 (d, $^3J_{HH}$ = 1.5, 2H, imid), 6.80 (d, $^3J_{HH}$ = 1.5, 2H, imid), 6.23 (d, $^2J_{HH}$ = 15, 2H, pyCH_2), 5.00 (d, $^2J_{HH}$ = 15, 2H, pyCH_2), 4.66 – 4.78 (m, 2H, *N*-CH_2), 3.65 – 3.79 (m, 2H, *N*-CH_2), 1.97 (br, 2H, CH_2), 1.61 (br, 2H, CH_2), 1.08 – 1.46 (m, 16H, CH_2).

Generation of [Ni(2c)Cl][BAr$^F_4$] (8) from *in-situ* 5: A mixture of [**2c**].2HBr (100 mg, 0.179 mmol), Ag_2O (45 mg, 0.194 mmol) and Na[BAr$^F_4$] (172 mg, 0.194 mmol) in CH_2Cl_2 (3 mL) was stirred in the absence of light for 16 hours before filtering onto a solution of $[NiCl_2(DME)]$ (40 mg, 0.182 mmol) in CH_2Cl_2 (*ca*. 3 mL). Stirring the resulting yellow solution for 6 h afforded a yellow suspension, which was filtered before purification on alumina to give the product as a yellow powder. Yield: 70 mg (29 %). Crystal suitable for XRD were grown from a mixture of toluene, Et_2O, cyclohexane and pentane at 20°C.

^{1}H NMR (500 MHz, CD_2Cl_2): δ 7.82 (t, $^3J_{HH}$ = 7.7, 1H, py), 7.72 (s, 8H, Ar^F), 7.55 (s, 4H, Ar^F), 7.45 (d, $^3J_{HH}$ = 7.7, 2H, py), 7.11 (d, $^3J_{HH}$ = 1.7, 2H, imid), 6.87 (d, $^3J_{HH}$ = 1.7, 2H, imid), 6.30 (d, $^2J_{HH}$ = 14.9, 2H, pyCH_2), 5.14 (d, $^2J_{HH}$ = 15.0, 2H, pyCH_2), 4.73 (app. t, *J* = 11, 2H, *N*-CH_2), 3.68 – 3.78 (m,

2H, *N*-CH_2), 1.94 (br, 2H, CH_2), 1.63 – 1.68 (m, 2H, CH_2), 1.34 – 1.42 (m, 12 H, CH_2), 1.27 (br, 2H, CH_2), 1.09 (br, 2H, CH_2). **^{13}C{^{1}H} NMR** (126 MHz, CD_2Cl_2): δ 162.3 (q, $^1J_{CB}$ = 50, Ar^F) 162.0 (s, Ni-C), 156.5 (s, py), 140.9 (s, py), 135.3 (s, Ar^F), 129.4 (qq, $^2J_{FC}$ = 32, $^3J_{CB}$ = 3, Ar^F), 125.2 (q, $^1J_{CF}$ = 273, Ar^F), 125.1 (s, py), 123.0 (s, imid), 121.4 (s, imid), 118.0 (quint, $^3J_{FC}$ = 4, Ar^F), 55.0 (s, py*C*H_2), 51.3 (s, *N*-*C*H_2), 30.83 (s, *N*-CH$_2$*C*H$_2$), 28.7 (s, *C*H_2), 27.5 (s, *C*H_2), 23.7 (s, *C*H_2). **ESI-HRMS** (CH_3CN, 180 °C, 4 kV) positive ion: 498.1929 *m/z*, $[M]^+$ (calc. 498.1929). **Elemental Analysis** Calc. for $C_{57}H_{47}BClF_{24}N_5Ni$ (1362.95 g mol^{-1}): C, 50.23; H, 3.48; N, 5.14. Found: C, 50.62; H, 3.74; N, 5.12.

Generation of [Rh(2c)(CO)][BAr$^F_4$] (9) from isolated 5 or 7: Use of 1.1 equiv. (0.0088 mmol) of $[Rh(CO)_2Cl]_2$ with **5** or **7** achieved total consumption of the starting materials in 2 h. Due to the air sensitivity of **9**, the sample was passed through a short Si plug under an atmosphere of nitrogen, washing with CH_2Cl_2. The filtrate was concentrated to obtain **9** as a yellow solid which was analysed by ^{1}H NMR spectroscopy in CD_2Cl_2 under argon. Yield using **7**: 9 mg (82 %). ^{1}H NMR data as for larger-scale synthesis, *vide infra*.

Generation of [Rh(2c)(CO)][BAr$^F_4$] (9) from *in-situ* 5: A mixture of [**2c**].2HBr (100 mg, 0.176 mmol), Ag_2O (41 mg, 0.176 mmol) and Na[BAr$^F_4$] (170 mg, 0.192 mmol) in CH_2Cl_2 (3 mL) was stirred in the absence of light for 16 hours. A solution of $[Rh(CO)_2Cl]_2$ (34 mg, 0.088 mmol) in CH_2Cl_2 (*ca*. 3 mL) was added and the yellow suspension stirred for a further 5 hours. The solution was filtered and the filtrate reduced to dryness in vacuo to afford the crude product. Purification was achieved by passing through a silica pad using CH_2Cl_2 eluent to give a vibrant yellow oil. To a solution of the oil in Et_2O was added hexane and the resulting suspension sonicated. The precipitate was filtered and washed with hexane to give **9** as a yellow powder. Yield: 129 mg (52 %).

^{1}H NMR (400 MHz, CD_2Cl_2) δ 7.89 (t, $^3J_{HH}$ = 7.7, 1H, py), 7.72 (m, 8H, Ar^F), 7.47 – 7.59 (m, 6H, py + Ar^F), 7.15 (d, $^3J_{HH}$ = 1.9, 2H, imid), 7.01 (d, $^3J_{HH}$ = 1.9, 2H, imid), 5.46 (d, $^2J_{HH}$ = 14.6, 2H, py*C*H_2), 5.04 (d, $^2J_{HH}$ = 14.8, 2H, py*C*H_2), 4.30 (m, 2H, *N*-*C*H_2), 3.99 (m, 2H, *N*-*C*H_2), 1.94 (m, 2H, CH_2), 1.84 (m, 2H, CH_2), 1.05 – 1.53 (m, 16H, CH_2). **^{13}C{^{1}H} NMR** (101 MHz, CD_2Cl_2) δ 194.0 (d, $^1J_{RhC}$ = 80, carbonyl), 181.8 (d, $^1J_{RhC}$ = 38, carbene), 162.3 (q, $^1J_{BC}$ = 50, Ar^F), 156.0 (s, py), 141.5 (s, py), 135.4 (s, Ar^F), 129.4 (q, $^2J_{CF}$ = 32, Ar^F), 125.2 (q, $^1J_{CF}$ = 273, Ar^F), 124.9 (s, py), 121.9 (s, imid), 121.5 (s, imid), 118.0 (s, Ar^F), 55.9 (s, py*C*H_2), 51.5 (s, *N*-*C*H_2), 31.6 (s, CH_2), 28.0 (s, CH_2), 27.9 (s, CH_2), 27.9 (s, CH_2), 24.6 (s, CH_2). **ESI-HRMS** (CH_3CN, 180 °C, 3 kV) positive ion: 536.190 *m/z*, $[M]^+$ (calc. 536.1891). **Elemental Analysis** Calc. for $C_{58}H_{47}BF_{24}N_5ORh$ (1399.70 g mol^{-1}): C, 49.77; H, 3.38; N, 5.00. Found: C, 49.92; H, 3.40; N, 5.21. **IR (CH_2Cl_2)** *ν*(CO) 1978 cm^{-1}; **IR (C_6H_6)** *ν*(CO)

1972 cm^{-1}. **UV-vis** (Cary 60, Agilent, CH_2Cl_2, 0.04mM) 304.3 nm (ε = 7779 $mol^{-1}dm^3cm^{-1}$), 394.5 nm (ε = 3529 $mol^{-1}dm^3cm^{-1}$) and 440.0 nm (ε = 1669 $mol^{-1}dm^3cm^{-1}$).

2.4.2 Variable Temperature NMR Experiments and Simulations

All measurements were performed using a DRX-500 spectrometer. Samples (0.014 M in CD_2Cl_2) were prepared in J. Young's NMR tubes under inert atmosphere and equilibrated at each temperature inside the spectrometer for 10 minutes prior to data acquisition.

Simulation of the fluxional process was conducted by Dr. Adrian Chaplin *via* line shape analysis of the imidazolylidene resonances using gNMR (v4.1.2). The $^3J_{HH}$ coupling constants and the line width parameters were fixed at 1.4 and 1.8 Hz following analysis of the 185 K and 298 K ^{1}H NMR spectra. Due to chemical shift changes of the signals with temperature, $\Delta\delta$ of the interchanging resonances were fixed using the 185 K data. Selected simulated data are shown in **Fig. 2.16**. Eyring analysis of the rate data gave $\Delta H^{\ddagger}$ = 43 ± 4 kJ mol^{-1}, $\Delta S^{\ddagger}$ = -7 ± 17 J $mol^{-1}K^{-1}$ and $\Delta G^{\ddagger}_{298\,K}$ = 45 ± 9 kJ mol^{-1} (**Fig. 2.17**).

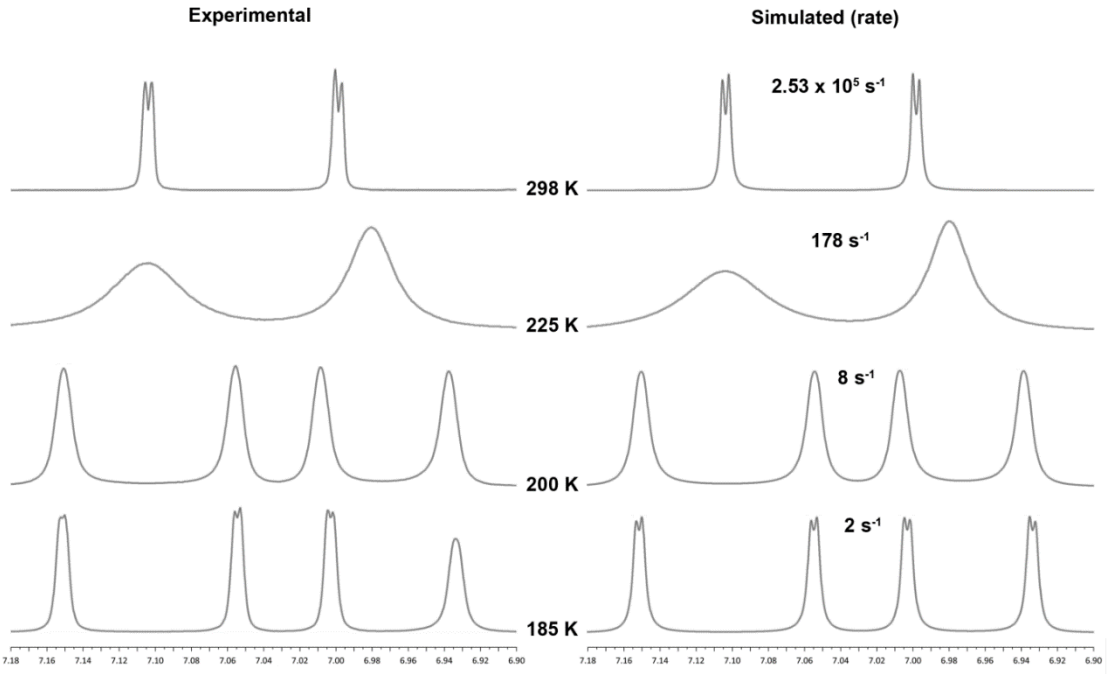

Fig. 2.16: *Selected experimental and simulated ^{1}H NMR spectra featuring the imidazolylidene protons of* ***3a*** *(CD_2Cl_2, 500 MHz).*

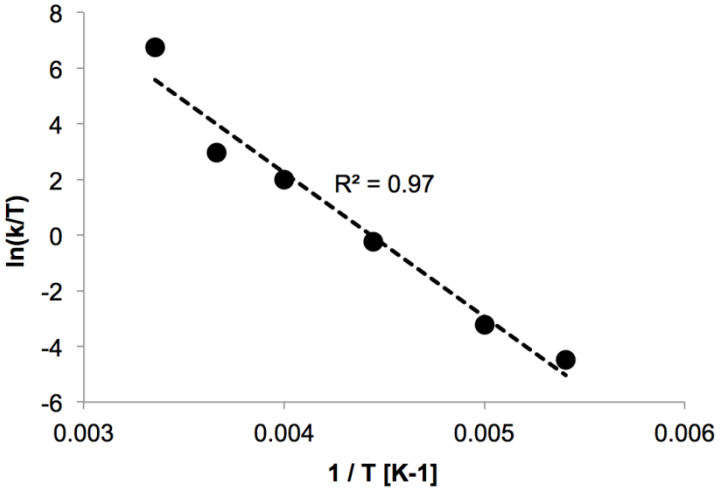

Fig. 2.17: *Eyring plot for the fluxional behaviour observed for* ***3a****.*

2.4.3 Crystallographic Data

Crystallographic data for [**2b**].2HBr, **3a**, **3b**, **3c**, **4a**, **4b**, **5**, **6**, **7** and **8** are summarised in **Table 2.7** and **Table 2.8**. With the exception of **8**, data were collected on an Oxford Diffraction Gemini Ruby CCD diffractometer using graphite monochromated Mo Kα (λ = 0.71073 Å) radiation and a low temperature device [150(2) K]. For **8**, data were collected on an Oxford Diffraction SuperNova AtlasS2 CCD diffractometer using micro-focused Mo Kα (λ = 0.71073) radiation and a low temperature device [150(2) K].

Data for all structures were collected and reduced using CrysAlisPro. All non-hydrogen atoms were refined anisotropically using SHELXL,[53] through the Olex2 interface.[54] Hydrogen atoms were placed in calculated positions using the riding model.

Table 2.7: *Crystallographic data for [**2b**].2HBr, **3a-c**, **4a** and **4b**.*

	[2b].2HBr · MeCN	3a	3b · 0.5(pentane)	3c · (OEt_2)	4a	4b
CCDC[a]/ID code	961289[a]	961290[a]	961291[a]	961292[a]	961293[a]	961294[a]
Figure	**2.2**	**2.3**	**2.3**	**2.3**	**2.8**	**2.8**
Formula	$C_{25}H_{36}Br_2N_6$	$C_{53}H_{39}BClF_{24}N_5Pd$	$C_{57.5}H_{49}BClF_{24}N_5Pd$	$C_{61}H_{57}BClF_{24}N_5OPd$	$C_{53}H_{39}BF_{25}N_5Pd$	$C_{55}H_{43}BF_{25}N_5Pd$
M	580.42	1354.55	1418.67	1484.77	1338.10	1366.15
Crystal system	Monoclinic	Triclinic	Monoclinic	Orthorhombic	Triclinic	Monoclinic
Space group	$P2_1$	$P\bar{1}$	$P2_1/c$	$P2_12_12_1$	$P\bar{1}$	C2/c
***T* [K]**	150(2)	150(2)	150(2)	150(2)	150(2)	150(2)
***a* [Å]**	8.6112(4)	13.8039(3)	12.92329(18)	9.7194(4)	12.7226(2)	35.3011(14)
***b* [Å]**	36.1437(11)	14.2173(3)	25.0749(3)	15.1274(5)	18.5028(3)	16.1372(3)
***c* [Å]**	8.7973(3)	15.6408(3)	19.5371(2)	43.507(2)	25.0641(5)	27.1414(11)
***α* [°]**	90	93.0635(17)	90	90	83.7891(16)	90
***β* [°]**	91.596(4)	102.8239(17)	108.9205(15)	90	78.0669(17)	133.337(7)
***γ* [°]**	90	110.5834(19)	90	90	82.1611(16)	90
***V* [$Å^3$]**	2737.01(17)	2772.73(10)	5988.95(13)	6396.7(5)	5699.2(2)	11245.5(12)
***Z* (Z′)**	4 (2)	2	4	4	4 (2)	8
Density [g cm^{-3}]	1.409	1.622	1.573	1.542	1.559	1.614
***μ* (mm^{-1})**	2.985	0.506	0.472	0.447	0.448	0.456
***ϑ* range [°]**	3.2 ≤ θ ≤ 25.0	2.9 ≤ θ ≤ 29.6	3.0 ≤ θ ≤ 27.9	3.1 ≤ θ ≤ 25.0	2.9 ≤ θ ≤ 25.7	2.9 ≤ θ ≤ 27.9
Reflns collected	19071	78258	88555	28972	50701	34662
R_{int}	0.0327	0.0360	0.0292	0.0820	0.0325	0.0319
Completeness [%]	99.8	99.9	99.9	99.7	99.8	99.8
No. of data/restr/param	9360/223/619	15538/605/850	14249/964/968	11264/753/934	21631/3975/2076	13379/710/836
R_1 **[I > 2σ(I)]**	0.0495	0.0358	0.0392	0.0937	0.0720	0.0412
wR_2 **[all data]**	0.1238	0.0862	0.0975	0.2105	0.1988	0.0988
GoF	1.101	1.021	1.058	0.2105	1.022	1.016
Largest diff. pk and hole [e $Å^{-3}$]	1.52/−0.47	0.82/−0.56	1.03/−0.57	2.11/−1.24	2.60/−1.27	0.93/−0.75
Flack (*x*)	0.024(15)	n/a	n/a	0.47(7)	n/a	n/a

[a] *Full crystallographic details are documented in CIF format and have been deposited with the Cambridge Crystallographic Data Centre. These data can be obtained free of charge via* ***www.ccdc.cam.ac.uk/data_request/cif***

Table 2.8: *Crystallographic data for* ***5 – 8.***

	5	**6**	**7**	**8**
CCDC[a]/ID code	1470494	1470495	1470496	1470497
Figure	**2.10**	**2.13**	**2.14**	**2.15**
Formula	$C_{114}H_{94}Ag_2B_2F_{48}N_{10}$	$C_{50}H_{70}Br_4Cu_4N_{10}$	$C_{57}H_{47}BCuF_{24}N_5$	$C_{57}H_{47}BClF_{24}N_5Ni$
M	2753.35	1384.96	1332.34	1362.96
Crystal system	Triclinic	Triclinic	Triclinic	Triclinic
Space group	P-1	P-1	P-1	P-1
***T* [K]**	150(2)	150(2)	150(2)	150(2)
***a* [Å]**	14.2080(4)	8.2779(2)	17.1195(4)	9.7990(4)
***b* [Å]**	14.8298(4)	10.9565(3)	18.1157(4)	14.7487(6)
***c* [Å]**	14.8366(4)	15.7732(5)	20.2735(4)	21.7093(12)
***α* [°]**	101.908(2)	100.004(2)	96.1858(17)	101.223(4)
***β* [°]**	91.158(2)	96.750(2)	103.2036(19)	99.989(4)
***γ* [°]**	109.055(2)	106.179(2)	90.5067(17)	101.393(3)
***V* [Å^3]**	2878.22(14)	1332.03(6)	5997.6(2)	2942.7(2)
***Z* (Z')**	1	1	4	2
Density [g cm^{-3}]	1.588	1.727	1.476	1.538
***μ* (mm^{-1})**	0.472	4.620	0.481	0.494
***ϑ* range [°]**	3.0 ≤ θ ≤ 27.1	3.0 ≤ θ ≤ 27.1	2.9 ≤ θ ≤ 27.1	3.2 ≤ θ ≤ 25.7
Reflns collected	67823	19990	86052	13369
R_{int}	0.0314	0.0392	0.0575	0.1528
Completeness [%]	99.9	99.9	99.9	99.8
No. of data/restr/param	12668/690/902	5863/0/307	26394/1974/1777	13369/342/858
R_1 **[I > 2σ(I)]**	0.0557	0.0292	0.0594	0.0643
wR_2 **[all data]**	0.1561	0.0685	0.1664	0.1479
GoF	1.059	1.036	1.015	1.048
Largest diff. pk and hole [e Å^{-3}]	1.11/-0.59	0.61/-0.74	1.11/-0.62	0.53/-0.47
Flack (*x*)	n/a	n/a	n/a	n/a

[a] *Full crystallographic details are documented in CIF format and have been deposited with the Cambridge Crystallographic Data Centre. These data can be obtained free of charge via* ***www.ccdc.cam.ac.uk/data_request/cif***

2.5 References

(1) Radloff, C.; Gong, H.-Y.; Schulte to Brinke, C.; Pape, T.; Lynch, V. M.; Sessler, J. L.; Hahn, F. E. *Chem. Eur. J.* **2010**, *16*, 13077-13081.
(2) Kumar, S.; Gupta, S. K. *Tetrahedron Letters* **2010**, *51*, 5459-5462.
(3) Gil-Rubio, J.; Cámara, V.; Bautista, D.; Vicente, J. *Inorg. Chem.* **2013**, *52*, 4071-4083.
(4) Nielsen, D. J.; Cavell, K. J.; Skelton, B. W.; White, A. H. *Inorg. Chim. Acta* **2006**, *359*, 1855-1869.
(5) Tulloch, A. A. D.; Danopoulos, A. A.; Winston, S.; Kleinhenz, S.; Eastham, G. *J. Chem. Soc., Dalton Trans.* **2000**, 4499-4506.
(6) Simons, R. S.; Custer, P.; Tessier, C. A.; Youngs, W. J. *Organometallics* **2003**, *22*, 1979-1982.
(7) Nielsen, D. J.; Cavell, K. J.; Skelton, B. W.; White, A. H. *Inorg. Chim. Acta* **2002**, *327*, 116-125.
(8) Buschmann, W. E.; Miller, J. S.; Bowman-James, K.; Miller, C. N. In *Inorg. Synth.*; John Wiley & Sons, Inc.: 2002, p 83-91.
(9) Miecznikowski, J. R.; Grundemann, S.; Albrecht, M.; Megret, C.; Clot, E.; Faller, J. W.; Eisenstein, O.; Crabtree, R. H. *Dalton Trans.* **2003**, 831-838.
(10) Tulloch, A. A. D.; Danopoulos, A. A.; Tizzard, G. J.; Coles, S. J.; Hursthouse, M. B.; Hay-Motherwell, R. S.; Motherwell, W. B. *Chem. Commun.* **2001**, 1270-1271.
(11) Danopoulos, A. A.; Tulloch, A. A. D.; Winston, S.; Eastham, G.; Hursthouse, M. B. *Dalton Trans.* **2003**, 1009-1015.
(12) Bröring, M.; Kleeberg, C. *Z. Anorg. Allg. Chem.* **2007**, *633*, 2210-2216.
(13) Szyszko, B.; Latos-Grażyński, L.; Szterenberg, L. *Angew. Chem. Int. Ed.* **2011**, *50*, 6587-6591.
(14) Gründemann, S.; Albrecht, M.; Loch, J. A.; Faller, J. W.; Crabtree, R. H. *Organometallics* **2001**, *20*, 5485-5488.
(15) Kemp, W. *NMR in Chemistry: A Multinuclear Introduction*; MacMillan, 1988.
(16) Huacuja, R.; Herbert, D. E.; Fafard, C. M.; Ozerov, O. V. *J. Fluorine Chem.* **2010**, *131*, 1257-1261.
(17) Sun, H.; DiMagno, S. G. *J. Am. Chem. Soc.* **2005**, *127*, 2050-2051.
(18) So, L.-C.; Liu, C.-C.; Chan, M. C. W.; Lo, J. C. Y.; Sze, K.-H.; Zhu, N. *Chem. Eur. J.* **2012**, *18*, 565-573.
(19) Hahn, F. E.; Jahnke, M. C.; Pape, T. *Organometallics* **2007**, *26*, 150-154.
(20) Hahn, F. E.; Jahnke, M. C.; Gomez-Benitez, V.; Morales-Morales, D.; Pape, T. *Organometallics* **2005**, *24*, 6458-6463.
(21) Watarai, N.; Kawasaki, H.; Azumaya, I.; Yamasaki, R.; Saito, S. *Heterocycles* **2009**, *79*, 531-548.
(22) Anton, D. R.; Crabtree, R. H. *Organometallics* **1983**, *2*, 855-859.
(23) Yu, K.; Sommer, W.; Richardson, J. M.; Weck, M.; Jones, C. W. *Adv. Synth. Catal.* **2005**, *347*, 161-171.
(24) Chapman, M. R.; Shafi, Y. M.; Kapur, N.; Nguyen, B. N.; Willans, C. E. *Chem. Commun.* **2015**, *51*, 1282-1284.
(25) Furst, M. R. L.; Cazin, C. S. J. *Chem. Commun.* **2010**, *46*, 6924-6925.
(26) Arnold, P. L.; Scarisbrick, A. C.; Blake, A. J.; Wilson, C. *Chem. Commun.* **2001**, 2340-2341.
(27) Bezuidenhout, D. I.; Kleinhans, G.; Guisado-Barrios, G.; Liles, D. C.; Ung, G.; Bertrand, G. *Chem. Commun.* **2014**, *50*, 2431-2433.
(28) Kwong, R. C.; Universal Display Corporation, USA . 2011, p 108pp.; Chemical Indexing Equivalent to 156:90028 (WO).
(29) Liu, X.; Pattacini, R.; Deglmann, P.; Braunstein, P. *Organometallics* **2011**, *30*, 3302-3310.
(30) Nakamura, T.; Ogushi, S.; Arikawa, Y.; Umakoshi, K. *J. Organomet. Chem.* **2016**, *803*, 67-72.

(31) Chen, C.; Qiu, H.; Chen, W. *J. Organomet. Chem.* **2012**, *696*, 4166-4172.
(32) Han, Y.-F.; Jin, G.-X.; Daniliuc, C. G.; Hahn, F. E. *Angew. Chem. Int. Ed.* **2015**, *54*, 4958-4962.
(33) Garrison, J. C.; Simons, R. S.; Kofron, W. G.; Tessier, C. A.; Youngs, W. J. *Chem. Commun.* **2001**, 1780-1781.
(34) Sinha, N.; Roelfes, F.; Hepp, A.; Mejuto, C.; Peris, E.; Hahn, F. E. *Organometallics* **2014**, *33*, 6898-6904.
(35) Segarra, C.; Guisado-Barrios, G.; Hahn, F. E.; Peris, E. *Organometallics* **2014**, *33*, 5077-5080.
(36) Nielsen, D. J.; Magill, A. M.; Yates, B. F.; Cavell, K. J.; Skelton, B. W.; White, A. H. *Chem. Commun.* **2002**, 2500-2501.
(37) Biffis, A.; Cipani, M.; Bressan, E.; Tubaro, C.; Graiff, C.; Venzo, A. *Organometallics* **2014**, *33*, 2182-2188.
(38) Biffis, A.; Cipani, M.; Tubaro, C.; Basato, M.; Costante, M.; Bressan, E.; Venzo, A.; Graiff, C. *New J. Chem.* **2013**, *37*, 4176-4184.
(39) Caytan, E.; Roland, S. *Organometallics* **2014**, *33*, 2115-2118.
(40) Diez-Gonzalez, S.; Escudero-Adan, E. C.; Benet-Buchholz, J.; Stevens, E. D.; Slawin, A. M. Z.; Nolan, S. P. *Dalton Trans.* **2010**, *39*, 7595-7606.
(41) Liu, B.; Zhang, Y.; Xu, D.; Chen, W. *Chem. Commun.* **2011**, *47*, 2883-2885.
(42) Catalano, V. J.; Munro, L. B.; Strasser, C. E.; Samin, A. F. *Inorg. Chem.* **2011**, *50*, 8465-8476.
(43) Liu, X.; Chen, W. *Organometallics* **2012**, *31*, 6614-6622.
(44) Large-scale synthesis and full characterisation of nickel complex conducted by Caroline Storey
(45) Yoshida, K.; Horiuchi, S.; Takeichi, T.; Shida, H.; Imamoto, T.; Yanagisawa, A. *Org. Lett.* **2010**, *12*, 1764-1767.
(46) Inamoto, K.; Kuroda, J.-i.; Kwon, E.; Hiroya, K.; Doi, T. *J. Organomet. Chem.* **2009**, *694*, 389-396.
(47) Large-scale synthesis and full characterisation of nickel complex conducted by Caroline Storey
(48) Zhang, J.; Leitus, G.; Ben-David, Y.; Milstein, D. *Angew. Chem. Int. Ed.* **2006**, *45*, 1113-1115.
(49) Feller, M.; Ben-Ari, E.; Gupta, T.; Shimon, L. J. W.; Leitus, G.; Diskin-Posner, Y.; Weiner, L.; Milstein, D. *Inorg. Chem.* **2007**, *46*, 10479-10490.
(50) Bertz, S. H.; Fairchild, E. H.; Denissova, I.; Barriault, L. In *Encyclopedia of Reagents for Organic Synthesis*; John Wiley & Sons, Ltd: 2004.
(51) Theis, A. B.; Townsend, C. A. *Synth. Commun.* **1981**, *11*, 157-166.
(52) McCleverty, J. A.; Wilkinson, G.; Lipson, L. G.; Maddox, M. L.; Kaesz, H. D. In *Inorg. Synth.*; John Wiley & Sons, Inc.: 2007, p 84-86.
(53) Sheldrick, G. *Acta Crystallogr. Sect. A* **2008**, *64*, 112-122.
(54) Dolomanov, O. V.; Bourhis, L. J.; Gildea, R. J.; Howard, J. A. K.; Puschmann, H. *J. Appl. Crystallogr.* **2009**, *42*, 339-341.

CHAPTER 3. RHODIUM CARBONYL COMPLEXES

Having established that the dodecamethylene-spaced ligand **2c** is of optimal size for accommodating a transition metal and a small molecular or ionic ligand, the focus of the project turned to complexes of this macrocycle with rhodium (*i.e.* **9**, **Fig. 3.1**). This chapter details the study of **9**; its structural behaviour and reactivity, alongside complementary studies of **Type I** variant **10**. Particular attention is given to the dynamic behaviour of **9** and its reactivity under basic conditions. **Type I** system **10** displays greater stability in higher oxidation states and a rhodium(III) derivative was further investigated for its application in transmetallation reactions.

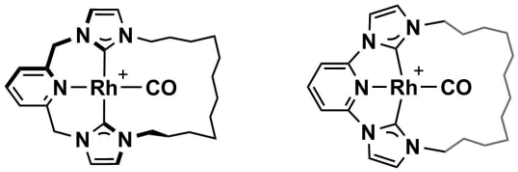

9 **10**

Fig. 3.1: *Structures of **9** and **10**.*

Publications resulting from work described in this chapter:

1. Andrew, R. E.; Chaplin, A. B. *Inorg. Chem.* **2015**, *54*, 312-322.
2. Andrew, R. E.; Ferdani, D. W.; Ohlin, C. A.; Chaplin, A. B. *Organometallics* **2015**, *34*, 913-917.

3.1 Synthesis and Characterisation of Rhodium(I) Carbonyl Complexes

While Pd(CNC)X complexes represent a significant proportion of reported NHC-based pincers (17 % of CEC complexes in the CSD database and present in *ca*. 26 % of articles where CEC pincers are discussed, as of September 2015), rhodium variants are limited to a handful of examples; these include **Type I** adducts **A114**[1-4] and **A34** and **A115**[5-7], which bear rigid anionic pincer ligands (**Fig. 3.2**). Where a neutral carbonyl is the ancillary ligand, these complexes undergo facile oxidative addition of organohalides, with adducts of MeI,[2,5] CD_2Cl_2[3] and benzyl and allyl halides[6] reported. Promoted by the strong *trans* influence of the amido group, rhodium(III) derivatives of **A34** demonstrate carbonyl exchange at room temperature, a feature probed using ^{13}CO and not observed for the rhodium(I) precursor.

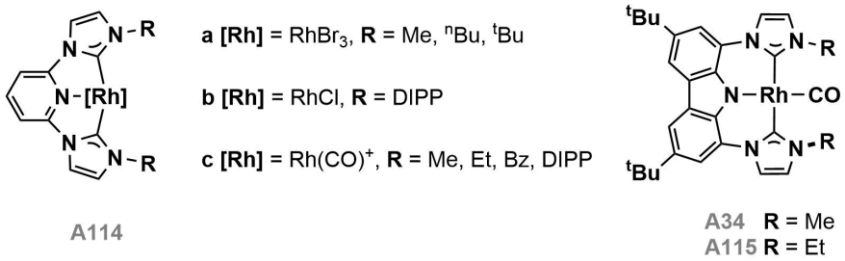

Fig. 3.2: *Rh(CNC)X precedents **A114, A34** and **A115**.*

As discussed in **Chapter 2**, complex **9** can be prepared in good yield *via* transmetallation from silver transfer agent **5**, either generated *in-situ* (52 % yield from [**2c**].2HBr) or isolated (*ca*. 59 % yield from [**2c**].2HBr over two steps). Attempts at utilising similar protocols for the synthesis of **10** were hindered by difficulty accessing the corresponding ligand precursor ([**11**].2HBr). Adaptation of routine literature procedures for the preparation of C-N-C pro-ligands instead afforded intractable mixtures, of which the target was only a minor component (**Scheme 3.1**).

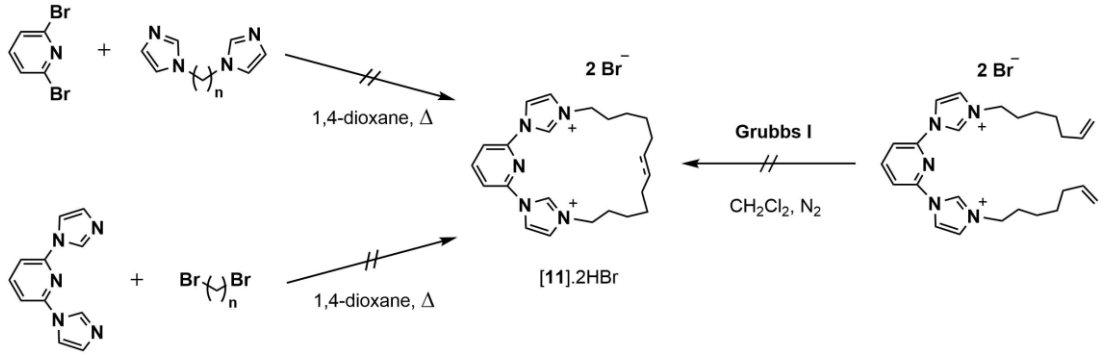

Scheme 3.1: *Attempted synthetic routes to ligand [**11**].2HBr.*

Minimising the production of oligomeric mixtures, *passive-metal* template synthesis (see **Chapter 1**, **Section 1.3.3**) is an established route to macrocyclic structures, with coordination of a metal centre favouring the macrocyclic product.[8] For example, Gladysz and co-workers

have demonstrated the effectiveness of this strategy by utilising a rhodium-template for ring-closing reactions, enabling preparation of gyroscope-like rhodium(I) carbonyl complexes **A116** in moderate yields following hydrogenation (**Scheme 3.2**).[9,10]

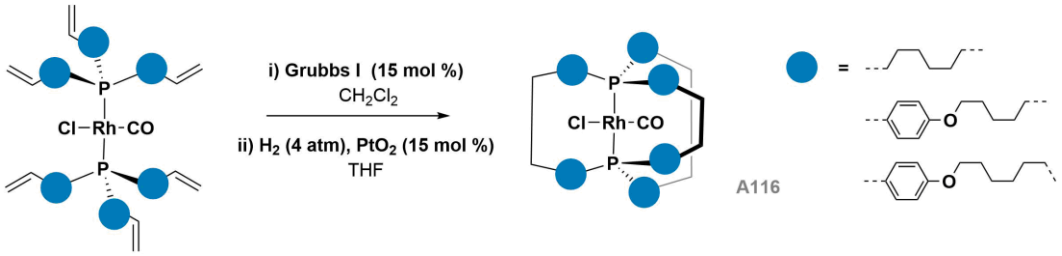

Scheme 3.2: *Example of passive-metal template synthesis using rhodium.*

Inspired by this example, a route to macrocyclic **9** and **10** employing acyclic bis(alkene) pro-ligands [**12**].2HBr was designed. These pro-ligands were readily synthesised using two-step alkylation procedures involving 7-bromo-1-heptene, imidazole and a suitable pyridine precursor (**Scheme 3.3**). Complexation using a modification of the *in-situ* transmetallation procedure previously employed for **3**, **8** and **9** afforded acyclic rhodium complexes **13** in moderate yields after purification on silica (58 %, **13a**; 83 %, **13b**). Complexes **13** are prone to alkene isomerisation during the transmetallation reaction and multiple modifications to the aforementioned reaction protocol were necessary to obtain pure samples (details in **Section 3.6.1.2**). On isolation, **13** are stable indefinitely in the solid-state and for up to 2 days in solution (CD_2Cl_2, under argon).

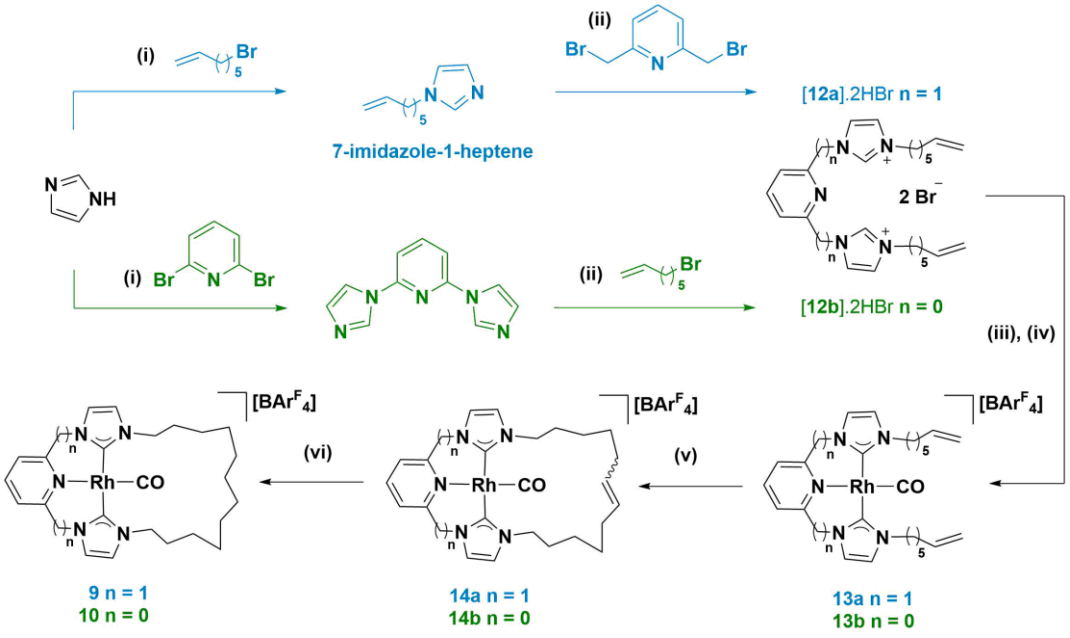

Scheme 3.3: *Template synthesis of **9** and **10**.*
(i) NaH, THF, reflux; (ii) 1,4-dioxane, reflux; (iii) Ag_2O, $Na[BAr^F_4]$, CH_2Cl_2 then (iv) $[Rh(CO)_2Cl]_2$; (v) Grubbs I (5-10 mol %), CH_2Cl_2, N_2; (vi) Pd/C (20 mol %), H_2 (4 bar), CH_2Cl_2 or $[Ir(COD)(py)(PCy_3)][BAr^F_4]$ (10 mol %), H_2 (1 bar), CH_2Cl_2.

Analytically pure bis-alkenes **13** were cyclised using Grubbs' 1st generation olefin metathesis catalyst (5 mol %). Consistent with the planar nature of **Type I** variant **13b**, where the alkene-terminated chains are directed into the same plane, metathesis is complete within 1 h (as determined by ESI-LRMS). Under the same conditions **13a**, which bears orthogonally-directed pendant alkenes, demonstrates only 69 % conversion and required addition of a further 5 mol % of catalyst to complete the ring-closing. After purification on silica to remove ruthenium salts, the internal-alkene intermediates **14a** (n = 1) and **14b** (n = 0) were isolated in high yield (95 % and 82 %, respectively) as mixtures of *E*- and *Z*-isomers, as determined by ^{1}H NMR spectroscopy (see **Section 3.6.1.2**).

Hydrogenation of **14a** (20 mol % Pd/C, 4 atm H_2) afforded **9** in 82 % yield after filtration, but as a further indication of the different reactivity of the two macrocycles, **10** was found to be unstable under the reaction conditions. Instead, rapid and selective hydrogenation of **14b** was effected using [Ir(COD)(py)(PCy_3)][BAr^F_4] (10 mol %) under 1 atm H_2.[11] Overall, **9** and **10** were obtained in high isolated yields from **14** (82 % (**9**); 83 % (**10**)). Despite the greater number of steps starting from bis(bromomethyl)pyridine, preparation of **9** *via* the template-synthesis route was achieved with an improved yield (43 %) compared to the one-pot procedure (20 %, *vide supra*). The lower yield *via* the latter procedure is attributed to lack of selectivity during the preparation of [**2c**].2HBr (**Scheme 2.1**, **Chapter 2**), thus demonstrating a clear advantage of the template approach.

Complexes **9**, **10** and **13** were fully characterised by ^{1}H, ^{13}C NMR, IR and UV-vis spectroscopy (*vide infra*), ESI-HRMS and elemental analysis. Each of the rhodium carbonyl complexes exhibit strong cation signals in their mass spectra with no loss of the carbonyl group. Microanalysis values are also consistent with the general formula [Rh(L)(CO)][BAr^F_4] (L = **2c**, **11** or **12**). In addition, the solid-state structures of **9** and **10** were determined by XRD (**Fig. 3.3**). Two polymorphs of **9** were obtained by variation of crystallisation conditions (Et_2O/hexane, N_2; CH_2Cl_2/pentane, CO), with the structure determined *via* crystallisation under CO (1 atm) denoted **9***.[12,13] Key solution and solid-state metrics are compiled in **Table 3.1**.

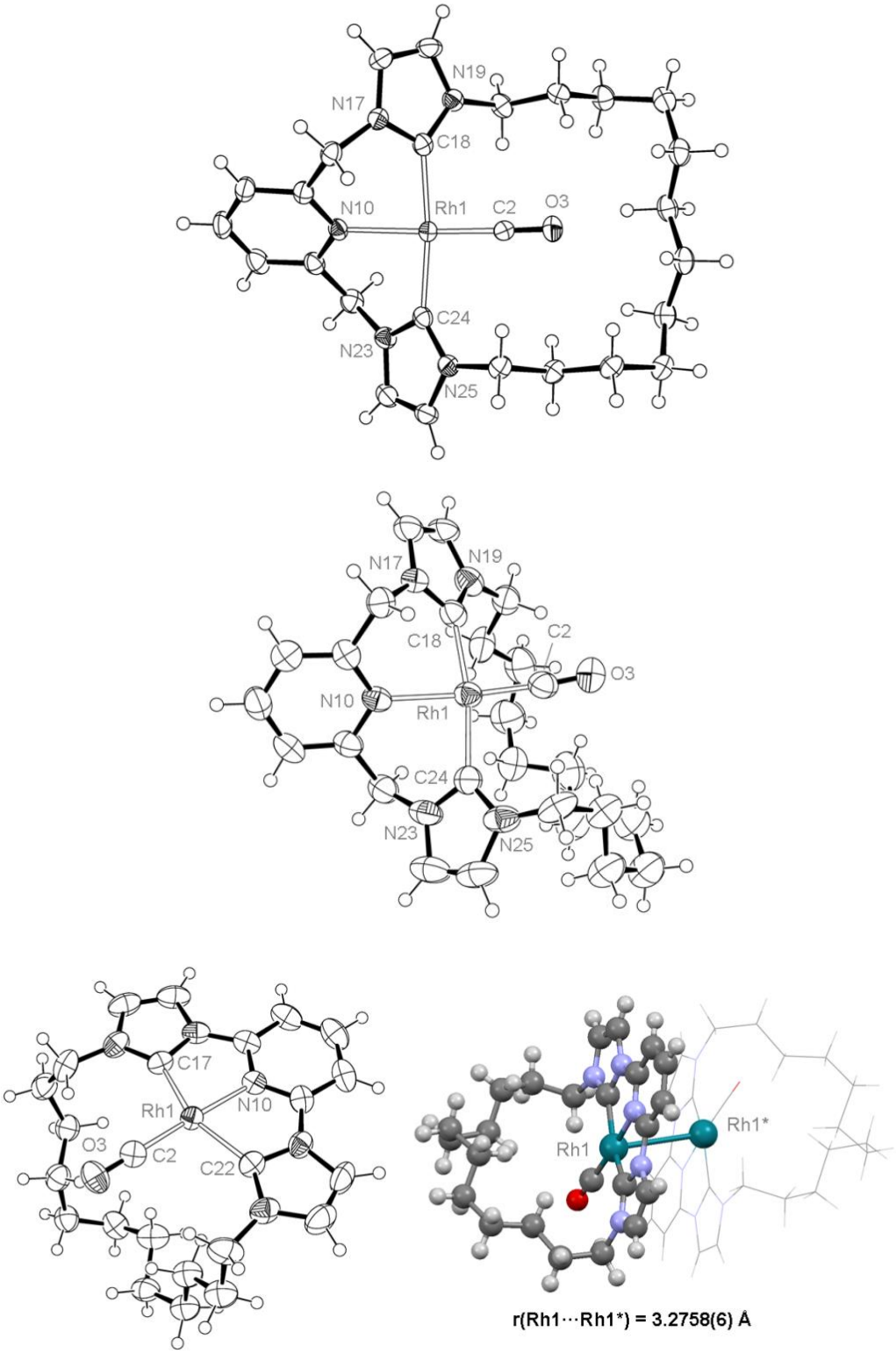

Fig. 3.3: *ORTEP representations of* ***9*** *(**top**),* ***9**** *(**middle**) and* ***10*** *(**bottom left**, as one half of dimer). Thermal ellipsoids at 50 %. [BAr$^{F}_{4}$]$^{-}$ counter anions omitted for clarity. Ball-and-stick structure of dimeric* ***10*** *shown with highlighted Rh···Rh interaction (**bottom right**).*

Table 3.1: *Selected solid-state metrics and spectroscopic data for* ***9****,* ***10*** *and* ***13****.*

	9	**9***	**13a**	**10**	**13b**
***ν*(CO)** /cm^{-1}	1979; 1972[a]	-	1978	1986; 1977[b]	1990; 1980[b]
δ_{CO} ($^1J_{RhC}$/Hz)	194.0 (80)	-	193.9 (79)	196.8 (78)	-[c]
δ_{NCN} ($^1J_{RhC}$/Hz)	181.8 (42)	-	182.2 (41)	186.5 (48)	186.6 (48)
Rh-C_{CO} /Å	1.804(3)	1.796(9)	-	1.836(4)	-
Rh-C_{NCN} /Å	2.036(3), 2.042(3)	2.020(7), 2.038(7)	-	2.029(4), 2.028(4)	-
Rh-N /Å	2.134(2)	2.150(7)	-	2.027(3)	-
N-Rh-C_{CO} /°	175.2(1)	175.0(4)	-	176.1(1)	-
C_{NCN}-Rh-C_{NCN} /°	172.77(12)	169.9(3)	-	155.18(15)	-

[a] *Recorded in C_6H_6.* [b] *Recorded in MeCN.* [c] *Not observed.*

As for Group 10 congeners utilising palladium (**3c**) and nickel (**8**), **9** is monomeric in the solid-state and adopts *pseudo-*C_2 symmetry with the dodecamethylene spacer arranged in a box-like conformation, slightly skewed to one side. The coordination geometry is square-planar, with N-Rh-C_{CO} and C_{NCN}-Rh-C_{NCN} bond angles that approach linearity; 175.2(1)° and 172.77(12)°, respectively. Demonstrating high flexibility of the dodecamethylene spacer, **9*** has clear C_1 symmetry with the alkyl chain displaced to one side of the coordination plane. However, structural metrics about the rhodium are similar to those of **9**, with no significant distortion of the square planar geometry and near-identical pincer-to-metal bond lengths. Although crystal-packing effects cannot be ruled out, this is hypothesised to be a result of reversible CO coordination during crystallisation, a process that is discussed in more detail in **Section 3.2**.

Further demonstrating high conformational flexibility of the dodecamethylene spacer, ^{1}H and ^{13}C{^{1}H} NMR spectra of **9** display time-averaged C_2 symmetry, which is retained from 298 to 200 K. Characteristic diastereotopic methylene bridge ^{1}H signals (δ 5.46 and 5.04, $^2J_{HH}$ = 14.8 Hz) are near identical to those of **13a** (δ 5.46 and 5.02, $^2J_{HH}$ = 14.7 Hz), suggesting no significant macrocyclic effect. Close agreement is also found between the ^{13}C{^{1}H} NMR spectra of **9** and **13a**, with carbenic and carbonyl resonances observed at *ca*. δ 182 ($^1J_{RhC}$ = *ca*. 41 Hz) and *ca*. δ 194 ($^1J_{RhC}$ = 80 Hz), respectively. The *ν*(CO) stretching bands are near-equivalent in shift, appearing at 1979 cm^{-1} (**9**) and 1978 cm^{-1} (**13a**). Likewise, key maxima in UV-vis spectra are found at 395 and 444 nm for both complexes (CH_2Cl_2, 40 μM). The latter absorption is consistent with the canary yellow appearance of both complexes in solution and in the solid-state (**Fig. 3.4**, **blue lines**).

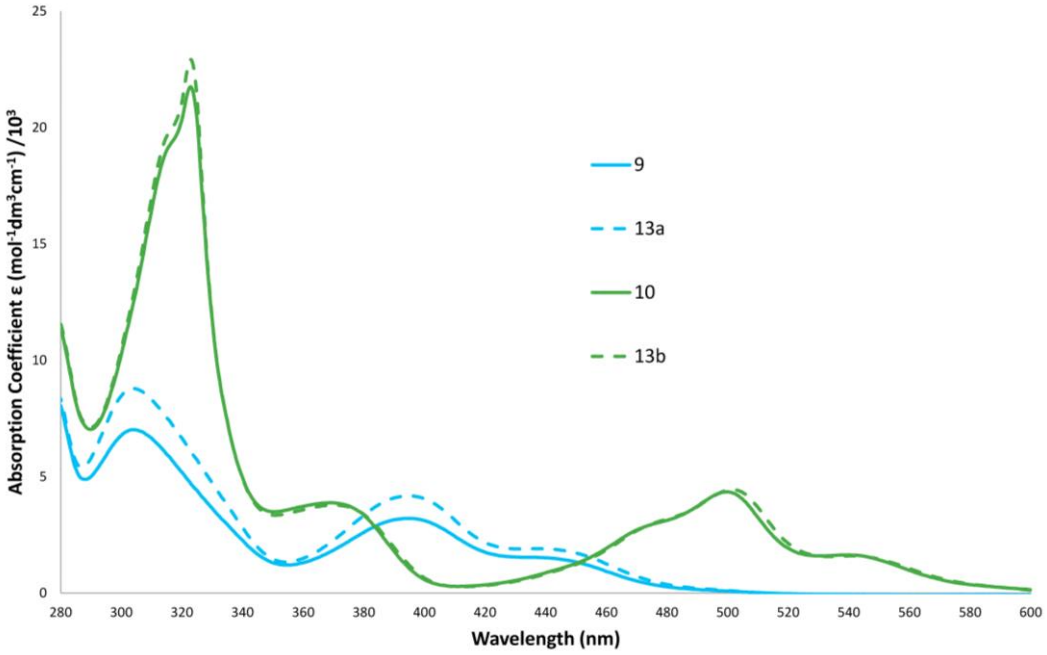

Fig. 3.4: *Superimposed UV-vis absorption spectra of* ***9***, ***13a***, ***10*** *and* ***13b*** *(CH_2Cl_2, 40 μM).*

Interestingly, **Type I** congener **10** crystallises as a di-cationic dimer, featuring an unsupported Rh···Rh interaction of 3.2758(6) Å and clear distortions of each dodecamethylene spacer away from the *anti*-orientated coordination planes. Despite the proximity of another metal, the rhodium exhibits square planar geometry, with a near-linear N-Rh-C_{CO} bond angle of 176.1(1)°. Reflecting the tighter bite angle of the **Type I** pincer, a slightly smaller Rh-N bond distance is observed (2.027(3) Å *c.f.* 2.134(2) Å) and the C_{NCN}-Rh-C_{NCN} bond angle is contracted to 155.18(15)° in **10**, compared with 172.77(12)° in **9**.

Metal-metal interactions are an established feature of many square planar d^8-metal complexes, with various dimeric, trimeric and polymeric chains reported.[14] Pt^{II}-Pt^{II} and Rh^{I}-Rh^{I} dimers are reasonably common and computational studies attribute the interaction to overlap of the d_z^2 and p_z orbitals.[15-21] Bearing resemblance to **10**, a Rh···Rh interaction of 3.3320(6) Å is observed in the solid-state for **A117** (**Fig. 3.5**), where the monomers are oriented in an *anti*-configuration about the metal-metal vector, ruling out stabilisation of the metal-metal bond *via* dispersion forces of the ligand.[20-22] Rh···Rh distances of *ca*. 3.2 Å are also observed for dimeric and trimeric forms of tetra-isocyanide **A118**.

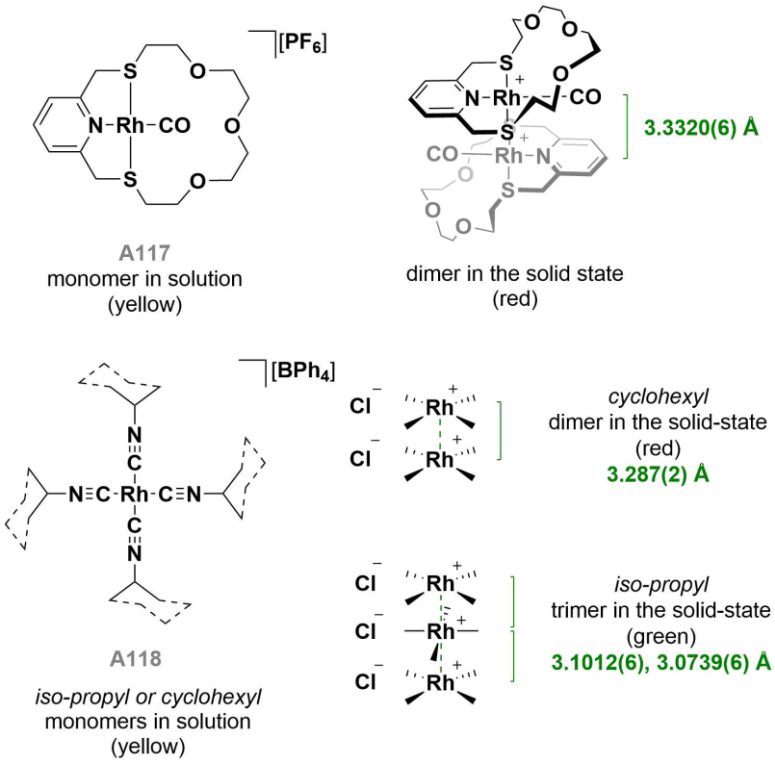

Fig. 3.5 *Rh···Rh interactions in the solid state.*

Contrary to the structure observed in the solid-state, ^{1}H and ^{13}C{^{1}H} NMR spectra of **10** (and **13b**) display time-averaged C_{2v} symmetry at 298 K (CD_2Cl_2, 500 MHz); indicating rapid, facile movement of the *N*-alkyl substituents to either side of the coordination plane. On cooling from 298 to 185 K (CD_2Cl_2, 500 MHz), ^{1}H NMR spectra of **10** show line-broadening then decoalescence (T_c = 225 K, $\Delta G^{\ddagger}_{est}$ = 45 kJ mol^{-1}) of signals for the *N*-$CH_2C\underline{H}_2$ protons, which become diastereotopic. The adoption of apparent C_s symmetry at low temperature suggests movement of the dodecamethylene spacer of **10** is more restricted than in **9**, and is consistent with the alkyl chain being pulled more tightly across the metal centre as a consequence of the more rigid backbone of the **Type I** pincer.

Room temperature ^{13}C{^{1}H} NMR spectra of **10** and **13b** are highly comparable, with carbene resonances at 186.5 and 186.6 ppm, respectively, exhibiting rhodium coupling ($^{1}J_{RhC}$ = 48 Hz). The carbonyl resonance for **13b** could not be located, but may be assumed to be similar to that of **10** ($\delta_{\underline{C}O}$ = 196.8, $^{1}J_{RhC}$ = 78 Hz) given the strong agreement between these and other spectroscopic data (**Table 3.1**). For example, the *ν*(CO) stretching bands of **10** and **13b** obtained from solution IR spectra are in good agreement in both CH_2Cl_2 and MeCN ($\Delta\nu_{(CO)} \leq 4$ cm^{-1}). The ν(CO) values bear close resemblance to those of literature precedents **A114c** in MeCN: 1977 cm^{-1}, **10**; 1980 cm^{-1}, **13b**; 1982 – 1983 cm^{-1}, **A114c** (R = Me, Et, Bz).[2]

Solutions of **10** and **13b** are deep violet with absorption maxima at 475, 500 and 540 nm in their UV-vis spectra (**Fig. 3.4**, **green lines**); values which are concentration invariant for **10**.

Minor changes in wavelength are observed on changing the solvent, but these are eclipsed by remarkable differences in the colour of solvated (as solution in CH_2Cl_2, *purple*), partially solvated (CH_2Cl_2 vapour or suspended in pentane, *green*) and dried samples (*grey*) of both **10** and **13b**.

Equally pronounced solvochromic behaviour has been assigned to solvent-metal and metal-metal interactions in the literature. Notably, **A71** displays striking differences in colour between monomeric (yellow), dimeric (red) and trimeric (green) forms (**Fig. 3.5**).[17] The observation of similarly drastic colour changes between **10** in solution and **10** in the solid-state suggests that the dimer is not retained in solution. This is consistent with the aforementioned concentration-invariant UV-vis absorption spectra, VT ^{1}H NMR data (*vide supra*) and integral-spaced isotopic distribution for the parent ion signal observed by ESI-HRMS.

3.2 Dynamic Behaviour of 9

While no loss of symmetry was observed on cooling CD_2Cl_2 solutions of **9** from 298 to 200 K, ^1H signals for the diastereotopic methylene bridge protons ($\Delta\delta$ = 0.42, $^2J_{HH}$ = 14.3 Hz, 500 MHz) sharpened slightly (Δ_{fwhm} = 5 Hz). Warming of C_6D_6 solutions of **9** resulted in coalescence of these signals (H_a and H_b; T_c = 350 K, C_6D_6, 500 MHz, **Fig. 3.6**) and adoption of time-averaged C_{2v} symmetry. These observations are consistent with atropisomerism between enantiomeric C_2 conformations on the NMR timescale (**Scheme 3.4**). Lineshape analysis of the corresponding VT ^1H NMR spectra (298 – 350 K) was used to calculate an activation barrier of $\Delta G^{\ddagger}_{298\,K}$ = 66 ± 8 kJ mol^{-1}. Estimation of the activation barrier using **Eq. 2.1** (**Chapter 2**) and the parameters of both H_a/H_b and H_c/H_d pairs (**Fig. 3.6**), afforded $\Delta G^{\ddagger}_{est}$ = 66.7 and 67.1 kJ mol^{-1}, respectively, in good agreement with the simulation.

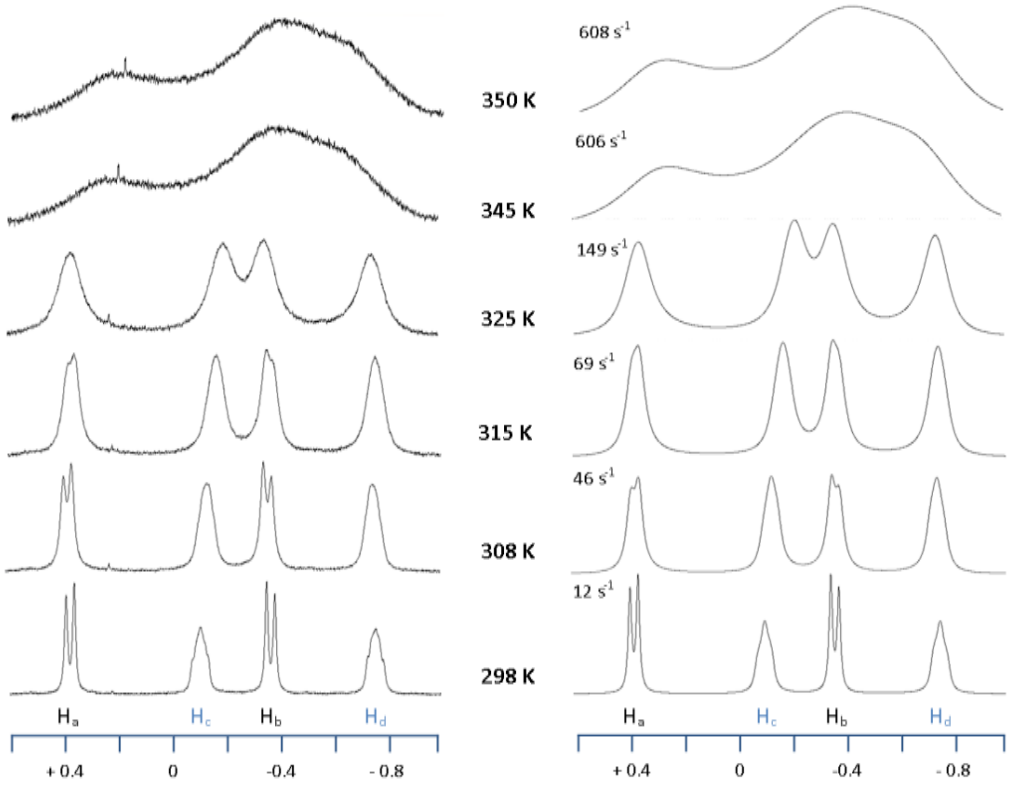

Fig. 3.6: *Experimental (**left**) and simulated (**right**) VT ^1H NMR spectra of **9** (C_6D_6, 500 MHz). The spectra are aligned by the centre of exchange for methylene bridge protons H_a and H_b (x = 0).*

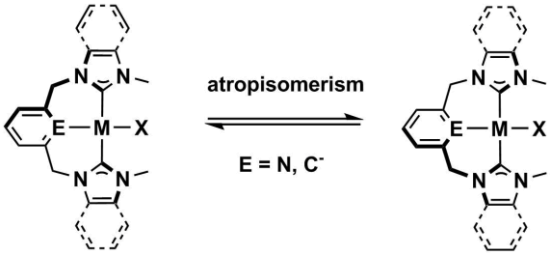

Scheme 3.4: *Atropisomerism of [M(C^E^C^R)X].*

For comparison, an acyclic variant of **9**, [Rh(**C^N^C^{Me}**)(CO)][BAr$^F_4$] (**16**) was prepared from the corresponding silver transfer reagent **15** (**Scheme 3.5**). Complex **16** demonstrates atropisomerism on the NMR timescale and, consistent with a slightly lower barrier to interconversion, the methylene bridge protons appear as broad resonances at room temperature, with the slow exchange limit not reached until 250 K ($\Delta\delta$ = 0.42, $^2J_{HH}$ = 15.1 Hz, CD_2Cl_2, 500 MHz). As for **9**, C_6D_6 solutions of **16** exhibit coalescence of the methylene bridge protons, with T_c = 325 K (500 MHz, for which $\Delta\delta$ = 0.79 and $^2J_{HH}$ = 14 Hz at 285 K). Estimation of the activation barrier using **Eq. 2.1** (**Chapter 2**), afforded $\Delta G^{\ddagger}_{est}$ = 61.5 and 61.1 kJ mol^{-1} for atropisomerism in C_6D_6 and CD_2Cl_2 respectively.

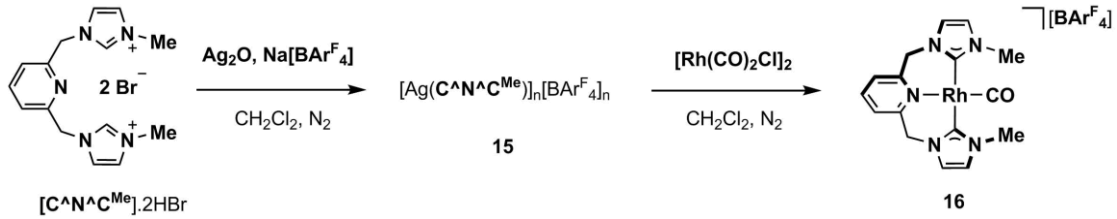

Scheme 3.5: *Synthesis of acyclic **16**.*

Facile atropsiomerism has been noted for a number of palladium complexes.[23-28] In their comprehensive experimental and computational investigation of Pd(C^E^C) systems, Faller, Eisenstein and Crabtree identify two mechanisms for interconversion. The pathway by which the enantiomers interconvert is dependent on the nature of the solvent, counter anion and the identity of central donor 'E'.[23]

In **Pathway A^{Pd}** (**Fig. 3.7**), interconversion occurs through a high-energy distortion of the κ^3-coordinate pincer, affording a puckered intermediate **PdInt$_A$**. Ligand-strain destabilises **PdInt$_A$**, which is not spectroscopically observed and readily reverts back to either C_2 symmetric enantiomer, thus mediating atropisomerism. Palladium complexes [Pd(C^C^C^{Me})X] and [Pd(C^N^C^{Me})X]Y, where X is a halide and Y is a weakly coordinating anion, are believed to undergo atropisomerism *via* this pathway. Coalescence temperatures of such systems are ≥ 340 K, with barrier heights of *ca*. 70 kJ mol^{-1} ($\Delta G^{\ddagger}_{298\,K}$). Higher values are observed when X is a neutral ligand and/or the solvent is non-coordinating.

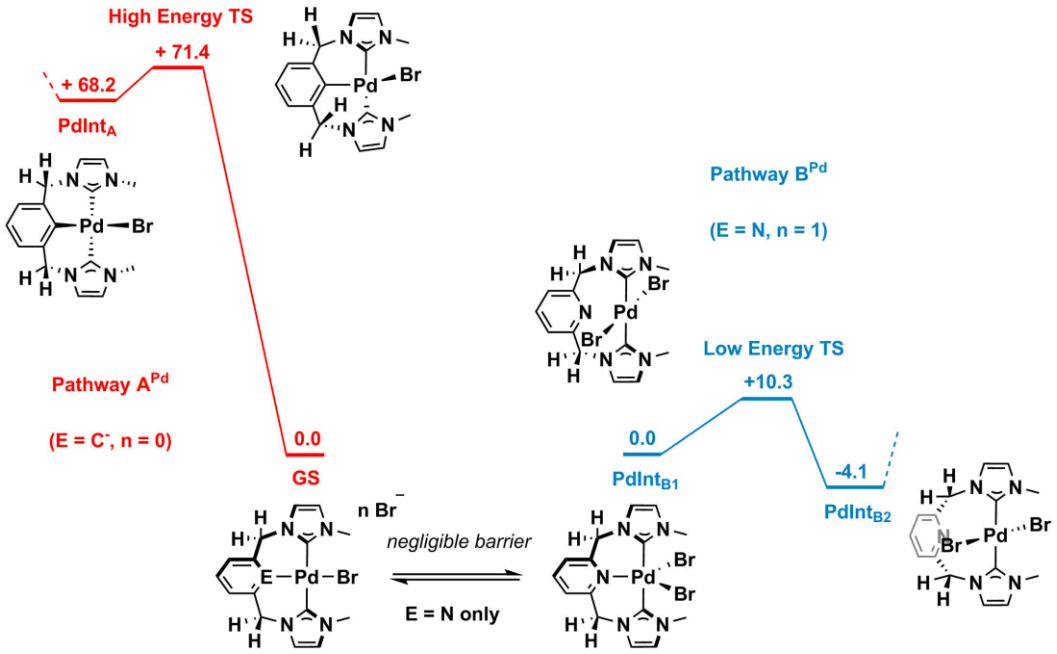

Fig. 3.7: *Mechanisms of atropisomerism in [Pd(C^C^C)Br] and [Pd(C^N^C)Br]Br systems. Energy in kJ mol^{-1}, relative to either ground state 'GS' (red) or 'PdInt$_{B1}$' (blue).*

When a halide is employed as the counter anion in lutidine-based [Pd(C^N^C^{Me})X]Y, barrier heights and coalescence temperatures drop significantly. For example, a loss of 29 kJ mol^{-1} and 130 K, respectively, is observed on substituting OTs$^-$ for I$^-$ as counter anion in [Pd(C^N^C^{Me})I]Y.[23] Here the counter anion appears to play an active role in the mechanism and, on the basis of DFT calculations using [Pd(C^N^C^{Me})Br]Br as model, Faller and co-workers propose **Pathway B^{Pd}** (**Fig. 3.7**). Pre-coordination of Br$^-$ (**PdInt$_{B1}$**, for which ΔS was not calculated) promotes dissociation of the pyridine group and formation of flexible *trans*-coordinate dihalo-intermediate **PdInt$_{B2}$**, where the pincer is κ^2-coordinated. In this state, twisting of the lutidine backbone is low energy (*ca*. 10 kJ mol^{-1} *c.f.* 71 kJ mol^{-1} for [Pd(C^C^C^{Me})X]) and enables rapid exchange between enantiomeric forms of **PdInt$_{B1}$** and hence [Pd(C^N^C^{Me})Br]Br.

Consistent with the mechanisms detailed in **Fig. 3.7**, no thermally-induced atropisomerism was observed for Pd complexes **3**, paired with weakly coordinating anions (**Chapter 2**), or sterically hindered *N*-aryl substituted [Pd(C^N^C^{Ar})X]X (Ar = DIPP, Mes; X = Cl$^-$, Br$^-$, $AgCl_2^-$) complexes, even up to 110°C.[29,30] A small increase in coalescence temperature and barrier height was observed experimentally on substitution of the *N*-methyl for *N*-^{n}butyl in [Pd(C^N^C^R)Br]Br (ΔT_c = 25 K, $\Delta\Delta G^{\ddagger}_{298\,K}$ = 4.5 kJ mol^{-1}).[23]

For rhodium complexes **9** and **16**, the weakly coordinating anion [BAr$^F{}_4$]$^-$ effectively rules out its participation, suggesting that a mechanism analogous to **Pathway A^{Pd}** is in force. Additionally, the small difference in activation barriers (ΔT_c = 25 K, $\Delta\Delta G^{\ddagger}_{298\,K}$ = *ca*. 6 kJ mol^{-1})

indicates a slight steric effect observed between *N*-methyl and *N*-alkyl substituents, analogous to that observed in the [Pd(C^N^C^{R})Br]Br systems above.

The observation of a high symmetry intermediate in ^{1}H NMR spectra of transmetallation reactions of **5** with $[Rh(CO)_2Cl]_2$ (**Chapter 2**, **Section 2.3.2**), indicates rapid atropisomerism on the NMR timescale with a significantly lower barrier than that of isolated **9**. To further investigate this process, a CD_2Cl_2 solution of **9** was placed under CO (1 atm). The resulting ^{1}H NMR spectrum (400 MHz, **Fig. 3.8**, **top left**) suggested a species of time-averaged C_{2v} symmetry; bearing a sharp singlet for the methylene bridge protons (5.24 ppm, 4H) in the same position as noted previously. Gradual reduction in the concentration of CO by successive freeze-pump-thaw (FPT) cycles regenerates **9**, but only after 18 cycles. These observations strongly suggest the C_{2v} symmetry (both that observed in crude reaction mixtures, and that from **9** under CO atmosphere) is induced by reversible interaction of **9** with CO, which significantly lowers the barrier to atropisomerism.

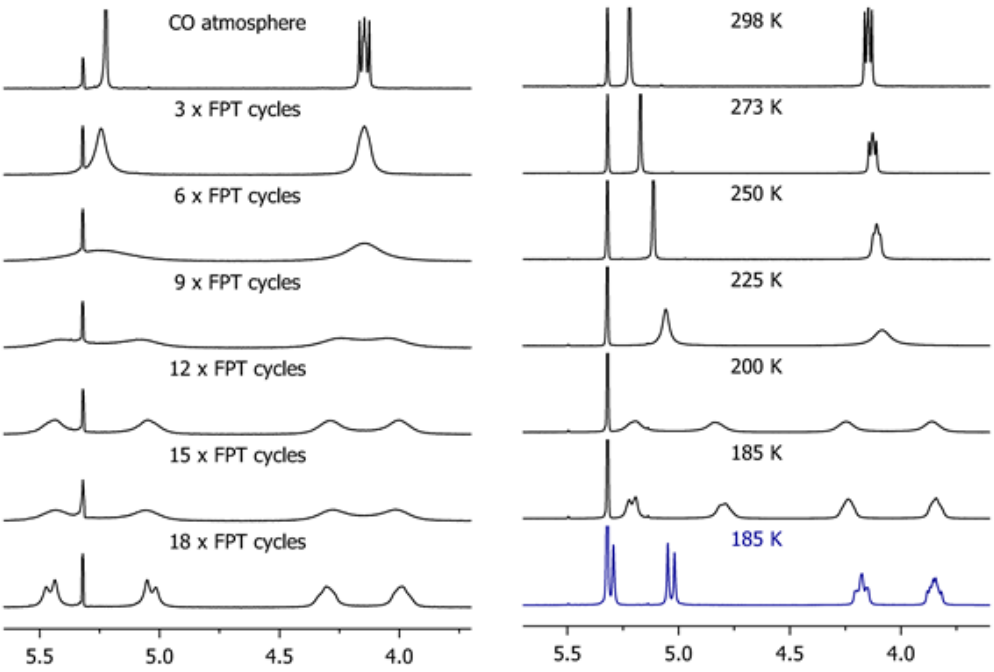

Fig. 3.8: *^{1}H NMR spectra depicting concentration and temperature dependence of the interaction of CO with **9** (11 mM in CD_2Cl_2). Decreasing CO concentration from 1 atm (top) at 400 MHz (**left**). Cooling produces a C_2 symmetric species with a different spectral profile to that of **9** (blue) under the same conditions (500 MHz) (**right**).*

To quantify the atropisomerism process, a CD_2Cl_2 solution of **9** under CO (1 atm) was cooled from 298 to 185 K, resulting in partial decoalescence. Lineshape analysis of VT ^{1}H NMR data (185 – 273 K, 500 MHz, CD_2Cl_2) enabled determination of a barrier height of $\Delta G^{\ddagger}_{298\,K}$ = 40 ± 9 kJ mol^{-1}, significantly lower than that of **9** under argon ($\Delta\Delta G^{\ddagger}_{298\,K}$ = 26 ± 18 kJ mol^{-1}). At 185 K the observed signals do not directly correspond to those of **9**; for instance the methylene bridge protons which appear at δ 5.31/5.03 ($^{2}J_{HH}$ = 15.0 Hz) in **9** *vs* δ 5.21/4.80 ($^{2}J_{HH}$ = 14.2 Hz) in the **9**

+ CO spectrum, indicating the presence of, or dynamic exchange with, a new C_2 symmetric species.

To further probe the atropisomerism of **9**, both alone and in the presence of CO, a range of mechanistic pathways were evaluated computationally, using **[Rh(C^N^C^{Me})(CO)]$^+$** as a convenient model. These DFT calculations were conducted by Dr. C. André Ohlin at Monash University (details in **Section 3.6.3**). Firstly, pathways involving dissociation of CO to form a three-coordinate intermediate were discounted due to prohibitively high values for the reaction enthalpy and associated free energy of the dissociation process (ΔH = + 240 kJ mol^{-1} and $\Delta G_{298\,K}$ = + 198 kJ mol^{-1}).

Bearing similarity to **Pathway A^{Pd}** for [Pd(C^E^C^{Me})X]Y, high-energy distortion of the κ^3-coordinated pincer **[Rh(C^N^C^{Me})(CO)]$^+$** to afford symmetric **RhInt$_A$** (**Pathway A^{Rh}**, **Fig. 3.9**) was evaluated using the Nudged Elastic Band method (NEB)[31] and calculated to proceed with an activation barrier of $\Delta H^{\ddagger}$ = 53 kJ mol^{-1} ($\Delta G^{\ddagger}_{298\,K}$ = 55 kJ mol^{-1}). Although lower than determined experimentally, these values lie close to those of acyclic **16** and the macrocycle **9**, for their thermal activation, and help validate use of **[Rh(C^N^C^{Me})(CO)]$^+$** as a model.

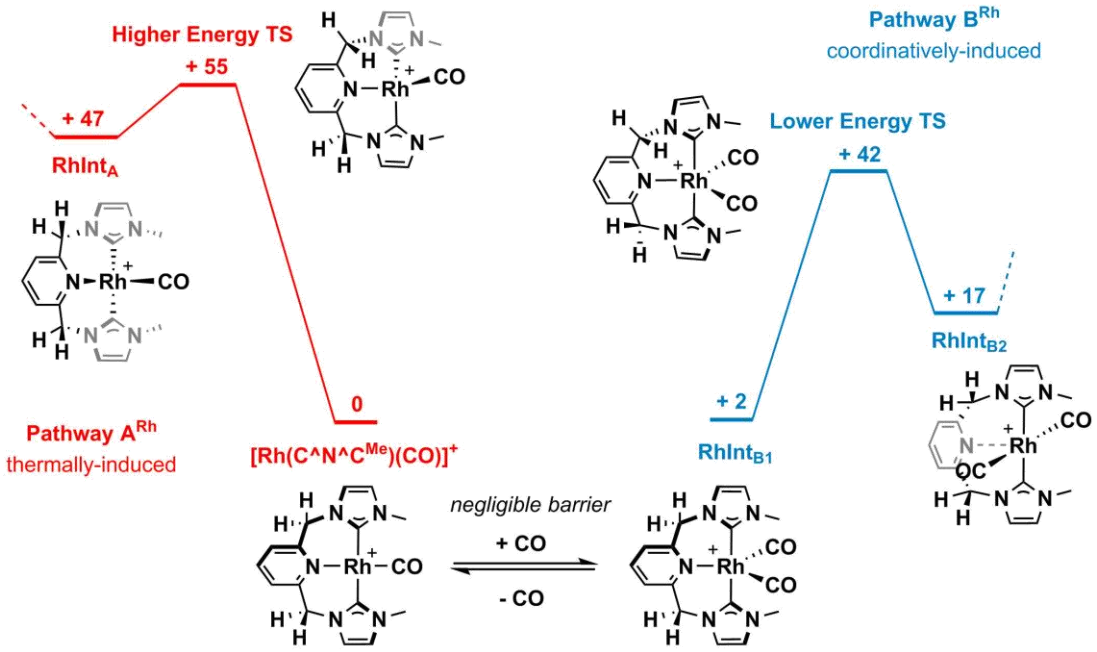

Fig. 3.9: *Mechanisms of atropisomerism for* ***[Rh(C^N^C^{Me})(CO)]$^+$****. All values are free energy, $\Delta G_{298\,K}$ (kJ mol^{-1}), relative to* ***[Rh(C^N^C^{Me})(CO)]$^+$****.*

Relevant to the CO-induced behaviour of **9**, an alternative mechanism, **Pathway B^{Rh}**, proceeds *via* coordination of CO to **[Rh(C^N^C^{Me})(CO)]$^+$** to afford 5-coordinate **RhInt$_{B1}$**. This transition entails a smooth increase in energy in the calculated reaction trajectory and the difference between the states is merely $\Delta G_{298\,K}$ = + 2 kJ mol^{-1} (ΔH = -41 kJ mol^{-1}, mitigated by an entropic penalty). A rapid equilibrium between **[Rh(C^N^C^{Me})(CO)]$^+$** and **RhInt$_{B1}$** is thus suggested and is

consistent with the observed differences in ^{1}H NMR spectra of **9** and **9 + CO** at 185 K, where exchange between the mono- and bis-carbonyl compounds under a CO atmosphere occurs faster than the NMR timescale.

Calculated bis-carbonyl **RhInt$_{B1}$** demonstrates a longer Rh-N bond than **[Rh(C^N^C^{Me})(CO)]$^{+}$** (+ 0.22 Å) with reduced NAO bond order (82 % of that in **[Rh(C^N^C^{Me})(CO)]$^{+}$**), facilitating a low-energy transition to symmetric intermediate **RhInt$_{B2}$**, where the pyridine is dissociated (Rh···N = 2.63 Å *c.f.* 2.19 Å for **[Rh(C^N^C^{Me})(CO)]$^{+}$**) and the ligand is therefore κ^{2}-coordinated. Overall, atropisomerism *via* reversible exchange of **RhInt$_{B1}$** and **RhInt$_{B2}$** (assuming a pre-equilibrium between mono- and bis-carbonyl states) has a calculated activation energy of $\Delta G^{\ddagger}_{298\,K}$ = 42 kJ mol^{-1}, in good agreement with the macrocyclic adduct **9 + CO** ($\Delta G^{\ddagger}_{298\,K}$ = 40 ± 9 kJ mol^{-1}).

Given the limitations of studying rapid processes using NMR spectroscopy, the interaction of **9** with CO was further interrogated experimentally by *in-situ* IR spectroscopy using a sealed solution cell (1 atm CO, 298 K, CH_2Cl_2; **Fig. 3.10**). The resulting spectrum shows the *ν*(CO) band of **9** at 1978 cm^{-1} along with two weak shoulders on either side. The difference spectrum of **9 + CO** minus **9** substantiates the presence of peaks at 1953 and 2007 cm^{-1}, which are assigned to *ν*(CO) stretching frequencies of a bis-carbonyl intermediate, with a bent OC-Rh-CO geometry as calculated for 5-coordinate **RhInt$_{B1}$** (C_{CO}-Rh-C_{CO} = 135°). The greater proportion of **9** is consistent with the small computed difference in Gibbs free energy and establishes **9** experimentally as the ground state configuration at 298 K.

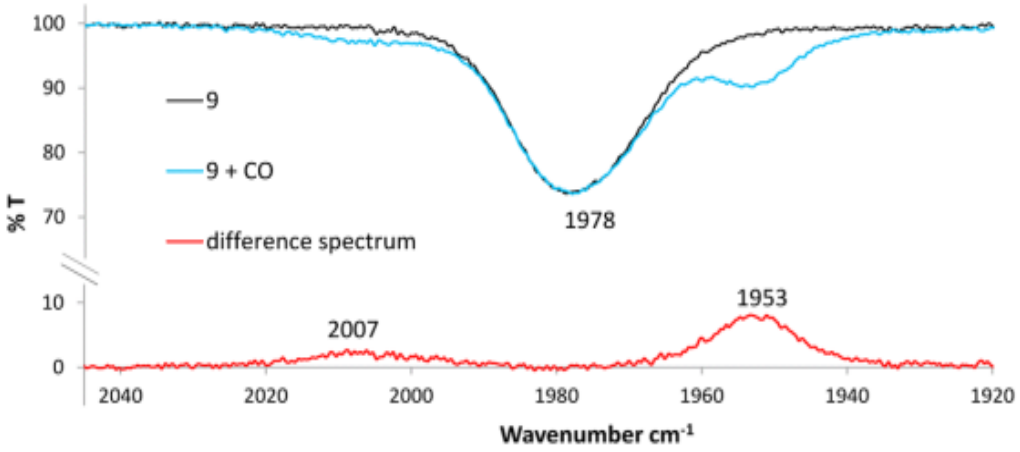

Fig. 3.10: *IR spectra of **9** and **9 + CO** with their difference spectrum (calculated using transmissions normalised at 1978 cm^{-1}).*

In addition to the computational and spectroscopic studies regarding atropisomerism of **9**, a structural analogue of 4-coordinate **RhInt$_{B2}$** was targeted by replacing the lutidine functionality with an *ortho*-xylene. Pro-ligand [**17**].2HBr was readily accessed via macrocyclisation of bis(imidazole)dodecamethylene **1c** and bis(bromomethyl)xylene as per the procedure for

[**2c**].2HBr (**Scheme 2.1**, **Chapter 2**). An *in-situ* silver-based transmetallation reaction afforded **18** in reasonable yield (46 %) following silica purification (**Scheme 3.6**).

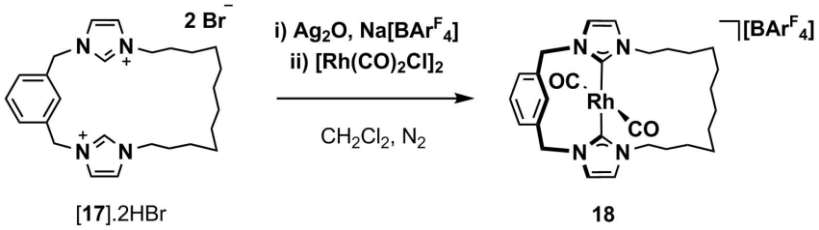

Scheme 3.6: *Synthesis of bis-carbonyl **18**.*

Bis-carbonyl **18** was comprehensively interrogated by NMR and IR spectroscopy, ESI-HRMS, elemental analysis and XRD. Bidentate metallation is marked in ^{1}H NMR spectra by disappearance of the acidic imidazolium protons of the pro-ligand and retention of the central aryl proton, which experiences a downfield shift of 0.42 ppm. The chelate demonstrates overall C_s symmetry, with diastereotopic methylene bridge protons (δ 5.09/5.02, $^{2}J_{HH}$ = 13.0 Hz) and equivalent carbenic carbons (δ 167.7, $^{1}J_{RhC}$ = 37 Hz). The carbonyl resonances both exhibit strong rhodium coupling, appearing separately at 187.8 ppm ($^{1}J_{RhC}$ = 74 Hz) and 182.4 ppm ($^{1}J_{RhC}$ = 69 Hz) in the ^{13}C{^{1}H} NMR spectrum.

In the IR spectrum, CO stretching frequencies are observed at 1993 and 2065 cm^{-1}, representing a significant hypsochromic shift with respect to the additional bands in the **9 + CO** spectrum (1953 and 2007 cm^{-1}). This data supports assignment of the latter signals to 5-coordinate **RhInt$_{B1}$**, as opposed to 4-coordinate **RhInt$_{B2}$,** which would be expected to display similar shifts to **18**.

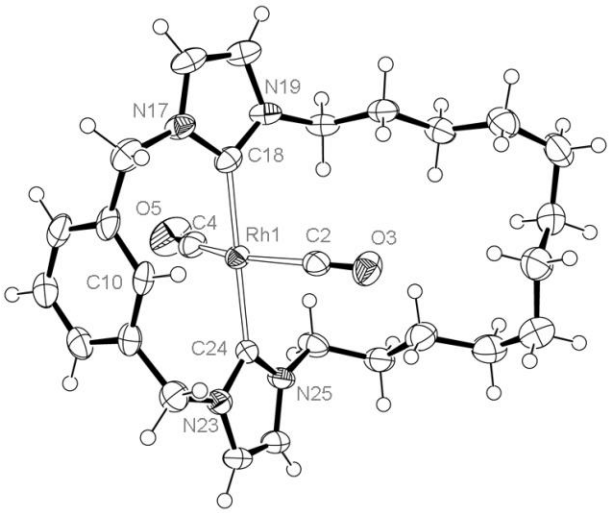

Fig. 3.11: *ORTEP representation of the solid-state structure of **18**. Thermal ellipsoids drawn at 50 % probability, [BAr$^{F}_{4}$]$^{-}$ counter anion and solvent molecule omitted for clarity. Selected bond lengths (Å) and angles (°): Rh1-C2, 1.895(6); Rh1-C4, 1.914(6); Rh1···C10, 2.585(5); Rh1-C18, 2.067(5); Rh1-C24, 2.050(5); C2-O3, 1.126(8), C4-O5, 1.130(8); C2-Rh1-C4, 151.8(2); C18-Rh1-C24, 178.8(2).*

Metal-carbene bonds of **18** are longer than those observed in the κ^3-coordinated pincer systems **9** and **10**, with Rh-C_{NCN} connections of *ca*. 2.06 Å (*c.f.* 2.02 – 2.04 Å for **9** and **10**), and Rh-C_{CO} that are significantly longer, at 1.895(6) and 1.914(6) Å (*c.f.* 1.804(3) and 1.836(4) Å for **9** and **10**, respectively). Much like the lutidine in the calculated structure of **$RhInt_{B2}$**, the aryl group is tilted away from the metal centre and 2.585(5) Å separate the rhodium and central carbon (**Fig. 3.12**). Similar separations have been observed in xylene-bridged bis(NHC) complexes of silver and copper, **A119**. In **A119**, agostic interactions are ruled out by DFT calculations and observation of a downfield shift in the proton NMR with respect to the imidazolium precursor, suggesting that the proximity is a result of geometric constraints of the ligand rather than interaction with the metal.[32,33] Similarly, the C10-H proton of **18** appears at 8.52 ppm in its ^{1}H NMR spectrum (298 K, CD_2Cl_2), shifted 0.42 ppm downfield with respect to the pro-ligand, with negligible change in $^1J_{CH}$ coupling constant (159 Hz *vs* 157 Hz for **17** and **18**, respectively). Addition of strong bases (KHMDS, KO^{t}Bu) does not promote cyclometallation to generate the pincer.

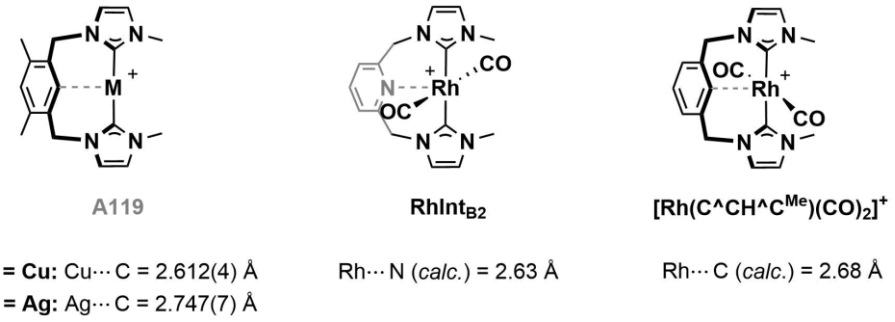

Fig. 3.12: *Arene-to-metal distances in CEC chelates obtained from single-crystal structures (**A119**) or DFT calculation.*

Computed **[Rh(C^CH^C^{Me})(CO)$_2$]$^+$** (**Fig. 3.12**), an acyclic analogue of **18**, has a calculated Rh···C distance of 2.68 Å and a non-negligible bond order of 41.6 %. These values are similar in magnitude to those calculated for the Rh···N interaction in **$RhInt_{B2}$** (2.63 Å, 46.3 %) and, combined with analysis of its spectroscopic and structural features, serve to aid the validation of **18** as a structural model of the bis-carbonyl intermediate **$RhInt_{B2}$** in the proposed atropisomerism mechanism.

3.3 Reactivity I – Deprotonation of 9

The methylene bridges of **Type II** complexes not only enable unique dynamic behaviour through introduction of conformational flexibility into the backbone, but also present an additional site of reactivity. Facilitated by pyridine dearomatisation to stabilise the resulting anion, the methylene bridge groups can be deprotonated by strong bases.[34-36]

Addition of KHMDS to a yellow solution of **9** in C_6D_6 at 293 K resulted in rapid formation of a dark red suspension. *In-situ* analysis by ^{1}H NMR spectroscopy (298 K, 500 MHz) revealed consumption of the C_2 symmetric starting material and quantitative conversion to C_1 symmetric, dearomatised **19** (**Scheme 3.7**). This structural assignment is strongly supported by the appearance of four signals for the inequivalent imidazolylidene protons and three coupled 1H resonances for the dearomatised pyridine: 6.35, 6.20 and 5.35 ppm (*c.f.* 6.62 (1H) and 6.25 (2H) ppm for **9**). A broad signal is observed for the vinylic proton at 5.79 ppm (298 K, 500 MHz, C_6D_6), which is partially resolved to a doublet, $^4J_{HH}$ = 1 Hz, on cooling from 298 to 280 K. Signals for the enduring methylene bridge and the methylene protons of the alkyl chain remain broad at 280 K, indicating that accommodation of the new sp^2 centre results in a lower barrier to movement of the dodecamethylene spacer. Time-averaged C_s symmetry for the alkyl chain is obtained on heating to 350 K, although the pincer backbone remains desymmetrised.

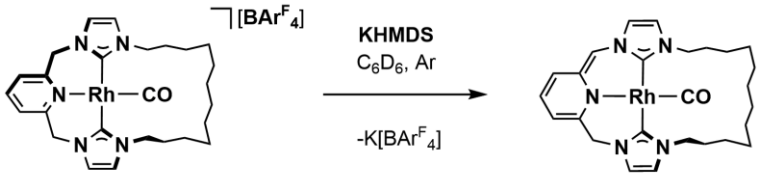

9 **19**

Scheme 3.7: *Dearomatisation of **9** to generate **19**.*

Complex **19** is highly reactive, displaying particular sensitivity to moisture, and is best characterised *in-situ*. However, crystalline material could be isolated on a small scale in moderate yield (52 %) by decantation of the reaction mixture to remove precipitated K[BAr$^F_4$] and layering of the supernatant with rigorously dried pentane. Fortuitously, single crystal samples suitable for XRD were obtained using this method and the resulting solid-state structure is shown in **Figures 3.13** and **3.14**.

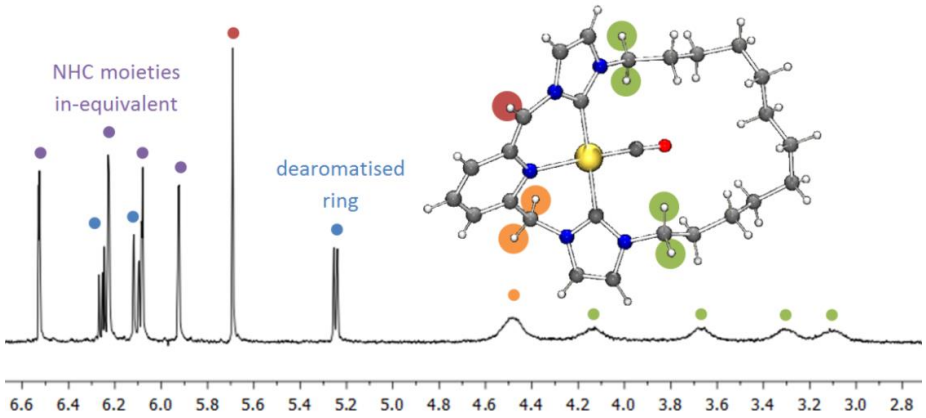

Fig. 3.13: *^{1}H NMR spectrum (C_6D_6, 500 MHz, 298 K) and POV-Ray representation of **19**.*

Formation of the new sp^2 centre results in contraction of the C11-C16 bond (1.356(4) Å) and expansion of the N17-C16-C11 bond angle (126.7(3)°) with respect to the corresponding pyridine-to-methylene connections in **9** (C_{py}-C_{CH2}: 1.506(5), 1.502(10) Å; C_{py}-C_{CH2}-N: 112.1(3)°, 110.8(6)°) and the remaining methylene group in **19** (C15-C22, 1.506(5) Å; C15-C22-N23, 111.3(2)°). The observation of bond-length alternation in the pyridine ring is consistent with a loss of aromaticity and transition of the pyridine nitrogen from neutral to anionic donor is evidenced by shortening of the Rh-N bond to 2.113(2) Å (*c.f.* 2.134(2) Å in **9**).

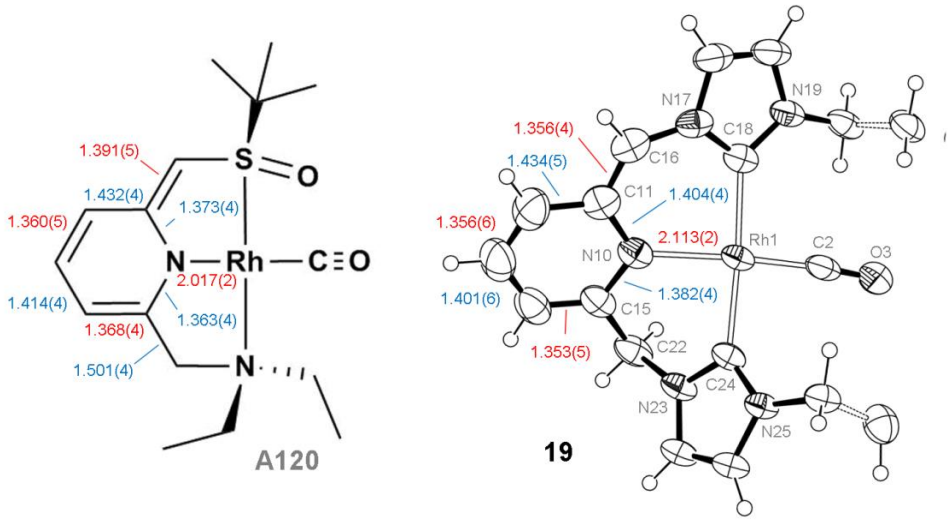

Fig. 3.14: *Comparison of bond length alternation in dearomatised **A120** and **19**. Shorter bonds than the corresponding parent cation (i.e. **9** for **19**) are indicated in red and longer bonds in blue. ORTEP representation of **19** has thermal ellipsoids at 50 % probability with minor disordered components, portion of alkyl chain and solvent omitted for clarity. Additional bond lengths (Å) and angles (°) for **19**: Rh1-C2, 1.799(3); Rh1-C18, 2.048(3); Rh1-C24, 2.045(3); C2-O3, 1.149(4); N10-Rh1-C2, 172.88(11); C18-Rh1-C24, 170.45(10); C11-C16-N17, 126.7(3); C15-C22-N23, 111.3(2)*

Due to their inherent reactivity, isolation and crystallographic study of dearomatised complexes of group 9 metals is rare.[37-39] Rhodium carbonyl SNN pincer **A120**, reported by Milstein *et al*, is a notable exception (**Fig. 3.14**). Despite the different terminal donors, there is good agreement between solid-state metrics of **19** and **A120**, which displays similar

desymmetrisation of the pyridine ring and contraction of the pyridine-CH bond from 1.502(4) to 1.391(5) Å (Δr_{CC} = 0.111(9) *vs.* Δr_{CC} = *ca.* 0.15 in **19**).[38] The transition of the pyridine nitrogen from neutral to anionic donor in **A120** is evidenced by a small contraction of the Rh-N bond from 2.031(2) Å, for the precursor, to 2.017(2) Å. Interestingly, no significant changes in solid-state metrics are observed between the rhodium carbonyl groups of **9** and **19**, despite a decrease of over 40 cm^{-1} in the carbonyl stretching frequency (1929 cm^{-1} *vs* 1972 cm^{-1} for **9** in C_6H_6), indicating greater π-backdonation.

Related PNP complexes of nickel, ruthenium, rhodium, rhenium and iridium (**A121-126**) have been explored for their application in bifunctional catalysis *via* base-induced dearomatisation of the lutidine backbone (**Fig. 3.15**).[39-44] Examples include the catalytic hydrogenation of imines,[45] ketones and esters[46] and the activation of CO_2,[42,43,47] and nitriles.[43,48,49] Bearing structural resemblance to **9**, a bis(NHC)-lutidine ruthenium carbonyl has been shown to catalyse the hydrogenation of esters *via* dearomatised intermediate **A126**, which may be trapped with CO_2 and nitriles.[35]

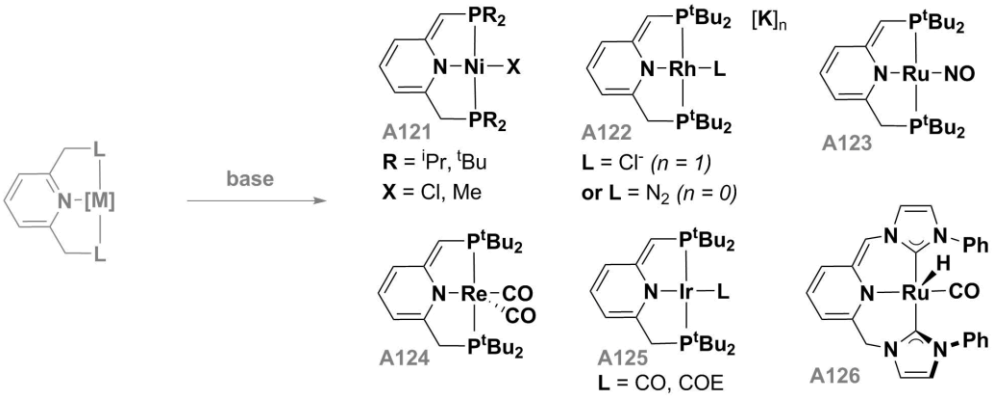

Fig. 3.15: *Dearomatised PNP and CNC complexes.*

3.4 Reactivity II – Oxidative Addition Reactions of 9 and 10

As a means to assess the differences in reactivity, oxidative-addition reactions of **9** and **10** with MeI and $PhICl_2$ were studied *in-situ* by ^{1}H NMR spectroscopy (CD_2Cl_2, 298 K, **Scheme 3.8**).

Much like **Type I** complexes **A114**[2] and amido-bridged **A115**,[5] the NMR-scale reaction of **10** with 3 equiv. of MeI proceeded rapidly and quantitatively to afford **20b** within 3 h. Under the same conditions, however, no significant reaction was apparent for **9** and instead 50 equiv. of MeI were required to convert **9** to **20a** within a similar timeframe. Despite the potential formation of three isomers (with CO, I, or Me *trans* to the pyridine) only one isomer is apparent in both cases and characteristic doublets ($^2J_{RhH}$ *ca*. 2 Hz) are observed for the Rh-C$\underline{H}_3$ groups at 1.20 and 0.59 ppm for **20a** and **20b**, respectively.

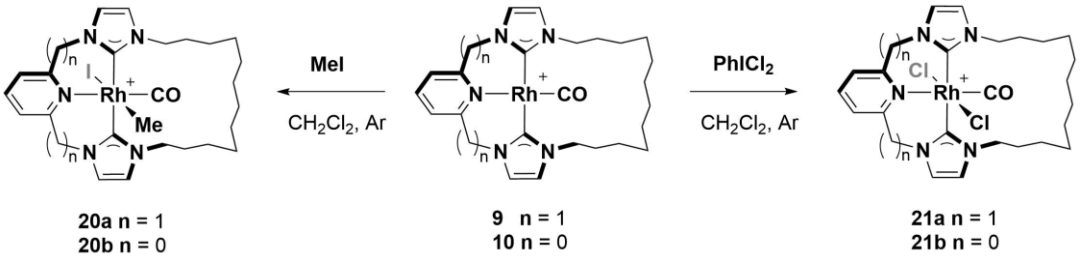

Scheme 3.8: *Oxidative addition reactions of **9** and **10**. [BAr$^F_4$]$^-$ counter anions omitted for clarity.*

On scaling up these reactions, **20a** was found to decompose slowly in solution, affording intractable mixtures containing C_1 symmetric species and free MeI, as detected by ^{1}H NMR spectroscopy. Facile decomposition frustrated attempts at isolation of **20a** and samples of high purity could not be obtained as a consequence. Instead, **20a** was characterised *in-situ* by ^{1}H and ^{13}C NMR spectroscopy; key spectral data are given in **Table 3.2**. Oxidation of **9** is accompanied by a shift of the pyridyl and imidazolylidene protons to higher frequency, which is found to be characteristic of rhodium(III) complexes of this type (*c.f.* **21a** and **40**, *vide infra*). In the ^{13}C{^{1}H} NMR spectrum, signals for the carbonyl and carbene carbons are shifted to lower frequency and display smaller $^1J_{RhC}$ coupling than the corresponding signals in the spectrum of **9**, appearing at 189.4 ppm ($^1J_{RhC}$ = 64 Hz) and 165.1 ppm ($^1J_{RhC}$ = 34 Hz), respectively (*c.f.* $\delta_{\underline{C}O}$ 194.0 ($^1J_{RhC}$ = 80 Hz) and $\delta_{N\underline{C}N}$ 181.8 ($^1J_{RhC}$ = 42 Hz)).

Table 3.2: *Selected spectroscopic data and solid-state metrics for rhodium(III) complexes* ***20*** *and* ***21****.*[a]

	20a	**20b**	**21a**	**21b**
***ν*(CO)** /cm^{-1}	2067	2070; 2066[b]	2110	2111
$\delta_{\underline{C}O}$ ($^1J_{RhC}$/Hz)	189.4 (64)	189.8 (61)	180.7 (57)	181.6 (57)
$\delta_{N\underline{C}N}$ ($^1J_{RhC}$/Hz)	165.1 (34)	180.2 (37)	160.1 (30)	173.9 (33)
$\delta_{C\underline{H}3}$ ($^1J_{RhH}$/Hz)	-1.2 (20)	-2.1 (18)	-	-
Rh-C_{CO} /Å	-	1.869(4)	-	1.945(3)
Rh-C_{NCN} /Å	-	2.041(3), 2.028(3)	-	2.043(3), 2.049(3)
Rh-N /Å	-	2.005(3)	-	1.997(3)
N-Rh-C_{CO} /°	-	175.42(15)	-	178.19(11)
C_{NCN}-Rh-C_{NCN} /°	-	156.47(15)	-	156.47(12)
R-Rh-X[c] **/°**	-	178.42(9)	-	179.49(3)

[a] IR spectra measured in CH_2Cl_2 solution, ^{1}H and ^{13}C{^{1}H} NMR spectra measured in CD_2Cl_2 solution. [b] Recorded in MeCN. [c] **R** = Me, **X** = I for **20**; **R** = **X** = Cl for **21**.

Demonstrating greater stability than **20a**, **20b** was readily isolated as a yellow microcrystalline solid in 75 % yield. Isolated **20b** showed no degradation in the solid-state or in CD_2Cl_2 solution over 15 hours, enabling its full characterisation by NMR and IR spectroscopy, ESI-HRMS and elemental analysis. Crystals suitable for XRD were also grown from slow diffusion of pentane into a CH_2Cl_2 solution; the resulting solid-state structure corroborates assignment of the single isomer to the *trans* methyl-iodide product (**Fig. 3.16**).

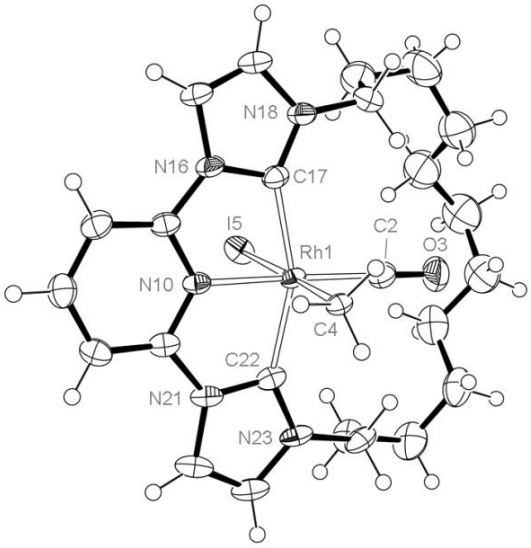

Fig. 3.16: *ORTEP representation of the solid state structure of* ***20b****. Thermal ellipsoids at 50 % probability, [BAr$^F{}_4$]$^-$ counter anion and minor disordered components omitted for clarity. Selected bond lengths (Å) and angles (°): Rh1–C2, 1.869(4); Rh1–C4, 2.297(3); Rh1–I5, 2.7539(4); Rh1–N10, 2.005(3); Rh1–C17, 2.041(3); Rh1–C22, 2.028(3); C2–O3, 1.122(5); N10–Rh1–C2, 175.42(15); C4–Rh1–I5, 178.42(9); C17–Rh1–C22, 156.47(15).*

Although *trans*-selective addition of methyl-iodide to Rh(CNC) systems is known (**A128**, **Scheme 3.9**),[5] closely related acyclic **A114c** (R = Me) affords two isomers **A129** and **A129'** in a 1:11 ratio when reacted with MeI in acetonitrile.[2] In the absence of their solid-state structures, these isomers cannot be definitively characterised. However, the similarity of the CO stretching frequencies of **20b** and **A129'** suggest that the *trans* methyl-iodide product is the major isomer. Moreover, **20a** can be tentatively assigned to the *trans* adduct due to

comparable spectroscopic properties associated with the carbonyl ligand, irrespective of the pincer ligand used: $\delta_{\underline{C}O}$ = 189.4 ($^1J_{RhC}$ = 64 Hz) for **20a** and $\delta_{\underline{C}O}$ = 189.8 ($^1J_{RhC}$ = 61 Hz) for **20b**. As for **20a**, the pyridyl and imidazolyl protons of **20b** are found to higher frequency in the ^{1}H NMR spectrum than their equivalents in **10**, and the carbonyl and carbene carbons appear at lower frequency in the $^{13}C\{^1H\}$ NMR spectrum, exhibiting smaller $^1J_{RhC}$ couplings (**Table 3.2**).

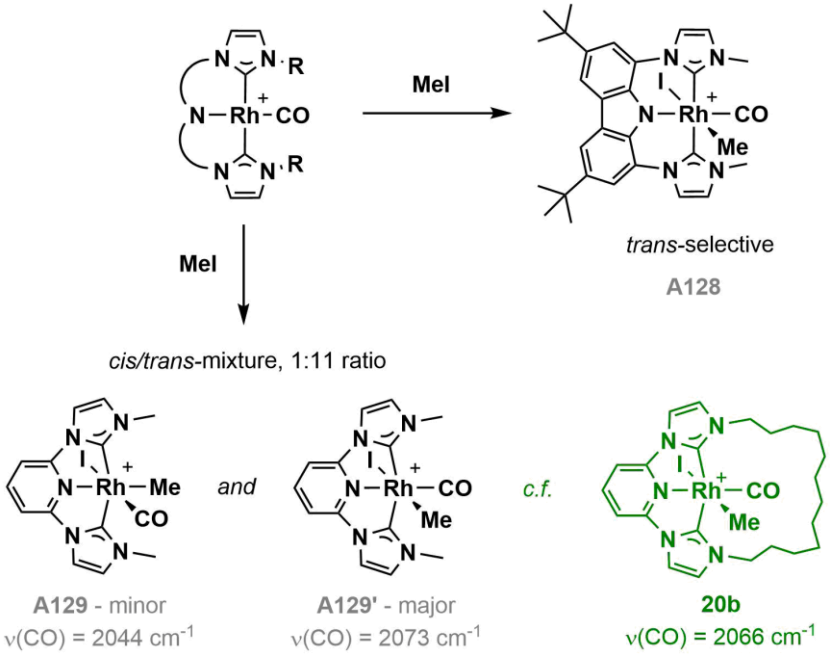

Scheme 3.9: *Comparison of **20b** with related literature precedents. IR data recorded in MeCN.*

Reaction of **9** and **10** with 1.1 equiv. of the stronger oxidant $PhICl_2$ is rapid in both cases, with complete conversion to **21** observed by ^{1}H NMR spectroscopy within 1 hour. Signals for the pyridine and imidazolylidene protons of **21** are higher in frequency than those of **9** and **10** and, consistent with formation of the *trans*-dichloride adducts, time-averaged C_2 or C_{2v} symmetry is observed for **21a** and **21b**, respectively (CD_2Cl_2, 500 MHz, 298 K). As for **20**, the carbonyl and carbene resonances in the $^{13}C\{^1H\}$ spectra of **21** are lower in frequency with respect to starting materials, and show smaller coupling constants. In addition, these resonances are shifted slightly further upfield with respect to methyl iodide adducts **20** ($\Delta\delta_{\underline{C}O}$ = 8.7 and 8.2, $\Delta\delta_{N\underline{C}N}$ = 5.0 and 6.3 for **Type II** and **Type I** respectively), although the coupling constants are similar.

As for **20a**, **21a** was found to be unstable in solution, undergoing partial disproportionation on isolation to afford an intractable mixture, a component of which is tentatively assigned to rhodium-trichloride complex [Rh(**2c**)Cl_3], on the basis of analysis by ^{1}H NMR spectroscopy and ESI-LRMS. As a consequence, **21a** was characterised *in-situ*. In contrast, **Type I** complex **21b** is air and moisture stable and was isolated in 67 % yield following recrystallization, enabling comparison of its solid-state structure (**Fig. 3.17**) to that of **20b**.

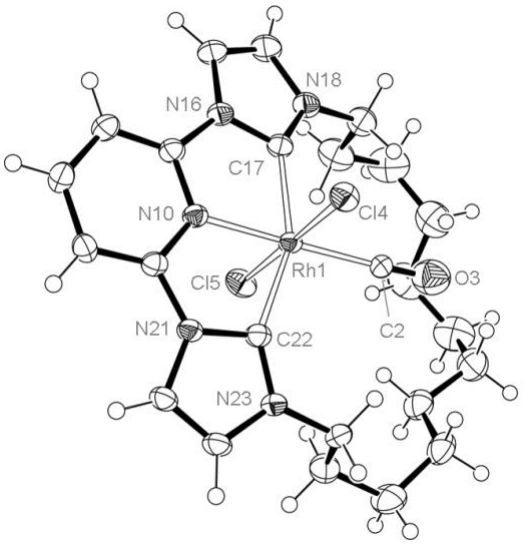

Fig. 3.17: *ORTEP representation of the solid-state structure of* ***21b****. Thermal ellipsoids at 50 % probability, [BAr$^F_4$]$^-$ counter anion and solvent molecules omitted for clarity. Selected bond lengths (Å) and angles (°): Rh1–C2, 1.945(3); Rh1–Cl4, 2.3514(8); Rh1–Cl5, 2.3150(8); Rh1–N10, 1.997(3); Rh1–C17, 2.043(3); Rh1–C22, 2.049(3); C2–O3, 1.046(4); N10–Rh1–C2, 178.19(11); Cl4–Rh1–Cl5, 179.49(3); C17–Rh1–C22, 156.47(12).*

In the solid-state, **20b** and **21b** adopt octahedral geometry typical of d^6 metal complexes, with values for the C_{NCN}-Rh-C_{NCN} bond angle comparable to **10**; 156.47(15)° (**20b**) and 156.47(12)° (**21b**) *c.f.* 155.18(15)° (**10**). Oxidation to rhodium(III) results in a minor contraction of the Rh-N bond from 2.027(3) Å to 2.005(3) Å, for the methyl-iodide, and 1.997(3) Å for the dichloride. Displacement of the dodecamethylene spacer to one side of the pincer is observed in both **20b** and **21b**, but is more pronounced in the methyl-iodide adduct, which also demonstrates a slightly distorted N-Rh-C_{CO} bond angle of 175.42(15)° (*c.f.* 178.19(11)° for **21b**); both observations are consistent with greater steric crowding at the metal.

The rapid formation, facile isolation and, most notably, greater stability of **20b**/**21b** in comparison with lutidine-based **20a**/**21a** indicate clear differences in reactivity between the **Type I** and **Type II** complexes, with the **Type I** adduct **10** showing greater disposition to oxidative addition, consistent with a more electron-rich metal centre. However, the ν(CO) bands of **9** and **10** (at 1979 and 1986 cm^{-1} respectively) suggest the opposite: that **9** is more electron rich. Interestingly, despite the disparity in CO-stretches observed for **9** and **10**, the *ν*(CO) bands of **20a** and **20b** differ only by 3 cm^{-1} (2067 *vs* 2070 cm^{-1}) and those of **21a** and **21b** by a mere 1 cm^{-1} (2110 *vs* 2111 cm^{-1}).

Similar observations have been made by Feller, Milstein, Goldberg and Heinekey,[50,51] whom note differences in reactivity between *iso*-propyl and *tert*-butyl substituted bis-phosphine pincers in oxidation-addition/reductive-elimination reactions (**Scheme 3.10**).

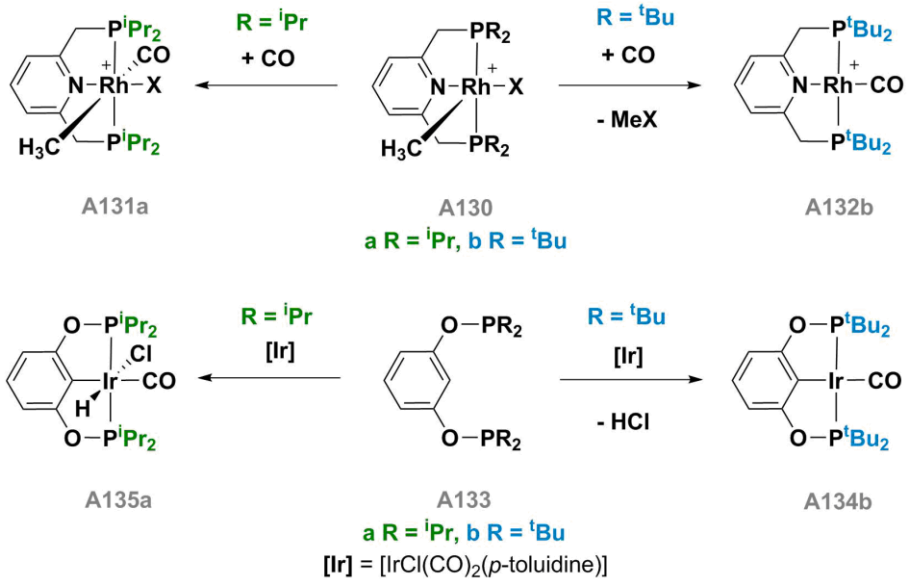

Scheme 3.10: *Role of phosphine substituents 'R' in the reactivity of complexes* ***A130*** *and* ***A133****.*

For instance, placing $[Rh^{III}(PNP^{R})(Me)(I)]^{+}$ **A130** under a carbon monoxide atmosphere results in formation of an isolable rhodium(III) carbonyl adduct **A131a** when R = ^{i}Pr, but when R = ^{t}Bu rapid reductive elimination of MeI is observed, affording $[Rh^{I}(PNP^{tBu})(CO)]^{+}$ **A132b**.[50] Similarly, reaction of $[IrCl(CO)_2(p\text{-toluidene})]$ and bis-phosphites **A133** gave iridium(I) complex **A134b** when ^{t}Bu substituents were used, but afforded an iridium(III) carbonyl **A135a** with the less sterically-encumbered bis-phosphite (R = ^{i}Pr).[51] When ^{i}Pr substituted iridium(I) carbonyl **A134a** is synthesised by an alternative method, the ν(CO) band resides at a higher frequency to that of **A134b** (1944 cm^{-1} for **A134a** *vs* 1937 cm^{-1} for **A134b**), indicating a system that is less favourable to oxidative addition.

The observations outlined above strongly implicate steric factors in the relative stability of Rh(III) and Ir(III) complexes of PEP-ligands, wherein higher oxidation states (and octahedral geometry) are disfavoured by steric bulk (R = ^{t}Bu) irrespective of the electronic properties of the metal. Given the substantial differences in geometry between lutidine-centred **9** and pyridine-centred **10**, the origin of their differences in reactivity could be purely steric in nature. However, in the absence of detailed calculations regarding the electronic structures of these complexes, the precise delineation of underlying steric or electronic effects remains to be determined.

With respect to the structural properties of the rhodium(III) products, introduction of two additional ligands into the metal coordination sphere has significant impact on the dynamics of **20** and **21** in solution. For the **Type I** complexes, **20b** and **21b**, displacement of the dodecamethylene spacer to one side of the coordination plane observed in the solid-state is corroborated by VT ^{1}H NMR spectroscopy (CD_2Cl_2, 500 MHz, 298 to 200 K), where C_s symmetry

is observed at 298 K for bulky methyl-iodide **20b** and at 250 K for less-hindered **21b**. Above 250 K, C_{2v} symmetry is observed for **21b**, presumably as a consequence of dynamic movement of the alkyl chain, resulting in a spectrum resembling that of **10**. Decoalescence of the *N*-$CH_2C\underline{H_2}$ proton signals is also observed for **10** (*vide supra*), but at lower temperatures, suggesting that oxidation results in a higher energy barrier to movement of the dodecamethylene spacer in **20b** and **21b**.

High flexibility of the dodecamethylene spacer is indicated in rhodium(III) complexes of **2c**, **20a** and **21a**, for which the ^{1}H NMR spectra indicate time-averaged C_2 symmetry at 298 K (CD_2Cl_2, 500 MHz, **Fig. 3.18**). The methylene resonances of **20a** are noticeably broadened with respect to the starting complex **9** at room temperature and cooling to 273 K results in complete decoalescence and C_1 symmetry, with the slow exchange limit reached at 250 K (CD_2Cl_2, 500 MHz). Supporting assignment of **21a** as the *trans*-dichloride, C_2 symmetry is retained from 298 to 200 K over the course of an analogous experiment.

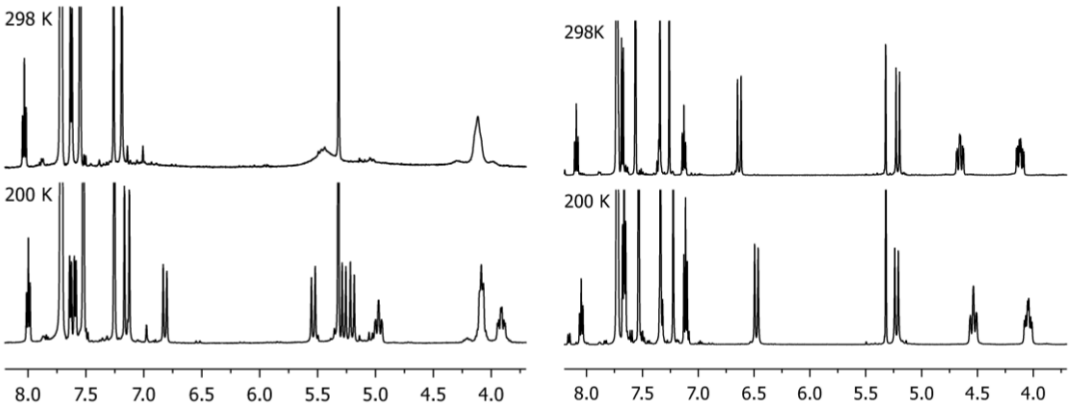

Fig. 3.18: *VT ^{1}H NMR spectra of **20a** (**left**) and **21a** (**right**), (CD_2Cl_2, 500 MHz).*

3.5 Transmetallation Reactions of 21b with Grignard Reagents

While the potential for dearomatisation (**Section 3.3**) and low-stability (**Section 3.4**) of **Type II** rhodium(III) adducts of **2c** limits their potential for further study, isolable air-stable **21b** is a promising starting point for the construction of more complex architectures *via* transmetallation of the *trans* chlorides. Accordingly, double transmetallation with phenyl acetylene magnesium bromide (3 equiv., 1.0 M solution in THF) affords diyne **22** in moderate yield of 34 % after recrystallization (**Scheme 3.11**).

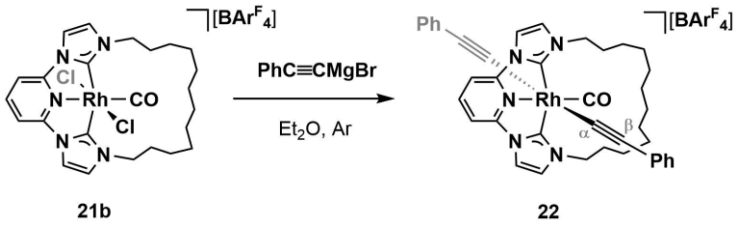

Scheme 3.11: *Synthesis of **22** from **21b**.*

The *trans*-geometry alkynyl ligands is corroborated by ^{1}H and ^{13}C NMR spectroscopy, which demonstrate C_{2v} symmetry at 298 K. Proton signals pertaining to the phenyl-alkyne substituents are present in a 2 : 1 ratio with respect to those of the macrocycle and the [BAr$^F_4$]$^-$ counter anion and, in the ^{13}C{^{1}H} NMR spectrum, doublet resonances for α and β carbons of the triple bonds appear at 84.5 ppm ($^{1}J_{RhC}$ = 31 Hz) and 106.7 ppm ($^{2}J_{RhC}$ = 6 Hz), respectively. These values are comparable to signals observed for the alkynes of Rh(III)-carbonyls **A136** and **A137** (δ_α 74 – 109 ($^{1}J_{RhC}$ = 35 – 45 Hz); δ_β 111 – 114 ($^{2}J_{RhC}$ = 7 – 9 Hz)).[52,53]

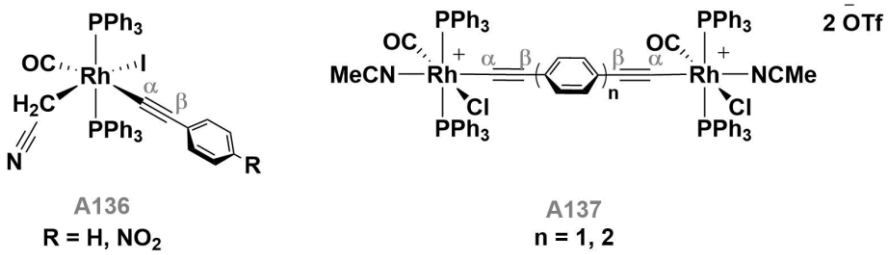

Fig. 3.19: *Literature precedents containing Rh-C_α≡C_β-Ar groups.*

A characteristic doublet for the carbene was observed at 176.8 ppm ($^{1}J_{RhC}$ = 34 Hz; *c.f.* δ 173.9 (33 Hz) for **21b**), but the carbonyl resonance could not be located (*c.f.* 184 ppm ($^{1}J_{RhC}$ = 47 Hz) for **A136**; 177 ppm ($^{1}J_{RhC}$ *ca*. 59 Hz) for **A137**). Retention of the carbonyl was instead corroborated by ESI-LRMS (710.2 *m/z*; calc. 710.2), elemental analysis consistent with the formula [Rh(**2c**)(CCPh)$_2$(CO)][BAr$^F_4$], and XRD (**Fig. 3.20**).

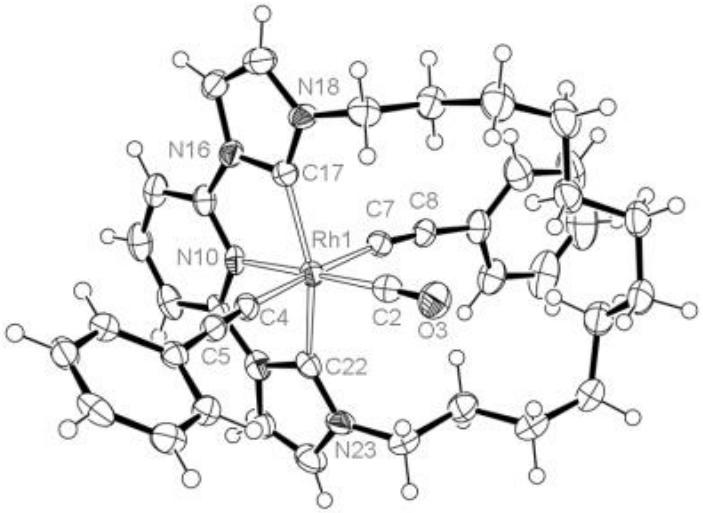

Fig. 3.20: *ORTEP representation of **22**. Thermal ellipsoids at 50 % probability. Solvent molecule and $[BAr^F{}_4]^-$ counter anion omitted for clarity. Selected bond lengths (Å) and angles (°): Rh1-C2, 1.875(5); Rh1-C4, 2.051(4); Rh1-C7, 2.043(4); Rh1-N10, 2.012(3); Rh1-C17, 2.039(4); Rh1-C22, 2.041(4); C2-O3, 1.222(5); C4-C5, 1.204(6); C7-C8, 1.198(6); N10-Rh1-C2, 178.74(16); C4-Rh1-C7, 175.31(16); C17-Rh1-C22, 156.10(17).*

Bonding interactions of the macrocycle with the metal in **22** are comparable to those of **21b** in the solid-state, a reflection of the rigid geometry of the planar pincer ligand. However, unlike the near-linear relationship between the *trans*-chlorides in **21b** (179.49(3)°), the C4-Rh1-C7 angle of the *trans*-alkynyls is partially contracted (175.31(16)°), with the phenyl-alkyne substituents tilted away from the pincer backbone. Interestingly, one of the phenyl groups appears to twist (estimated Rh-C_α≡C_β-Ph torsion angle of 36(7)°, *c.f.* -5(16)° of opposing substituent) in order to adopt a CH-π interaction with a distance of 3.07 Å between the centroid of the phenyl ring and the nearest proton of the alkyl chain. Previously reported CH-π aryl interaction distances are in the range 2.4 – 3.5 Å.[54]

Encouraged by the straightforward synthesis and isolation of **22**, the preparation of other *trans*-substituted rhodium(III) complexes from **21b**, *via* transmetallation, was attempted. To this end, reactions with commercially available Grignard reagents (methyl magnesium bromide, phenyl ethyl magnesium chloride) and a range of *in-situ* generated organometallic reagents from bromide **23** (alkyl Grignard) and alkynes **24** and **25** (copper, magnesium and lithium acetylides), were investigated.

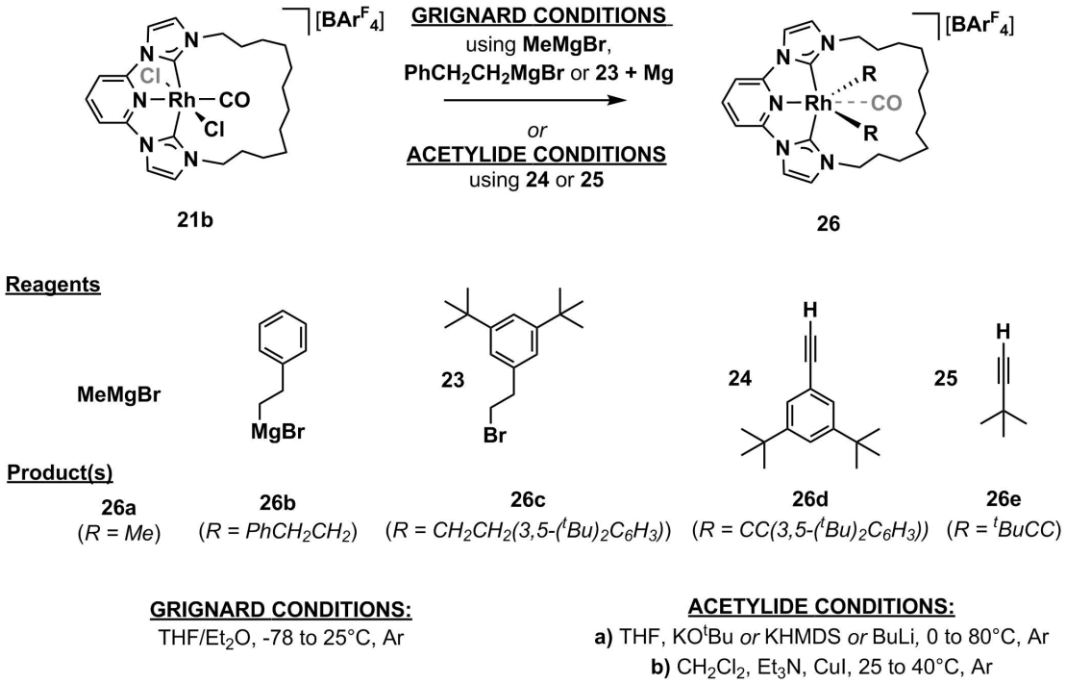

Scheme 3.12: *Attempted syntheses of dialkyls and diynes* ***26****.*

Initial sampling of reaction mixtures using ESI-LRMS was promising, with apparent consumption of [Rh(**2c**)Cl$_2$]$^+$ and concomitant production of mono or di-substituted products. Mixtures of fragment ions with and without the carbonyl ligand were observed by ESI-LRMS, with [Rh(**2c**)(**R**)$_2$]$^+$ the predominant product in all cases. Frustratingly, the resulting mixtures proved intractable and were not investigated further.

To investigate the possibility for inducing C-C bond formation *via* abstraction of CO from well-defined **22**, a degassed solution of the diyne in difluorobenzene was heated at 80°C in a sealed tube. After 20 h, multiple products were apparent in the ^{1}H NMR spectrum and, while no loss of the carbonyl was observed by ESI-LRMS, a signal for rhodium(I) carbonyl **10** was noted. Addition of CO abstraction agent NMe$_3$O[55] to difluorobenzene solutions of **22** was more successful and resulted in complete consumption of the starting material to afford both loss of the carbonyl ligand and production of **10**, by ESI-LRMS. However, ^{1}H NMR spectra (CD$_2$Cl$_2$) revealed multiple, pincer-ligand containing species alongside sharp singlets in the alkyl region pertaining to NMe$_3$, NMe$_3$O and similar NMe$_3$-derived signals (2.9 - 3.7 ppm).

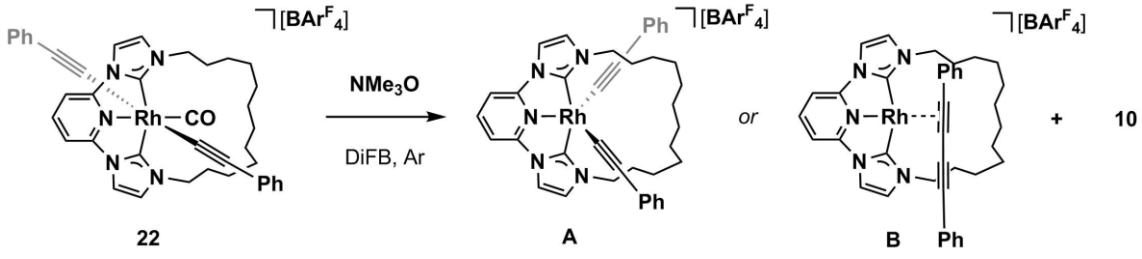

Scheme 3.13: *CO abstraction from* ***22****.*

Coordination of NMe_3O to rhenium, rhodium and platinum centres has been observed crystallographically[56] and by solution NMR spectroscopy.[57] The presence of NMe_3-containing products in crude mixtures, as analysed by ^1H NMR spectroscopy, is not reduced by various solvent extraction methods or the employment of high vacuum. As a consequence, pure samples of the decarbonylated product could not be obtained and its identity – either as rhodium(III) dialkynyl **A** or rhodium(I) diyne **B** – could not be verified (**Scheme 3.13**).

The strength of the rhodium-carbonyl bond is a significant hurdle to further application of **10** and its derivatives. Similarly, the CO bond of **9** is resistant to photochemical promoted dissociation (either by 365 nm LED source or broad irradiation from 100 W Hg lamp) and studies of CO-abstraction using NMe_3O are frustrated by poor-selectivity and the generation of intractable mixtures.[58] In light of these findings, the investigation of macrocyclic complexes of rhodium bearing more labile ancillary ligands was targeted and is discussed in **Chapter 4**.

3.6 Experimental Procedures and Selected Data

3.6.1 Experimental Procedure

General considerations. Manipulations were performed under an inert atmosphere, using Schlenk (nitrogen, argon, carbon monoxide and hydrogen) and glove box (argon) techniques unless otherwise stated. Glassware was oven dried at 130°C overnight and flamed under vacuum prior to use. Anhydrous solvents (<0.005 % H_2O) were purchased from ACROS Organics or Sigma Aldrich and used as supplied: DMF, MeCN, CH_2Cl_2, THF, 1,4-dioxane, hexane, pentane and Et_2O. 1,2-Difluorobenzene (DiFB) was stirred over neutral aluminum oxide, filtered, dried over CaH_2, vacuum distilled, and freeze-pump-thaw degassed three times before being placed under argon over 3 Å molecular sieves. CD_2Cl_2 and C_6D_6 were dried over CaH_2 and sodium metal respectively prior to vacuum-distillation, and stored under an atmosphere of argon. $Na[BAr^F{}_4]$,[59] $[Rh(CO)_2Cl]_2$,[60] 2,6-bis(imidazolyl)pyridine,[61] 3,5-di(*tert*-butyl)phenyl acetylene,[62] [C^N^C^{Me}].2HBr,[63,64] $PhICl_2$[65] and $[Ir(COD)(py)(PCy_3)][BAr^F{}_4]$[11] were synthesised using literature procedures. Complex **9** was synthesised from [**2c**].2HBr as described in **Chapter 2**. All other solvents and reagents are commercial products and were used as received. NMR spectra were recorded on Bruker DPX-300, DPX-400, AV-400, AV-500, AVIII-500 HD and AV-600 spectrometers at 298 K unless otherwise stated. Chemical shifts are quoted in ppm and coupling constants in Hz. IR spectra were recorded using a cell with a Perkin-Elmer spectrum 100 spectrometer. UV-vis absorption spectra were recorded on an Agilent Cary 60 spectrometer. ESI-LRMS were recorded on an Agilent 6130B mass spectrometer. ESI-HRMS were recorded on a Bruker MaXis mass spectrometer. Microanalyses were performed at the London Metropolitan University by Stephen Boyer.

*3.6.1.1 Preparation of Acyclic Ligands **13***

7-imidazole-1-heptene: NaH (60 wt % suspension in mineral oil, 0.32 g, 8.03 mmol) was added portionwise to a stirred solution of imidazole (0.50 g, 7.34 mmol) in 50 mL THF at 0°C, over 5 min., 7-Bromo-1-heptene (1.18 mL, 7.73 mmol) was then added *via* syringe. The mixture was heated at reflux for 16 h and then quenched by addition of H_2O, after cooling to room temperature. The product was extracted with CH_2Cl_2 (3 × 50 mL), and the combined organic extracts were washed with H_2O and then dried over Na_2SO_4. The crude product (yellow oil) was then purified by silica column chromatography (10 % MeOH in CH_2Cl_2) to yield the pure product as a colourless oil. Yield: 0.880 g (46 %).

^{1}H NMR (300 MHz, $CDCl_3$): δ 7.45 (s, 1H, imid), 7.05 (s, 1H, imid), 6.90 (s, 1H, imid), 5.77 (ddt, $^3J_{HH}$ = 16.9, 9.9, 6.6, 1H, C*H*═CH_2), 4.90–5.07 (m, 2H, CH═CH_2), 3.92 (t, $^3J_{HH}$ = 7.1, 2H, *N*-CH_2),

1.98–2.09 (m, 2H, C*H*$_2$), 1.78 (app. quint, *J* = 7, 2H, CH$_2$), 1.22–1.49 (m, 4H, CH$_2$). **^{13}C{^{1}H} NMR** (75 MHz, $CDCl_3$): δ 138.5, 137.2, 129.5, 118.9, 114.9, 47.1, 33.6, 31.1, 28.4, 26.1. **ESI-HRMS** (CH_3CN, 180 °C, 3 kV): positive ion: 165.1391 *m*/*z*, $[M]H^+$ (calc. 165.1386). **Elemental Analysis** Calc. for $C_{10}H_{16}N_2$ (164.25 g mol^{-1}): C, 73.13; H, 9.82; N, 17.06. Found: C, 72.97; H, 9.68; N, 16.96.

[C^N^C-((CH$_2$)$_5$CH═CH$_2$)$_2$].2HBr ([**12a**].2HBr): A mixture of 2,6-bis(bromomethyl)pyridine (1.30 g, 4.90 mmol) and 7-imidazole-1-heptene (2.41 g, 14.7 mmol) in 1,4-dioxane (50 mL) was heated at reflux for 5 h. The solvent was removed *in vacuo* to give an orange oil, which was then extracted with MeCN (50 mL). The filtrate was reduced in volume, and excess Et_2O was added to separate the product as an oil, which was separated by decantation. The remaining oil was washed with Et_2O (3 × 50 mL) before drying *in vacuo* to a yield a yellow foam. Yield: 2.737 g (94 %).

^{1}H NMR (400 MHz, $CDCl_3$): δ 10.51 (br, 2H, imid), 8.17 (app. t, *J* = 2, 2H, imid), 7.73 (d, $^3J_{HH}$ = 7.6, 2H, py), 7.62 (dd, $^3J_{HH}$ = 8.3, 7.1, 1H, py), 7.37 (app. t, *J* = 2, 2H, imid), 5.73 (s, 4H, pyC*H*$_2$), 5.65 (ddt, $^3J_{HH}$ = 16.9, 10.1, 6.7, 2H, C*H*═CH$_2$), 4.88 (d app. q, $^3J_{HH}$ = 16.9, *J* = 2, 2H, CH═C*H*$_2$), 4.83 (br d, $^3J_{HH}$ = 10.1, 2H, CH═C*H*$_2$), 4.34 (t, $^3J_{HH}$ = 7.5, 4H, N-C*H*$_2$), 1.94 (app. q, *J* = 7, 4H, CH$_2$), 1.86 (app. quint, *J* = 8, 4H, CH$_2$), 1.20–1.40 (m, 8H, CH$_2$). **^{13}C{^{1}H} NMR** (101 MHz, $CDCl_3$): δ 153.3, 139.1, 138.2, 137.2, 137.1, 124.0, 123.9, 121.5, 115.0, 53.4, 50.1, 33.4, 30.3, 28.2, 25.6. **ESI-HRMS** (CH_3CN, 180 °C, 3 kV): positive ion: 216.6598 *m*/*z*, $[M]^{2+}$ (calc. 216.6597). **Elemental Analysis** Calc. for $C_{27}H_{39}Br_2N_5$ (593.44 g mol^{-1}): C, 54.65; H, 6.62; N, 11.80. Found: C, 54.49; H, 6.57; N, 11.74.

[CNC-((CH$_2$)$_5$CH═CH$_2$)$_2$].2HBr ([**12b**].2HBr): A mixture of 2,6-bis(imidazolyl)pyridine (0.634 g, 2.77 mmol) and 7-bromo-1-heptene (1.05 mL, 6.91 mmol) in 1,4-dioxane (2 mL) was stirred at 100°C in a sealed J. Young's flask for 16 h. After cooling, the reaction mixture was extracted with MeCN (3 × 10 mL). To the filtrate was added Et_2O (20 mL) to form a white suspension, which was left to stand for 4 h before filtration. The remaining white solid was washed with Et_2O and dried *in vacuo* to give the product. Yield: 1.067 g (68 %).

^{1}H NMR (300 MHz, $CDCl_3$): δ 11.92 (br, 2H, imid), 9.27 (app. t, *J* = 2, 2H, imid), 8.78 (d, $^3J_{HH}$ = 8.2, 2H, py), 8.31 (t, $^3J_{HH}$ = 8.1, 1H, py), 7.52 (app. t, *J* = 2, 2H, imid), 5.75 (ddt, $^3J_{HH}$ = 16.9, 10.1, 6.7, 2H, C*H*═CH$_2$), 4.98 (d app. q, $^3J_{HH}$ = 16.9, *J* = 2, 2H, CH═C*H*$_2$), 4.93 (br d, $^3J_{HH}$ = 10.1, 2H, CH═C*H*$_2$), 4.59 (t, $^3J_{HH}$ = 7.3, 4H, *N*-C*H*$_2$), 1.95–2.12 (m, 8H, CH$_2$), 1.34–1.54 (m, 8H, CH$_2$). **^{13}C{^{1}H} NMR** (75 MHz, $CDCl_3$): δ 145.4, 145.3, 138.3, 136.7, 123.3, 120.9, 115.6, 115.1, 50.9, 33.4, 30.3, 28.2, 25.7. **ESI-HRMS** (CH_3CN, 180 °C, 3 kV): positive ion: 202.6458 *m*/*z*, $[M]^{2+}$/2 (calc.

202.6441). **Elemental Analysis** Calc. for $C_{25}H_{35}Br_2N_5$ (565.39 g mol^{-1}): C, 53.11; H, 6.24; N, 12.39. Found: C, 52.92; H, 6.11; N, 12.28.

*3.6.1.2 Preparation of Rhodium Carbonyl Complexes **9**, **10**, **16** and **18***

[Rh(**12a**)(CO)][BAr$^F_4$] (**13a**): A mixture of [**12a**].2HBr (0.050 g, 0.084 mmol), Ag_2O (0.020 g, 0.084 mmol), and Na[BAr$^F_4$] (0.075 g, 0.084 mmol) in CH_2Cl_2 (3 mL) was stirred in the absence of light for 16 h. A solution of $[Rh(CO)_2Cl]_2$ (0.016 g, 0.042 mmol) in CH_2Cl_2 (3 mL) was added, and the resulting suspension was stirred for a further 20 h. The suspension was filtered through a pad of silica, eluting with CH_2Cl_2, to yield the crude product upon removal of solvent. The crude material was then purified by precipitation from Et_2O–pentane to yield the pure product as a yellow powder. Yield: 0.070 g (58 %).

^{1}H NMR (400 MHz, CD_2Cl_2): δ 7.86 (t, $^3J_{HH}$ = 7.7, 1H, py), 7.70–7.75 (m, 8H, Ar^F), 7.55 (br, 4H, Ar^F), 7.49 (d, $^3J_{HH}$ = 7.7, 2H, py), 7.14 (d, $^3J_{HH}$ = 1.9, 2H, imid), 6.99 (d, $^3J_{HH}$ = 2.0, 2H, imid), 5.75 (ddt, $^3J_{HH}$ = 16.9, 10.2, 6.7, 2H, C*H*═CH$_2$), 5.46 (d, $^2J_{HH}$ = 14.7, 2H, pyC*H*$_2$), 5.02 (d, $^2J_{HH}$ = 14.7, 2H, pyC*H*$_2$), 4.94 (d app. q, $^3J_{HH}$ = 16.9, *J* = 2, 2H, CH═C*H*$_2$), 4.89 (br d, $^3J_{HH}$ = 10.2, 2H, CH═C*H*$_2$), 4.13 (t, $^3J_{HH}$ = 7.6, 4H, N-C*H*$_2$), 2.02 (app. q, *J* = 7, 4H, CH$_2$), 1.82–1.95 (m, 4H, CH$_2$), 1.30–1.48 (m, 8H, CH$_2$). **^{13}C{^{1}H} NMR** (101 MHz, CD_2Cl_2): δ 193.9 (d, $^1J_{RhC}$ = 79, carbonyl), 182.2 (d, $^1J_{RhC}$ = 41, carbene), 162.2 (q, $^1J_{CB}$ = 49, Ar^F), 156.0 (s, py), 141.4 (s, py), 139.1 (s, *C*H═CH$_2$), 135.3 (s, Ar^F), 129.3 (q, $^2J_{CF}$ = 32, Ar^F), 125.1 (q, $^1J_{CF}$ = 272, Ar^F), 124.8 (s, py), 121.8 (s, imid), 121.3 (s, imid), 118.0 (sept., $^3J_{FC}$ = 4, Ar^F), 114.8 (s, CH═*C*H$_2$), 55.8 (s, py*C*H$_2$), 51.4 (s, N-*C*H$_2$), 34.0 (s, CH$_2$), 31.7 (s, CH$_2$), 28.8 (s, CH$_2$), 26.5 (s, CH$_2$). **ESI-HRMS** (CH_3CN, 180 °C, 3 kV): positive ion: 562.2067 *m*/*z*, [M]$^+$ (calc. 562.2048). **Elemental Analysis** Calc. for $C_{60}H_{49}BF_{24}N_5ORh$ (1425.74 g mol^{-1}): C, 50.55; H, 3.46; N, 4.91. Found: C, 50.43; H, 3.36; N, 4.90. **IR (CH_2Cl_2):** *ν*(CO) 1978 cm^{-1}.

[Rh(**12b**)(CO)][BAr$^F_4$] (**13b**): A mixture of [**12b**].2HBr (0.100 g, 0.177 mmol), Ag_2O (0.041 g, 0.176 mmol), and Na[BAr$^F_4$] (0.173 g, 0.195 mmol) in CH_2Cl_2 (2 mL) was stirred in the absence of light for 16 h. The reaction mixture was filtered onto $[Rh(CO)_2Cl]_2$ (0.035 g, 0.088 mmol), and the resulting suspension was stirred for a further 5 min before further filtration. The filtrate was reduced to dryness and purified on silica (CH_2Cl_2) to afford the product as a purple foam on removal of the solvent. Yield: 0.218 g (83 %).

^{1}H NMR (400 MHz, CD_2Cl_2): δ 8.01 (t, $^3J_{HH}$ = 8.2, 1H, py), 7.72–7.80 (m, 8H, Ar^F), 7.58 (br, 4H, Ar^F), 7.43 (d, $^3J_{HH}$ = 2.2, 2H, imid), 7.15 (d, $^3J_{HH}$ = 8.2, 2H, py), 7.10 (d, $^3J_{HH}$ = 2.2, 2H, imid), 5.81 (ddt, $^3J_{HH}$ = 16.9, 10.2, 6.7 Hz, 2H, C*H*═CH$_2$), 5.00 (d app. q, $^3J_{HH}$ = 16.9, *J* = 2, 2H, CH═C*H*$_2$), 4.95 (br d, $^3J_{HH}$ = 10.2, 2H, CH═C*H*$_2$), 4.14 (t, $^3J_{HH}$ = 7.5, 4H, *N*-C*H*$_2$), 2.08 (app. q, *J* = 7, 4H, CH$_2$), 1.93 (app. quint, *J* = 7, 4H, CH$_2$), 1.38–1.54 (m, 8H, CH$_2$). **^{13}C{^{1}H} NMR** (101 MHz, CD_2Cl_2): δ 186.6 (d,

$^1J_{RhC}$ = 48, carbene), 162.4 (q, $^1J_{CB}$ = 50, Ar^F), 152.7 (s, py), 146.3 (s, py), 139.0 (s, *C*H═CH_2), 135.4 (s, Ar^F), 129.5 (q, $^2J_{FC}$ = 32, Ar^F), 125.2 (q, $^1J_{FC}$ = 272, Ar^F), 123.8 (s, imid), 118.1 (sept., $^3J_{FC}$ = 4, Ar^F), 117.0 (s, imid), 115.0 (s, CH═*C*H_2), 106.7 (s, py), 53.0 (s, *N*-*C*H_2), 34.0 (s, CH_2), 31.6 (s, CH_2), 28.8 (s, CH_2), 26.4 (s, CH_2); *carbonyl resonance not observed*. **ESI-HRMS** (CH_3CN, 180 °C, 3 kV): positive ion: 534.1726 *m*/*z*, $[M]^+$ (calc. 534.1735). **Elemental Analysis** Calc. for $C_{58}H_{45}BF_{24}N_5ORh$ (1397.69 g mol^{-1}): C, 49.84; H, 3.25; N, 5.01. Found: C, 49.72; H, 3.25; N, 5.12. **IR (CH_2Cl_2):** *ν*(CO) 1990 cm^{-1}. **IR (CH_3CN):** *ν*(CO) 1980 cm^{-1}.

[Rh(**2c**)(CO)][BAr^F_4] (**9**): N_2 was bubbled through a solution of **13a** (0.100 g, 0.070 mmol) and Grubbs I (0.003 g, 0.004 mmol) in CH_2Cl_2 (70 mL) for 1 h. After this time, ESI-LRMS indicated 69 % reaction conversion. A further portion of Grubbs I (0.003 g, 0.004 mmol) was added, and N_2 was bubbled through for an additional hour, at which time ESI-LRMS indicated the reaction had gone to completion. The resulting solution was concentrated and passed through a silica pad using CH_2Cl_2 as the eluent to afford [Rh(C^N^C-$C_{12}H_{22}$)(CO)][BAr^F_4] (**14a**) as a yellow glass (*cis*:*trans* ~ 1:3). Yield: 0.096 g (95 %). A solution of **14a** (0.096 g, 0.065 mmol) in CH_2Cl_2 (5 mL) was added to a J. Young's flask charged with palladium on carbon (10 wt % Pd, 0.014 g, 0.013 mmol, *ca*. 20 mol % Pd), and the solution was placed under H_2 (4 bar). After stirring for 72 h, the reaction mixture was degassed, concentrated, and filtered through a Celite pad. The filtrate was concentrated *in vacuo* to give **9** as a yellow–orange foam. Yield: 0.075 g (82 %). Data consistent with those reported for alternative route (see **Chapter 2**).

Data for [Rh(C^N^C–$C_{12}H_{22}$)(CO)][BAr^F_4] (**14a**): **^{1}H NMR** (400 MHz, CD_2Cl_2, *trans isomer only*): δ 7.88 (t, $^3J_{HH}$ = 7.7, 1H, py), 7.70–7.75 (m, 8H, Ar^F), 7.55 (br, 4H, Ar^F), 7.50 (d, $^3J_{HH}$ = 7.7, 2H, py), 7.15 (d, $^3J_{HH}$ = 1.9, 2H, imid), 7.01 (d, $^3J_{HH}$ = 1.9, 2H, imid), 5.40 (br, 2H, pyC*H*$_2$), 5.35–5.39 (m, 2H,C*H*═C*H*), 5.03 (br, 2H, pyC*H*$_2$), 3.90–4.36 (m, 4H, N-C*H*$_2$), 1.14–2.24 (m, 16H, CH_2). **ESI-HRMS** (CH_3CN, 180 °C, 3 kV): positive ion: 534.1762 *m*/*z*, $[M]^+$ (calc. 534.1735).

Additional data in C_6D_6/C_6H_6 for [Rh(**2c**)(CO)][BAr^F_4] (**9**): **^{1}H NMR** (500 MHz, C_6D_6): δ 8.35 (br, 8H, Ar^F), 7.58 (br, 4H, Ar^F), 6.62 (t, $^3J_{HH}$ = 7.7, 1H, py), 6.25 (d, $^3J_{HH}$ = 7.7, 2H, py), 6.10 (d, $^3J_{HH}$ = 1.6, 2H, imid), 5.99 (d, $^3J_{HH}$ = 1.6, 2H, imid), 4.43 (d, $^2J_{HH}$ = 14.9, 2H, pyC*H*$_2$), 3.92 – 3.99 (m, 2H, *N*-C*H*$_2$), 3.70 (d, $^2J_{HH}$ = 14.8, 2H, pyC*H*$_2$), 3.27 – 3.35 (m, 2H, *N*-C*H*$_2$),1.45 – 1.57 (m, 4H, CH_2), 1.10 – 1.43 (m, 16H, CH_2). **IR (C_6H_6):** *ν*(CO) 1972 cm^{-1}.

[Rh(**11**)(CO)][BAr^F_4] (**10**): N_2 was bubbled through a solution of **13b** (0.100 g, 0.074 mmol) and Grubbs I (0.003 g, 0.004 mmol) in CH_2Cl_2 (70 mL) for 30 min (reaction completion observed by ESI-LRMS). The resulting solution was concentrated to dryness and purified on silica (CH_2Cl_2). [Rh(CNC-$C_{12}H_{22}$)(CO)][BAr^F_4] (**14b**) was obtained as a purple powder by precipitation from CH_2Cl_2 with excess pentane and subsequent filtration (*cis* : *trans* ~ 1:1). Yield: 0.083 g (82 %). A

solution of **14b** (0.050 g, 0.037 mol) and [Ir(COD)(py)(PCy_3)][BAr^F_4] (0.003 g, 0.004 mol) in CH_2Cl_2 (2 mL) was placed under hydrogen (1 bar). After stirring for 2 h, the reaction mixture was concentrated in vacuo. The residue was then purified on silica (CH_2Cl_2). The eluted solvent was concentrated to 2 mL before precipitation of the product with excess pentane. Complex **10** as a dark green powder was obtained by filtration and washed with pentane (3 × 5 mL). Yield: 0.042 g (83 %).

Data for [Rh(CNC-$C_{12}H_{22}$)(CO)][BAr^F_4] (**14b**): **^{1}H NMR** (400 MHz, CD_2Cl_2, *both isomers*): δ 8.04 (t, $^3J_{HH}$ = 8.2, 1H, py), 7.70–7.75 (m, 8H, Ar^F), 7.56 (s, 4H, Ar^F), 7.48/7.49 (d, $^3J_{HH}$ = 2.3, 2H, imid), 7.17 (d, $^3J_{HH}$ = 8.1, 2H, py), 7.09/7.10 (d, $^3J_{HH}$ = 2.3, 2H, imid), 5.27–5.37 (m, 2H, C*H*═C*H*), 4.13–4.21 (m, 4H, *N*-CH_2), 1.97–2.09 (m, 4H, CH_2), 1.80–1.91 (m, 4H, CH_2), 1.24–1.50 (m, 8H, CH_2). **ESI-HRMS** (CH_3CN, 180 °C, 3 kV) positive ion: 506.1422 *m/z*, $[M]^+$ (calc. 506.1422).

Data for [Rh(**11**)(CO)][BAr^F_4] (**10**): **^{1}H NMR** (500 MHz, CD_2Cl_2): δ 8.05 (t, $^3J_{HH}$ = 8.2, 1H, py), 7.70–7.75 (m, 8H, Ar^F), 7.56 (br, 4H, Ar^F), 7.49 (d, $^3J_{HH}$ = 2.3, 2H, imid), 7.18 (d, $^3J_{HH}$ = 8.2, 2H, py), 7.12 (d, $^3J_{HH}$ = 2.3, 2H, imid), 4.17 (t, $^3J_{HH}$ = 6.5, 4H, *N*-CH_2), 1.91 (app. quint, *J* = 6, 4H, CH_2), 1.24–1.48 (m, 16H, CH_2). **^{13}C{^{1}H} NMR** (101 MHz, CD_2Cl_2): δ 196.8 (d, $^1J_{RhC}$ = 78, carbonyl), 186.5 (d, $^1J_{RhC}$ = 48, carbene), 162.3 (q, $^1J_{CB}$ = 50, Ar^F), 152.7 (s, py), 146.3 (s, py), 135.4 (s, Ar^F), 129.5 (q, $^2J_{FC}$ = 32, Ar^F), 125.2 (q, $^1J_{FC}$ = 272, Ar^F), 123.2 (s, imid), 118.1 (sept., $^3J_{FC}$ = 4, Ar^F), 117.5 (s, imid), 106.7 (s, py), 51.7 (s, N-*C*H_2), 30.6 (s, CH_2), 29.0 (s, CH_2), 28.8 (s, CH_2), 28.5 (s, CH_2), 25.4 (s, CH_2). **ESI-HRMS** (CH_3CN, 180 °C, 3 kV): positive ion: 508.1570 *m/z*, $[M]^+$ (calc. 508.1578). **Elemental Analysis** Calc. for $C_{56}H_{43}BF_{24}N_5ORh$ (1371.65 g mol^{-1}): C, 49.04; H, 3.16; N, 5.11. Found: C, 49.17; H, 3.07; N, 5.10. **IR (CH_2Cl_2):** *ν*(CO) 1986 cm^{-1}. **IR (CH_3CN):** *ν*(CO) 1977 cm^{-1}.

[Ag(**C^N^C^{Me}**)][BAr^F_4] (**15**): In a Schlenk flask under argon, **[C^N^C^{Me}].2HBr** (0.100 g, 0.293 mmol), Na[BAr^F_4] (0.284 g, 0.320 mmol) and Ag_2O (0.070 g, 0.303 mmol) were suspended in CH_2Cl_2 (5 mL) and stirred in the absence of light for 18 hours before filtering through a celite plug to afford a colourless solution. Removal of the solvent *in vacuo* afforded the product as a white solid. Yield: 0.314 g (86 %).

^{1}H NMR (500 MHz, CD_2Cl_2) δ 7.70 – 7.74 (m, 8H, Ar^F), 7.66 (t, $^3J_{HH}$ = 7.7, 1H, py), 7.54 – 7.56 (br, 4H, Ar^F), 7.10 – 7.18 (br, 2H, py), 7.06 – 7.09 (br, 2H, imid), 7.02 (d, $^3J_{HH}$ = 1.7, 2H, imid), 5.20 (s, 4H, py*C*H_2), 3.79 (s, 6H, *N*-CH_3). **^{13}C{^{1}H} NMR** (126 MHz, CD_2Cl_2) δ 181.1 (carbene) 162.3 (q, $^1J_{CB}$ = 50, Ar^F), 155.7 (s, py), 139.9 (s, py), 135.4 (s, Ar^F), 129.4 (qq, $^2J_{FC}$ = 32, $^3J_{CB}$ = 3, Ar^F), 125.1 (q, $^1J_{FC}$ = 272, Ar^F), 123.3 (br, imid + py), 122.7 (br, imid), 118.0 (m, Ar^F), 57.2 (s, py*C*H_2), 39.8 (s, *N*-*C*H_3). **ESI-HRMS** (CH_3CN, 180°C, 3 kV) positive ion: 374.0528 *m/z*, $[M]^+$ (calc. 374.0529). **Elemental Analysis** Calc. for $C_{47}H_{29}AgBF_{24}N_5$ (1238.42 g mol^{-1}): C, 45.58; H, 2.36; N, 5.66. Found: C, 45.52; H, 2.25; N, 5.57.

[Rh(**C^N^C^{Me}**)(CO)][BAr$^F_4$] (**16**): In a Schlenk flask under N_2, **15** (0.090 g, 0.0727 mmol) and $[Rh(CO)_2Cl]_2$ (0.015 g, 0.0386 mmol) were solubilised in CH_2Cl_2 (5 mL) to give a yellow suspension, which was sonicated before filtering onto a short silica column (*ca*. 15 cm^3, under N_2). A yellow solution was eluted in CH_2Cl_2 and diluted with pentane. N_2 was bubbled through the solution until production of a yellow microcrystalline solid and loss of colour in the mother liquor, which was removed by filtration. The resulting yellow solid was washed with pentane and dried to afford **16** as a yellow microcrystalline powder. Yield: 0.050 g (61 %).

^{1}H NMR (400 MHz, CD_2Cl_2) δ 7.87 (t, $^3J_{HH}$ = 7.7, 1H, py), 7.67 – 7.77 (m, 8H, Ar^F), 7.55 (s, 4H, Ar^F), 7.50 (d, $^3J_{HH}$ = 7.7, 2H, py), 7.13 (d, $^3J_{HH}$ = 1.9, 2H, imid), 6.97 (d, $^3J_{HH}$ = 1.8, 2H, imid), 5.46 (br, 2H, pyCH_2), 5.05 (br, 2H, pyCH_2), 3.83 (s, 6H, *N*-CH_3). **^{13}C{^{1}H} NMR** (101 MHz, CD_2Cl_2) δ 193.6 (d, $^1J_{RhC}$ = 80, carbonyl), 182.9 (d, $^1J_{RhC}$ = 42, carbene), 162.3 (q, $^1J_{CB}$ = 50, Ar^F), 158.0 (s, py), 141.5 (s, py), 135.4 (s, Ar^F), 129.5 (qq, $^2J_{FC}$ = 32, $^3J_{CB}$ = 3, Ar^F), 125.2 (q, $^1J_{FC}$ = 271, Ar^F), 124.9 (s, py), 122.7 (s, imid), 121.7 (s, imid), 118.1 (pent., $^3J_{FC}$ = 4, Ar^F), 55.8 (d, $^3J_{RhC}$ = 2, pyCH_2), 38.4 (d, $^3J_{RhC}$ = 1, *N*-CH_3). **ESI-HRMS** (CH_3CN, 180°C, 3 kV) positive ion: 398.0485 *m/z*, $[M]^+$ (calc. 398.0483). **Elemental Analysis** Calc. for $C_{48}H_{29}BF_{24}N_5ORh$ (1261.47 g mol^{-1}): C, 45.70; H, 2.32; N, 5.55. Found: C, 45.59; H, 2.37; N, 5.67).

[C^CH^C-$(CH_2)_{12}$].2HBr ([**17**].2HBr): Solutions of α,α′-Dibromo-*m*-xylene (1.000 g, 3.79 mmol) and 1,12-bis(imidazole)dodecane (1.25 g, 3.79 mmol) in 1,4-dioxane (*ca*. 0.075 M) were simultaneously added dropwise over 30 min to a flask charged with warm 1,4-dioxane (150 mL, 90 °C). The suspension was heated at reflux for 16 h then cooled and the solvent removed *in vacuo*. The resulting off-white residue was extracted with MeCN (*ca*. 200 mL) with vigorous stirring. The MeCN solution was filtered and concentrated, and excess Et_2O was added. The resulting precipitate was isolated by filtration and washed with excess Et_2O to obtain [**17**].2HBr as a white crystalline solid. Yield: 0.500 g (23 %).

^{1}H NMR (500 MHz, CD_2Cl_2): δ 10.66 (app. t, *J* = 1, 2H, imid), 8.23 (app. t, *J* = 2, 2H, imid), 8.10 (app. t, *J* = 2 Hz, 1H, Ar), 7.62 (dd, $^3J_{HH}$ = 7.7, *J* = 2, 2H, Ar), 7.34 (t, $^3J_{HH}$ = 7.6, 1H, Ar), 7.32 (app. t, *J* = 2, 2H, imid), 5.63 (s, 4H, ArCH_2), 4.27 (t, $^3J_{HH}$ = 7.2, 4H, *N*-CH_2), 1.90 (app. quint, *J* = 7, 4H, CH_2), 1.18–1.32 (m, 16H, CH_2). **^{13}C{^{1}H} NMR** (126 MHz, CD_2Cl_2): δ 137.8, 135.4, 131.5, 130.4, 130.4, 123.9, 122.0, 54.0, 53.0, 50. 5, 29.7, 28.6, 28.3, 28.2, 25.8. **^{13}C NMR** (126 MHz, CD_2Cl_2, *selected data only*): δ 131.5 (d app. quint, $^1J_{CH}$ = 159, *J* = 4, Ar-C10). **ESI-HRMS** (CH_3CN, 180 °C, 3 kV) positive ion: 203.155 *m/z* $[M]^{2+}$ (calc. 203.154). **Elemental Analysis** Calc. for $C_{26}H_{38}Br_2N_4$ (566.144 g mol^{-1}): C, 55.13; H, 6.76; N, 9.89. Found: C, 55.20; H, 6.90; N, 9.80.

[Rh(**17**)$(CO)_2$][BAr$^F_4$] (**18**): To a Schlenk flask charged with [**17**].2HBr (0.140 g, 0.247 mmol), Ag_2O (0.057 g, 0.247 mmol), and Na[BAr$^F_4$] (0.239 g, 0.269 mmol) was added CH_2Cl_2 (5 mL). The

resulting solution was stirred at room temperature for 16 h, a solution of $[Rh(CO)_2Cl]_2$ (0.048 g, 0.124 mmol) in CH_2Cl_2 (2 mL) added, and then the solution was stirred for a further 53 h. The solution was then filtered and passed through a silica plug (CH_2Cl_2). The product **18** was precipitated as a yellow solid by addition of excess pentane. Yield: 0.162 g (46 %).

^{1}H NMR (500 MHz, CD_2Cl_2): δ 8.52 (s, 1H, aryl C10H), 7.70–7.75 (m, 8H, Ar^F), 7.56 (s, 4H, Ar^F), 7.52 (t, $^3J_{HH}$ = 7.7, 1H, Ar), 7.36 (dd, $^3J_{HH}$ = 7.6, *J* = 2, 2H, Ar), 7.20 (d, $^3J_{HH}$ = 2.0, 2H, imid), 7.12 (d, $^3J_{HH}$ = 2.1, 2H, imid), 5.09 (d, $^2J_{HH}$ = 13.0, 2H, ArC*H*$_2$), 5.02 (d, $^2J_{HH}$ = 13.0, 2H, ArC*H*$_2$), 4.19 (t, $^3J_{HH}$ = 8.2, 4H, *N*-C*H*$_2$), 1.66–1.81 (m, 4H), 1.25–1.42 (m, 16H). **^{13}C{^{1}H} NMR** (126 MHz, CD_2Cl_2): δ 187.8 (d, $^1J_{RhC}$ = 74, carbonyl), 182.4 (d, $^1J_{RhC}$ = 69, carbonyl), 167.7 (d, $^1J_{RhC}$ = 37, carbene), 162.3 (q, $^1J_{CB}$ = 49, Ar^F), 139.5 (s, Ar), 135.4 (s, Ar^F), 130.8 (s, Ar), 129.4 (qq, $^2J_{FC}$ = 32, $^3J_{BC}$ = 3, Ar^F), 129.4 (s, Ar), 125.1 (q, $^1J_{FC}$ = 272, Ar^F), 124.8 (s, imid), 122.0 (s, imid), 118.1 (sept., $^3J_{FC}$ = 4, Ar^F), 110.8 (s, Ar-C10), 54.8 (s, Ar*C*H$_2$), 54.4 (s, *N*-*C*H$_2$), 31.2 (s, CH$_2$), 27.3 (s, CH$_2$), 27.2 (s, CH$_2$), 25.8 (s, CH$_2$), 25.6 (s, CH$_2$). **^{13}C NMR** (126 MHz, CD_2Cl_2, *selected data only*): δ 110.8 (d app. quint, $^1J_{CH}$ = 157, *J* = 4, Ar-C10). **ESI-HRMS** (CH_3CN, 180 °C, 3 kV) positive ion: 563.189 *m*/*z*, $[M]^+$ (calc. 563.188). **Elemental Analysis** Calc. for $C_{60}H_{48}BF_{24}N_4O_2Rh$ (1426.75 g mol^{-1}): C, 50.51; H, 3.39; N, 3.93. Found: C, 50.35; H, 3.24; N, 4.14. **IR (CH_2Cl_2):** *ν*(CO) 1993 cm^{-1} (s), 2065 cm^{-1} (w).

*3.6.1.3 Preparation of Dearomatised Rhodium Carbonyl **19***

[Rh(C^N^C*-(CH$_2$)$_{12}$)(CO)] (**19**): To a J. Young's NMR tube charged with **9** (0.020 g, 0.014 mmol) and K[N(SiMe$_3$)$_2$] (0.004 g, 0.020 mmol) was added C_6D_6 (0.5 mL) under an argon atmosphere. This resulted in the formation of a red solution and brown precipitate. Quantitative formation of 1**9** was observed by ^{1}H NMR spectroscopy alongside HN(SiMe$_3$)$_2$ (δ_{CH_3} = 0.10, δ_{NH} = −0.07). The red solution was separated by decantation and layered with pentane (under argon). Diffusion of the solvent over 4 h afforded dark red crystals, which were isolated by decantation, washed with pentane, and dried. Yield: 0.003 g (52 %). The extremely high reactivity of 1**9** has prevented accurate elemental analysis results from being obtained (on two separate sample batches). Complex **19** is best characterized directly *in-situ* by NMR spectroscopy.

^{1}H NMR (500 MHz, C_6D_6, 280 K): δ 6.61 (app. t, *J* = 1, 1H, imid), 6.37 (ddd, $^3J_{HH}$ = 9.1, 5.9, *J* = 1, 1H, py), 6.30 (app. t, *J* = 1, 1H, imid), 6.23 (d app. t, $^3J_{HH}$ = 9.1, *J* = 1, 1H, py), 6.15 (app. t, *J* = 1, 1H, imid), 5.99 (app. t, *J* = 1, 1H, imid), 5.81 (br d, *J* = 1, 1H, pyC*H*), 5.36 (d app. t, $^3J_{HH}$ = 5.8, *J* = 1, 1H, py), 4.60 (app. t, *J* = 13, 1H, *N*-C*H*$_2$), 4.58 (d, $^2J_{HH}$ = 12.8, 1H, pyC*H*$_2$), 4.25 (app. t, *J* = 13, 1H, *N*-C*H*$_2$), 3.72 (d, $^2J_{HH}$ = 12.8, 1H, pyC*H*$_2$), 3.32–3.40 (m, 1H, *N*-C*H*$_2$), 3.08–3.22 (m, 1H, *N*-C*H*$_2$), 1.94–2.07 (m, 1H, CH$_2$), 1.72–1.83 (m, 1H, CH$_2$), 1.03–1.63 (m, 18H, CH$_2$). **^{1}H NMR** (500 MHz, C_6D_6, 298 K): δ 6.63 (app. t, *J* = 1, 1H, imid), 6.35 (dd, $^3J_{HH}$ = 9.1, 5.9, 1H, py), 6.33 (app. t, *J*

= 1, 1H, imid), 6.20 (d, $^{3}J_{HH}$ = 9.0, 1H, py), 6.19 (app. t, *J* = 2, 1H, imid), 6.04 (app. t, *J* = 1, 1H, imid), 5.79 (br, 1H, py*CH*), 5.35 (d, $^{3}J_{HH}$ = 5.8, 1H, py), 4.58 (br, 2H, pyCH_2 + N-CH_2), 4.23 (s, 1H, N-CH_2CH_2), 3.76 (br, 1H, pyCH_2), 3.41 (br, 1H, N-CH_2), 3.22 (br, 1H, N-CH_2), 1.99 (br, 1H, CH_2), 1.75 (br, 1H, CH_2), 1.00–1.66 (m, 18H, CH_2). **$^{13}C\{^{1}H\}$ NMR** (101 MHz, C_6D_6): δ 197.4 (d, $^{1}J_{RhC}$ = 73, carbonyl) 185.5 (d, $^{1}J_{RhC}$ = 43, carbene), 174.2 (d, $^{1}J_{RhC}$ = 44, carbene), 149.5 (s, py), 143.2 (s, py), 126.6 (s, py), 119.7 (s, py), 119.5 (s, imid), 119.3 (s, imid), 119.1 (s, imid), 117.7 (s, imid), 100.1 (s, py), 94.4 (s, py*C*H), 58.2 (s, pyCH_2), 51.4 (s, *N*-CH_2), 50.7 (s, *N*-CH_2), 32.1 (s, CH_2), 31.0 (s, CH_2), 28.0 (s, CH_2), 27.8 (s, CH_2), 27.7 (s, CH_2), 27.6 (s, CH_2), 26.5 (s, CH_2), 24.8 (s, CH_2), 24.0 (s, CH_2). **IR (C_6H_6):** *ν*(CO): 1929 cm^{-1}.

*3.6.1.4 Preparation of Rhodium(III) Carbonyl Complexes **20-22***

[Rh(**2c**)(CO)(CH_3)I][BAr^F_4] (**20a**): To a solution of **9** (0.008 g, 0.006 mmol) in CD_2Cl_2 (0.5 mL) inside a J. Young's NMR tube was added MeI (0.018 mL, 0.285 mmol) under an argon atmosphere. The J. Young's NMR tube was sealed and monitored periodically by ^{1}H NMR spectroscopy. After 3 h, less than 5 % **9** was present. The reaction tube was left to stand for a further 17 h, after which no signals of **9** were observable. The product **20a** was characterized *in-situ* by NMR spectroscopy. ESI-HRMS and IR data were obtained from crude (impure) mixtures of **20a** prepared in a similar manner, with excess MeI removed in vacuo.

^{1}H NMR (500 MHz, CD_2Cl_2): δ 8.04 (t, $^{3}J_{HH}$ = 7.8, 1H, py), 7.70–7.75 (m, 8H, Ar^F), 7.63 (d, $^{3}J_{HH}$ = 7.8, 2H, py), 7.55 (br, 4H, Ar^F), 7.26 (d, $^{3}J_{HH}$ = 1.7, 2H, imid), 7.19 (d, $^{3}J_{HH}$ = 1.7, 2H, imid), 5.4 (br, 2H, pyCH_2), 5.1 (v. br, 2H, *N*-CH_2), 4.1 (br, 2H, *N*-CH_2), 1.76–2.05 (br m, 4H, CH_2), 1.23–1.55 (m, CH_2, 16H), 1.20 (d, $^{2}J_{RhH}$ = 1.8, Rh-CH_3); one pyCH_2 resonance (2H) was too broad to definitively locate at this temperature. **$^{13}C\{^{1}H\}$ NMR** (126 MHz, CD_2Cl_2, *selected data only*): δ 189.4 (d, $^{1}J_{RhC}$ = 64, carbonyl), 165.1 (d, $^{1}J_{RhC}$ = 34, carbene), −1.2 (d, $^{2}J_{RhH}$ = 20, Rh-CH_3). **ESI-HRMS** (CH_3CN, 180 °C, 3 kV) positive ion: 678.1169 *m*/*z*, $[M]^+$ (calc. 678.1171). **IR (CH_2Cl_2):** *ν*(CO) 2067 cm^{-1}.

[Rh(**11**)(CO)(CH_3)I][BAr^F_4] (**20b**): To a purple solution of **10** (0.033 g, 0.024 mmol) in CH_2Cl_2 (5 mL) was added MeI (0.0075 mL, 0.120 mmol). The solution was stirred at room temperature for 3 h, and the product was precipitated by addition of excess pentane. The product was isolated by filtration, washed with pentane (2 × 5 mL), and dried in vacuo to afford **20b** as a cream powder. Yield: 0.028 g (75 %).

^{1}H NMR (500 MHz, CD_2Cl_2): δ 8.34 (t, $^{3}J_{HH}$ = 8.2, 1H, py), 7.78 (d, $^{3}J_{HH}$ = 2.2, 2H, imid), 7.70–7.74 (m, 8H, Ar^F), 7.56 (d, $^{3}J_{HH}$ = 8.2, 2H, py), 7.55 (br, 4H, Ar^F), 7.28 (d, $^{3}J_{HH}$ = 2.2, 2H, imid), 4.25 (app. t, *J* = 8, 4H, *N*-CH_2), 2.39–2.50 (m, 2H, *N*-CH_2CH_2), 1.84–1.95 (m, 2H, *N*-CH_2CH_2), 1.30–1.75 (m, 16H, CH_2), 0.59 (d, $^{2}J_{RhH}$ = 2.1, 3H, Rh-CH_3). **$^{13}C\{^{1}H\}$ NMR** (151 MHz, CD_2Cl_2): δ 189.8 (d, $^{1}J_{RhC}$

= 61, carbonyl), 180.2 ($^1J_{RhC}$ = 37, carbene), 162.3 (q, $^1J_{CB}$ = 50, Ar^F), 150.2 (s, py), 145.7 (s, py), 135.3 (s, Ar^F), 129.4 (q, $^2J_{CF}$ = 32, Ar^F), 125.1 (q, $^1J_{CF}$ = 272, Ar^F), 124.3 (s, imid), 118.2 (s, imid), 118.0 (sept., $^3J_{FC}$ = 4, Ar^F), 108.8 (s, py), 53.1 (s, *N*-*C*H_2), 30.1 (s, *N*-CH_2*C*H_2), 29.5 (s, CH_2), 28.6 (s, CH_2), 28.5 (s, CH_2), 25.9 (s, CH_2), −2.1 (d, $^1J_{RhC}$ = 18, Rh-CH_3). **ESI-HRMS** (CH_3CN, 180 °C, 3 kV): positive ion: 650.0849 *m*/*z*, $[M]^+$ (calc. 650.0858). **Elemental Analysis** Calc. for $C_{57}H_{46}BF_{24}IN_5ORh$ (1513.15 g mol^{-1}): C, 45.23; H, 3.06; N, 4.63. Found: C, 45.18; H, 2.97; N, 4.58. **IR (CH_2Cl_2):** *v*(CO) 2070 cm^{-1}. **IR (CH_3CN):** *v*(CO) 2066 cm^{-1}.

[Rh(**2c**)(CO)Cl_2][BAr^F_4] (**21a**): To a J. Young's NMR tube charged with **9** (0.008 g, 0.006 mmol) and $PhICl_2$ (0.002 g, 0.007 mmol) was added CD_2Cl_2 (0.5 mL) under an argon atmosphere. This resulted in a rapid color change from yellow to pale yellow and quantitative formation of **21a**, which was characterized immediately in situ by NMR spectroscopy. ESI-HRMS and IR data were obtained from crude (impure) mixtures of **21a** prepared in a similar manner and passed through a silica plug.

^{1}H NMR (500 MHz, CD_2Cl_2): δ 8.09 (t, $^3J_{HH}$ = 7.7, 1H, py), 7.70–7.75 (m, 8H, Ar^F), 7.68 (d, $^3J_{HH}$ = 7.8, 2H, py), 7.56 (br, 4H, Ar^F), 7.34 (d, $^3J_{HH}$ = 1.6, 2H, imid), 7.26 (d, $^3J_{HH}$ = 1.8, 2H, imid), 6.63 (d, $^2J_{HH}$ = 15.8, 2H, py*CH*$_2$), 5.21 (d, $^2J_{HH}$ = 15.8, 2H, py*CH*$_2$), 4.65 (ddd, $^2J_{HH}$ = 14.7, $^3J_{HH}$ = 12.8, 4.2, 2H, *N*-*CH*$_2$), 4.12 (ddd, $^2J_{HH}$ = 14.7, $^3J_{HH}$ = 12.5, 5.7, 2H, *N*-*CH*$_2$), 1.98–2.11 (m, 2H, CH_2), 1.86–1.98 (m, 2H, CH_2), 1.38–1.61 (m, 10H, CH_2), 1.12–1.36 (m, 6H, CH_2). **^{13}C{^{1}H} NMR** (126 MHz, CD_2Cl_2, *selected data only*): δ 180.7 (d, $^1J_{RhC}$ = 57, carbonyl), 160.1 (d, $^1J_{RhC}$ = 30, carbene). **ESI-HRMS** (CH_3CN, 180 °C, 3 kV) positive ion: 606.1271 *m*/*z*, $[M]^+$ (calc. 606.1268). **IR (CH_2Cl_2):** *v*(CO) 2110 cm^{-1}.

[Rh(**11**)(CO)Cl_2][BAr^F_4] (**21b**): A solution of **10** (0.020 g, 0.015 mmol) and $PhICl_2$ (0.004 g, 0.015 mmol) in CH_2Cl_2 (2 mL) was stirred at room temperature for 3 h. The reaction mixture was layered with pentane and left to stand for 16 h to give the yellow crystalline product, which was isolated by filtration and washed with pentane (2 × 5 mL). Yield: 0.014 g (67 %).

^{1}H NMR (500 MHz, CD_2Cl_2): δ 8.43 (t, $^3J_{HH}$ = 8.2, 1H, py), 7.84 (d, $^3J_{HH}$ = 2.2, 2H, imid), 7.70–7.75 (m, 8H, Ar^F), 7.64 (d, $^3J_{HH}$ = 8.2, 2H, py), 7.56 (s, 4H, Ar^F), 7.36 (d, $^3J_{HH}$ = 2.2, 2H, imid), 4.41 (t, $^3J_{HH}$ = 7.7, 4H, *N*-*CH*$_2$), 2.09 (app. quint, *J* = 7, 4H, *N*-CH_2*CH*$_2$), 1.56 (app. quint, *J* = 6, 4H, CH_2), 1.34–1.51 (m, 12H, CH_2). **^{13}C{^{1}H} NMR** (101 MHz, CD_2Cl_2): δ 181.6 (d, $^1J_{RhC}$ = 57, carbonyl), 173.9 (d, $^1J_{RhC}$ = 33, carbene), 162.3 (q, $^1J_{CB}$ = 49, Ar^F), 150.9 (s, py), 147.6 (s, py), 135.4 (s, Ar^F), 129.5 (q, $^2J_{CF}$ = 32, Ar^F), 125.2 (q, $^1J_{FC}$ = 272, Ar^F), 124.7 (s, imid), 119.1 (s, imid), 118.1 (sept., $^3J_{FC}$ = 4, Ar^F), 109.9 (s, py), 53.3 (s, *N*-*C*H_2), 31.1 (s, *N*-CH_2*C*H_2), 29.2 (s, CH_2), 28.6 (s, CH_2), 28.1 (s, CH_2), 25.6 (s, CH_2). **ESI-HRMS** (CH_3CN, 180 °C, 3 kV): positive ion: 578.0958 *m*/*z*, $[M]^+$ (calc.

578.0955). **Elemental Analysis** Calc. for $C_{56}H_{43}BCl_2F_{24}N_5ORh$ (1442.57 g mol^{-1}): C, 46.63; H, 3.00; N, 4.85. Found: C, 46.52; H, 2.85; N, 4.89. **IR (CH_2Cl_2):** *ν*(CO) 2111 cm^{-1}.

[Rh(**11**)(CO)$(CCPh)_2$][BAr^F_4] (**22**): To a solution of **21b** (0.040 g, 0.0277 mmol) in Et_2O (2 mL) at -78°C under argon was added 0.100 mL of phenyl acetylene magnesium bromide as 1.0 M solution in THF (0.100 mmol). The resulting yellow suspension was allowed to warm to room temperature and filtered onto an alumina plug (pipette, 3 cm). The alumina was washed with Et_2O before elution of the product in CH_2Cl_2. An excess of pentane was added to the filtrate to precipitate fine white crystals before the solvent was removed by filtration. Successive washings with pentane afforded the product **22** as an off-white crystalline solid. Yield: 0.015 g (34 %).

^{1}H NMR (500 MHz, CD_2Cl_2) δ 8.41 (t, $^3J_{HH}$ = 8.3, 1H, py), 7.86 (d, $^3J_{HH}$ = 2.2, 2H, imid), 7.71 - 7.74 (br, 8H, Ar^F), 7.65 (d, $^3J_{HH}$ = 8.3, 2H, py), 7.55 - 7.57 (br, 4H, Ar^F), 7.36 (d, $^3J_{HH}$ = 2.2, 2H, imid), 7.06 - 7.09 (m, 6H, Ph), 6.92 - 6.96 (m, 4H, Ph), 4.36 (t, $^3J_{HH}$ = 8.5, 4H, *N*-CH_2), 2.21 - 2.28 (m, 4H, CH_2), 1.58 - 1.64 (m, 4H, CH_2), 1.39 - 1.46 (m, 4H, CH_2), 1.30 - 1.38 (m, 4H, CH_2), 1.23 - 1.28 (m, 4H, CH_2). **^{13}C{^{1}H} NMR** (151 MHz, CD_2Cl_2) δ 176.8 (d, $^1J_{RhC}$ = 34, carbene), 162.3 (q, $^1J_{CB}$ = 50, Ar^F), 150.2 (s, py), 145.9 (s, py), 135.3 (s, Ar^F), 131.7 (s, Ph), 129.4 (q, $^2J_{CF}$ = 32, Ar^F), 128.4 (s, Ph), 127.1 (s, Ph), 126.6 (s, Ph), 125.1 (q, $^1J_{CF}$ = 272, Ar^F), 124.4 (s, imid), 118.3 (s, imid), 118.0 (sept., $^3J_{FC}$ = 4, Ar^F), 109.1 (s, py), 106.7 (d, $^2J_{RhC}$ = 6, Rh-C_α≡C_β-Ph), 84.5 (d, $^1J_{RhC}$ = 31, Rh-C_α≡C_β-Ph), 53.5 (s, *N*-CH_2), 30.6 (s, CH_2), 29.3, (s, CH_2), 28.7 (s, CH_2), 28.2 (s, CH_2), 25.9 (s, CH_2); *carbonyl resonance not observed*. **Elemental Analysis** Calc. for $C_{72}H_{53}BF_{24}N_5ORh$ (1573.93 g mol^{-1}): C, 54.94; H, 3.39; N, 4.45. Found: C, 55.03; H, 3.28; N, 4.46).

3.6.1.5 Other Transmetallation Reactions

General Procedure for Reactions with Grignards: To a solution of **21b** in Et_2O or THF at -78°C under argon, in a flask equipped with a suba-seal, was added an excess of the corresponding Grignard reagent. Aliquots were taken by syringe under a dynamic flow of argon and analysed by ESI-LRMS. The reactions were allowed to come to room temperature before further purification or analysis.

Reaction with methyl magnesium bromide (**26a**): Following the general procedure with 0.020 g of **21b** (0.014 mmol) and a 3.0 M solution of MeMgBr in Et_2O (0.05 mL, 0.150 mmol) afforded a pale lilac reaction mixture which was allowed to warm to approx. 5°C before sampling for ESI-LRMS, dominant ion: 510 *m/z* consistent with product. Stirring at room temperature for 1 h afforded a deep purple/indigo solution, an aliquot of which gave an identical MS spectrum.

Attempts at filtration, precipitation or removal of solvent resulted loss of colour and the observation of solvent-adducts of magnesium salts by ^{1}H NMR spectroscopy.

Reaction with phenyl ethyl magnesium bromide (**26b**): Following the general procedure with 0.010 g of **21b** (0.007 mmol) and a 1.0 M solution of $PhCH_2CH_2MgBr$ in THF (0.05 mL, 0.050 mmol) afforded a pale lilac reaction mixture which was allowed to warm to room temperature (dark blue suspension) before sampling for ESI-LRMS, dominant ion: 690.3 *m/z* consistent with product. After a further hour at room temperature, reaction mixture was a suspension of brown solid in a purple solution with green residues on the sides of the flask; mass spectrum unchanged. After 5 h, purple solution filtered into a J. Young's reaction flask and diluted with pentane to afforded a brown solid. Analysis by ^{1}H NMR spectroscopy indicated dominant presence of THF-magnesium salts.

Reaction with 3,5-di(*tert*-butyl)phenyl ethyl magnesium bromide (**26c**): A solution of **3,5-di(^{t}Bu)phenyl ethyl bromide** (**23**, see **Section 3.6.1.6**) (0.010 g, 0.034 mmol) in Et_2O was transferred by cannula into a Schlenk flask containing magnesium turnings (approx. 0.002 g, 0.080 mmol). Addition of a crystal of I_2 gave an orange solution that became colourless after 10 minutes of stirring. This solution was stirred overnight at room temperature before transfer onto a solid sample of **21b** (0.010 g, 0.007 mmol) in a J. Young's NMR tube under argon containing a sealed capillary of C_6D_6 for machine-lock. The NMR tube was sealed and shaken to afford a blue suspension, which was kept at -72°C until analysis at room temperature. Consumption of **21b** was clear by ^{1}H NMR spectroscopy alongside appearance of two sets of coupled doublets at 6.71 (J = 18 Hz), 6.66 (J = 11 Hz), 5.66 (J = 18 Hz) and 5.11 (J = 11 Hz) ppm, but no coherent product identified. Analysis of the NMR sample or of mixtures generated following the general procedure showed no clear signals in the mass spectra.

Reaction with 3,5-di(*tert*-butyl)phenyl acetylene (**26d**): To a solution of **24** (0.025 g, 0.117 mmol) in THF (3 mL) at -78°C under argon was added 0.08 mL (0.128 mmol) of ^{n}BuLi as 1.6M solution in hexanes. Warming to room temperature afforded a yellow solution, which was stirred for 2 h before returning to -78°C and addition of a solution of **21b** (0.035 g, 0.024 mmol) in THF (1 mL, -78°C) by cannula. The resulting orange solution rapidly turned brown before giving a purple solution on warming to room temperature. Aliquot analysis by ESI-LRMS showed no **21b** but products of mono and bis-transmetallation, +/- CO. After heating at 75°C for 1 h, only bis-transmetallation products were observed. Heating for a further 2 days did not achieve further loss of the carbonyl ligand. Concentration of the reaction mixture and extraction with toluene afforded a mixture of products by proton NMR spectroscopy, which resisted attempts at purification.

Reaction with *tert*-butyl acetylene (**26e**): Following the procedure reported by Chan and Yam for the *in-situ* generation of copper-acetylides for transmetallation with gold(III) chloride pincer complexes,[66] a solution of **21b** (0.010 g, 0.007 mmol) and copper(I) iodide (approx. 0.1 mg, 0.7 μmol) in CH_2Cl_2 was cannula transferred onto ***tert*-butyl acetylene** (**25**) (approx. 10 μL, 0.01 mmol) in triethylamine (0.5 mL). The resulting pink-red solution was stirred at 45°C for 3 h before aliquot analysis by ESI-LRMS showed product (670.2 *m/z*) and reduction-product **10**. The reaction mixture was filtered at room temperature to remove excess copper iodide and diluted with pentane to afford a purple precipitate, which was washed with pentane and dried by analysis by NMR spectroscopy. Proton NMR spectra were consistent with an asymmetric pincer-ligand containing species also incorporating two inequivalent ^{t}Bu groups but minimal $[BAr^F{}_4]^-$ counter anion. The complex did not prove amenable to further purification and characterisation.

*3.6.1.6 Synthesis of 3,5-Di(tert-butyl)phenyl Ethyl Bromide **23***

3,5-di(*tert*-butyl)phenyl ethyl bromide (**23**) was accessed in 4 steps from **3,5-di(*tert*-butyl)phenyl acetylene** (**24**)[62] using a modification of the procedure reported for the stepwise reduction of *p*-(*t*Bu)phenyl acetylene to *p*-(*t*Bu)phenyl ethyl bromide.[67]

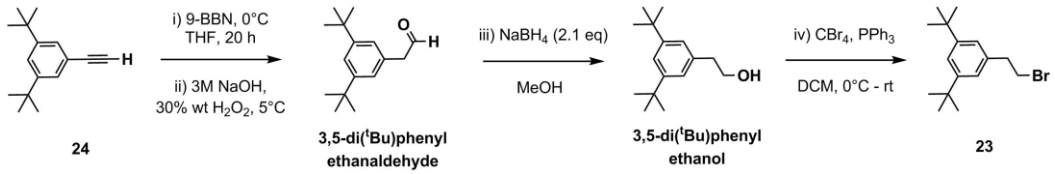

Scheme 3.14:** Synthesis of **23** from **25.

3,5-di(*tert*-butyl)phenyl ethanaldehyde: To a solution of **3,5-di(*tert*-butyl)phenyl acetylene** (**24**) (1.00 g, 4.67 mmol) in THF (5 mL) at 0°C under nitrogen was added 9-borabicyclo[3.3.1]nonane as 0.5 M solution in THF (9.8 mL, 4.90 mmol). The reaction mixture was stirred at 0°C for 20 h before addition of a fresh 1 : 1 mixture of 3M NaOH (7.8 mL) and 30 % wt H_2O_2 (7.8 mL) and a further 2 h of stirring. The reaction was quenched at 5°C by dilution in H_2O and extraction in EtOAc. Combined organics were washed with brine before drying over Na_2SO_4 and concentration to a yellow oil, which was purified by column chromatography (10 % Et_2O in pentane) to afford **3,5-di(*tert*-butyl)phenyl ethanaldehyde** as a colourless oil. Yield: 0.330 g (30 %). **^{1}H NMR** (400 MHz, $CDCl_3$) δ 9.75 (s, 1H, C(O)*H*), 7.37 (s, 1H, *p*-Ar), 7.05 (s, 2H, *o*-Ar), 3.67 (s, 2H, CH_2COH), 1.33 (s, 18H, C(CH_3)$_3$).

3,5-di(*tert*-butyl)phenyl ethanol: A solution of **3,5-di(*tert*-butyl)phenyl ethanaldehyde** (0.280 g, 1.21 mmol) in anhydrous MeOH (15 mL) was transferred onto sodium borohydride (0.096 g, 2.53 mmol) under argon. The resulting reaction mixture was stirred for 1.5 h before addition of

a 5 % solution of $NaHCO_3$ and extraction with CH_2Cl_2 (5 x 10 mL). Combined organics were dried over Na_2SO_4 and concentrated to a yellow oil, which was purified by column chromatography (CH_2Cl_2) to afford a crude mixture of **3,5-di(*tert*-butyl)phenyl ethanol** of approx. 90 % purity by ^{1}H NMR. Yield: 0.144 g (51 %). Selected ^{1}H NMR data for **3,5-di(*tert*-butyl)phenyl ethanol** in mixture: **^{1}H NMR** (400 MHz, $CDCl_3$) δ 7.31 (s, 1H, *p*-Ar), 7.07 (s, 2H, *o*-Ar), 3.87 (t, $^3J_{HH}$ = 6.5, 2H, CH_2CH_2OH), 2.87 (t, $^3J_{HH}$ = 6.5, 2H, CH_2CH_2OH), 1.56 (br, 1H, O*H*), 1.32 (s, 18H, $C(CH_3)_3$). *Used without further purification.*

3,5-di(*tert*-butyl)phenyl ethyl bromide (**23**): PPh_3 (0.177 g, 0.676 mmol) was added portionwise to a solution of CBr_4 (0.224 g, 0.676 mmol) and **3,5-di(*tert*-butyl)phenyl ethanol** (0.144 g, 0.614 mmol) in CH_2Cl_2 at 0°C to afford a dark orange suspension. The reaction mixture was stirred at 0°C for 30 minutes before warming to room temperature, whereupon it was stirred for a further 3 h. Addition of excess hexane gave a white suspension that was filtered through silica and concentrated to a colourless oil, which was subjected to column chromatography (hexane) to afford a crude mixture of **3,5-di(*tert*-butyl)phenyl ethyl bromide** of approx. 90 % purity by ^{1}H NMR. Yield: 0.100 g (55 %). Selected ^{1}H NMR data for **3,5-di(*tert*-butyl)phenyl ethyl bromide** in mixture: **^{1}H NMR** (400 MHz, $CDCl_3$) δ 7.32 (s, 1H, *p*-Ar), 7.05 (s, 2H, *o*-Ar), 3.56 (t, $^3J_{HH}$ = 8.0, 2H, CH_2CH_2Br), 3.16 (t, $^3J_{HH}$ = 8.0, 2H, CH_2CH_2Br), 1.32 (s, 18H, $C(CH_3)_3$). *Used without further purification.*

3.6.2 Variable Temperature NMR Simulations

Simulation of the fluxional process was carried out by line shape analysis of the methylene bridge resonances using gNMR (v4.1.2).

*3.6.2.1 Rhodium(I) Complex **9** in C_6D_6 (285 – 350 K)*

See **Fig. 3.6**. To better model the shape of the exchanging methylene bridge resonances H_a and H_b, exchange calculations for $H_a \leftrightarrow H_b$ and $H_c \leftrightarrow H_d$ (*N*-$C\underline{H}_2CH_2$ resonances) were computed simultaneously. The linewidth for each spectrum was taken from the solvent peak. Coupling constants ($^3J_{HaHb}$ = 14.63 Hz and $^3J_{HcHd}$ = 13.05 Hz) were calculated separately at 298 K then fixed for all temperatures. Coupling of H_c and H_d to $NCH_2C\underline{H}_2$ protons was simulated with constants $^3J_{HcHe}/^3J_{HdHf}$ = 10.25 Hz and $^3J_{HdHe}/^3J_{HcHf}$ = 4.90 Hz, estimated from the spectrum at 298 K. Separation of H_a and H_b ($\Delta\delta_{ab}$) was fixed at 0.73 ppm from the 298 K spectrum. The relative positions of H_c and H_d do not have a clear dependence on temperature and were fixed by analysis of individual spectra. Hence simulation of $H_c \leftrightarrow H_d$ only served to facilitate measurement of $H_a \leftrightarrow H_b$ and the computed rates are not used in calculations of $\Delta G^{\ddagger}$, but show rough agreement with values for $H_a \leftrightarrow H_b$.

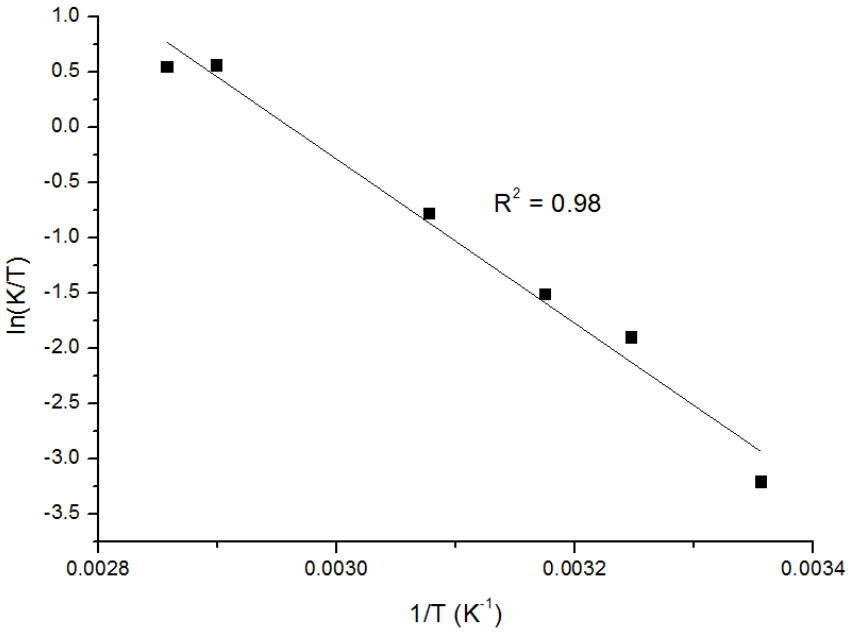

Fig. 3.21: *Eyring Plot for the fluxional behaviour of **9** in C_6D_6 from 298 to 350 K, as determined from $H_a \leftrightarrow H_b$.*

Eyring analysis of the rate data gave $\Delta H^{\ddagger}$ = 62 ± 4 kJ mol^{-1}, $\Delta S^{\ddagger}$ = -15 ± 13 J mol^{-1} K^{-1} and $\Delta G^{\ddagger}_{298\,K}$ = 66 ± 8 kJ mol^{-1}. As an independent check of the simulation, $\Delta G^{\ddagger}_{est}$ was calculated using **Eq. 2.1** (**Chapter 2**) for the resonance pairs H_a/H_b and H_c/H_d, giving 66.7 kJ mol^{-1} and 67.1 kJ mol^{-1} respectively.

*3.6.2.2 Rhodium(I) Complex **16** in C_6D_6 (285 – 350 K) and in CD_2Cl_2 (250 – 308 K)*

Lineshape analysis of VT ^{1}H NMR spectra of **16** in both C_6D_6 and CD_2Cl_2 was conducted but gave unsatisfactory results, with large entropy values, that did not correlate with estimated values using **Eq. 2.1**. $\Delta\delta_{ab}$ in both spectra (particularly CD_2Cl_2) was found to have a positive dependence on temperature and, as a result, only the $\Delta G^{\ddagger}_{est}$ values (calculated using **Eq. 2.1**) are used in comparison of **9** and **16**. It is worth noting that **Eq. 2.1** is known to be sensitive to changes of $\Delta\nu$ with temperature,[68] but this does not explain the disparity between calculation and estimation in C_6D_6. Nevertheless, details of the simulations are given below.

C_6D_6 (285 – 350 K): The separation of H_a and H_b was fixed at $\Delta\delta_{ab}$ = 0.79 after analysis of the 285 K spectrum. Similarly, $^3J_{HH}$ and linewidth parameters were fixed at 14 Hz and 2 Hz respectively. Eyring analysis of the rate data gave $\Delta H^{\ddagger}$ = 60 ± 3 kJ mol^{-1}, $\Delta S^{\ddagger}$ = 93 ± 9 J mol^{-1} K^{-1} and $\Delta G^{\ddagger}_{298\,K}$ = 32 ± 5 kJ mol^{-1}. As an independent check of the simulation, $\Delta G^{\ddagger}_{est}$ was calculated using **Eq. 2.1** (**Chapter 2**) with T_c = 325 K and $\Delta\nu$ = 398 Hz, giving 61.5 kJ mol^{-1}, which is markedly different.

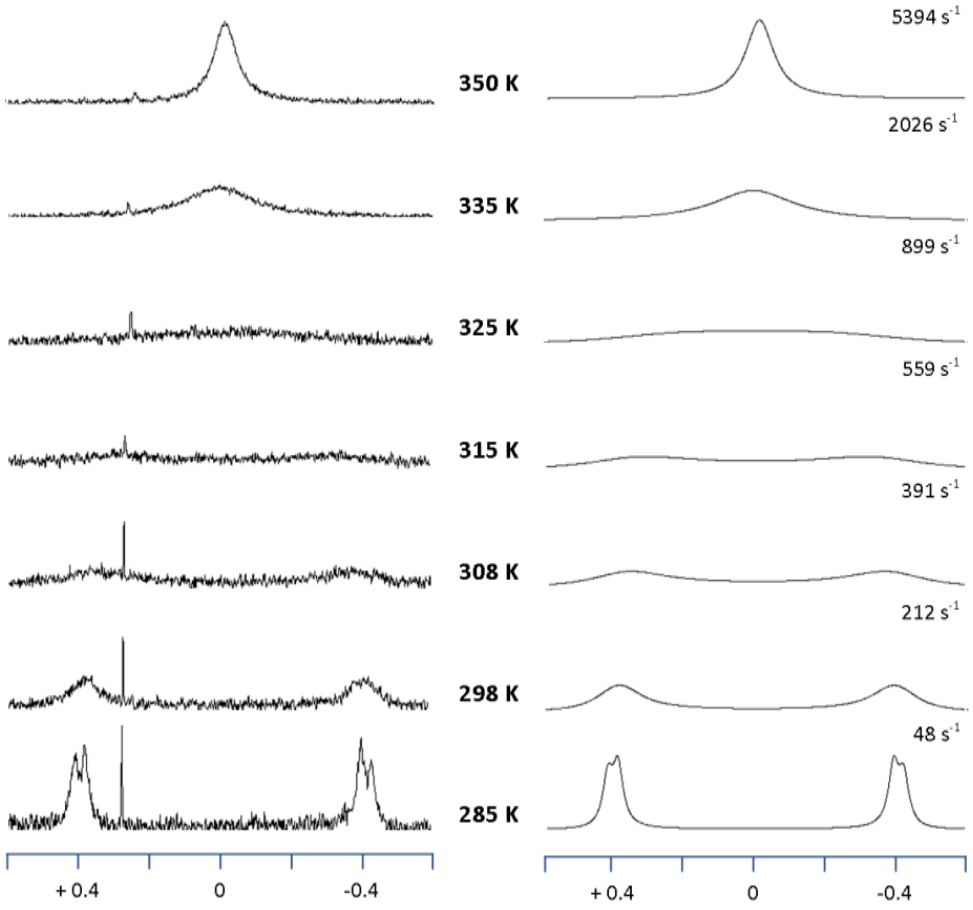

Fig. 3.22: *Experimental (left) and simulated spectra (right) for ^{1}H NMR spectra of **16** (C_6D_6, 500 MHz). The spectra are aligned by the centre of exchange for protons H_a and H_b (x = 0).*

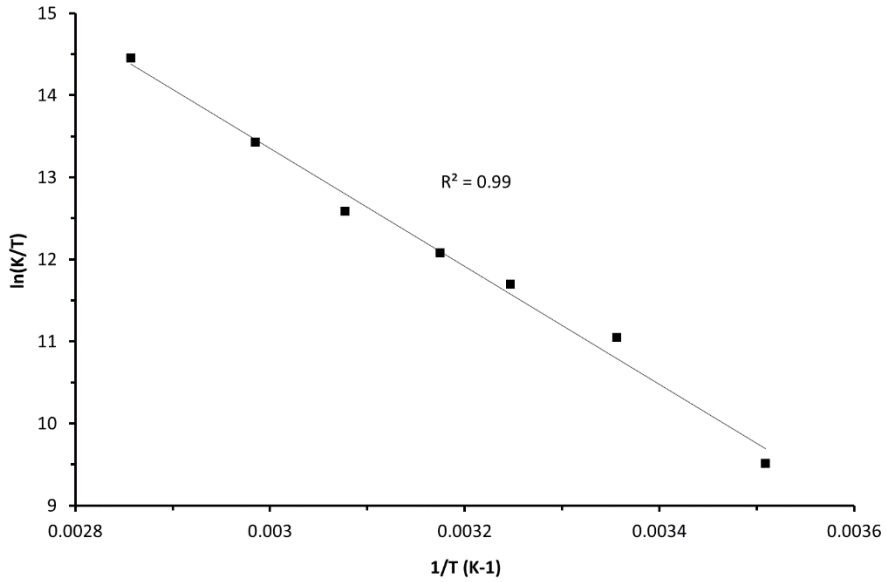

Fig. 3.23: *Eyring Plot for the fluxional behaviour of **16** in C_6D_6 from 285 to 350 K, as determined by $H_a \leftrightarrow H_b$.*

CD_2Cl_2 (250 – 308 K): Fixed parameters for the coupling constant $^{3}J_{HH}$ = 14.9 Hz and linewidth = 2 Hz, were taken from the 250 K spectrum. Through analysis of the experimental spectra, positive temperature dependence was found for both $\Delta\delta_{ab}$ (0.001**T** + 0.1578, where **T** is the

temperature in Kelvin) and the centrepoint (0.0005**T** + 5.1126 ppm). Values of H_a and H_b thus obtained were employed in the simulations and resulting Eyring analysis to obtain $\Delta H^{\ddagger}$ = 46 ± 4 kJ mol^{-1}, $\Delta S^{\ddagger}$ = 46 ± 15 J mol^{-1} K^{-1} and $\Delta G^{\ddagger}_{298\,K}$ = 32 ± 9 kJ mol^{-1}, showing good agreement with those in C_6D_6. As an independent check of the simulation, $\Delta G^{\ddagger}_{est}$ was calculated using **Eq. 2.1** with estimated T_c = 315 K (due to approaching coalescence in 308 K spectrum) and $\Delta\nu$ = 213 Hz, giving 61.1 kJ mol^{-1}. As noted for the C_6D_6-derived estimation, this is markedly different from the result from lineshape analysis.

*3.6.2.3 Rhodium(I) complex **9** in CD_2Cl_2 under 1 atm CO (185 – 273 K)*

The separation of H_a and H_b was fixed at $\Delta\delta_{ab}$ = 0.411 after analysis of the 185 K spectrum. Similarly, $^3J_{HH}$ and linewidth parameters were fixed at 14.16 Hz and 2 Hz respectively.

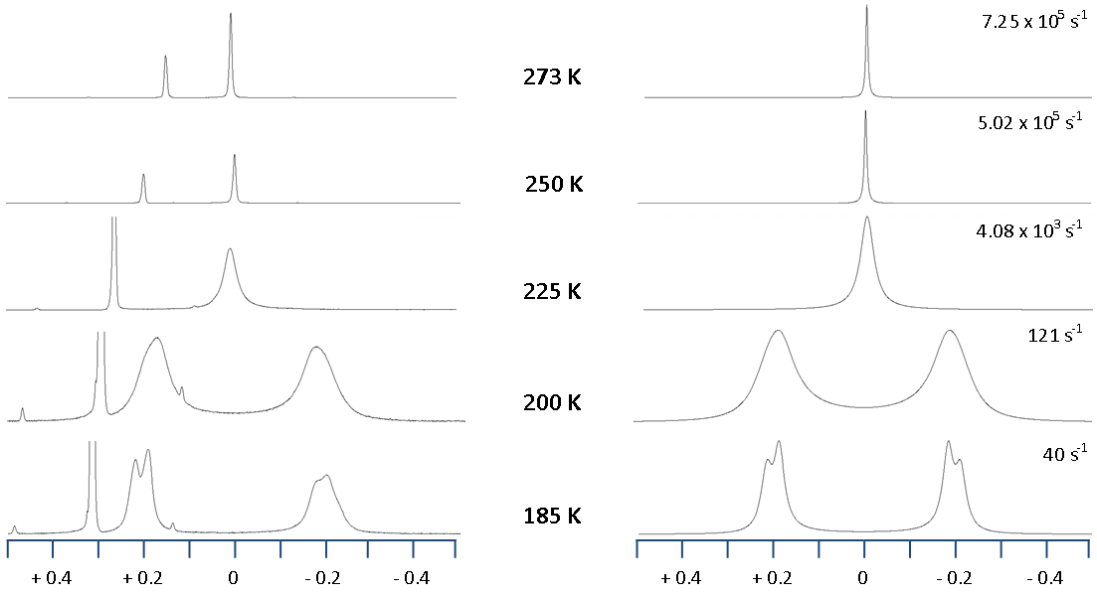

Fig. 3.24: *Experimental (left, with solvent peak) and simulated spectra (right) for ^{1}H NMR spectra of **9** (CD_2Cl_2, 1 atm CO, 500 MHz). The spectra are aligned by the centre of exchange for protons H_a and H_b (x = 0).*

Eyring analysis of the rate data gave $\Delta H^{\ddagger}$ = 38 ± 4 kJ mol^{-1}, $\Delta S^{\ddagger}$ = -9 ± 17 J mol^{-1} K^{-1} and $\Delta G^{\ddagger}_{298\,K}$ = 40 ± 9 kJ mol^{-1}. As an independent check of the simulation, $\Delta G^{\ddagger}_{est}$ was calculated using **Eq. 2.1** for the resonance pairs H_a/H_b, giving 41.1 kJ mol^{-1}.

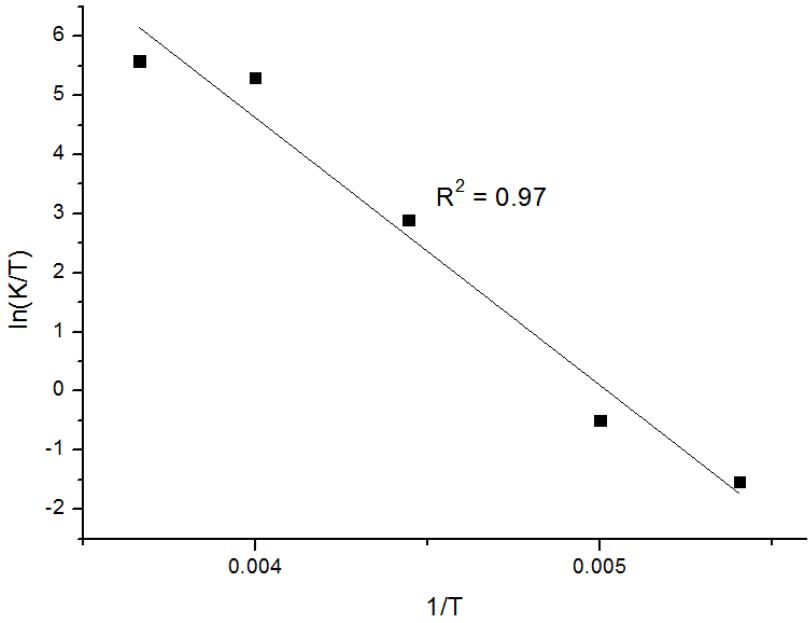

Fig. 3.25: *Eyring Plot for the fluxional behaviour of* ***9*** *in* CD_2Cl_2 *(1 atm CO, 185 - 273 K) as determined from* $H_a \leftrightarrow H_b$.

3.6.3 Computational Studies

Mechanisms **Pathway A**^{Rh} and **Pathway B**^{Rh} were evaluated for their potential in the rhodium carbonyl system with all structures optimised using dispersion-inclusive exchange correlation functional M06,[69] and combinations of the Stuttgart RSC 1997 ECP (Rh) and 6-31G(d,p) (C, H, N, O) basis sets.[70,71]

3.6.4 Selected Crystallographic Data

Crystallographic data for **9**, **9***, **10**, **18**, **19**, **20**, **21** and **22** are summarised in **Table 3.3** and **Table 3.4**. Data were collected on an Oxford Diffraction Gemini Ruby CCD disffractometer using graphite monochromated Mo Kα (λ = 0.71073 Å, for **9**, **10**, **18**, **19**, **20**, **21** and **22**) or Cu Kα (λ = 1.54178 Å, for **9***) radiation and a low temperature device [150(2) K]. Data were collected and reduced using CrysAlisPro. All non-hydrogen atoms were refined anisotropically using SHELXL,[72] through the Olex2 interface.[73] Hydrogen atoms were placed in calculated positions using the riding model.

Table 3.3: *Crystallographic data for* ***9****,* ***9****,* ***10*** *and* ***18****.*

	9	**9***	**10**	**18**.$CHCl_3$
CCDC[a]/ID code	1025594[a]	1027503[a]	1025595[a]	1038863
Figure	**3.3**	**3.3**	**3.3**	**3.11**
Formula	$C_{58}H_{47}BF_{24}N_5ORh$	$C_{58}H_{47}BF_{24}N_5ORh$	$C_{56}H_{43}BF_{24}N_5ORh$	$C_{61}H_{49}BCl_3F_{24}N_4O_2Rh$
M	1399.72	1399.72	1371.67	1546.11
Crystal system	triclinic	triclinic	monoclinic	triclinic
Space group	$P\bar{1}$	$P\bar{1}$	$P2_1/c$	P-1
***T* [K]**	150(2)	150(2)	150(2)	150(2)
***a* [Å]**	9.3661(3)	13.0450(10)	13.3809(5)	13.0625(12)
***b* [Å]**	18.7809(6)	14.5880(14)	28.7207(11)	15.7650(13)
***c* [Å]**	19.3860(6)	17.4059(11)	16.9649(7)	17.5041(14)
***α* [°]**	116.409(3)	104.723(7)	90	70.987(7)
***β* [°]**	94.878(3)	105.186(7)	105.369(4)	83.584(7)
***γ* [°]**	92.986(3)	102.973(8)	90	70.335(8)
***V* [$Å^3$]**	3027.66(18)	2937.5(4)	6286.6(5)	3209.2
***Z* (*Z'*)**	2	2	4	2
Density [g cm^{-3}]	1.535	1.582	1.449	1.600
***μ* (mm^{-1})**	0.400	3.452	0.384	0.507
***ϑ* range [°]**	3.16 ≤ θ ≤ 26.37	6.49 ≤ θ ≤ 66.58	3.32 ≤ θ ≤ 26.37	2.96 ≤ θ ≤ 26.37
Reflns collected	23522	18880	96566	35179
R_{int}	0.0340	0.1078	0.0638	0.0726
Completeness [%]	99.8	99.8	99.8	
No. of data/restr/param	12359/852/960	10378/830/924	12828/1087/955	13106/1164/1066
R_1 **[I > 2σ(I)]**	0.0495	0.0803	0.0546	0.0810
wR_2 **[all data]**	0.1117	0.2151	0.1572	0.1587
GoF	1.051	1.018	1.040	1.071
Largest diff. pk and hole [e $Å^{-3}$]	0.69/-0.53	0.89/-1.10	0.94/-0.59	0.67/-0.67
Flack (*x*)	n/a	n/a	n/a	n/a

[a] Full crystallographic details are documented in CIF format and have been deposited with the Cambridge Crystallographic Data Centre. These data can be obtained free of charge via www.ccdc.cam.ac.uk/data_request/cif

Table 3.4: *Crystallographic data for* ***19, 20b, 21b*** *and* ***22****.*

	19.1/3(C_6H_6)	**20b**	**21b.**1/2(CH_2Cl_2)	**22**
CCDC[a]/ID code	1025598[a]	1025596[a]	1025597[a]	0154abc15
Figure	**3.13/3.14**	**3.16**	**3.18**	**3.22**
Formula	$C_{28}H_{36}N_5ORh$	$C_{57}H_{46}BF_{24}IN_5ORh$	$C_{56.5}H_{44}BCl_3F_{24}N_5ORh$	$C_{79}H_{61}BF_{24}N_5ORh$
M	531.53	1513.61	1485.03	1666.04
Crystal system	trigonal	triclinic	triclinic	monoclinc
Space group	$R\bar{3}$	$P\bar{1}$	$P\bar{1}$	$P2_1/n$
***T* [K]**	150(2)	150(2)	150(2)	150(2)
***a* [Å]**	19.2242(2)	14.26866(15)	12.7330(4)	23.7608(6)
***b* [Å]**	19.2242(2)	17.1057(2)	15.5875(4)	10.7739(2)
***c* [Å]**	37.5121(8)	24.6768(3)	17.0556(5)	29.6225(8)
***α* [°]**	90	90	100.337(2)	90
***β* [°]**	90	94.4576(10)	97.165(2)	99.904(3)
***γ* [°]**	120	90	113.343(3)	90
***V* [Å^3]**	12003.0(4)	6004.78(12)	2984.89(16)	7470.3(3)
***Z* (Z')**	18	4	2	4
Density [g cm^{-3}]	1.398	1.674	1.652	1.481
***μ* (mm^{-1})**	0.669	0.918	0.541	0.338
***ϑ* range [°]**	2.98 ≤ θ ≤ 26.37	3.10 ≤ θ ≤ 26.37	2.94 ≤ θ ≤ 26.37	3.03 ≤ θ ≤ 26.37
Reflns collected	89168	70014	29569	82806
R $_{int}$	0.0444	0.0348	0.0287	0.1056
Completeness [%]	99.8	99.8	99.8	99.8
No. of data/restr/param	5442/459/389	12268/885/909	12186/373/852	15259/144/1001
***R $_1$* [I > 2σ(I)]**	0.0374	0.0446	0.0474	0.0608
***wR$_2$* [all data]**	0.0958	0.1141	0.1184	0.1495
GoF	1.078	1.053	1.037	1.007
Largest diff. pk and hole [e Å^{-3}]	1.75/-0.22	2.62/-0.96	1.05/-0.92	0.83/-0.59
Flack (*x*)	n/a	n/a	n/a	n/a

[a] Full crystallographic details are documented in CIF format and have been deposited with the Cambridge Crystallographic Data Centre. These data can be obtained free of charge via www.ccdc.cam.ac.uk/data_request/cif

3.7 References

(1) Poyatos, M.; Mas-Marzá, E.; Mata, José A.; Sanaú, M.; Peris, E. *Eur. J. Inorg. Chem.* **2003**, *2003*, 1215-1221.
(2) Wilson, J. M.; Sunley, G. J.; Adams, H.; Haynes, A. *J. Organomet. Chem.* **2005**, *690*, 6089-6095.
(3) Wright, J. A.; Danopoulos, A. A.; Motherwell, W. B.; Carroll, R. J.; Ellwood, S.; Saßmannshausen, J. *Eur. J. Inorg. Chem.* **2006**, *2006*, 4857-4865.
(4) Frey, G. D.; Rentzsch, C. F.; von Preysing, D.; Scherg, T.; Mühlhofer, M.; Herdtweck, E.; Herrmann, W. A. *J. Organomet. Chem.* **2006**, *691*, 5725-5738.
(5) Moser, M.; Wucher, B.; Kunz, D.; Rominger, F. *Organometallics* **2007**, *26*, 1024-1030.
(6) Wucher, B.; Moser, M.; Schumacher, S. A.; Rominger, F.; Kunz, D. *Angew. Chem., Int. Ed.* **2009**, *48*, 4417-4421.
(7) Juergens, E.; Wucher, B.; Rominger, F.; Toernroos, K. W.; Kunz, D. *Chem. Commun.* **2015**, *51*, 1897-1900.
(8) Ruwwe, J.; Martín-Alvarez, J. M.; Horn, C. R.; Bauer, E. B.; Szafert, S.; Lis, T.; Hampel, F.; Cagle, P. C.; Gladysz, J. A. *Chem. Eur. J.* **2001**, *7*, 3931-3950.
(9) Wang, L.; Hampel, F.; Gladysz, J. A. *Angew. Chem. Int. Ed.* **2006**, *45*, 4372-4375.
(10) Wang, L.; Shima, T.; Hampel, F.; Gladysz, J. A. *Chem. Commun.* **2006**, 4075-4077.
(11) Vazquez-Serrano, L. D.; Owens, B. T.; Buriak, J. M. *Inorg. Chim. Acta* **2006**, *359*, 2786-2797.
(12) Solid-state structure of **9** obtained by removal of a highly disorded solvent molecule using the SQUEEZE algorithm (see following reference). No solvent present in solid-state structure of **9***.
(13) Spek, A. *Acta Crystallographica Section D* **2009**, *65*, 148-155.
(14) Bera, J. K.; Dunbar, K. R. *Angew. Chem. Int. Ed.* **2002**, *41*, 4453-4457.
(15) Laurila, E.; Oresmaa, L.; Hassinen, J.; Hirva, P.; Haukka, M. *Dalton Trans.* **2013**, *42*, 395-398.
(16) Inoki, D.; Matsumoto, T.; Nakai, H.; Ogo, S. *Organometallics* **2012**, *31*, 2996-3001.
(17) Tran, N. T.; Stork, J. R.; Pham, D.; Olmstead, M. M.; Fettinger, J. C.; Balch, A. L. *Chem. Commun.* **2006**, 1130-1132.
(18) Novoa, J. J.; Aullon, G.; Alemany, P.; Alvarez, S. *J. Am. Chem. Soc.* **1995**, *117*, 7169-7171.
(19) Aullón, G.; Alemany, P.; Alvarez, S. *Inorg. Chem.* **1996**, *35*, 5061-5067.
(20) Helps, I. M.; Matthes, K. E.; Parker, D.; Ferguson, G. *J. Chem. Soc., Dalton Trans.* **1989**, 915-920.
(21) Parker, D.; Lehn, J.-M.; Rimmer, J. *J. Chem. Soc., Dalton Trans.* **1985**, 1517-1521.
(22) Grimme, S.; Djukic, J.-P. *Inorg. Chem.* **2011**, *50*, 2619-2628.
(23) Miecznikowski, J. R.; Grundemann, S.; Albrecht, M.; Megret, C.; Clot, E.; Faller, J. W.; Eisenstein, O.; Crabtree, R. H. *Dalton Trans.* **2003**, 831-838.
(24) Hahn, F. E.; Jahnke, M. C.; Pape, T. *Organometallics* **2007**, *26*, 150-154.
(25) Gründemann, S.; Albrecht, M.; Loch, J. A.; Faller, J. W.; Crabtree, R. H. *Organometallics* **2001**, *20*, 5485-5488.
(26) Hahn, F. E.; Jahnke, M. C.; Gomez-Benitez, V.; Morales-Morales, D.; Pape, T. *Organometallics* **2005**, *24*, 6458-6463.
(27) Schultz, K. M.; Goldberg, K. I.; Gusev, D. G.; Heinekey, D. M. *Organometallics* **2011**, *30*, 1429-1437.
(28) Watarai, N.; Kawasaki, H.; Azumaya, I.; Yamasaki, R.; Saito, S. *Heterocycles* **2009**, *79*, 531-548.
(29) Tulloch, A. A. D.; Danopoulos, A. A.; Tizzard, G. J.; Coles, S. J.; Hursthouse, M. B.; Hay-Motherwell, R. S.; Motherwell, W. B. *Chem. Commun.* **2001**, 1270-1271.
(30) Danopoulos, A. A.; Tulloch, A. A. D.; Winston, S.; Eastham, G.; Hursthouse, M. B. *Dalton Trans.* **2003**, 1009-1015.

(31) Mills, G.; Jónsson, H. *Phys. Rev. Lett.* **1994**, *72*, 1124-1127.
(32) Liu, X.; Pattacini, R.; Deglmann, P.; Braunstein, P. *Organometallics* **2011**, *30*, 3302-3310.
(33) Brookhart, M.; Green, M. L. H.; Parkin, G. *Proc. Natl. Acad. Sci. USA* **2007**, *104*, 6908-6914.
(34) Filonenko, G. A.; Smykowski, D.; Szyja, B. M.; Li, G.; Szczygiel, J.; Hensen, E. J. M.; Pidko, E. A. *ACS Catal.* **2015**, *5*, 1145-1154.
(35) Filonenko, G. A.; Cosimi, E.; Lefort, L.; Conley, M. P.; Copéret, C.; Lutz, M.; Hensen, E. J. M.; Pidko, E. A. *ACS Catal.* **2014**, *4*, 2667-2671.
(36) del Pozo, C.; Iglesias, M.; Sánchez, F. l. *Organometallics* **2011**, *30*, 2180-2188.
(37) Ben-Ari, E.; Leitus, G.; Shimon, L. J. W.; Milstein, D. *J. Am. Chem. Soc.* **2006**, *128*, 15390-15391.
(38) Schaub, T.; Radius, U.; Diskin-Posner, Y.; Leitus, G.; Shimon, L. J. W.; Milstein, D. *Organometallics* **2008**, *27*, 1892-1901.
(39) Schwartsburd, L.; Iron, M. A.; Konstantinovski, L.; Diskin-Posner, Y.; Leitus, G.; Shimon, L. J. W.; Milstein, D. *Organometallics* **2010**, *29*, 3817-3827.
(40) Gunanathan, C.; Milstein, D. *Chem. Rev.* **2014**, *114*, 12024-12087.
(41) Fogler, E.; Iron, M. A.; Zhang, J.; Ben-David, Y.; Diskin−Posner, Y.; Leitus, G.; Shimon, L. J. W.; Milstein, D. *Inorg. Chem.* **2013**, *52*, 11469-11479.
(42) Vogt, M.; Rivada-Wheelaghan, O.; Iron, M. A.; Leitus, G.; Diskin-Posner, Y.; Shimon, L. J. W.; Ben-David, Y.; Milstein, D. *Organometallics* **2012**, *32*, 300-308.
(43) Vogt, M.; Nerush, A.; Iron, M. A.; Leitus, G.; Diskin-Posner, Y.; Shimon, L. J. W.; Ben-David, Y.; Milstein, D. *J. Am. Chem. Soc.* **2013**, *135*, 17004-17018.
(44) Schwartsburd, L.; Iron, M. A.; Konstantinovski, L.; Ben-Ari, E.; Milstein, D. *Organometallics* **2011**, *30*, 2721-2729.
(45) Hernandez-Juarez, M.; Vaquero, M.; Alvarez, E.; Salazar, V.; Suarez, A. *Dalton Trans.* **2013**, *42*, 351-354.
(46) Gunanathan, C.; Milstein, D. *Science* **2013**, *341*, 1229712.
(47) Khusnutdinova, J. R.; Garg, J. A.; Milstein, D. *ACS Catal.* **2015**, 2416-2422.
(48) Mukherjee, A.; Srimani, D.; Chakraborty, S.; Ben-David, Y.; Milstein, D. *J. Am. Chem. Soc.* **2015**, *137*, 8888-8891.
(49) Chang, Y.-H.; Takeuchi, K.; Wakioka, M.; Ozawa, F. *Organometallics* **2015**, *34*, 1957-1962.
(50) Feller, M.; Diskin-Posner, Y.; Leitus, G.; Shimon, L. J. W.; Milstein, D. *J. Am. Chem. Soc.* **2013**, *135*, 11040-11047.
(51) Goldberg, J. M.; Wong, G. W.; Brastow, K. E.; Kaminsky, W.; Goldberg, K. I.; Heinekey, D. M. *Organometallics* **2015**, *34*, 753-762.
(52) Tykwinski, R. R.; Stang, P. J. *Organometallics* **1994**, *13*, 3203-3208.
(53) Lee, C.-C.; Lin, Y.-C.; Liu, Y.-H.; Wang, Y. *Organometallics* **2005**, *24*, 136-143.
(54) Nishio, M. *CrystEngComm* **2004**, *6*, 130-158.
(55) Albers, M. O.; Coville, N. J. *Coord. Chem. Rev.* **1984**, *53*, 227-259.
(56) Nubel, P. O.; Wilson, S.; Brown, T. L. *Organometallics* **1983**, *2*, 515-525.
(57) Webb, J. R.; Figg, T. M.; Otten, B. M.; Cundari, T. R.; Gunnoe, T. B.; Sabat, M. *Eur. J. Inorg. Chem.* **2013**, *2013*, 4515-4525.
(58) Heating **9** in the presence of trimethylamine *N*-oxide and terminal alkynes afforded mixtures of hydro and dehydro-coupled products. Attempts at displacement of the activated CO with internal alkynes and acetonitrile were unsuccessful.
(59) Buschmann, W. E.; Miller, J. S.; Bowman-James, K.; Miller, C. N. In *Inorg. Synth.*; John Wiley & Sons, Inc.: 2002, p 83-91.
(60) McCleverty, J. A.; Wilkinson, G.; Lipson, L. G.; Maddox, M. L.; Kaesz, H. D. In *Inorg. Synth.*; John Wiley & Sons, Inc.: 2007, p 84-86.
(61) Raba, A.; Anneser, M. R.; Jantke, D.; Cokoja, M.; Herrmann, W. A.; Kühn, F. E. *Tetrahedron Letters* **2013**, *54*, 3384-3387.
(62) Philp, D.; Gramlich, V.; Seiler, P.; Diederich, F. *J. Chem. Soc., Perkin Trans. 2* **1995**, 875-886.

(63) Nielsen, D. J.; Cavell, K. J.; Skelton, B. W.; White, A. H. *Inorg. Chim. Acta* **2002**, *327*, 116-125.
(64) Ibrahim, H.; Bala, M. D. *Tetrahedron Letters* **2014**, *55*, 6351-6353.
(65) Taylor, R. T.; Stevenson, T. A. *Tetrahedron Letters* **1988**, *29*, 2033-2036.
(66) Au, V. K.-M.; Tsang, D. P.-K.; Wong, K. M.-C.; Chan, M.-Y.; Zhu, N.; Yam, V. W.-W. *Inorg. Chem.* **2013**, *52*, 12713-12725.
(67) Iwasaki, T.; Takagawa, H.; Singh, S. P.; Kuniyasu, H.; Kambe, N. *J. Am. Chem. Soc.* **2013**, *135*, 9604-9607.
(68) Kemp, W. *NMR in Chemistry: A Multinuclear Introduction*; MacMillan, 1988.
(69) Zhao, Y.; Truhlar, D. G. *Theor. Chem. Acc.* **2007**, *120*, 215-241.
(70) Francl, M. M.; Pietro, W. J.; Hehre, W. J.; Binkley, J. S.; Gordon, M. S.; DeFrees, D. J.; Pople, J. A. *J. Chem. Phys.* **1982**, *77*, 3654-3665.
(71) Hehre, W. J.; Ditchfield, R.; Pople, J. A. *J. Chem. Phys.* **1972**, *56*, 2257-2261.
(72) Sheldrick, G. *Acta Crystallogr. Sect. A* **2008**, *64*, 112-122.
(73) Dolomanov, O. V.; Bourhis, L. J.; Gildea, R. J.; Howard, J. A. K.; Puschmann, H. *J. Appl. Crystallogr.* **2009**, *42*, 339-341.

CHAPTER 4. SYNTHESIS AND REACTIVITY OF RHODIUM ETHYLENE COMPLEXES

This chapter describes the synthesis of rhodium(I) ethylene complexes **27** and **28**, and their application in the homo-coupling of terminal alkynes. Acyclic **27** catalyses the formation of *E*-1,4-enynes, while use of **28** resulted in the formation of interlocked complexes (**Scheme 4.1**). The effect of the substituent **R** on the structural behaviour and reactivity of the latter complexes is also discussed, along with the mechanism of their formation.

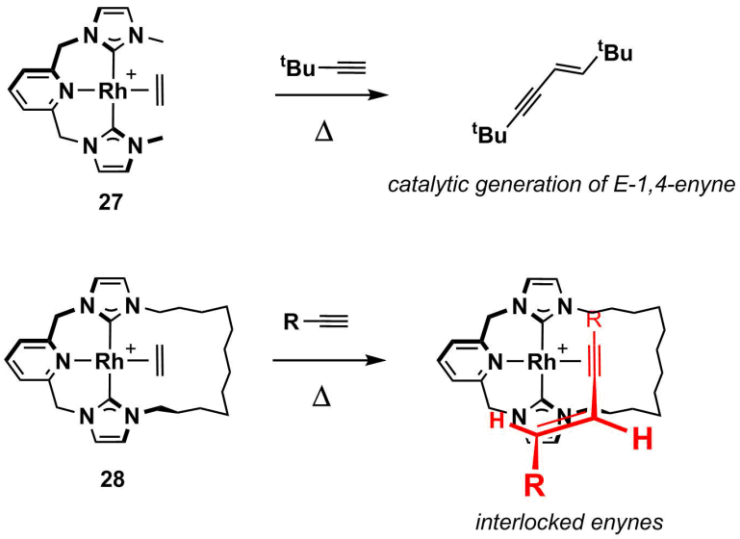

Scheme 4.1: *Terminal alkyne coupling reactions of **27** and **28**.*

4.1 Catalytic Dimerisation of Terminal Alkynes

Alkyne dimerisation is an atom-economical method for the generation of enynes from terminal alkynes and has been catalysed by a range of transition metal complexes, many of which have demonstrated high selectivity despite the large product distribution possible (**Scheme 4.2**).[1,2,3] Empirically, three regioisomers may result from the formal addition of one alkyne C-H bond across the C≡C bond of another; these are the *gem*-1,3-enyne, *Z*-1,4-enyne and *E*-1,4-enynes. Blum, Schumann and co-workers have demonstrated that 1,4-enynes are the thermodynamic products and that thermal isomerisation of *gem*-1,3-enynes to mixtures of *Z*- and *E*-1,4-enynes is possible in the absence of a catalyst.[4] Further activation of the enynes can afford butatrienes,[5] arenes (*via* cyclotrimerisation)[6,7] or other polyenes.[4,8]

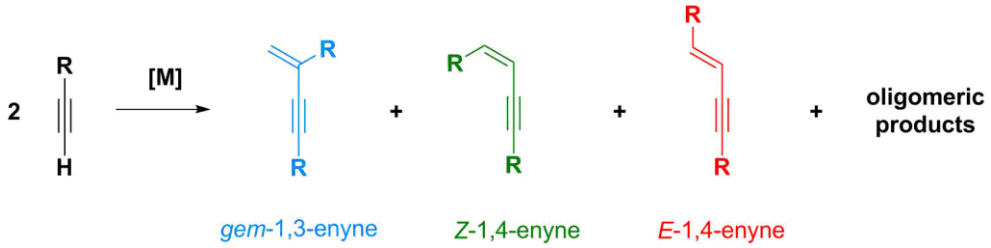

Scheme 4.2: *Key alkyne dimerisation products.*

Pioneering the use of palladium catalysts in this field, Trost showed selective generation of *gem*-1,3-enynes in moderate to high yields could be achieved using a combination of $Pd(OAc)_2$ and a phosphone ligand.[1] A range of functional groups are tolerated and, in addition to homo-coupling, cross-coupling reactions with internal alkynes were successful, affording mixed enynes in up to 92 % yield. More recently, sterically-hindered palladium(NHC) complex **A138** has proved highly selective for the generation of *E*-1,4-enynes.[9]

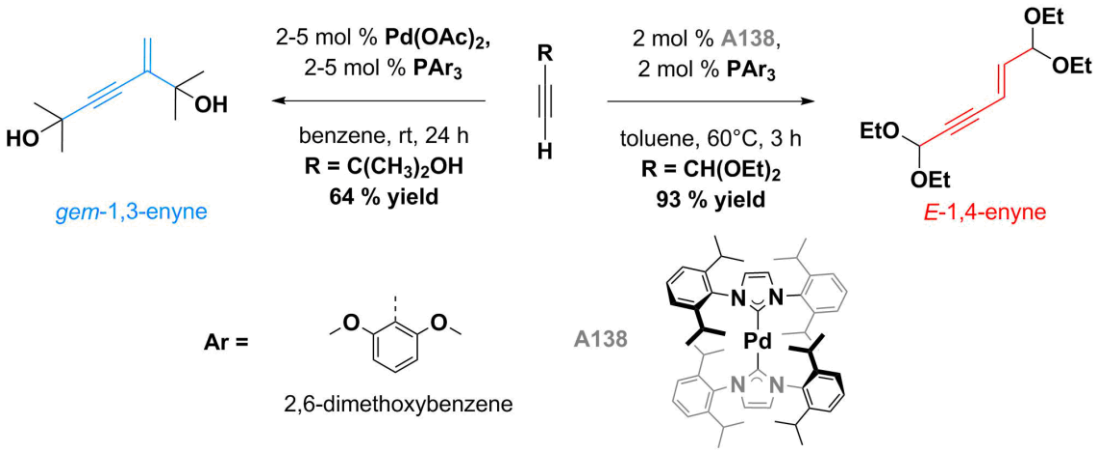

Scheme 4.3: *Palladium-based systems for alkyne dimerisation.*

Rhodium(I) pincers **A139** and **A140** are effective for the production of *E*-1,4-enynes and *gem*-1,3-enynes, respectively (**Scheme 4.4**).[10,11] Dihydride **A139** affords *E*-isomers in 90 – 100 %

yields at 100°C (0.5 mol % catalyst loading) within 10 hours, although more sterically hindered substrates (R = ^{t}Bu, CH_2NMe_2 when R-C≡C-H is alkyne) require longer reaction times and are associated with lower product selectivity.[10] Triazole-based **A140** is the only CNC pincer reported to date for this transformation, showing a high functional group tolerance (amines, ethers, alcohols, halides) and high selectivity for the formation of *gem*-1,3-enynes in moderate-to-quantitative yields at 80°C (1 mol % loading).[11]

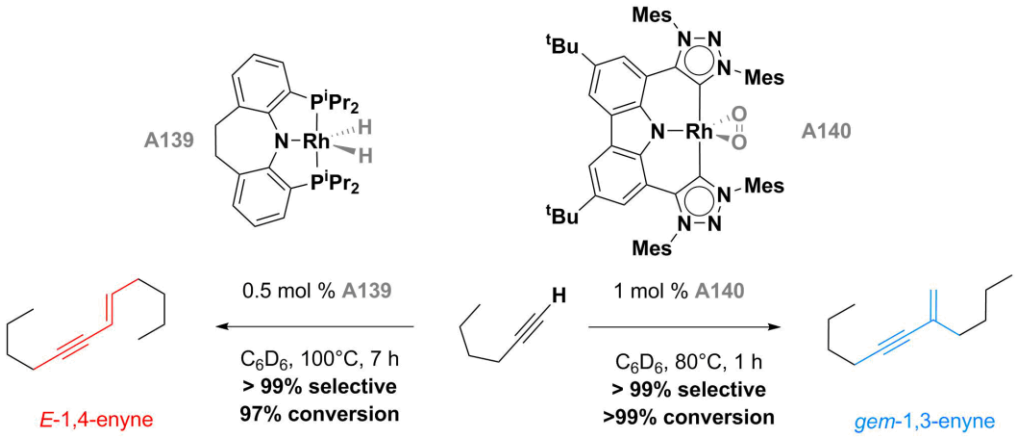

Scheme 4.4: *Rhodium-based pincers for alkyne dimerisation.*

As demonstrated by the divergent capabilities of palladium(0)/palladium(II) and rhodium(I)/rhodium(III) systems (**Scheme 4.3** and **4.4**), multiple mechanistic pathways are possible.[1,3,4,9,10,12-14]

For the majority of palladium and rhodium-based systems reported to date, *E*-1,4-enynes and *gem*-1,3-enynes are the dominant products.[13,14] Two distinct mechanistic pathways that account for these observations are shown in **Scheme 4.5**. Both pathways proceed *via* initial C-H bond activation of the alkyne but diverge during the subsequent insertion of the second alkyne, for which both insertion into the Rh-C (carbometallation),[14] or Rh-H (hydrometallation) bond is possible.[3,13] Selectivity for head-to-tail (*gem*-1,3-enynes) or head-to-head (*E*-1,4-enynes) migratory insertion dictates the regioselectivity in both pathways, and the products are generated by reductive elimination.

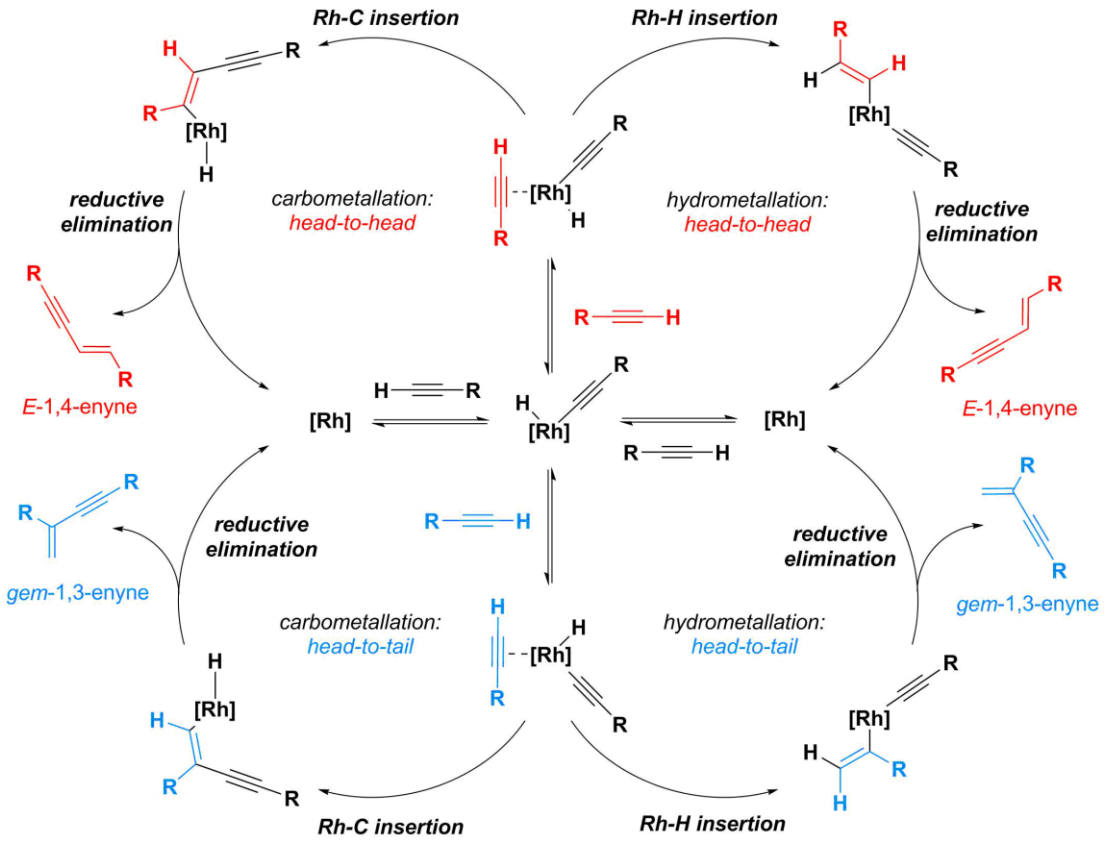

Scheme 4.5: *Carbometallation and hydrometallation pathways for the generation of gem-1,3- and E-1,4-enynes.*

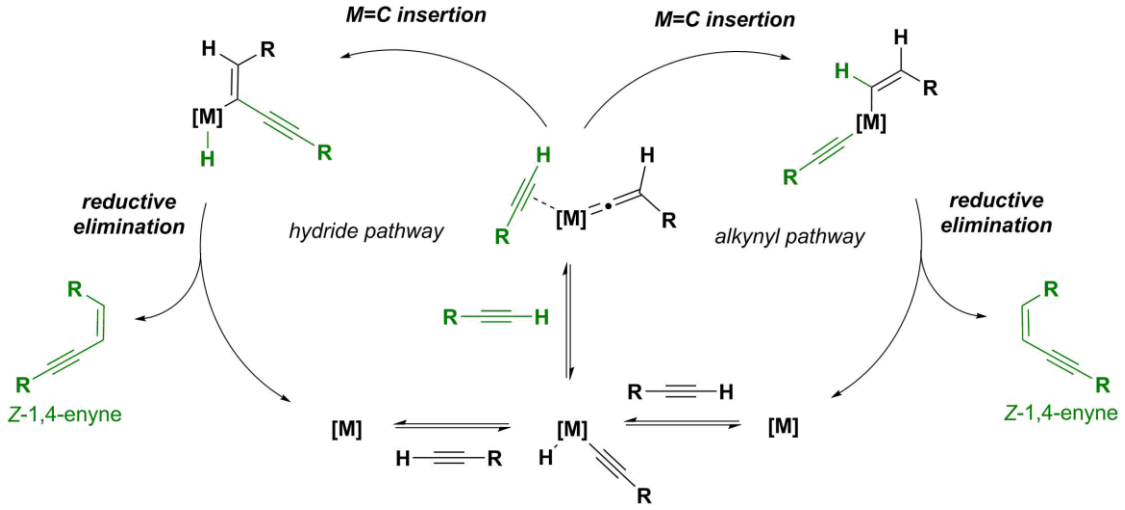

Scheme 4.6: *Mechanistic pathways for the generation of Z-1,4-enynes.*

Generation of the *Z*-1,4-enyne is believed to proceed by a different mechanism, *via* a vinylidene intermediate (**Scheme 4.6**).[3,15,16] While generation of *Z*-1,4-enynes has been observed in sterically hindered rhodium systems,[3,15] *Z*-selective pre-catalysts **A141**, **A142** and **A143** (**Fig. 4.1**) incorporate zirconium[12] and ruthenium[17,18] centres, respectively. The ruthenium POP pincer complex **A142** is notable for the highly selective generation of *Z*-1,4-diphenyl-enyne from phenyl acetylene in 97 % yield with 1 mol % catalyst loading at 80°C, demonstrating a turnover frequency (TOF) of 215 h^{-1}.[17] Similarly, ruthenium-based **A143**,

containing a tetradentate ligand, is highly effective in the dimerisation of alkynes bearing a range of functional groups, affording *Z*-1,4-enynes in 80 – 95 % yields over 24 h at 110°C (0.03 – 2 mol % loadings).[18]

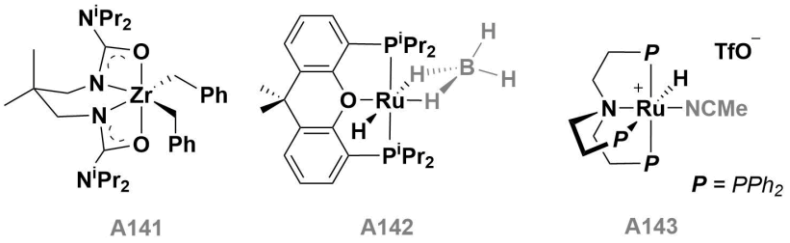

Fig. 4.1: *Catalyst precursors demonstrating high selectivity for Z-1,4-enynes.*

From the aforementioned examples it is clear that the product distribution is highly sensitive to both steric and electronic properties of the ligand. The three enynes are readily distinguishable by ^{1}H NMR spectroscopy due to the coupling constants of the alkene protons (< 7 Hz for *gem*-1,3-enynes,[19] 10 – 12 Hz for *Z*-1,4-enynes,[18] 14 – 16 Hz for *E*-1,4-enynes).[10] Reflecting the preponderance of labile ligands in efficient catalysts **A139 – A143** (highlighted in grey in **Scheme 4.4** and **Fig. 4.1**), rhodium(I) ethylene complexes bearing **2c** (**28**) and an acyclic analogue (**27**) were targeted in order to study their application in alkyne dimerisation reactions.

4.2 Rhodium(I) Ethylene Complexes

In an analogous procedure to the synthesis of **9** and **16**, from their respective silver(I) transfer agents and $[Rh(CO)_2Cl]$, reaction of **5** or **15** with rhodium(I) bis-ethylene dimer $[Rh(C_2H_4)_2Cl]_2$ under an atmosphere of ethylene in Et_2O rapidly afforded **27** and **28**, along with precipitation of silver(I) chloride (**Scheme 4.7**). Unlike the rhodium carbonyls, **27** and **28** are unstable in CH_2Cl_2, demonstrating slow decomposition and generation of free ethylene (approximate $t_{1/2}$ = 24 h), and cannot be purified effectively by silica chromatography.

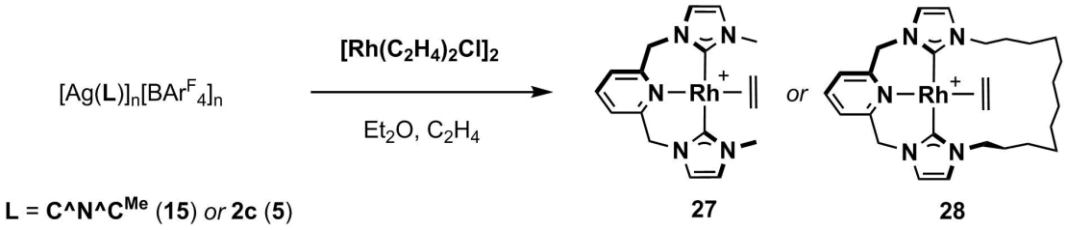

Scheme 4.7: *Synthesis of rhodium(I) ethylene complexes **27** and **28**. $[BAr^F_4]^-$ counter anions omitted in products.*

Purification of **27** was achieved by recrystallization, involving filtration of the reaction mixture and dilution with pentane under ethylene, to afford crystals suitable for XRD that were stored and handled under argon. Elemental analysis values are consistent with the formula $[Rh(\mathbf{C^N^C^{Me}})(C_2H_4)][BAr^F_4]$ and, while the parent cation was not observed, ESI-HRMS showed a major signal corresponding to $[Rh(\mathbf{C^N^C^{Me}})(O_2)]^+$ (402.0424 *m/z*, calc. 402.0432), indicating ready substitution of C_2H_4 during analysis.

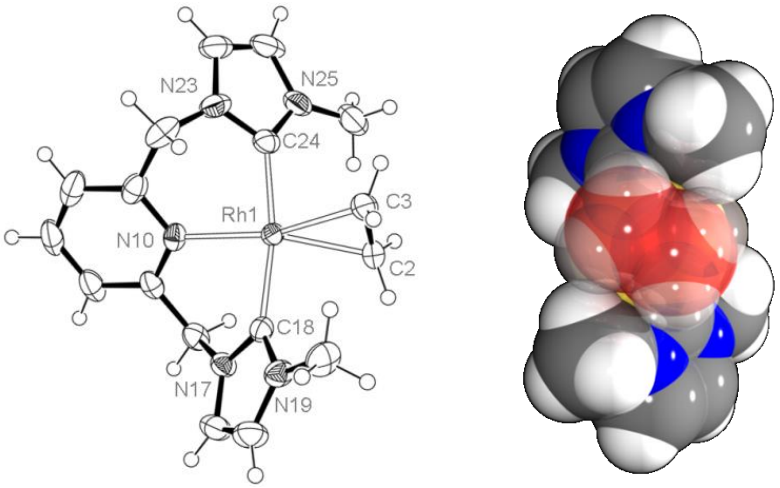

Fig. 4.2: *ORTEP (**left**) and spacefill (**right**) representations of **27**, $[BAr^F_4]^-$ counter anion omitted for clarity. Thermal ellipsoids at 50 % for ORTEP image. Coordinated ethylene highlighted in red to show packing. Selected bond lengths (Å) and angles (°): Rh1-N10, 2.116(2); Rh1-C2, 2.148(2); Rh1-C3, 2.143(3); Rh1-C18, 2.037(2); Rh1-C24, 2.042(2); C2-C3, 1.373(4); C18-Rh1-C24, 169.60(10); N10-Rh1-C2, 161.26(10); N10-Rh1-C3, 161.41(10).*

In the solid-state (**Fig. 4.2**), the rhodium-ethylene interaction in **27** is noticeably weaker than in previously reported NHC systems (**Scheme 4.8**), with Rh-C_{C2H4} bond lengths of *ca*. 2.14 Å (*c.f.* 2.09 – 2.13 Å).[20-22] A short C=C bond of 1.373(4) Å more closely resembles those observed in

saturated-NHC variants of **A144a** (1.38 – 1.40 Å) than unsaturated and/or monomeric derivatives **A144b-A147** (1.40 – 1.42 Å, *c.f.* 1.3391(13) for free ethylene).[20-23]

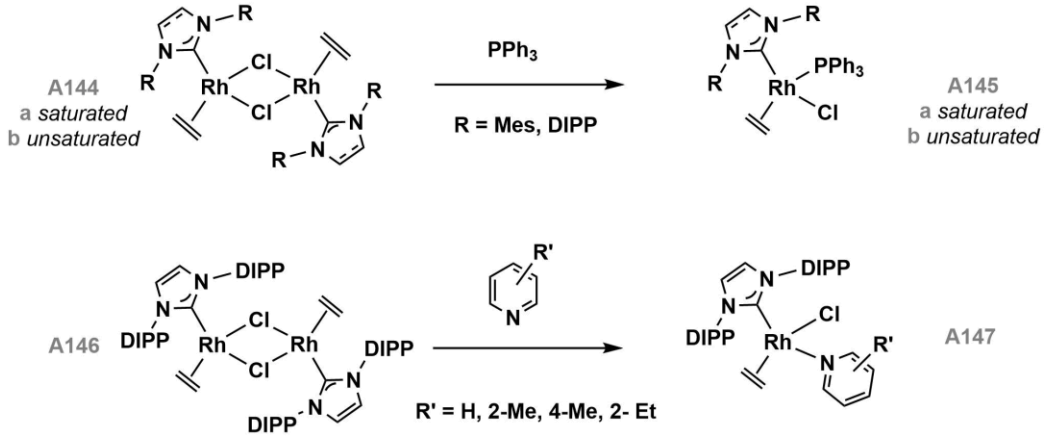

Scheme 4.8: *Rhodium NHC complexes coordinating ethylene.*

Despite established catalytic utility of pincer complexes coordinating ethylene,[24,25] well-defined NHC-based variants are scarce (**Fig. 4.3**). The only reported rhodium precedent is PCP complex **A148b**,[26] which was identified as a component of the equilibrium mixture formed on placing **A148a** under ethylene atmosphere, using ^{31}P NMR spectroscopy. Instead, Fe,[27] Ir[28] and Pt[29,30] complexes of **Type I** pincer ligands account for the majority. Platinum complex **A149** is implicated in hydrovinylation catalysis and has been structurally characterised, revealing an ethylene ligand with C=C bond length comparable to **27** (1.371(7) Å) and orthogonal orientation with respect to the coordination plane of the metal (*c.f*. 59.7(2)[a] in **27**).[30]

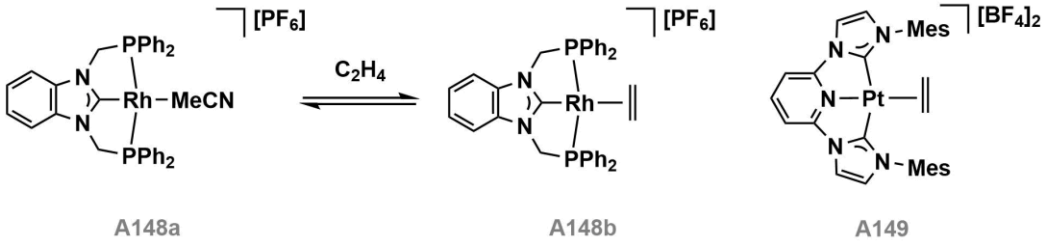

Fig. 4.3: *NHC pincer complexes bearing ethylene.*

Solution ^{1}H and ^{13}C{^{1}H} NMR spectra of **27** display C_2 symmetry at room temperature, with broad signals for the diastereotopic methylene bridge protons (δ 5.04, 5.73; CD_2Cl_2, 500 MHz) suggesting atropisomerism of the pincer backbone, though these signals remain broad on cooling from 298 to 205 K in CD_2Cl_2. Although decomposition was observed on heating in DiFB, coalescence was achieved at 350 K (500 MHz) and, using **Eq. 2.1** with Δν of 317 Hz, the barrier to atropisomerism may be approximated as $\Delta G^{\ddagger}_{est}$ = 67 kJ mol^{-1}, slightly higher than that estimated for carbonyl-complex **16** ($\Delta G^{\ddagger}_{est}$ = 61 kJ mol^{-1}). In the ^{13}C{^{1}H} NMR spectrum at 298

[a] Angle between least squares planes containing 'N10, Rh1, C18, C24, the centroid of C2 and C3' and 'Rh1, C2, C3'

K, weak rhodium coupling is observed for the methylene bridge carbons (δ 56.2, $^{3}J_{RhC}$ = 2 Hz) and coordination of the pincer ligand is corroborated by a carbene resonance at 184.8 ppm, which shows stronger coupling to rhodium: $^{1}J_{RhC}$ = 40 Hz.

Coordination of ethylene is denoted by a broad 4H resonance at δ 3.50 in the ^{1}H NMR spectrum at 298 K (CD_2Cl_2, 500 MHz), but no corresponding resonance was found in the $^{13}C\{^{1}H\}$ NMR spectrum (101 MHz). These observations are indicative of a highly fluxional ethylene ligand, with a ^{1}H resonance that lies within the range of rhodium-bound precedents (δ 1.3 – 3.5),[20-22] but bears closer resemblance to free ethylene (δ 5.40, CD_2Cl_2)[31] than a strongly bound molecule (*ca*. 2 ppm).

The observed instability of **27** in CD_2Cl_2 and DiFB solutions is presumably due to weak coordination of the alkene. To probe this observation, **27** was dissolved in THF-d^8 and sealed in a J. Young's NMR tube under argon. The resulting ^{1}H NMR spectra evolved over 3 days to give a mixture of **27**, free ethylene, and a new compound tentatively assigned as [Rh(**2c**)(THF)]$^{+}$ (1 : 0.1 : 0.7). Placing the mixture under 1 atm CO afforded compound **16** (exhibiting time averaged C_{2v} symmetry under CO) and free ethylene (**Fig. 4.4**).

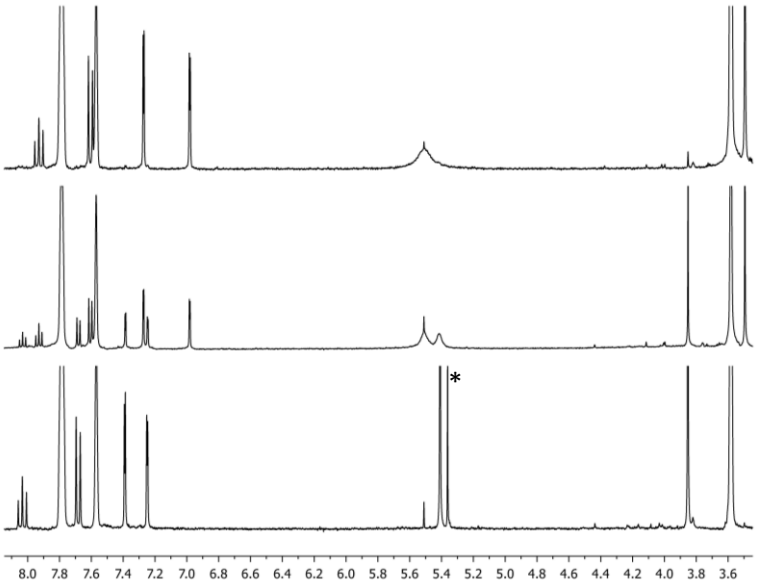

Fig. 4.4: *^{1}H NMR spectra of **27** in d^8-THF after approx. 15 minutes (**top**), 3 days (**middle**) and under an atmosphere of CO after 4 days under argon (**bottom**).* * = free ethylene*

Prepared independently (**Scheme 3.5**, **Chapter 3**), **16** bears close resemblance to **27**, both in solution and in the solid-state (**Fig. 4.5**). Resonances in the $^{13}C\{^{1}H\}$ NMR spectrum of **16** for the carbene (δ 182.9, $^{1}J_{RhC}$ = 42 Hz) and methylene bridge atoms (δ 55.8, $^{3}J_{RhC}$ = 2 Hz) are particularly comparable to those of **27** (*vide supra*). Between the solid-state structures of **16** and **27**, the coordination geometry of the **C^N^C^{Me}** ligand is almost unchanged, with Rh-C_{NCN} bond lengths of *ca*. 2.04 Å and only a small difference in the Rh-N bond distances (2.140(2) Å

for **16** *vs* 2.116(2) Å for **27**). Both **16** and **27** adopt square planar geometry with C_{NCN}-Rh-C_{NCN} angles of 172.89(10)° and 169.60(10)°, respectively.

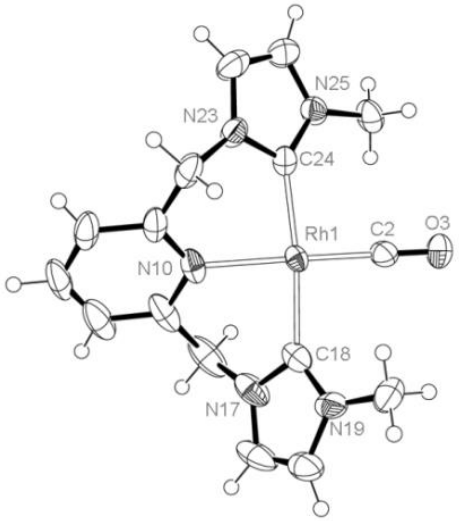

Fig. 4.5: *ORTEP representation of **16**. Thermal ellipsoids at 50 % probability and $[BAr^F_4]^-$ counter anion omitted for clarity. Selected bond lengths (Å) and angles (°): Rh1-C2, 1.809(3); Rh1-N10, 2.140(2); Rh1-C18, 2.039(3); Rh1-C24, 2.031(3); C2-O3, 1.145(3); N10-Rh1-C2, 179.00(11); C18-Rh1-C24, 172.89(10).*

Obtaining analytically pure samples of **28** proved difficult and the macrocyclic complex did not crystallise readily from a range of solvents. For instance, filtration of the reaction mixture in Et_2O enabled removal of precipitated silver salts, but addition of hydrocarbon solvents resulted in the formation of oils, which were washed by decantation and dried to afford orange-red foams. Samples obtained in this way demonstrated larger-than-expected integration values for the Ar^F protons (>12H *vs* 8H expected for the *ortho* protons relative to those of the ligand). Despite slow decomposition of **28** in CH_2Cl_2, conducting the reaction in this solvent before rapid filtration through a silica plug consistently afforded foams in *ca*. 60 % yield. This process produced marginally improved integration ratios, of 10-11H *vs* 8H, suggesting purity of 73-80 %. In both cases, coordination of ethylene was confirmed by ^{1}H NMR spectroscopy, with a sharp 4H singlet at 3.46 ppm (CD_2Cl_2, 400 MHz, *c.f.* 3.50 ppm for **27**).

Silver(I) ethylene salts, partnered with the weakly coordinating anion $[BAr^F_4]^-$, are potential culprits for such observations and would explain the larger-than-expected integration values of Ar^F protons observed in isolated material. Supporting this hypothesis, $[Ag(PCy_3)_2][BAr^F_4]$ can be detected by ^{31}P NMR spectroscopy and ESI-LRMS on addition of PCy_3 to crude isolated samples of **28** in CH_2Cl_2.[32] While a number of $[Ag(C_2H_4)_n]^+$ adducts (n = 1, 2, 3) have been spectroscopically and structurally characterised,[33,34] persistence of such species, especially on silica, would not be expected. An alternative explanation could be the partial one-electron oxidation of **27**, mediated by silver salts, to produce paramagnetic species not readily apparent by NMR spectroscopy.

To aid understanding of the structure of **28** in solution, ^{1}H and $^{13}C\{^{1}H\}$ NMR spectra were also obtained for **28** generated *in-situ* from **5** and $[Rh(C_2H_4)_2Cl]_2$ under argon atmosphere, with partial stabilisation offered by the liberation of 1 equiv. of ethylene (**Table 4.1**). Although **28**, demonstrating C_{2v} symmetry and a broad resonance for the methylene bridge protons at *ca*. 5.3 ppm, is notably more fluxional than **27** in solution, good agreement is established between the room temperature NMR spectra of these complexes. For instance, the carbene resonance of **28** is found at 181.2 ppm with rhodium coupling of 40 Hz (*c.f.* δ 184.8, $^{1}J_{RhC}$ = 40 Hz for **27**) and the methylene bridge carbons are represented by a singlet at 56.3 ppm (*c.f.* 56.2 ppm, $^{1}J_{RhC}$ = 2 Hz for **27**). The *in-situ* generated sample of **28** exhibits notable broadening of the ethylene proton resonance with respect to that of isolated material, presumably as a result of exchange with free ethylene. Additionally, a broad resonance between 111.0 and 113.5 ppm (*c.f.* free ethylene at 123 ppm)[31] can be observed in the $^{13}C\{^{1}H\}$ NMR spectrum of isolated **28** in Et_2O under argon, and is tentatively assigned to coordinated ethylene.

Table 4.1: *Selected ^{1}H and $^{13}C\{^{1}H\}$ NMR data for **27** and **28**.*[a]

Sample	δ_{1H}		δ_{13C} (J_{RhC} / Hz)		
	$H_2C{=}CH_2$	pyCH_2	N$\underline{C}$N	$H_2C{=}CH_2$	py$\underline{C}H_2$
27	3.50	5.04, 5.73	184.8 (40)	-	56.2 (2)
28[b]	3.46	5.31	-	-	-
28[c]	3.5 – 5.5	5.29	181.2 (40)	-	56.3

[a] Recorded in CD_2Cl_2 under argon at 298 K. [b] Impure isolated product. [c] In-situ reaction of **5** and $[Rh(C_2H_4)_2Cl]_2$.

While the agreement of NMR data obtained for **28** with **27** is encouraging, pure samples of **28** could ultimately not be obtained and it was instead used *in-situ*. Substantiating this procedure, as well as the ready displacement of ethylene from **27**, clean conversion to **9** was observed when *in-situ* generated **28** was placed under CO (**Scheme 4.9**).

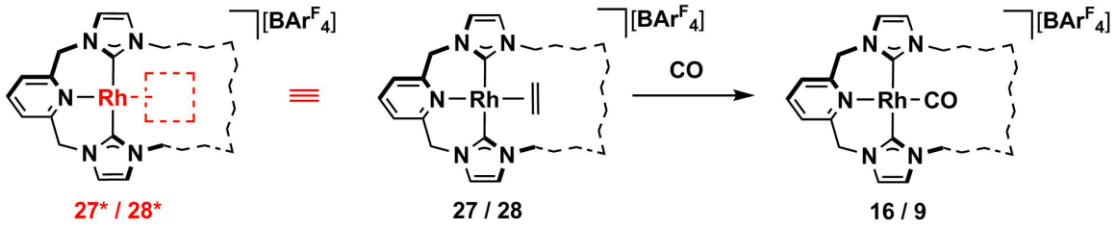

Scheme 4.9: *Reaction of **27** and **28** with CO, demonstrating facile substitution of C_2H_4.*

4.3 Catalytic Terminal Alkyne Coupling Using 27

Addition of *tert*-butyl alkyne **25** (15 equiv.) to a J. Young's NMR tube containing a solution of **27** (0.005 mmol, 6.7 mol %) in DiFB under argon afforded a dark orange solution that was monitored by ^{1}H NMR spectroscopy, using the Ar^{F} resonances as an internal standard (**Fig. 4.6**). After 4 hours at room temperature the major species observed was *tert*-butyl enyne **29** (4 : 1 *vs* [BAr$^{F}_{4}$]$^{-}$), identified from comparison with data obtained in C_6D_6[35] and $CDCl_3$[9] and a characteristic *trans*-alkene $^{3}J_{HH}$ coupling constant of 16.5 Hz. Some terminal alkyne remained (roughly 1 : 1 with [BAr$^{F}_{4}$]$^{-}$, representing approx. 93 % conversion) alongside other poorly defined species. After a further 16 hours, **25** had been consumed and a 3.5 : 1 ratio of **29** to [BAr$^{F}_{4}$]$^{-}$ was observed. Additional signals pertaining to ene-enyne **30** also became prominent, integrating to 0.6 equiv. against [BAr$^{F}_{4}$]$^{-}$. A summary of the assignment and relevant spectra of **30** are given in **Section 4.6.1.4**.

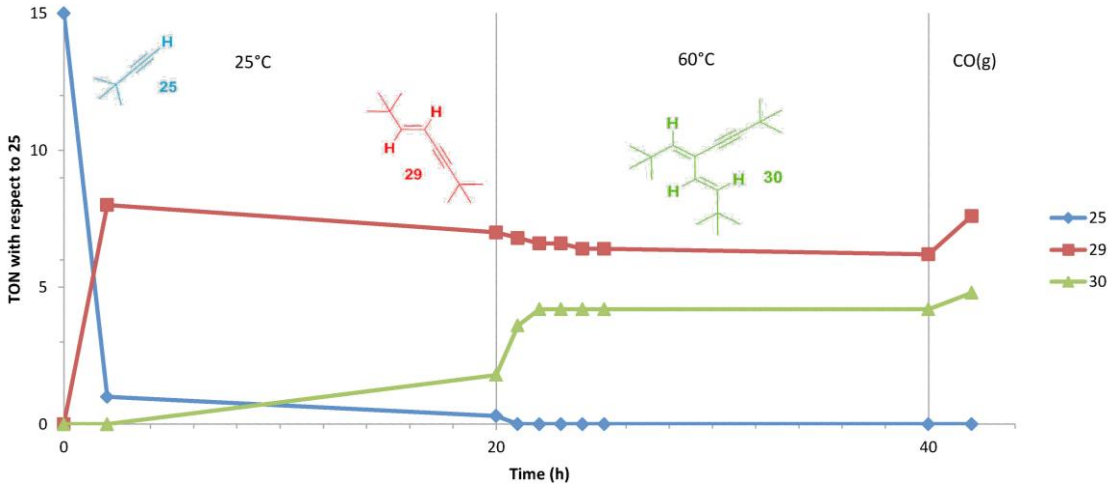

Fig. 4.6: *Homo-coupling of **25** using **27**.*

After subsequent heating at 60°C for 1 h, the ^{1}H NMR spectrum showed further reduction of **29** and corresponding rise in **30**, bringing the ratio to roughly 3.3 : 1.2 : 1 (**29**/**30**/[BAr$^{F}_{4}$]). Two singlets at 3.28 and 3.31 ppm were also assigned to the *N*-methyl groups of an asymmetric pincer complex, consistent with coordination of a bulky, non-linear hydrocarbon. The reaction was monitored for a further 20 h, during which product distribution plateaued at 3.0 : 1.4 : 1.0 (**29**/**30**/[BAr$^{F}_{4}$]). Finally, the sample was cooled, degassed and placed under 1 atm of CO, which generated greater populations of both **29** (3.8 equiv.) and **30** (1.6 equiv.) alongside **16** (0.8 equiv.). These results support the earlier observation of asymmetric pincer complex(es) and suggest 2 equiv. of **25** in total (*e.g.* as **29** or **30**) are bound to a metal complex during the reaction.

Encouraged by this initial experiment, and the selectivity for *E*-1,4-enyne derived products, work was undertaken to study the effects of solvent, catalyst loading and temperature on the selectivity for **29**, using **27** as catalyst; the results of which are summarised in **Table 4.2**.

Table 4.2: *Homo-coupling of **25** using **27**.*

Trial	Solvent	Loading (mol %)	Reaction Coordinate	**Ratio of products** against $[BAr^F_4]^-$ (***TON***[a])			Conversion of 25[b]
				29	**30**	**pincer**	
i	**DiFB**	**6.7**	20 h @ 25°C	3.5 (***7.0***)	0.6 (***1.8***)	-	93 %
			+20 h @ 60°C	3.0 (***6.2***)	1.4 (***4.2***)	0.8 (***1.4***)[b]	> 95 %
ii	**THF**	**6.7**	1 h @ 25°C	-	-	1.0 (***2.0***)[b]	88 %
			+20 h @ 60°C	2.8 (***5.6***)	0.5 (***1.5***)	-	> 95 %
iii	**DiFB/THF**	**6.7**	3 h @ 25°C	1.3 (***2.6***)	-	-	46 %
			+20 h @ 60°C	3.0 (***6.0***)	1.5 (***4.5***)	-	> 95 %
iv	**DiFB**	**0.5**	1 h @ 25°C	11 (***22***)	-	-	11 %
			+20 h @ 60°C	24 (***48***)	-	-	30 %

[a] Relative to **25**. [b] Assuming coordination of 2 equiv. of **29**.

Repeating the homo-coupling in THF (**ii**, **Table 4.2**) afforded negligible **29** after 1 h. Instead, the observation of a pair of inequivalent *N*-methyl signals and two corresponding ^{t}Bu resonances (1 : 1) indicated coordination of a bis(tert-butyl) species, such as **29**. Heating this sample to 60°C for 1 h afforded **29** (1.3 equiv. *vs* $[BAr^F_4]^-$) alongside reduction in the signals for the free alkyne; no signals for **30** were observed. The reaction was monitored over the course of a further 19 hours, during which time the signals for **29** grew in intensity and the consumption of **25** was observed alongside generation of multiple impurities in the aromatic region. The product ratio after 20 hours at 60°C was 2.8 : 0.5 : 1 for **29**/**30**/$[BAr^F_4]^-$, thus demonstrating slower turnover, but greater selectivity for **29** in THF than in DiFB. A mixture of THF and DiFB was also trialled but demonstrated similar final conversion to that achieved in DiFB alone (**iii**, **Table 4.2**).

Noting complete consumption of **25** in reactions **i** – **iii**, lower loadings of **27** were pursued. Using 0.5 mol % **27** in DiFB, 22 turnovers of **25** were achieved within 1 hour at room temperature (**iv**, **Table 4.2**). Conversion was enhanced by heating overnight at 60°C, yet complete consumption of **25** was not observed. At a loading of approximately 0.1 mol %, the catalytic activity of **27** in neat alkyne is negligible at room temperature, but 6 equiv. of **29** were produced after 20 h at 60°C. Interestingly, no evidence for **30** or adducts of the pincer were observed during either reaction, implying further reaction of **29** is competitive with homo-coupling of **25** at high catalyst loadings.

To probe the recyclability of the catalyst, a J. Young's NMR tube containing 2 mol % **27** with respect to **25**, in toluene under argon, was heated at 100°C for 16 h. All starting alkyne was consumed and a 5 : 1 ratio of **29** to **30** was determined by ^{1}H NMR spectroscopy. The sample

was replenished with 50 equiv. of alkyne **25** and heated overnight, resulting again in complete consumption of the alkyne and a 3 : 1 ratio of **29** to **30**. A further 50 equiv. of alkyne and another 16 hours of heating gave the same outcome, however, additional signals in the alkyl region indicated the production of ^{t}Bu-containing by-products and another cycle was not attempted. Extraction with pentane afforded a mixture of **29** and **30** that was used to characterise **30** (see **Section 4.6.1.4**).

Overall, **27** is a poor catalyst, significantly inferior to rhodium PNP and CNC precedents **A139** and **A140** (**Scheme 4.4**). These benchmark catalysts bear central anionic amido-donors that, in comparison to the neutral lutidine donor of **27**, would be expected to promote more facile oxidative addition of substrate alkynes, and hence faster catalysis.

4.4 Synthesis of Interlocked Enynes Using 28

4.4.1 Reaction of 28 and tert-Butyl Alkyne 25

The reaction of *tert*-butyl alkyne **25** with the macrocyclic ethylene complex (**28**) was probed *in-situ* using ^{1}H NMR spectroscopy. Addition of **25** (15 equiv.) to a DiFB solution of crude **28** in a J. Young's NMR tube under argon at room temperature resulted in initial formation of *ca.* 0.6 equiv. of **29**, with no further increase observed 3 hours after mixing. Clear signals in the aromatic region were assigned to the pyridine moiety of the pincer ligand (1 : 1 with $[BAr^{F}_{4}]^{-}$), but the methylene bridge protons could not be conclusively identified. Heating the reaction mixture at 60°C for 1 hour resulted in an increased amount of **29** (1.6 equiv.), a concomitant decrease in **25**, and the appearance of several sharp resonances pertaining to the methylene bridge protons of a new C_1 symmetric complex.

No change was observed after heating for a further hour and the reaction mixture was diluted with pentane prior to passing through a silica plug, from which an orange organometallic compound was obtained on extraction with CH_2Cl_2. Analysis of this material by ^{1}H NMR spectroscopy (*vide infra*) and ESI-LRMS (672.4 *m/z*), enabled assignment of this species as [Rh(**2c**)(**29**)]$^{+}$ **31** (**Scheme 4.10**).

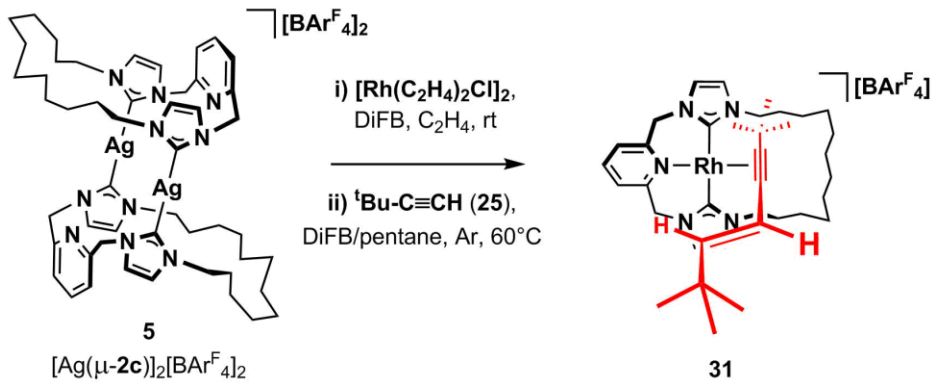

Scheme 4.10: *In-situ generation and reaction of **28** with **25**.*

Seeking to isolate **31** on a larger scale, an excess of **25** was reacted with **28** (from 0.015 mmol of **5**). After heating for 3 hours at 60°C, the reaction mixture was extracted with Et_2O onto a silica plug, which was washed generously with Et_2O before elution of the product as a striking orange solution in CH_2Cl_2. Precipitation with pentane afforded **31** as an orange powder (66 % yield), which was fully characterised by NMR spectroscopy and XRD (*vide infra*, **Fig. 4.7**). In addition, elemental analysis values are consistent with the formula [Rh(**2c**)(**29**)][BAr$^{F}_{4}$], as is ESI-HRMS data (672.3513 *m/z*; calc. 672.3507, $[M]^{+}$), with no loss of the enyne detected. Complex **31** is indefinitely air and moisture-stable in the solid-state and can be crystallised from bench solvents. No reaction is apparent on heating isolated **31** with excess **25**.

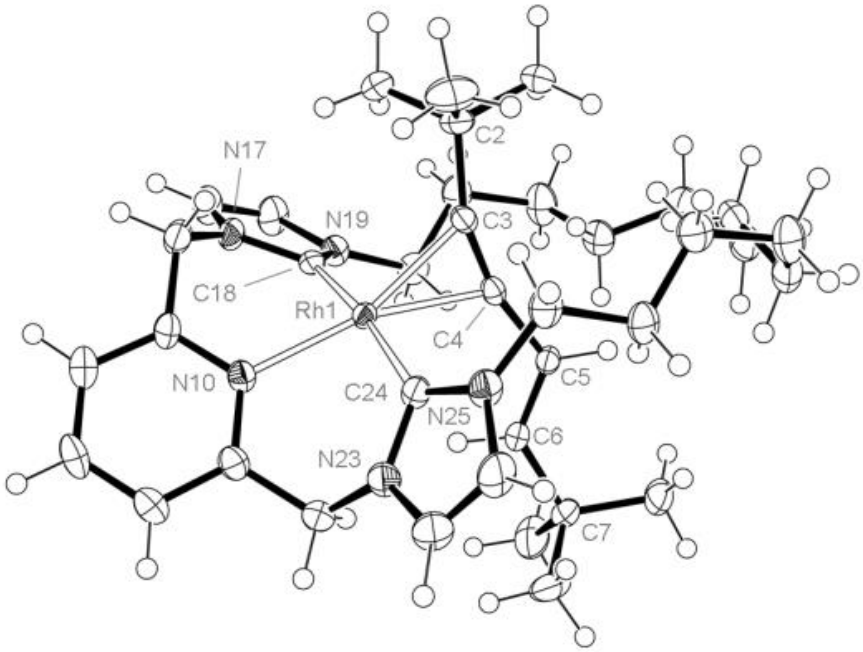

Fig. 4.7: *ORTEP representation of **31**. Thermal ellipsoids at 50 % probability. [BAr$^F_4$]$^-$ counter anion and solvent molecule omitted for clarity. Selected bond lengths (Å) and angles (°): Rh1-C3, 2.132(3); Rh1-C4, 2.093(3); Rh1-N10, 2.103(3); Rh1-C18, 2.039(3); Rh1-C24, 2.071(3); C3-C4, 1.245(6); C4-C5, 1.451(5); C5-C6, 1.335(5); C18-Rh1-C24, 171.41(18); N10-Rh1-C4, 164.14(14); N10-Rh1-C3, 161.59(15); C2-C3-C4, 160.3(4); C3-C4-C5, 164.8(4).*

In the solid-state, binding of the enyne *via* the C≡C bond is confirmed by close interaction of the C4 (alkene-bearing) and C3 atoms with the metal (2.093(3) and 2.132(3) Å, respectively); tilting the alkyne 70.2(2)° from the coordination plane of the pincer.[a] The C-C≡C-C connection is distorted from linearity and exhibits angles of 160.3(4)° and 164.8(4)° for the ^{t}Bu-C≡C and $C_{sp}{}^2$-C≡C bonds, respectively, indicating significant π-donation into the C≡C anti-bonding orbitals. The macrocycle comfortably surrounds the enyne and adopts pseudo-C_2 symmetry. The geometry about the metal is distorted square planar, with inequivalent Rh-C_{NCN} distances of 2.039(3) and 2.071(3) Å and a C_{NCN}-Rh-C_{NCN} bond angle of 171.41(18)°.

Retention of the solid-state structure in solution is confirmed by NMR spectroscopy, with inequivalent diastereotopic methylene bridge groups giving rise to two signals in the $^{13}C\{^1H\}$ NMR spectrum (δ 56.2 and 56.3) and four doublets ($^2J_{HH}$ *ca*. 15 Hz) in the ^{1}H NMR spectrum. The carbene resonances are also inequivalent, appearing at 184.4 and 181.9 ppm ($^1J_{RhC}$ = 43 Hz). Coordination of the enyne results in a marked change in the alkene proton signals from those of the free enyne **29**, appearing at 7.44 and 6.05 ppm ($\Delta\delta$ = 1.39 and $^3J_{HH}$ = 15.3 Hz, CD_2Cl_2) *c.f.* 6.09 and 5.41 ppm ($\Delta\delta$ = 0.68 and $^3J_{HH}$ = 16.2 Hz, $CDCl_3$, **29**).[9] The alkyne carbons

[a] Angle between least squares planes containing 'N10, Rh1, C18, C24, the centroid of C3 and C4' and 'Rh1, C3, C4'

appear as doublets in the $^{13}C\{^{1}H\}$ NMR spectrum at 72.8 ppm ($^{1}J_{RhC}$ = 10 Hz, C4) and 89.5 ppm ($^{1}J_{RhC}$ = 14 Hz, C3).

The spacefill representation shown in **Fig. 4.8** (**top**) highlights the mechanical entrapment of the enyne, which is interlocked through the macrocyclic ring by steric-encumberment of the *tert*-butyl substituents. Unlike ethylene in **27** and **28**, the enyne of **31** cannot be displaced by CO, addition of which results instead in time-averaged C_2 symmetry by ^{1}H NMR spectroscopy (CD_2Cl_2, CO, 400 MHz), presumably *via* coordinatively-induced atropisomerism of the macrocycle (*c.f.* **9 + CO**, **Chapter 3**). The close proximity of the enyne protons to those of the macrocycle is apparent in the solid-state structure and is corroborated in solution by associated through-space interactions, identified by a NOESY experiment (highlighted in **Fig. 4.8** (**bottom**)).

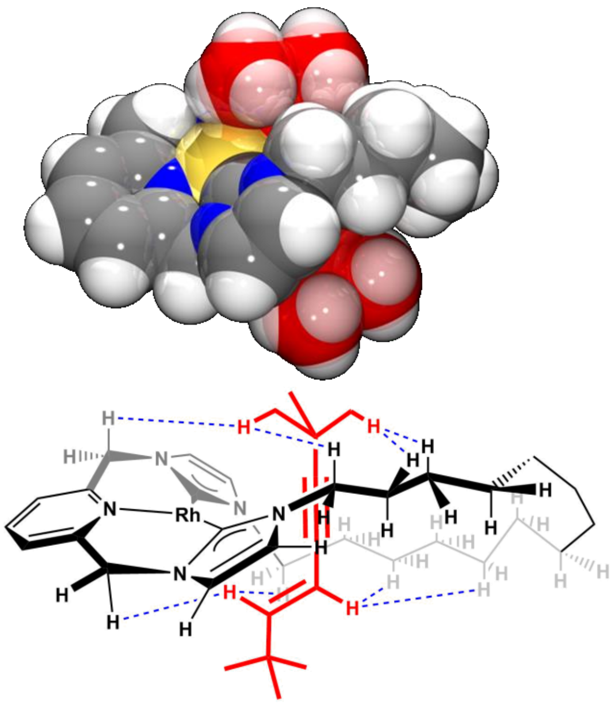

Fig. 4.8: *Spacefill representation (POV-ray) of **31** with interlocked enyne **29** highlighted in red **(top)**. ChemDraw diagram of through-space interactions identified from a NOESY experiment **(bottom)**.*

With **31** in hand, observations from the *in-situ* NMR experiment were reconsidered. At high temperature **31** is clearly produced, however, while a small amount of homo-coupling outside of the macrocyclic cavity takes place initially at room temperature, no signals consistent with either **31** or the starting material were observed, inferring the presence of an intermediate. In an attempt to isolate such an intermediate, and further interrogate the mechanism of reaction, the alkyne dimerisation was conducted at room temperature on a preparative scale (**Scheme 4.11**).

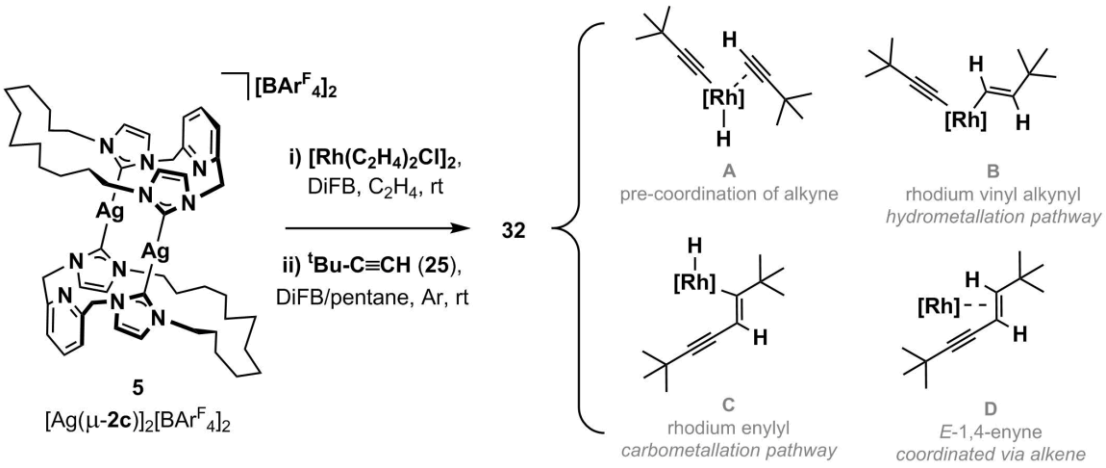

Scheme 4.11: *Formation and potential structures of intermediate* ***32****.*

Gratifyingly, concentration of the reaction mixture after 30 minutes and purification on silica afforded **32** in 34 % yield. Complex **32** proved to be more air and moisture sensitive than **31**, necessitating handling under argon, and was stored at -27°C in an argon-filled glove box. Corroborating its function as an intermediate *en route* to **31**, ^{1}H NMR spectra of **32** show gradual isomerisation to **31** at room temperature over 16 h.

The observation of two inequivalent ^{t}Bu signals (δ 0.71 and 1.24, each 9H with respect to Ar^F) in the ^{1}H NMR spectrum of **32** (CD_2Cl_2) is consistent with ligand(s) derived from two units of **25.** In addition, a strong signal at 672.3 *m/z* in the ESI-LRMS spectrum indicated a parent cation isomeric with **31** (calc. 672.4 *m/z*). ^{1}H NMR signals at δ 3.55 (dd, $^3J_{HH}$ = 13.6 and $^3J_{RhH}$ = 3 Hz) and δ 6.53 (d, $^3J_{HH}$ = 13.5 Hz) exhibit a strong cross-peak in a HH-COSY experiment and indicate the presence of a *trans*-alkene, with separation of *ca*. 3 ppm and rhodium-coupling further suggesting a close interaction with the metal centre (*c.f.* J_{RhH} coupling constants of **A151-A153**, **Fig. 4.9**).[13,15] These data, along with the absence of hydride signals (from δ_H 0 to -35), rule out a hydrido-complex such as **32A** and **32C**, and are more consistent with vinyl alkynyl **32B**. As a consequence of the low stability of **32**, good quality $^{13}C\{^1H\}$ NMR spectra could not be obtained, precluding conclusive identification of all proton or carbon resonances; selected unassigned $^{13}C\{^1H\}$ NMR data is given in **Section 4.6.1.3**. However, heteronuclear correlation experiments (CD_2Cl_2) identify the alkene carbons at 144.8 (one-bond correlation with vinyl proton at δ 3.55) and *ca*. 121.3 ppm (one-bond correlation with vinyl proton at δ 6.53), although the latter resonance coincides with those of the imidazolylidenes and no rhodium coupling is observed for the signal at 144.8 ppm. Of the two inequivalent *tert*-butyl groups, one proton resonance shows a strong multiple-bond correlation with the vinyl carbon signal at 144.8 ppm, the other with a broad resonance at 115.1 ppm, consistent with the C_β of complex **A150** (115.8 ppm).[36] The alkynyl signal is also comparable with the C_β resonance in diyne **22**

(**Chapter 3**), which was found at 106.7 ppm ($^1J_{RhC}$ = 6 Hz). The C_α resonance of **32** could not be identified and rhodium(I) *E*-enyne complex **32D** cannot be definitively ruled out.

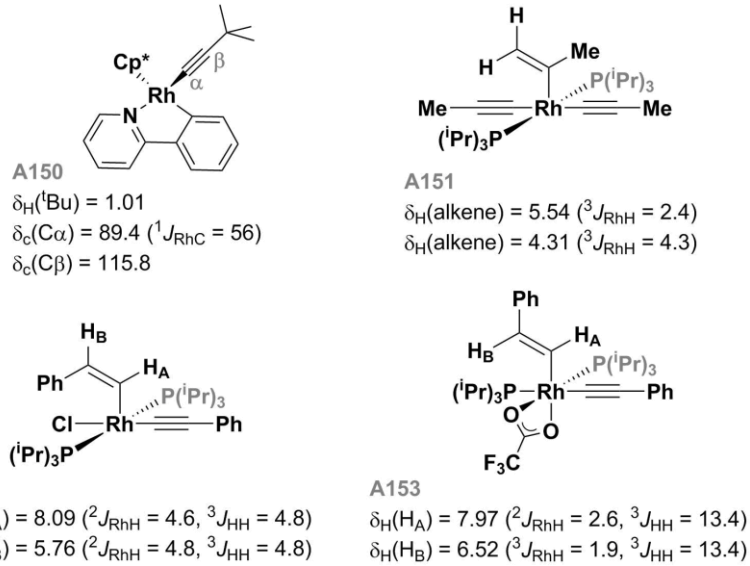

Fig. 4.9: *Existing rhodium vinyl and alkynyl complexes* ***A150-A153.***

Vinyl alkynyl complexes **A151 – A153** undergo reductive elimination at room temperature to afford coordinated enynes within 24 h. The relative longevity of **32** could potentially be a result of the macrocycle encumbering the conformational flexibility at the metal centre, which could also help explain the broad resonances observed in the ^{1}H NMR spectrum for the methylene bridge and *N*-CH_2 protons. Cooling from 308 to 225 K resulted in decoalescence of these signals and appearance of C_1 symmetry (CD_2Cl_2, 500 MHz, **Fig. 4.10**). Two sets of diastereotopic methylene bridge groups are observed, along with three inequivalent resonances for the pyridyl protons. Interestingly, signals pertaining to the hydrocarbon ligand(s), in particular the vinyl resonances denoted by the dotted line in **Fig. 4.10**, remain unchanged between 225 and 308 K, suggesting that the dynamics observed for **32** are related to movement of the dodecamethylene spacer alone.

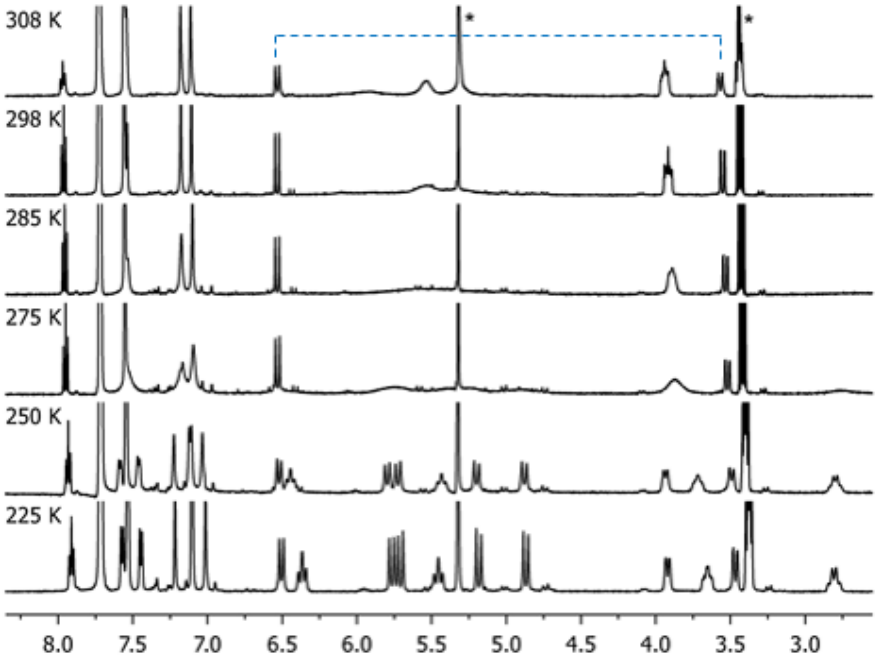

Fig. 4.10: *VT ^{1}H NMR spectra of **32** (225 – 308 K, 500 MHz, CD_2Cl_2). Positions of the vinyl protons denoted by dotted line. * = CD_2Cl_2, Et_2O.*

Further supporting an assignment as **32B**, reaction of **32** with H_2 (4 bar, DiFB, 25°C) resulted in gradual decomposition, in parallel to slow isomerisation to **31**. Resonances consistent with $^{t}BuCH_2CH_3$ [δ = 1.07 (t, $^{3}J_{HH}$ = 7.4, 2H), 0.72 (s, 9H, ^{t}Bu) and 0.69 (t, $^{3}J_{HH}$ = 7.4, 3H)] were observed, refuting formation of an alkyne-coupled product such as in **32D**, which would necessitate cleavage of an alkyne-alkene bond to obtain this observation. As discussed in **Section 4.4.3**, **31** does not react with H_2 under forcing conditions, demonstrating neither hydride formation nor insertion into the coordinated enyne.

4.4.2 Reaction of 28 and 3,5-Di(tert-butyl)phenyl Acetylene 24

Seeking to further explore the formation of interlocked compounds with other alkynes, **28** was heated with 4 equiv. of 3,5-di(*tert*-butyl)phenyl acetylene **24** (**Scheme 3.8**, **Chapter 3**) at 60°C for 20 h to afford analytically pure **33** in 38 % yield, after silica purification and recrystallization (**Scheme 4.12**). Complex **33** is air and moisture stable and was fully characterised by NMR spectroscopy and XRD (**Fig. 4.11**). In addition, microanalysis values are consistent with the structure given in **Scheme 4.12** and, like **31**, a strong parent cation signal is observed at 936.5391 *m/z* (calc. 936.5385), with no signals to indicate fragmentation by loss of the enyne.

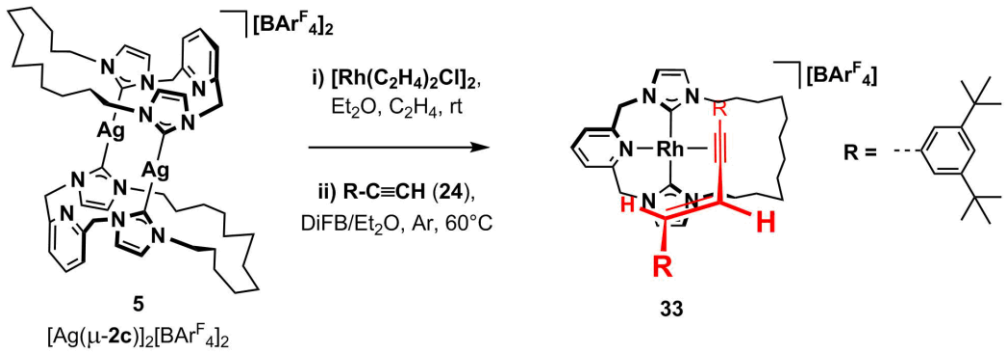

Scheme 4.12: *Synthesis of interlocked complex* ***33****.*

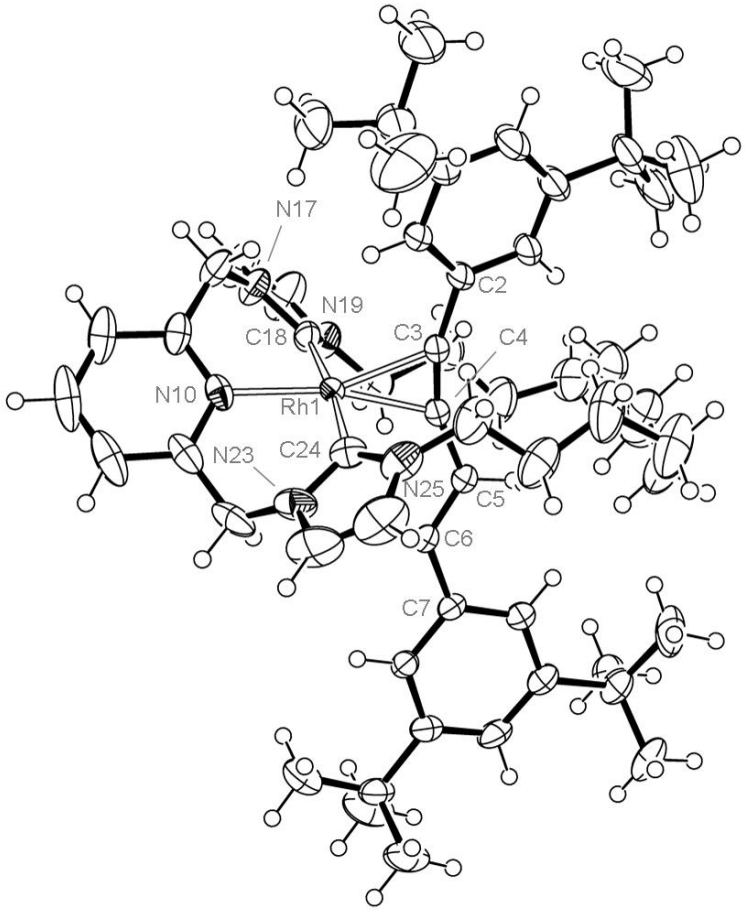

Fig. 4.11: *ORTEP representation of* ***33****. Thermal ellipsoids at 50 % probability. Solvent molecule, [BAr$^F_4$]$^-$ counter anion and minor disordered component omitted for clarity. Selected bond lengths (Å) and angles (°): Rh1-C3, 2.081(3); Rh1-C4, 2.076(3); Rh1-N10, 2.104(2); Rh1-C18, 2.0342(3); Rh1-C24, 2.053(3); C3-C4, 1.254(4); C4-C5, 1.425(4); C5-C6, 1.340(4); C18-Rh1-C24, 173.93(11); N10-Rh1-C3, 158.75(10); N10-Rh1-C4, 166.09(10); C2-C3-C4, 162.0(3); C3-C4-C5, 159.4(3).*

In comparison to **31**, the solid-state structure of **33** reveals shorter metal-carbon bond distances of *ca*. 2.08 Å (*c.f.* 2.12 Å) and a more distorted C-C≡C-C connection, with bond angles of 162.0(3)° and 159.4(3)° for Ar-C≡C and $C_{sp}{}^2$-C≡C, respectively, suggesting a greater loss of sp-character (bond angles of 160.3(4) and 164.8(4)° in **31**, respectively). The coordination geometry of **33** lies marginally closer to square planar than in **31**, with a C_{NCN}-Rh-C_{NCN} bond

angle of 173.93(11)° (*c.f.* 171.41(18)°), and the C≡C bond intersects the pincer coordination plane at an angle of 78.1(2)°,[a] demonstrating a more orthogonal binding mode (*c.f.* 70.2(2)°).

Corroborating the solid-state structure, solution NMR spectra of **33** in CD_2Cl_2 indicate C_1 symmetry with 2 sets of diastereotopic methylene bridge protons exhibiting coupling of *ca*. 14.7 Hz. In comparison to **31**, signals for the alkene protons of **33** appear significantly more downfield at 8.05 and 7.01 ppm, with small rhodium-coupling visible in the $^{13}C\{^1H\}$ NMR spectrum for the corresponding peaks at 142.8 ppm ($^2J_{RhC}$ = 2 Hz) and 117.1 ppm ($^3J_{RhC}$ = 1 Hz), respectively. The inequivalent carbene resonances appear at δ 182.0 and 181.4 ($^1J_{RhC}$ = 42 Hz) and, relative to **31**, a slightly larger Rh-C coupling constant of 12 Hz is observed for the C3 carbon at 83.6 ppm, which lies closer to C4, at 88.9 ppm ($^1J_{RhC}$ = 13 Hz).

The data described above indicate a stronger rhodium-alkyne interaction, facilitated by fewer steric clashes of enyne with the macrocyclic ligand. As shown by the spacefill representation (**Fig. 4.12** (**left**)), the aryl groups of the enyne are held close to the macrocycle, but the majority of the steric bulk is located further from the metal than in **31**. Accordingly, fewer through-space interactions were observed in the NOESY spectrum of **33** than in that of **31**. Nevertheless, key interactions are noted between the *ortho* protons of the C3-aryl ring and one of the methylene bridge protons, and between the alkene proton at 8.05 ppm and another of the methylene bridge protons; both further corroborate conservation of the solid-state structure in solution (**Fig. 4.12** (**right**)).

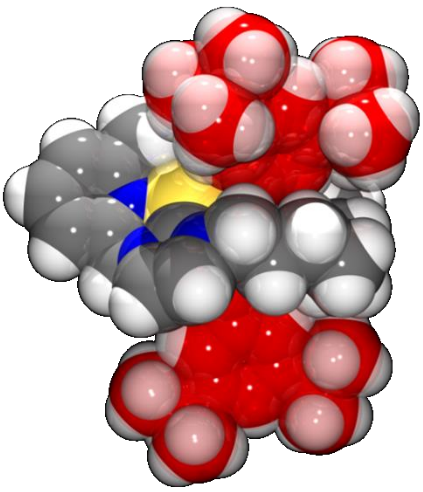

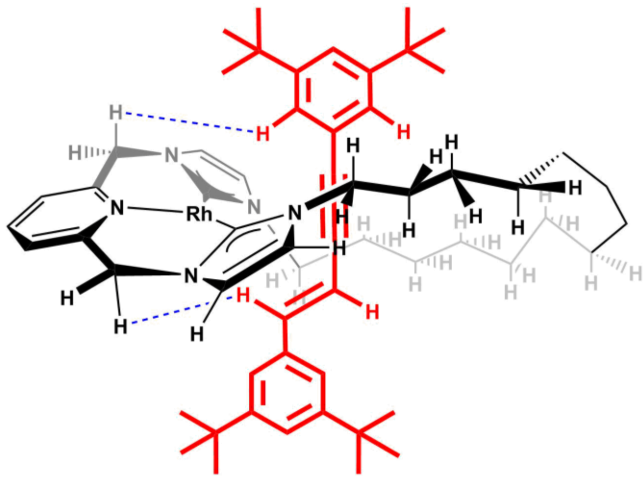

***Fig. 4.12:** Spacefill representation (POV-ray) of **33** with interlocked enyne highlighted in red **(left)**. ChemDraw diagram of through-space interactions identified from NOESY experiment **(right)**.*

---

[a] Angle between least squares planes containing 'N10, Rh1, C18, C24, the centroid of C3 and C4' and 'Rh1, C3, C4'

With **33** in hand and structurally characterised, the mechanism of its formation was investigated. Following on from the work conducted with *tert*-butyl alkyne **25**, for which two distinct organometallic products were obtained by varying the reaction temperature (*vide supra*), **28** was reacted with 4 equiv. of **24** at room temperature to afford **34** in 39 % yield, after silica purification (**Scheme 4.13**). Although demonstrating some moisture sensitivity, **34** undergoes negligible isomerisation over 24 h in $CDCl_3$, enabling its full characterisation by NMR spectroscopy, ESI-LRMS and microanalysis. Values for the latter are consistent with the formula [Rh(**2c**)($C_{12}H_{38}$)][BAr^F_4], isomeric with **33**, as is the observation of the parent cation at 936.5 *m/z* (calc. 936.5) with no observed fragmentation in the ESI-LRMS spectrum. Using ^1H and ^{13}C NMR spectroscopy in CD_2Cl_2, in particular cross-correlation experiments, it was possible to unambiguously assign **34** to a complex of the *gem*-1,3-enyne derived from **24.**

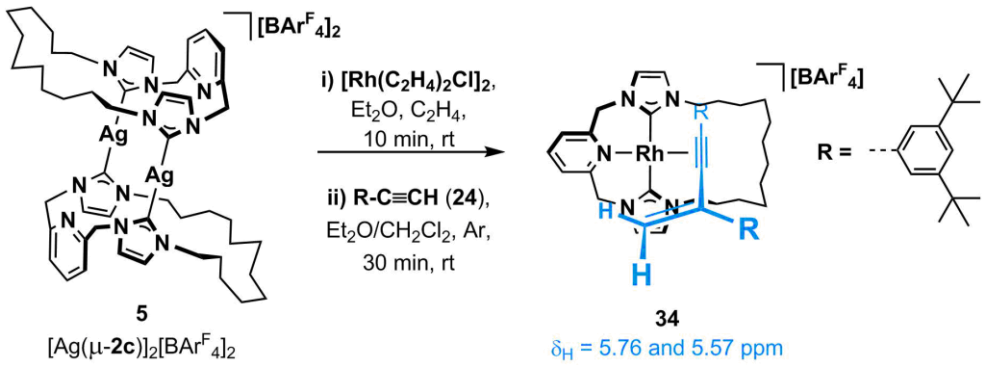

Scheme 4.13: *Synthesis of gem-1,3-enyne complex **34**.*

Characterised as a finely-coupled doublet ($^3J_{HH}$ = 2 Hz) at 5.76 ppm and a broadened singlet at 5.57 ppm in the ^1H NMR spectrum, the vinylic protons of **34** do not exhibit the distinctive $^3J_{HH}$ couplings of *cis* or *trans* alkene protons. Instead, through-bond HSQC and HMBC experiments confirmed the location of both protons on the same alkene carbon (δ 114.7), adjacent to a di-substituted alkene resonance, that displays rhodium-coupling (δ 157.7, $^2J_{RhC}$ = 27 Hz). A cross-peak is also present in the HMBC spectrum between the doublet at 5.76 ppm and an alkyne carbon resonance (δ 85.0, $^1J_{RhC}$ = 72 Hz), verifying the presence of a sp-sp^2 bond. The other alkyne carbon resonance (δ 104.7, $^1J_{RhC}$ = 17 Hz) instead shows a 3-bond correlation in the HMBC spectrum with *ortho*-protons of the adjacent aryl ring.

In the ^1H NMR spectrum of **34** at 298 K, two singlets at 0.99 and 1.25 ppm pertain to the *tert*-butyl groups of the aryl rings and each integrate to 18 H, against resonances for the pincer backbone and the alkene protons. The lower frequency shift, assigned to *tert*-butyl groups on the vinyl-bound aryl ring, is significantly broader (*fwhm* = 7.0 *vs* 1.6 Hz). Broad signals are also observed for neighbouring proton and carbon resonances, as well as some pertaining to the macrocyclic ligand. These observations indicate restricted rotation about the C_{vinyl}-C_{aryl} bond.

Cooling from 298 to 207 K partially resolves broad resonances of both the bound enyne and the macrocycle, with low temperature ^{1}H NMR spectra suggesting C_1 symmetry, although the slow exchange limit was not reached in all cases (CD_2Cl_2, 500 MHz, **Fig. 4.13**). In the 207 K spectrum, the previously broad 18 H resonance at 0.99 ppm has decoalesced into two singlets (δ 1.14, 0.67; both 9H), corroborating restricted rotation about the C_{vinyl}-C_{aryl} bond. Suggesting a less congested metal centre, the barrier to atropisomerism of the macrocycle in **34** would appear to be lower than in **32**, with *meta*-protons of the pyridyl ring not fully resolved until the 207 K spectrum (*c.f.* 225 K for **32**), where they appear as apparent doublets (J = 8 Hz) at 7.22 and 7.14 ppm.

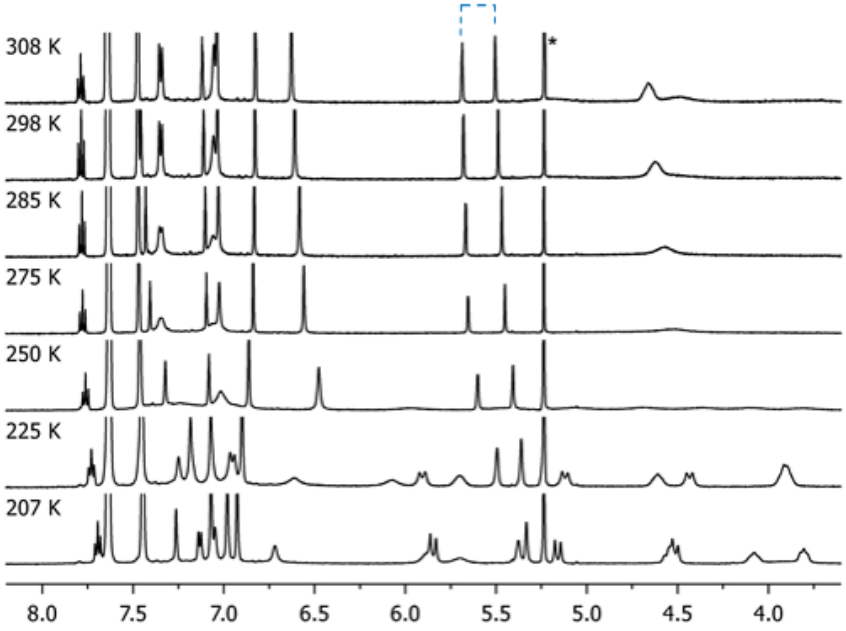

Fig. 4.13: *VT ^{1}H NMR spectra of **34** (207 – 308 K, 500 MHz, CD_2Cl_2). Dotted line indicates vinyl protons. * = CH_2Cl_2.*

^{1}H NMR spectra recorded after 4 days in CD_2Cl_2 at 293 K show *ca*. 20 % conversion of **34** to **33**, which is accelerated to over 60 % by heating of the sample at 40°C overnight. Heating isolated **34** at 60°C in C_6D_6 for 20 h resulted in complete conversion of **34** to **33**. Suggesting inhibition by solvent coordination, heating **34** in CD_3CN at 60°C for 2 days gave negligible **33** (< 10 %).

The stability of **34** in solution, in comparison with **32**, enables study of its reaction with H_2 in the absence of isomerisation to **33**. Further supporting assignment to the *gem*-1,3-enyne, **34** showed no reaction with H_2 at room temperature for 20 h (*c.f.* **32**). Unlike thermodynamically favoured **33** (*vide infra*), heating at 80°C in DiFB under H_2 (1 atm) resulted in decomposition, alongside formation of $ArCH_2CH_3$ [δ = 2.51 (app. q, $^3J_{HH}$ = 7.6, 2H), 1.22 (s, 18H, ^{t}Bu) and 1.12 (t, $^3J_{HH}$ = 7.7, 3H)]. Production of this hydrocarbon requires cleavage of the C_{vinyl}-C_{alkyne} bond; a necessary step in the isomerisation of **34** to **33** (see **Section 4.5**).

4.4.3 Reactions of 28 with Other Alkynes

Encouraged by the facile access to isolable complexes **31** and **33**, reaction of **28** with other alkynes at elevated temperature was attempted (**Scheme 4.14**).

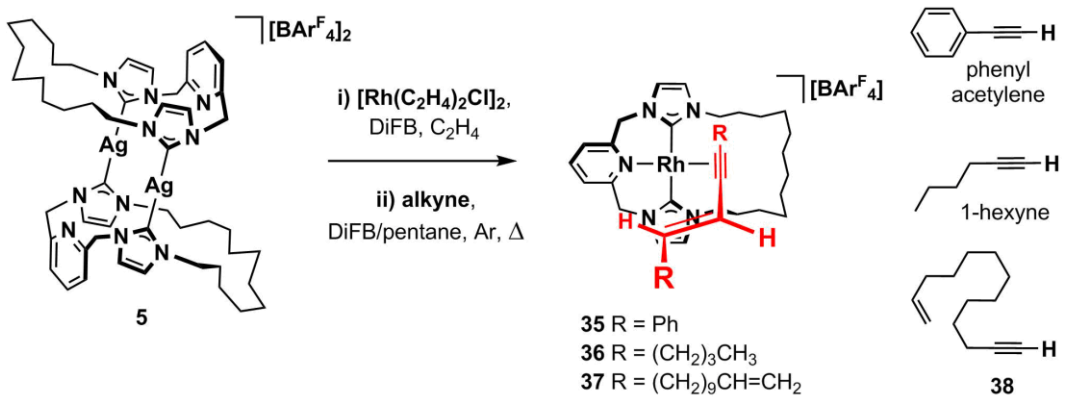

Scheme 4.14: *Synthesis of complexes* ***35 – 37****.*

When phenyl acetylene was reacted with **28**, a mixture containing two major products was obtained, after silica purification. Representing roughly 80 % of the mixture, the major product is tentatively assigned to [Rh(**2c**)(1,4-diphenyl-*E*-enyne)][BAr$^F_4$] **35** with resonances of the alkene identified at 7.95 and 7.06 ppm ($^3J_{HH}$ = 15.3 Hz); downfield to those of the free enyne (7.06 and 6.40 ppm, $^3J_{HH}$ = 16.3 Hz, $CDCl_3$).[9] The methylene bridge protons appear as two pairs of diastereotopic resonances at δ 5.84, 5.81 ($^2J_{HH}$ = 14.7 Hz) and 5.20, 5.13 ($^2J_{HH}$ = 14.9 Hz). In addition, a single signal pertaining to the parent cation was observed at 712.2 *m/z* (calc. 712.3) by ESI-LRMS. Frustratingly, the mixture proved resistant to further purification on silica or recrystallisation and neither major nor minor product were isolated nor conclusively characterised.

When alkyl-substituted alkynes were used, less well-defined products were obtained. After silica purification, the reaction of 1-hexyne with **28** afforded a complex mixture by ^{1}H NMR spectroscopy (CD_2Cl_2) and multiple signals by ESI-LRMS, including a strong peak for the expected product **36** at 672.2 *m/z* (calc. 672.4), but also a signal at 836.4 *m/z*, suggesting coupling of an additional 2 equiv. of the alkyne (calc. 836.5 *m/z*).

Seeking to explore the potential of the alkyne dimerisation reaction for the preparation of [2]catenanes, di-functionalised alkene-alkyne **38** was reacted with **28**. Initial product formation at room temperature was suggested by a strong cation signal at 864.5389 *m/z* (calc. 864.5385 for **37**) by ESI-HRMS and broad signals in the ^{1}H NMR spectrum, akin to those of **32** and **34**. After heating and silica purification, the broad proton signals were replaced by multiple sharp resonances to afford a complicated spectrum that, despite no change in ESI-HRMS spectra, indicated the formation of a mixture of products.

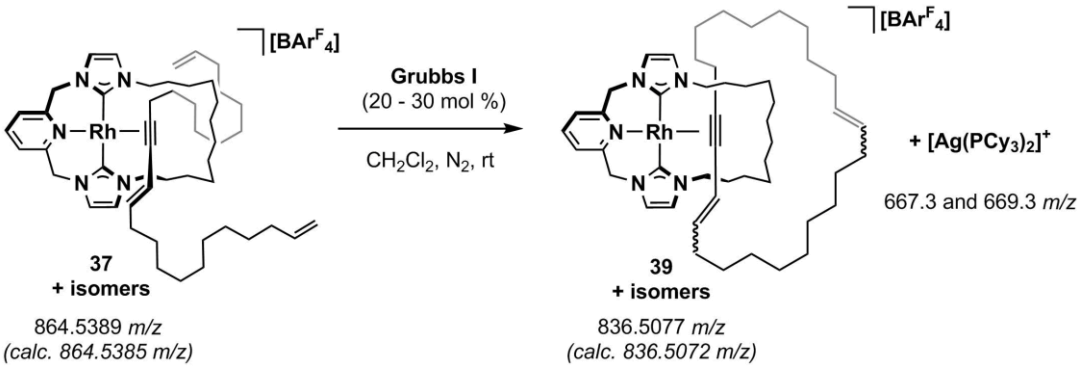

Scheme 4.15: *Ring-closing metathesis of* ***37****.*

Crude samples of **37** were subjected to alkene metathesis using the 1st Generation Grubbs catalyst (20 – 30 mol %) resulting in replacement of distinctive terminal alkene resonances with internal alkene signals in the ^{1}H NMR spectrum and a mass change of -28 Da by ESI-HRMS, indicating formation of catenate **39** (**Scheme 4.15**). These changes were accompanied by observation of signals at 667.3 and 669.3 *m/z* in the ESI-LRMS spectrum, indicating the presence of $[Ag(PCy_3)_2]^+$, which was further corroborated by ^{31}P and ^{1}H NMR spectroscopy and isolation of $[Ag(PCy_3)_2][BAr^F_4]$ from the reaction mixture.[32]

Generation of $[Ag(PCy_3)_2]^+$ and complexity of NMR spectra limited characterisation of **39**. Samples proved resistant to silica purification or crystallisation from a range of solvent systems. However, crude samples were placed under hydrogen to investigate the possibility of generating a catenane *via* hydrogenation of the 24-carbon ring. This resulted in loss of signals pertaining to an interlocked complex by ESI-LRMS analysis, and generation of diagnostic resonances for terminal alkane groups (-C*H*$_2$C*H*$_3$) in ^{1}H NMR spectra.

4.4.4 Further Reactivity of Enynes 31, 33 and 39

Complexes **31** and **33** are remarkably air and moisture stable and show no change in their ^{1}H NMR spectra after three days in $CDCl_3$ solution, in air, indicating that the metal-centres are less prone to oxidation than those of the rhodium(I) carbonyl complexes of **Chapter 3**, which must be characterised in CD_2Cl_2 under inert atmosphere.

Both complexes are notably unreactive to hydrogen, with no hydrogenation of either bound enyne observed under 4 bar pressure of H_2 at 80°C for extended reaction times (2 – 3 days). During these small scale reactions, monitored by ^{1}H NMR spectroscopy, no hydride signals are observed down to -20 ppm. Moreover, **31** was heated to 80°C in toluene under 80 bar pressure of H_2 for 20 h without degradation. Additionally, mixtures of **31** with Wilkinson's catalyst or palladium on carbon under hydrogen atmospheres do not show any reduction of the enyne, despite the latter conditions being effective in the hydrogenation of **29** to 2,2,7,7-

tetra-methyl octane (**Scheme 4.16**). The robustness of **31** and **33** is in sharp contrast to the reactivity of intermediates **32** and **34**, both of which degrade under pressure of H_2 (**Sections 4.4.1** and **4.4.2**).

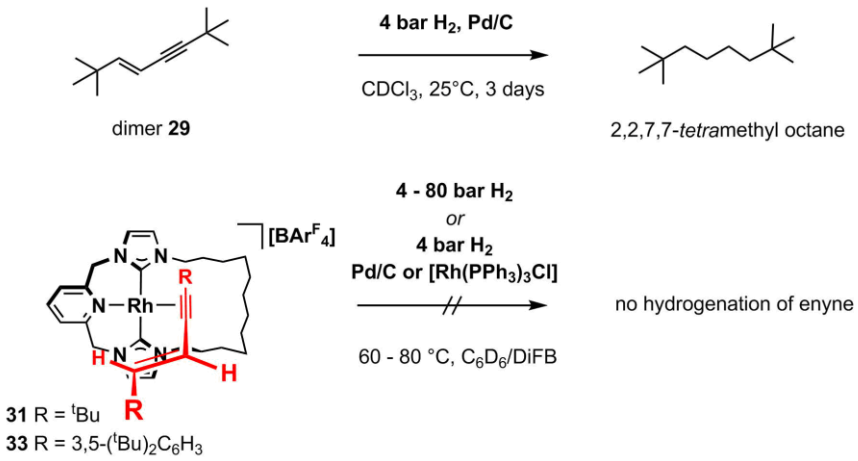

Scheme 4.16: *Contrasting reactivity of **29** with that of **31** and **33**.*

Reaction of **31** and **33** with strong oxidants is possible, however, and the addition of $PhICl_2$ to CH_2Cl_2/CD_2Cl_2 solutions of **31** or **33** resulted in loss of their distinctive orange colour. In the case of **31**, yellow rhodium(III) dichloride complex **40** (**Scheme 4.17**) was isolated and fully characterised by NMR spectroscopy, XRD, ESI-HRMS and microanalysis. The latter afforded values consistent with the formula [Rh(**2c**)(**29**)$(Cl)_2$][BAr^F_4], which was further corroborated by a strong parent cation signal at 742.2881 *m/z* (calc. 742.2884) by ESI-HRMS.

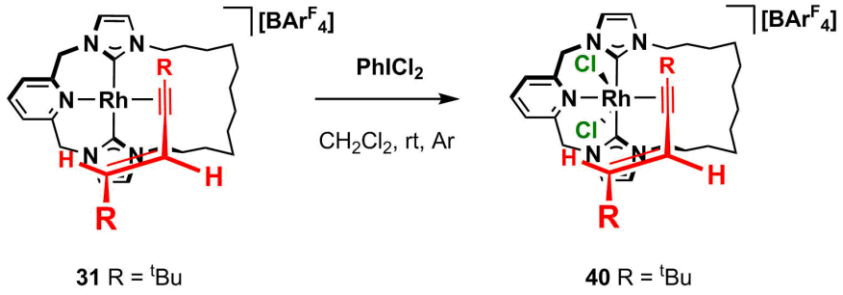

Scheme 4.17: *Reaction of **31** with $PhICl_2$.*

In the $^{13}C\{^1H\}$ NMR spectrum of **40**, oxidation from rhodium(I) to rhodium(III) is marked by an upfield shift in the carbene signals and a contraction in the rhodium-coupling constant, affording doublets at 164.8 and 163.3 ppm with $^1J_{RhC}$ = 30 Hz (*c.f.* 184.4 and 181.9 ppm, $^1J_{RhC}$ = 43 Hz, **31**). The alkene protons are also shifted upfield by *ca.* 0.4 ppm, appearing at 7.03 and 5.73 ppm ($^3J_{HH}$ = 15.9 Hz) *c.f.* 7.44 and 6.05 ppm ($^3J_{HH}$ = 15.3 Hz, **31**). Further corroborating the reduction in available electron density at the metal, rhodium-coupling for the alkyne carbon resonances (δ 65.3 and 83.2) is reduced to *ca.* 7 Hz from $^1J_{RhC}$ values of 10 and 14 Hz observed for the corresponding resonances of **31** (72.8 and 89.5 ppm, respectively).

The solid-state structure of **40** (**Fig. 4.14**) reveals longer Rh-C_{alkyne} distances of 2.444(10) and 2.239(7) Å, compared to **31** (2.093(4) and 2.132(3) Å). However, bonding angles of the alkyne suggest greater distortion of the C-C≡C-C group than observed previously, which is attributed to a steric clash between hydrocarbon and chloride ligands rather than π-backbonding into the π*(C≡C). Consistent with this suggestion, the Cl8-Rh1-Cl9 bond angle (167.04(8)°) is distorted significantly from linearity (*c.f.* 179.49(3) in **21b**) and the C≡C bond intersects the pincer coordination plane at *ca*. 60°,[a] presumably to reduce unfavourable steric interaction between the *tert*-butyl groups and the chloride ligands (**Fig. 4.15**). The mechanical entrapment of the enyne in **40** may help confer the observed air and moisture stability, in contrast to unstable **21a** ([Rh(**2c**)(CO)$(Cl)_2$], **Chapter 3**, **Section 3.4**).

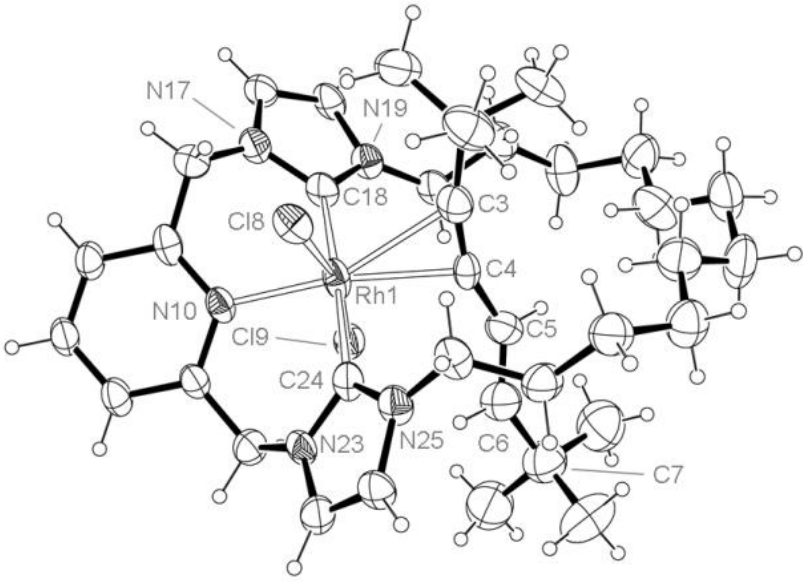

Fig. 4.14: *ORTEP representation of complex **40**. Thermal ellipsoids at 30 % probability. Only one of two unique cations shown (Z' = 2). $[BAr^F_4]^-$ counter anion removed for clarity. Selected bond lengths (Å) and angles(°): Rh1-C3, 2.444(10); Rh1-C4, 2.239(7); Rh1-Cl8, 2.378(2); Rh1-Cl9, 2.383(2); Rh1-N10, 2.074(3); Rh1-C18, 2.015(3); Rh1-C24, 2.089(4); C3-C4, 1.266(13); C5-C6, 1.280(14); Cl8-Rh1-Cl9, 167.04(8); C18-Rh1-C24, 176.1(2); C3-Rh1-N10, 159.7(3); C4-Rh1-N10, 169.1(3).*

[a] Average angle (using both independent units in cell) between least squares planes containing 'N10, Rh1, C18, C24' and 'Rh1, C3, C4'.

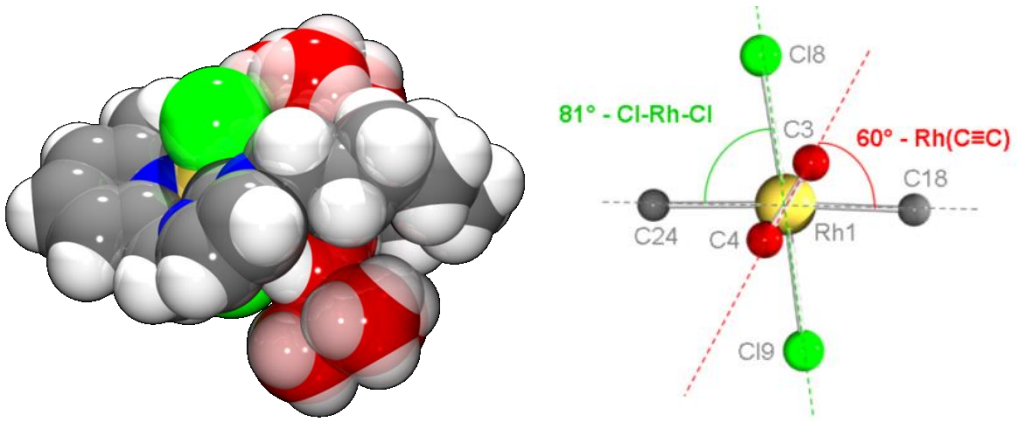

Fig. 4.15: *PoV-Ray representations of **40** demonstrating steric clash of chlorides with interlocked enyne (spacefill, **left**) and resulting displacement (ball-and-stick, **right**).*

Oxidation of **33** with $PhICl_2$ in CD_2Cl_2 at room temperature resulted in complete consumption of starting material, with the ^1H NMR spectrum indicating formation of a single product, **41**, of reduced conformational flexibility due to hindered rotation about C-C_{Ar} bonds. Unlike **40**, **41** is not air-stable and exposure of the solution results in further reaction. Initial sampling by ESI-LRMS (MeCN, air) is consistent with the dichloride (1006.5 *m/z*, calc. 1006.5) being the dominant product of reaction between $PhICl_2$ and **33**, but other signals were apparent and, on prolonged exposure of the reaction mixture to air, the dichloride signal was depleted. After 10 days, a statistical distribution of chloride additions (+ 35 Da by ESI-LRMS) from 1 to 6 Cl atoms was observed, indicating addition into the enyne unit, as well as onto the metal centre. A similar result was obtained when $PhICl_2$ was added to a CH_2Cl_2 solution of crude **39**, with up to 9 chloride additions (tentatively suggested by ESI-LRMS), consistent with Cl_2 addition into all of the unsaturated bonds available (**Scheme 4.18**).

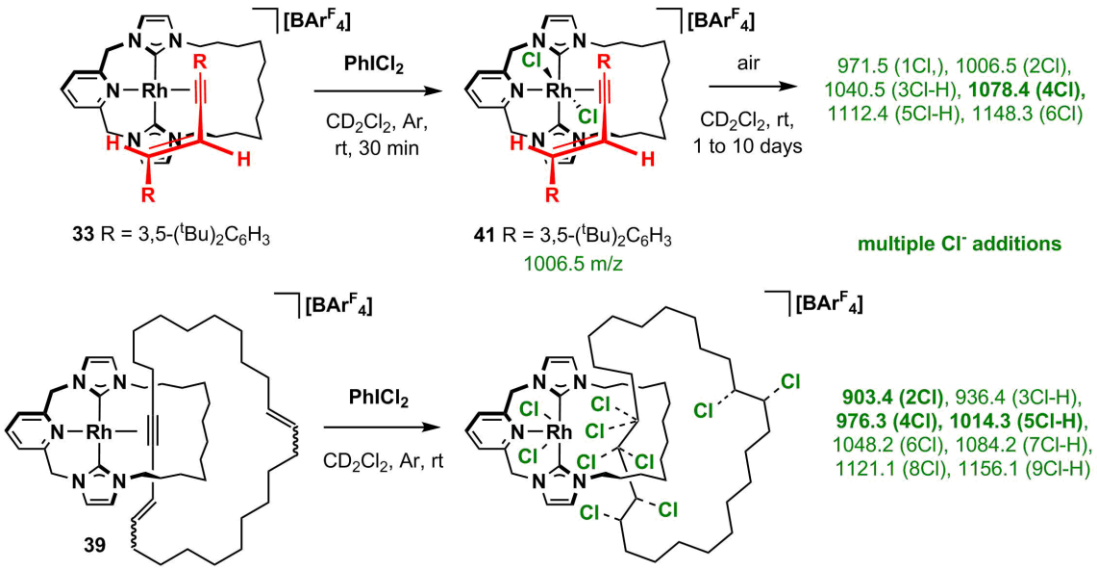

Scheme 4.18: *Reaction of **33** and **39** with $PhICl_2$. Bold m/z values denote dominant signals.*

4.5 Summary of Observations

In summary, the contrasting reactivity of acyclic **27** and macrocyclic **28** in terminal alkyne homo-coupling reactions has shown that the macrocyclic ligand in **28** exerts clear kinetic and thermodynamic control, resulting in a potential means for the construction of complex supramolecular assemblies. Notably, the observed substituent dependence of the reactions of **28** with alkynes enabled the isolation and characterisation of two distinct intermediates *en route* to thermally stable interlocked *E*-1,4-enynes, providing insights into the mechanism.

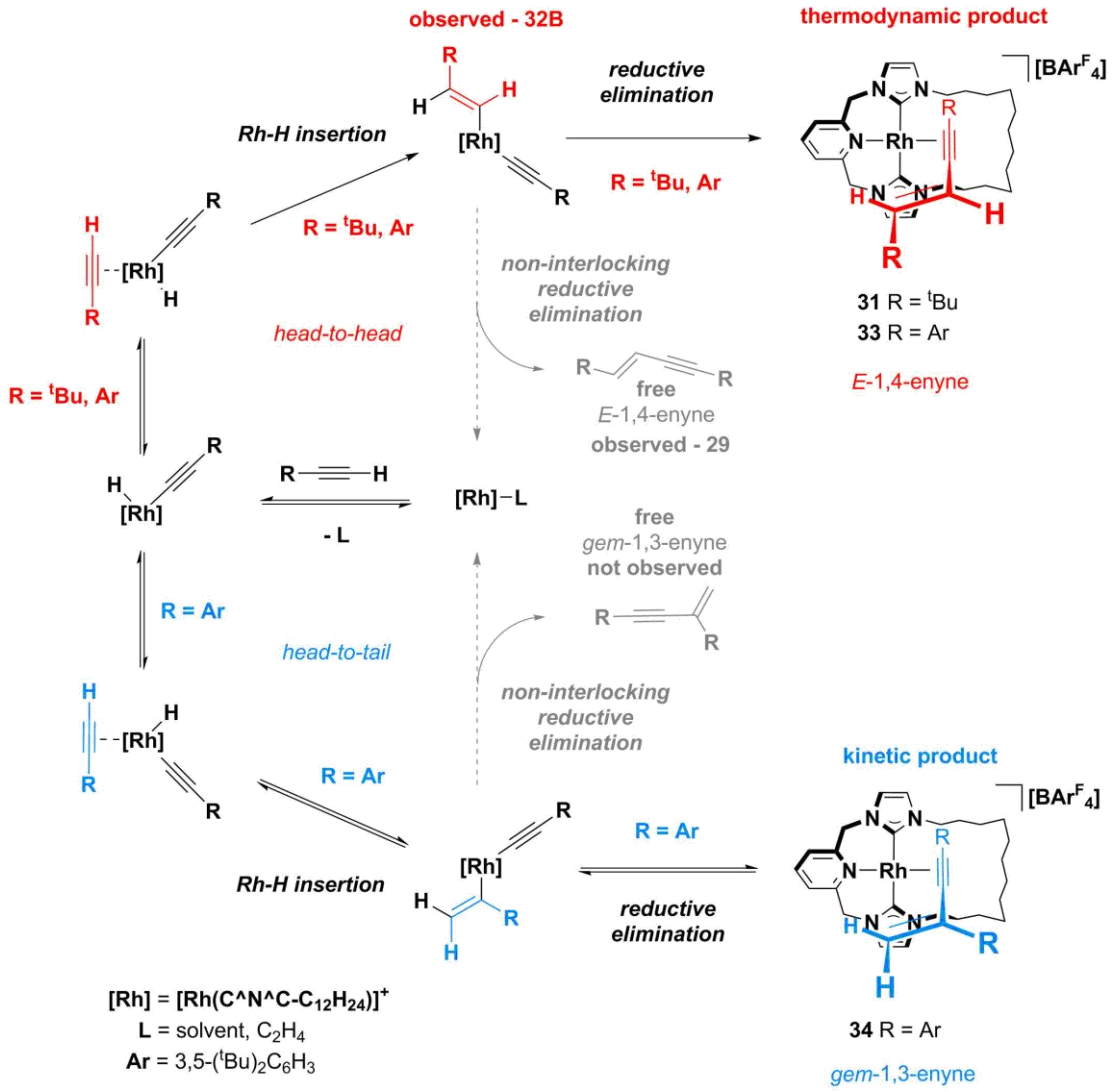

Scheme 4.19: *Placement of **31 – 34** on hydrometallation mechanism pathways.*

With the data available, the Rh(C^N^C) systems reported herein appear to proceed *via* the hydrometallation pathways suggested by Ozerov and Werner (**Scheme 4.5**),[3,13,15] as illustrated by the isolation of intermediate **32**, which is assigned to a vinyl-alkynyl complex **32B** (**Scheme 4.19**). Significant steric effects are implied in the regioselectivity-determining Rh-H insertion step. Aryl-substituted alkyne **24** kinetically disfavours *head-to-head* insertion, resulting instead in formation of *gem*-1,3-enyne **34**, which shows restricted C-C_{Ar} bond rotation, indicating a

congested coordination sphere. This process is reversible; heating enables *head-to-head* insertion and the formation of thermodynamically favoured *E*-1,4-enyne as part of an interlocked, but less congested, complex **33**.

The robust nature of **31** under forcing hydrogenation conditions precludes reduction of the bound enyne, which as free enyne **29** can be hydrogenated using Pd/C. Although no reaction with H_2 is observed, **31** can be oxidised using $PhICl_2$ to afford a well-defined Rh(III) derivative. In contrast, the attempted oxidation of **33** and **39** lead to more complicated product distributions, whereby reaction of the bound enyne was observed.

4.6 Experimental Procedures and Selected Data

4.6.1 Experimental Procedures

General considerations. Manipulations were performed under an inert atmosphere, using Schlenk (nitrogen, argon, carbon monoxide, ethylene, hydrogen) and glove box (argon) techniques unless otherwise stated. Glassware was oven dried at 130°C overnight and flamed under vacuum prior to use. Anhydrous solvents (<0.005 % H_2O) were purchased from ACROS Organics or Sigma Aldrich and used as supplied: CH_2Cl_2, THF, 1,4-dioxane, hexane, pentane and Et_2O. DiFB was stirred over neutral aluminum oxide, filtered, dried over CaH_2, vacuum distilled, and freeze-pump-thaw degassed three times before being placed under argon over 3 Å molecular sieves. CD_2Cl_2 and C_6D_6 were dried over CaH_2 and sodium metal respectively prior to vacuum-distillation, and stored under an atmosphere of argon. $[Rh(C_2H_4)_2Cl]_2$,[37] $PhICl_2$,[38] 3,5-di(*tert*-butyl)phenyl acetylene (**24**, see **Chapter 3**),[39] and $HC{\equiv}C(CH_2)_9CH{=}CH_2$ (**38**)[40] were synthesised using literature procedures. Silver transmetallation reagents $[Ag(\mu\text{-}\mathbf{2c})]_2[BAr^F{}_4]_2$ (**5**) and $[Ag(\mathbf{C\text{^}N\text{^}C^{Me}})][BAr^F{}_4]$ (**15**) were synthesised as described in **Chapters 2 and 3**, respectively. All other solvents and reagents are commercial products and were used as received. NMR spectra were recorded on Bruker DPX-300, DPX-400, AV-400, AV-500, AVIII-500 HD, AV-600 and AV-700 spectrometers at 298 K unless otherwise stated. Chemical shifts are quoted in ppm and coupling constants in Hz. Where DiFB was used as NMR solvent, proton spectra were referenced using the highest intensity peak of the highest frequency fluoroarene multiplet (δ 6.865). ESI-LRMS were recorded on an Agilent 6130B mass spectrometer. ESI-HRMS were recorded on a Bruker MaXis mass spectrometer. Microanalyses were performed at the London Metropolitan University by Stephen Boyer.

4.6.1.1 Synthesis of Rhodium(I) Ethylene Complexes

$[Rh(\mathbf{C\text{^}N\text{^}C^{Me}})(C_2H_4)][BAr^F{}_4]$ (**27**): A J. Young's flask under argon was charged with $[Ag(\mathbf{C\text{^}N\text{^}C^{Me}})][BAr^F{}_4]$ (**15**) (60 mg, 0.0485 mmol) and $[Rh(C_2H_4)_2Cl]_2$ (10 mg, 0.0257 mmol). The flask was evacuated then back-filled with ethylene. The following reaction and work-up was conducted under an ethylene atmosphere using solvents stored under ethylene. Addition of Et_2O rapidly afforded an orange suspension. The reaction mixture was stirred for 10 minutes before filtration and the filtrate layered with pentane. After 4 hours the sealed crystallisation tube was inverted and the resulting red oil allowed to move slowly through the pentane-ether mixture overnight, affording red-orange feather-like crystals. The solvent was removed by filtration and the crystalline solid washed with pentane before drying *in vacuo*. Once dry, the red-orange product was stored under argon at -27°C. Yield: 40 mg (65 %).

^{1}H NMR (500 MHz, CD_2Cl_2) δ 7.79 (t, $^{3}J_{HH}$ = 7.7, 1H, py), 7.70 – 7.74 (m, 8H, Ar^F), 7.55 (br, 4H, Ar^F), 7.44 (d, $^{3}J_{HH}$ = 7.7, 2H, py), 7.04 (d, $^{3}J_{HH}$ = 1.8, 2H, imid), 6.73 (d, $^{3}J_{HH}$ = 1.8, 2H, imid), 5.74 (br, 2H, pyCH_2), 5.03 (br, 2H, pyCH_2) 3.50 (br, 4H, C_2H_4), 3.46 (s, 6H, *N*-CH_3). **$^{13}C\{^{1}H\}$ NMR** (101 MHz, CD_2Cl_2) δ 184.8 (d, $^{1}J_{RhC}$ = 40, carbene), 162.3 (q, $^{1}J_{CB}$ = 50, Ar^F), 155.9 (s, py), 139.5 (s, py), 135.4 (s, Ar^F), 129.5 (qq, $^{2}J_{FC}$ = 32, $^{3}J_{CB}$ = 3, Ar^F), 125.2 (q, $^{1}J_{FC}$ = 271, Ar^F), 124.0 (s, py), 123.0 (s, imid), 120.8 (s, imid), 118.1 (pent., $^{3}J_{FC}$ = 4, Ar^F), 56.2 (d, $^{3}J_{RhC}$ = 2, pyCH_2), 36.5 (s, *N*-CH_3). **ESI-HRMS** (CH_3CN, 180°C, 3 kV) positive ion: 402.0424 *m/z*, $[M\text{-}C_2H_4]+[O_2]^+$ (calc. 402.0432). **Elemental Analysis** Calc. for $C_{49}H_{33}BF_{24}N_5Rh$ (1261.52 g mol^{-1}): C, 46.65; H, 2.64; N, 5.61. Found: C, 46.72; H, 2.69; N, 5.61).

[Rh(**2c**)(C_2H_4)][BAr^F_4] (**28**): *To obtain a sample of ca. 80 % purity (as per comparison of [BAr^F_4] and ligand integrals in the proton NMR spectrum)* - A Schlenk flask under argon was charged with [Ag(μ-**2c**)]$_2$[$BArF_4$]$_2$ (**5**) (60 mg, 0.0243 mmol) and [Rh(C_2H_4)$_2$Cl]$_2$ (10 mg, 0.0257 mmol). The flask was evacuated then back-filled with ethylene. The following reaction and work-up was conducted under an ethylene atmosphere using solvents stored under ethylene. Addition of CH_2Cl_2 rapidly afforded an orange suspension. The reaction mixture was stirred for 10 minutes before filtration onto a large silica plug (*ca*. 15 cm^3) and elution of an orange solution in CH_2Cl_2. Concentration of the eluent afforded a red oil, which was sonicated in pentane. Removal of the solvent by decantation and subsequent washes (with sonication) afforded the **28** as an orange-red foam after drying. Complex **28** was stored under argon at -27°C. Yield: 70 mg (57 %).

*4.6.1.2 Selected ^{1}H and $^{13}C\{^{1}H\}$ NMR Data for In-Situ and Crude Samples of **28***

Crude sample in CD_2Cl_2 under argon atmosphere: **^{1}H NMR** (400 MHz, CD_2Cl_2, Ar) δ 7.84 (t, $^{3}J_{HH}$= 7.7, 1H, py), 7.72 (br, 10H, 1.25x Ar^F), 7.55 (br, 5H, 1.25x Ar^F), 7.48 (d, $^{3}J_{HH}$ = 7.7, 2H, py), 7.05 (s, 2H, imid), 6.79 (s, 2H, imid), 5.31 (br, 4H, pyCH_2), 3.76 (app. t, *J* = 8, *N*-CH_2), 3.45 (br, 4H, C_2H_4), 1.72 – 1.85 (br, 4H, CH_2), 1.22 – 1.50 (m, 20H, CH_2).

Crude sample in Et_2O under ethylene atmosphere (C_6D_6 capillary used for machine-lock, proton spectrum referenced to centre of triplet resonance of EtO-CH_2CH_3 at 1.11 ppm, carbon spectrum referenced to singlet resonance of EtO-CH_2CH_3 at 15.46 ppm)[31]*:* **^{1}H NMR** (400 MHz, CD_2Cl_2, C_2H_4) δ 7.86 (t, $^{3}J_{HH}$ = 7.7, 1H, py), 7.70 (br, 11H, 1.38xAr^F), 7.50 (d, $^{3}J_{HH}$ = 7.7, 2H, py), 7.47 (br, 5.5H, 1.38xAr^F), 7.17 (s, 2H, imid), 6.91 (s, 2H, imid), 5.36 (s, 4H, pyCH_2), 4.75 – 5.25 (br, 32H, 8xC_2H_4), 3.77 (m, 4H, *N*-CH_2), 1.74 – 1.84 (br, 4H, CH_2), 1.30 – 1.51 (m, 20H, CH_2). **$^{13}C\{^{1}H\}$ NMR** (101 MHz, CD_2Cl_2, C_2H_4, *selected data only*) δ 181.7 (d, $^{1}J_{RhC}$ = 40, carbene), 156.5 (s, py), 140.2 (s, py), 124.2 (s, py), 122.2 (s, imid), 121.9 (s, imid), 111.0 – 113.0 (br, C_2H_4).

Generation of in-situ sample under argon: In an argon-filled glove box, 0.5 mL of CD_2Cl_2 was added to a J. Young's NMR tube containing **5** (8.0 mg, 0.006 mmol) and $[Rh(C_2H_4)_2Cl]_2$ (1.4 mg, 0.004 mmol) to afford a thick red suspension. **^{1}H NMR** (400 MHz, CD_2Cl_2, Ar) δ 7.84 (t, $^3J_{HH}$ = 7.7, 1H, py), 7.73 (m, 8H, Ar^F), 7.56 (s, 4H, Ar^F), 7.48 (d, $^3J_{HH}$ = 7.7, 2H, py), 7.04 (d, $^3J_{HH}$ = 2, 2H, imid), 6.79 (d, $^3J_{HH}$ = 2, 2H, imid), 5.29 (s, 4H, pyCH_2), 3.50 – 5.50 (br, 64H, 16xC_2H_4), 3.72 – 3.82 (m, 4H, *N*-CH_2), 1.74 – 1.87 (m, 4H, CH_2), 1.25 – 1.85 (m, 20H, CH_2). **^{13}C{^{1}H} NMR** (101 MHz, CD_2Cl_2, C_2H_4) δ 181.2 (d, $^1J_{RhC}$ = 40, py), 162.3 (q, $^1J_{CB}$ = 50, Ar^F), 156.0 (s, py), 139.8 (s, py), 135.4 (s, Ar^F), 129.4 (qq, $^2J_{FC}$ = 31, $^3J_{CB}$ = 3, Ar^F), 125.2 (q, $^1J_{FC}$ = 271, Ar^F), 124.2 (s, py), 121.8 (s, imid), 121.5 (s, imid), 118.1 (pent., $^3J_{FC}$ = 4, Ar^F), 56.3 (s, py), 49.9 (s, *N*-CH_2), 31.5 (s, CH_2), 28.9 (s, CH_2), 27.8 (s, CH_2), 27.6 (s, CH_2), 24.5 (s, CH_2). *The ethylene resonance was not observed*.

*4.6.1.3 Reactions of **27** with tert-Butyl Acetylene **25***

General Procedure for reactions of 27 with 15 equiv. of *tert*-butyl acetylene: Using a micro-litre syringe, 8 µL (5 mg, 0.065 mmol) of *tert*-butyl acetylene was added to a J. Young's NMR tube containing a sealed capillary of C_6D_6 and a solution of [Rh(**C^N^C^{Me}**)(C_2H_4)][$BAr^F{}_4$] (**27**) (6 mg, 0.005 mmol) in DiFB (0.5 mL) or THF (0.5 mL). The tube was maintained under a flow of argon during addition then sealed and shaken. ^{1}H NMR spectra were recorded at 298 K at the intervals specified. After the experiments, reaction mixtures were diluted with pentane and passed through a silica plug. The filtrate was concentrated and analysed by ^{1}H NMR spectroscopy ($CDCl_3$) to confirm the identity of the products.

For run **iii** (see **Table 4.2**), 20 µL (13 mg, 0.162 mmol) of THF was added to the DiFB solution.

For run **iv** (see **Table 4.2**), 60 µL (40 mg, 0.487 mmol) of *tert*-butyl acetylene was added to a solution of [Rh(**C^N^C^{Me}**)(C_2H_4)][$BAr^F{}_4$] (**27**) (6 mg, 0.005 mmol) in DiFB (2 mL) in a J. Young's flask, which was sampled at the specified intervals for analysis by ^{1}H NMR spectroscopy.

For run **v** (see **Table 4.2**), 500 µL (333 mg, 4.060 mmol) of *tert*-butyl acetylene was added by cannula to a J. Young's NMR tube containing solid [Rh(**C^N^C^{Me}**)(C_2H_4)][$BAr^F{}_4$] (**27**) (6 mg, 0.005 mmol) and a sealed capillary of C_6D_6.

For run **vi** (see **Table 4.2**), 25 µL (17 mg, 0.203 mmol) of *tert*-butyl acetylene was added to a suspension of [Rh(**C^N^C^{Me}**)(C_2H_4)][$BAr^F{}_4$] (**27**) (6 mg, 0.005 mmol) in toluene (0.5 mL). Sonication of the J. Young's NMR tube afforded a yellow-orange solution. Further addition of *tert*-butyl acetylene was conducted under a flow of argon.

*4.6.1.4 Characterisation of Alkyne Dimerisation Products **29** and **30***

Data for dimer 29:

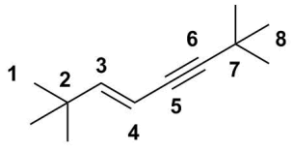

***Fig. 4.16:** Structure of dimer **29**.*

Isolated. **^{1}H NMR** (500 MHz, $CDCl_3$) δ 6.09 (d, $^{3}J_{HH}$ = 16.1, 1H, H-3), 5.41 (d, $^{3}J_{HH}$ = 16.2, 1H, H-4), 1.24 (s, 9H, H-8), 1.01 (s, 9H, H-1). **^{13}C{^{1}H} NMR** (126 MHz, $CDCl_3$) δ 153.5 (s, C-3), 105.4 (s, C-4), 97.4 (s, C-6), 77.8 (s, C-5), 33.9 (s, C-2), 31.3 (s, C-8), 29.2 (s, C-1), 28.0 (s, C-7). *During reactions in DiFB.* **^{1}H NMR** (400 MHz, 1,2-DiFB, C_6D_6 cap.) δ 5.95 (d, $^{3}J_{HH}$ = 16.1, 1H, alkene), 5.29 (d, $^{3}J_{HH}$ = 16.2, 1H, alkene), 1.16 (s, 9H, C(CH_3)$_3$), 0.83 (s, 9H, C(CH_3)$_3$).

Data for 30:

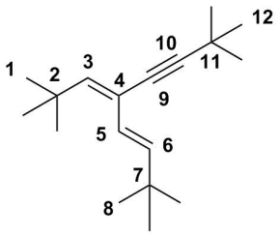

***Fig. 4.17:** Structure of **30**.*

*Mixture with **29**. Resonance for C-11 could not be identified. NOESY experiment shows interaction between H-5 and H-1, but none between H-5 and H-3, indicating the isomer shown.* **^{1}H NMR** (500 MHz, $CDCl_3$) δ 6.43 (d, $^{3}J_{HH}$ = 15.5, H-5), 6.13 (d, $^{3}J_{HH}$ = 15.6, H-6), 5.84 (s, H-3), 1.28 (s, 9H, H-12), 1.18 (s, 9H, H-1), 1.07 (s, 9H, H-8). **^{13}C{^{1}H} NMR** (126 MHz, $CDCl_3$) δ 146.3 (s, C-3), 145.6 (s, C-6), 121.1 (s, C-4), 120.5 (s, C-5), 96.8 (s, C-10), 78.9 (s, C-9), 33.5 (s, C-2/C-7), 33.4 (s, C-2/C-7), 31.5 (s, C-1/C-12), 31.3 (s, C-1/C-12), 29.8 (s, C-8). *During reactions in DiFB.* **^{1}H NMR** (400 MHz, 1,2-DiFB, C_6D_6 cap.) δ 5.84 (s, 1H, H-3) 1.20 (s, 9H, C(CH_3)$_3$), 1.06 (s, 9H, C(CH_3)$_3$), 0.98 (s, 9H, C(CH_3)$_3$). *H-5 and H-6 resonances obscured by DiFB signals.*

4.6.1.5 Reactions of Rhodium(I) Ethylene Complexes with Terminal Alkynes

[Rh(**2c**)(**29**)][BAr$^{F}_{4}$] (**31**): A Schlenk flask under argon was charged with 40 mg (0.015 mmol) of [Ag(μ-**2c**)]$_2$[BAr$^{F}_{4}$]$_2$ (**5**) and 6.5 mg (0.016 mmol) of [Rh(C_2H_4)$_2$Cl]$_2$. The flask was evacuated then back-filled with ethylene before addition of DiFB under ethylene, affording a red solution. This reaction mixture was stirred for 5 minutes in the absence of light before addition of *tert*-butyl acetylene (**25**) in pentane and degas by bubbling argon, giving an orange solution. The reaction

mixture was heated for 3 hours at 60°C, at which point aliquot analysis by ^{1}H NMR spectroscopy showed only signals for the product, and the solution was concentrated. The concentrate was taken up in Et_2O and filtered through a silica plug, which was washed generously with Et_2O before elution of the product in CH_2Cl_2. Sonication of the concentrated eluent in pentane afforded an orange suspension. The solvent was removed by filtration and the precipitate washed with pentane and dried to provide **31** as an orange solid. Yield: 30 mg (66 %).

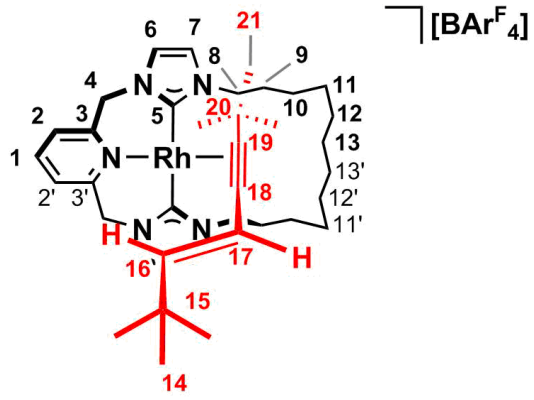

Fig. 4.18: *Structure of **31** with numbering scheme.*

^{1}H NMR (600 MHz, CD_2Cl_2) δ 7.83 (app. t, *J* = 8, 1H, H-1), 7.66 – 7.75 (m, 8H, Ar^F), 7.55 (s, 4H, Ar^F), 7.53 (d, $^{3}J_{HH}$ = 7.7, 1H, H-2), 7.48 (d, $^{3}J_{HH}$ = 7.7, 1H, H-2'), 7.44 (d, $^{3}J_{HH}$ = 15.3, 1H, H-16), 7.03 (d, $^{3}J_{HH}$ = 1.8, 1H, H-6), 7.02 (d, $^{3}J_{HH}$ = 1.8, 1H, H-6'), 6.75 (d, $^{3}J_{HH}$ = 1.9, 1H, H-7), 6.73 (d, $^{3}J_{HH}$ = 1.9, 1H, H-7'), 6.05 (d, $^{3}J_{HH}$ = 15.3, 1H, H-17), 5.87 (d, $^{2}J_{HH}$ = 14.8, 1H, H-4a), 5.45 (d, $^{2}J_{HH}$ = 14.7, 1H, H-4a'), 5.11 (d, $^{2}J_{HH}$ = 14.8, 1H, H-4b), 5.05 (d, $^{2}J_{HH}$ = 14.7, 1H, H-4b'), 4.13 – 4.27 (m, 2H, H-8a and H-8a'), 3.49 – 3.68 (m, 1H, H-8b'), 3.31 – 3.40 (m, 1H, H-8b), 1.39 – 1.87 (m, 20H, H-9 to H-13 and H-9' to H-13'), 1.37 (s, 9H, H-21), 1.04 (s, 9H, H-14). **^{13}C{^{1}H} NMR** (151 MHz, CD_2Cl_2) δ 184.4 (d, $^{1}J_{RhC}$ = 43, C-5), 181.9 (d, $^{1}J_{RhC}$ = 43, C-5'), 162.3 (q, $^{1}J_{CB}$ = 50, Ar^F), 158.0 (s, C-16), 155.7 (s, C-3'), 155.5 (s, C-3), 139.0 (s, C-1), 135.4 (s, Ar^F), 129.4 (q, $^{2}J_{FC}$ = 32, Ar^F), 125.2 (q, $^{1}J_{FC}$ = 272, Ar^F), 124.7 (s, C-2/2'), 124.5 (s, C-2/2'), 121.9 (s, C-6/7), 121.1 (s, C-6/7), 121.0 (s, C-6/7), 120.6 (s, C-6/7), 118.0 (m, Ar^F), 114.7 (s, C-17), 89.5 (d, $^{1}J_{RhC}$ = 14, C-19), 72.8 (d, $^{1}J_{RhC}$ = 10, C-18), 56.3 (s, C-4/4'), 56.2 (s, C-4/4'), 50.0 (s, C-8'), 49.4 (s, C-8), 34.7 (s, C-15), 34.0 (s, C-20), 32.5 (s, C-9), 32.2 (s, C-14), 30.8 (s, C-9'), 29.9 (s, C-21), 29.8 (s, CH_2), 29.6 (s, CH_2), 29.3 (s, CH_2), 28.7 (s, CH_2), 28.7 (s, CH_2), 28.6 (s, CH_2), 25.5 (s, CH_2), 25.1 (s, CH_2). *Carbons C10 – C13 represented by 'CH$_2$'*. **ESI-HRMS** (CH_3CN, 180 °C, 3 kV) positive ion: 672.3513 *m/z*, $[M]^+$ (calc. 672.3507). **Elemental Analysis** Calc. for $C_{69}H_{69}BF_{24}N_5Rh$ (1538.02 g mol^{-1}): C, 53.96; H, 4.40; N, 4.56. Found: C, 53.86; H, 4.36; N, 4.49).

[Rh(**2c**)($C_{12}H_{20}$)][BAr^F_4] (**32**): A Schlenk flask under argon was charged with 50 mg (0.018 mmol) of [Ag(μ-**2c**)][BAr^F_4]$_2$ (**5**) and 7 mg (0.018 mmol) of [Rh(C_2H_4)$_2$Cl]$_2$. The flask was evacuated then back-filled with ethylene before addition of DiFB under ethylene, affording a red solution. This reaction mixture was stirred for 5 minutes in the absence of light before addition of *tert*-butyl acetylene (**25**) in CH_2Cl_2 and degas by bubbling argon, giving a brown solution. Analysis by ESI-LRMS showed a single peak at 672.3 *m/z*, consistent with product. The reaction mixture was stirred for 30 minutes before concentrating *in vacuo* to afford a brown oil, which was taken up in Et_2O, under nitrogen, and filtered through a silica plug, which was washed generously with Et_2O before elution of the product in CH_2Cl_2. The resulting yellow eluent was concentrated to a yellow-orange glass, which was handled and stored under argon. Yield: 19 mg (34 %).

^{1}H NMR (500 MHz, CD_2Cl_2) δ 7.96 (t, $^3J_{HH}$ = 7.7, 1H, py), 7.72 (s, 8H, Ar^F), 7.53 – 7.57 (m, 6H, Ar^F + py), 7.18 (s, 2H, imid), 7.11 (s, 2H, imid), 6.54 (d, $^3J_{HH}$ = 13.5, 1H, alkene), 5.00 – 6.20 (br m, 6H, 4 pyCH_2 + 2 *N*-CH_2), 3.88 – 3.95 (m, 2H, *N*-CH_2), 3.55 (dd, $^3J_{HH}$ = 13.6, J_{RhH} = 3, 1H, alkene), 1.84 – 1.96 (m, 2H, CH_2), 1.68 – 1.82 (m, 4H, CH_2), 1.55 – 1.67 (m, 2H, CH_2), 1.27 – 1.40 (m, 4H, CH_2), 1.24 (s, 9H, C(CH_3)$_3$), 1.05 – 1.20 (m, 8H, CH_2), 0.71 (s, 9H, C(CH_3)$_3$). **^{13}C{^{1}H} NMR** (101 MHz, CD_2Cl_2, *selected data only*) δ 156.4 (s), 144.8 (s), 140.3 (s), 125.8 (s), 121.3 (br), 119.7 (br), 115.6 (s), 115.0-115.3 (m), 66.2 (s,), 55.6 (s), 35.7 – 35.8 (m), 33.0 (s), 28.9 – 30.7 (m).

[Rh(**2c**)((3,5-(^{t}Bu)$_2$$C_6H_3$)CH=CHC≡C(3,5-(^{t}Bu)$_2$$C_6H_3$))][$BAr^F_4$] (**33**): A Schlenk flask under argon was charged with 48 mg (0.017 mmol) of [Ag(μ-**2c**)]$_2$[BAr^F_4]$_2$ (**5**) and 8 mg (0.021 mmol) of [Rh(C_2H_4)$_2$Cl]$_2$. The flask was evacuated then back-filled with ethylene before addition of DiFB under ethylene, affording a red solution. This reaction mixture was stirred for 5 minutes in the absence of light before addition of 3,5-di(*tert*-butyl)phenyl acetylene (**24**) in Et_2O and degas by bubbling argon, giving a dark-orange solution. The reaction flask was sealed and heated overnight at 60°C. The concentrated reaction mixture was taken up in Et_2O, in air, and filtered through a silica plug, which was washed generously with Et_2O before elution of the product in CH_2Cl_2. The concentrated eluent was dissolved in pentane and filtered through a celite pad. Slow evaporation of the eluent afforded an orange microcrystalline powder, which was washed with cold pentane to provide the product. Yield: 24 mg (39 %).

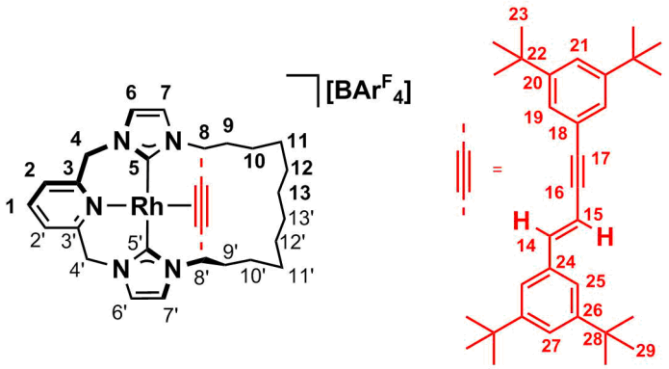

Fig. 4.19: *Structure of* ***33*** *with numbering scheme.*

^{1}H NMR (400 MHz, CD_2Cl_2) δ 8.23 (d, $^4J_{HH}$ = 1.7, 2H, H-19), 8.05 (d, $^3J_{HH}$ = 15.3, 1H, H-15), 7.90 (t, $^3J_{HH}$ = 7.7, 1H, H-1), 7.72 (br, 8H, Ar^F), 7.59 (d, $^3J_{HH}$ = 7.8, 2H, H-2), 7.55 (br, 4H, Ar^F), 7.42 – 7.45 (m, 2H, H-27 + H-21), 7.39 (d, $^4J_{HH}$ = 1.4, 2H, H-25), 7.02 (d, $^3J_{HH}$ = 1.8, 1H, H-6'), 7.01 (d, $^3J_{HH}$ = 15.3, 1H, H-14), 6.98 (d, $^3J_{HH}$ = 1.8, 1H, H-6), 6.67 (d, $^3J_{HH}$ = 1.8, 1H, H-7'), 6.65 (d, $^3J_{HH}$ = 1.8, 1H, H-7), 5.95 (d, $^2J_{HH}$ = 14.6, 1H, H-4a), 5.81 (d, $^2J_{HH}$ = 14.7, 1H, H-4a'), 5.20 (d, $^2J_{HH}$ = 14.8, 1H, H-4b'), 5.16 (d, $^2J_{HH}$ = 14.7, 1H, H-4b), 4.21 (app. dt, *J* = 13, *J* = 2, 1H, H-8a/8a'), 3.75 (app. dt, *J* = 13, *J* = 2, 1H, H-8a/8a'), 3.33 – 3.45 (m, 2H, H-8b/8b'), 2.18 – 2.31 (m, 1H, H-9a), 1.05 – 1.81 (m, 23H, H-9 to H-13), 1.36 (s, 18H, H-23/29), 1.35 (s, 18H, H-23/29). **^{13}C{^{1}H} NMR** (101 MHz, CD_2Cl_2) δ 182.0 (d, $^1J_{RhC}$ = 42, C-5), 181.3 (d, $^1J_{RhC}$ = 42, C-5'), 162.3 (q, $^1J_{CB}$ = 50, Ar^F), 155.7 (s, C-3 + C-3'), 152.4 (s, C-20), 151.5 (s, C-26), 142.8 (d, $^2J_{RhC}$ = 2, C-15), 139.8 (s, C-1), 136.6 (s, C-24), 135.4 (s, Ar^F), 129.5 (qq, $^2J_{FC}$ = 32, $^3J_{CB}$ = 3, Ar^F), 127.1 (s, C-19), 125.2 (q, $^1J_{FC}$ = 271, Ar^F), 124.9 (s, C-2/2'), 124.8 (s, C-2/2'), 123.9 (s, C-21/27), 123.2 (s, C-21/27), 121.58 – 121.71 (m, C-25 + C-7 + C-7'), 120.9 (s, C-6/6'), 120.7 (s, C-6/6'), 118.1 (quint, $^3J_{FC}$ = 4, Ar^F), 117.2 (br, C-14), 88.9 (d, $^1J_{RhC}$ = 14, C-17), 83.6 (d, $^1J_{RhC}$ = 13, C-16), 56.3 (s, C-4 + C-4'), 49.8 (s, C-8/8'), 49.5 (s, C-8/8'), 35.6 (s, C-20/28), 35.4 (s, C-20/28), 33.2 (s, CH_2), 31.9 (s, C-23/29), 31.8 (s, C-23/29), 31.6 (s, CH_2), 29.8 (s, CH_2), 29.5 (s, CH_2), 28.9 (s, CH_2), 28.7 (s, CH_2), 28.5 (s, CH_2), 28.3 (s, CH_2), 25.4 (s, CH_2), 24.0 (s, CH_2). *Carbons C9 – C13 represented by 'CH_2'. Resonance for C-18 not identified.* **ESI-HRMS** (CH_3CN, 180 °C, 3 kV) positive ion: 936.5391 *m/z*, $[M]^+$ (calc. 936.5385). **Elemental Analysis** Calc. for $C_{89}H_{91}BF_{24}N_5Rh$ (1799.60 g mol^{-1}): C, 59.37; H, 5.09; N, 3.89. Found: C, 59.36; H, 4.99; N, 4.01).

[Rh(**2c**)(H_2C=C(3,5-(^{t}Bu)$_2C_6H_3$)C≡C(3,5-(^{t}Bu)$_2C_6H_3$))][BAr$^F_4$] (**34**): A Schlenk flask under argon was charged with 50 mg (0.018 mmol) of [Ag(μ-**2c**)]$_2$[BAr$^F_4$]$_2$ (**5**) and 7 mg (0.018 mmol) of [Rh(C_2H_4)$_2$Cl]$_2$. The flask was evacuated then back-filled with ethylene before addition of Et_2O under ethylene, affording an orange-red suspension. This reaction mixture was stirred for 5 minutes in the absence of light before addition of 3,5-di(*tert*-butyl)phenyl acetylene (**24**) in CH_2Cl_2 and degas by bubbling argon, affording a brown suspension. The reaction mixture was

stirred for 30 minutes before filtration onto a silica plug, under argon, which was washed generously with Et_2O before elution of the product in CH_2Cl_2. The eluent was concentrated to a brown foam, which was handled and stored under argon. Yield: 25 mg (39 %).

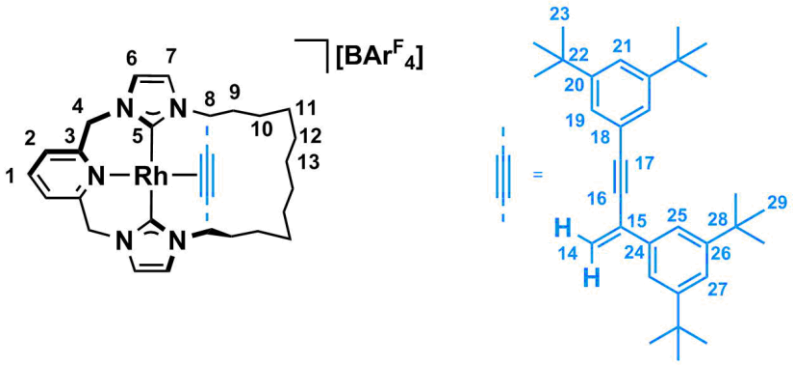

Fig. 4.20: *Structure of* ***34*** *with numbering scheme.*

^{1}H NMR (500 MHz, CD_2Cl_2) δ 7.86 (t, $^3J_{HH}$ = 7.7, 1H, H-1), 7.73 (s, 8H, Ar^F), 7.53 – 7.57 (m, 5H, Ar^F + H-27), 7.43 (d, $^3J_{HH}$ = 7.6, 2H, H-2), 7.20 (app. t, *J* = 2, 1H, H-21), 7.14 (br, 2H, H-6), 7.12 (s, 2H, H-7), 6.92 (d, $^4J_{HH}$ = 1.6, 2H, H-19), 6.69 (br, 2H, H-25), 5.76 (d, *J* = 1.6, 1H, H-14a), 5.57 (s, 1H, H-14b), 3.50 – 5.50 (v. br, 8 H, H-4 and H-8), 2.10 – 2.21 (br, 2H, H-9a), 1.86 – 1.98 (br, 2H, H-9b), 1.27 – 1.62 (m, 16 H, H-10 to H-13), 1.25 (s, 18H, H-23), 1.10 – 1.21 (m, 4H, H-9 to H-13), 0.99 (br, 18H, H-29). **^{13}C{^{1}H} NMR** (126 MHz, CD_2Cl_2) δ 172.9 (d, $^1J_{RhC}$ = 38, C-5), 162.3 (q, $^1J_{CB}$ = 50, Ar^F), 157.7 (d, $^2J_{RhC}$ = 27, C-15), 156.1 (s, C-3), 155.4 (br, C-26), 151.0 (s, C-20), 141.1 (s, C-1), 135.4 (s, Ar^F), 129.5 (qq, $^2J_{FC}$ = 32, $^3J_{CB}$ = 3, Ar^F), 127.0 (s, C-18), 125.8 (s, C-19), 125.4 (br, C-27), 125.2 (q, $^1J_{FC}$ = 271, Ar^F), 122.9 (br, C-6), 122.6 (br, C-7), 122.3 (br, C-24), 120.8 (s, C-21), 118.1 (pent., $^3J_{FC}$ = 4, Ar^F), 114.7 (s, C-14), 104.7 (d, $^1J_{RhC}$ = 15, C-17), 85.0 (d, $^1J_{RhC}$ = 72, C-16), 55.0 (br, C-4), 50.9 (br, C-8), 35.4 (s, C-28), 35.1 (s, C-22), 31.7 (s, C-23), 31.4 (s, C-29), 28.9 (s, CH_2), 28.4 – 28.5 (s, CH_2). *Carbons C10 – C13 represented by 'CH_2'. Resonances for C-25 and C-9 not identified. 2D correlation spectra suggest C-9 coincides with a signal of opposite phase at 31 ppm.* **Elemental Analysis** Calc. for $C_{89}H_{91}BF_{24}N_5Rh$ (1799.60 g mol^{-1}): C, 59.37; H, 5.09; N, 3.89. Found: C, 59.37; H, 4.94; N, 3.93).

[Rh(**2c**)(PhCH=CHC≡CPh)][BAr^F_4] (**35**): A Schlenk flask under argon was charged with 40 mg (0.015 mmol) of [Ag(μ-**2c**)]$_2$[BAr^F_4]$_2$ (**5**) and 6.0 mg (0.015 mmol) of [Rh(C_2H_4)$_2$Cl]$_2$. The flask was evacuated then back-filled with ethylene before addition of DiFB under ethylene, affording a red solution. This reaction mixture was stirred for 5 minutes in the absence of light before addition of phenyl acetylene (30 mg, 0.291 mmol) in Et_2O and degas by bubbling argon, affording a brown solution. Aliquot analysis by ESI-LRMS showed a dominant peak at 712.3 *m/z*, consistent with product (calc. 712.3), and another for the mono-addition at 610.2 *m/z* (calc. 610.2). The reaction mixture was heated for 2 days at 80°C, at which point aliquot

analysis by ESI-LRMS showed a single peak at 712.3 *m/z*, then concentrated. The concentrate was taken up in Et_2O, under nitrogen, and filtered through a silica plug, which was washed generously with Et_2O before elution of the product in CH_2Cl_2. The eluent was concentrated to an orange glass. Approx. 4 : 1 mixture of **35** to similar material. Yield not obtained.

*Selected ^1H NMR data for **35**, major product:* **^{1}H NMR** (400 MHz, CD_2Cl_2) δ 8.37 (d, $^3J_{HH}$= 7.1, 2H, *o*-Ph), 7.95 (d, $^3J_{HH}$ = 15.3, 1H, alkene), 7.89 (t, $^3J_{HH}$ = 7.7, py), 7.06 (d, $^3J_{HH}$= 15.3, 1H, alkene), 7.02 (d, $^3J_{HH}$ = 1.5, 1H, imid), 6.93 (d, $^3J_{HH}$ = 1.5, 1H, imid), 6.66 (d, $^3J_{HH}$ = 1.5, 1H, imid), 6.62 (d, $^3J_{HH}$ = 1.5, 1H, imid), 5.84 (d, $^2J_{HH}$ = 14.7, 1H, pyCH_2), 5.81 (d, $^2J_{HH}$ = 14.7, 1H, pyCH_2), 5.20 (d, $^2J_{HH}$ = 14.9, 1H, pyCH_2) and 5.13 (d, $^2J_{HH}$ = 15.0, 1H, pyCH_2).

[Rh(**2c**)(H_2C=CH(CH_2)$_9$CH=CHC≡C(CH_2)$_9$CH=CH_2)][BAr^F_4] (**37**): A Schlenk flask under argon was charged with 44 mg (0.016 mmol) of [Ag(μ-**2c**)]$_2$[BAr^F_4]$_2$ (**5**) and 6.0 mg (0.015 mmol) of [Rh(C_2H_4)$_2$Cl]$_2$. The flask was evacuated then back-filled with ethylene before addition of DiFB under ethylene, affording a red solution. This reaction mixture was stirred for 5 minutes in the absence of light before addition of **HC≡C(CH_2)$_9$CH=CH_2** (**38**) (26 mg, 0.146 mmol) in pentane and degas by bubbling argon, affording a brown solution. Aliquot analysis by ESI-LRMS showed peaks for both mono- and bis-alkyne addition (1:4). The reaction mixture was heated at 60°C for 4 h, affording a 1:20 ratio by ESI-LRMS analysis, which was concentrated *in vacuo*. The concentrated was taken up in Et_2O, under nitrogen, and filtered through a silica plug, which was washed generously with Et_2O before elution of the product in CH_2Cl_2. The eluent was concentrated to an orange oil. Yield: 26 mg (47 %). **ESI-HRMS** (CH_3CN, 180 °C, 3 kV) positive ion: 864.5389 *m/z*, $[M]^+$ (calc. 864.5385).

[Rh(**2c**)(CH$_2$(CH_2)$_8$CH=CHC≡C(CH_2)$_9$CH=CH)][BAr^F_4] (**39**): A solution of Grubbs 1st Generation catalyst (1.3 mg, 0.0015 mmol) in CH_2Cl_2 (1 mL) was washed into a stirred CH_2Cl_2 (20 mL) solution of [Rh(**2c**)(H_2C=CH(CH_2)$_9$CH=CHC≡C(CH_2)$_9$CH=CH_2)][BAr^F_4] (**37**) (26 mg, 0.0150 mmol). A steady stream of nitrogen was bubbled through the solution for 2 h before aliquot analysis by ESI-LRMS indicated no further change in conversion (at *ca*. 90 %). A further 1.5 mg (0.0018 mmol) of catalyst was added and N_2 passed through the solution for 0.5 h before aliquot analysis by ESI-LRMS indicated completion. The reaction mixture was concentrated then taken up in Et_2O, under nitrogen, and filtered through a silica plug, which was washed generously with Et_2O before elution of the product in CH_2Cl_2. The eluent was concentrated to a yellow-orange oil. Yield: 11 mg (43 %). **ESI-HRMS** (CH_3CN, 180 °C, 3 kV) positive ion: 836.5077 *m/z*, $[M]^+$ (calc. 836.5072).

*4.6.1.6 Hydrogenation of **29***

A solution of **29** (5 mg, 0.030 mmol) in $CDCl_3$ was added to a high pressure NMR tube containing approx. 2 mg (0.002 mmol) of 10 % wt palladium on carbon. The reaction tube was degassed by successive freeze-pump-thaw cycles, then pressured to 1 atmosphere of H_2 at -197°C before sealing and allowing to come to room temperature. The reaction was monitored by ^{1}H NMR spectroscopy until consumption of signals in the alkene region was observed, after which the reaction medium was filtered through a celite plug in $CDCl_3$ and the filtrate studied by ^{1}H NMR without further purification (yield not obtained). **^{1}H NMR** (600 MHz, $CDCl_3$) δ 0.86 (s, 18H, 2xC(C*H*$_3$)$_3$), 1.14 – 1.23 (m, 8H, 2xC*H*$_2$C*H*$_2$). **^{13}C{^{1}H} NMR** (151 MHz, $CDCl_3$) δ 44.5 (s, *C*H$_2$C(CH$_3$)$_3$), 29.6 (s, C(*C*H$_3$)$_3$), 25.7 (s, *C*H$_2$CH$_2$C(CH$_3$)$_3$). *Resonance for C(CH$_3$)$_3$ not observed.*

4.6.1.7 Reactions of Interlocked Complexes with $PhICl_2$

[Rh(**2c**)(**29**)(Cl)$_2$][BAr$^F_4$] (**40**): A mixture of [Rh(**2c**)(**29**)][BAr$^F_4$] (**31**) (20 mg, 0.013 mmol) and $PhICl_2$ (10 mg, 0.036 mmol) was solubilised in CH_2Cl_2 in air to afford a yellow solution. Addition of excess pentane precipitated a pale yellow solid, which was washed with pentane and dried to afford the product. Yield: 10 mg (48 %). Crystals suitable for XRD could be obtained by slow diffusion of pentane into a toluene solution of the product.

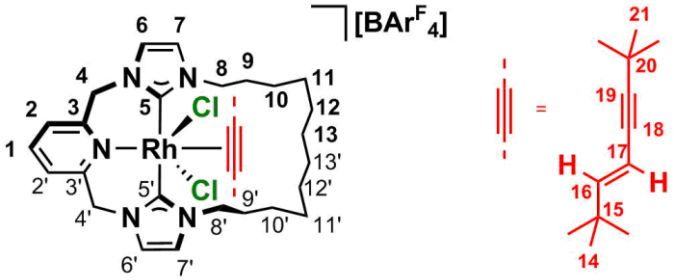

***Fig. 4.21:** Structure of **40** with numbering scheme.*

^{1}H NMR (700 MHz, CD_2Cl_2) δ 7.98 (t, $^3J_{HH}$ = 7.7, 1H, H-1), 7.72 (br, 8H, Ar^F), 7.63 (d, $^3J_{HH}$ = 7.6, 1H, H-2), 7.56 (br, 5H, Ar^F + H-2'), 7.34 (d, $^3J_{HH}$ = 1.7, 1H, H-6'), 7.29 (d, $^3J_{HH}$ = 1.8, 1H, H-6), 7.15 (s, 2H, H-7 + H-7'), 7.03 (d, $^2J_{HH}$ = 15.6, 1H, H-4a'), 6.99 (d, $^2J_{HH}$ = 15.5, 1H, H-4a), 5.88 (d, $^3J_{HH}$ = 15.9, 1H, H-17), 5.76 (d, $^3J_{HH}$ = 15.9, 1H, H-16), 5.27 (d, $^2J_{HH}$ = 15.6, 1H, H-4b), 5.23 (d, $^2J_{HH}$ = 15.6, 1H, H-4b'), 4.54 - 4.59 (m, 1H, H-8a'), 4.31 - 4.37 (m, 1H, H-8a), 3.78 - 3.84 (m, 1H, H-8b'), 3.56 – 3.65 (m, 1H, H-8b), 2.20 - 2.28 (m, 1H, H-9a), 2.10 – 2.19 (m, 1H, H-9a'), 1.81 – 1.91 (m, 2H, H-9b and H-9b'), 1.66 – 1.80 (m, 4H, CH_2), 1.46 - 1.65 (s, 17H, 4xCH_2 + H-21), 1.34 – 1.44 (m, 2H, CH_2), 1.18 - 1.23 (m, 1H, CH_2), 1.05 - 1.11 (m, 1H, CH_2), 1.03 (s, 9H, H-14). *Protons H10 – H13 represented by 'CH$_2$'.* **^{13}C{^{1}H} NMR** (176 MHz, CD_2Cl_2) δ 164.8 (d, $^1J_{RhC}$ = 30, C-5), 163.3 (d, $^1J_{RhC}$ = 30, C-5'), 162.3 (q, $^1J_{BC}$ = 50, Ar^F), 162.2 (s, C-16), 157.7 (s, C-3), 157.3 (s, C-3'), 141.4 (s,

C-1), 135.3 (s, Ar^F), 129.4 (qq, $^2J_{FC}$ = 32, $^3J_{BC}$ = 3, Ar^F), 128.0 (s, C-2), 127.5 (s, C-2'), 125.1 (q, $^1J_{FC}$ = 272, Ar^F), 123.5 (s, C-7/7'), 123.3 (s, C-7/7'), 122.3 (s, C-6'), 121.6 (s, C-6), 118.0 (m, Ar^F), 106.4 (s, C-17), 83.2 (d, $^1J_{RhC}$ = 7, C-19), 65.3 (d, $^1J_{RhC}$ = 7, C-18), 56.9 (s, C-4), 56.4 (s, C-4'), 50.5 (s, C-8), 49.8 (s, C-8'), 36.3 (s, C-20), 35.7 (s, C-15), 33.2 (s, C-21), 31.4 (s, CH_2), 31.3 (s, CH_2), 31.3 (s, CH_2), 30.7 (s, CH_2), 30.3 (s, CH_2), 30.1 (s, CH_2), 29.7 (s, C-14), 29.6 (s, CH_2), 29.4 (s, CH_2), 26.9 (s, CH_2), 26.2 (s, CH_2). *Carbons C9 – C13 represented by 'CH$_2$'.* **ESI-HRMS** (CH_3CN, 180 °C, 3 kV) positive ion: 742.2881 *m/z*, $[M]^+$ (calc. 742.2884). **Elemental Analysis** Calc. for $C_{69}H_{69}BCl_2F_{24}N_5Rh$ (1608.92 g mol^{-1}): C, 51.57; H, 4.20; N, 4.36. Found: C, 51.63; H, 3.94; N, 4.36).

[Rh(**2c**)((3,5-(^{t}Bu)$_2$C$_6$H$_3$)CH=CHC≡C(3,5-(^{t}Bu)$_2$C$_6$H$_3$))(Cl)$_2$][BAr$^F_4$] (**41**): Inside an argon-filled glove box, CD_2Cl_2 (0.5 mL) was added to a J. Young's NMR tube charged with [Rh(**2c**)((3,5-(^{t}Bu)$_2$C$_6$H$_3$)CH=CHC≡C(3,5-(^{t}Bu)$_2$C$_6$H$_3$))][BAr$^F_4$] (**33**) (10 mg, 0.006 mmol) and $PhICl_2$ (7 mg, 0.026 mmol) to give an orange solution which rapidly turned dark red. Analysis by ^{1}H NMR spectroscopy showed no signals for the starting material and shift in signals of the methylene and *N*-CH_2 protons consistent with oxidation to a rhodium(III) complex. Exposed to air for sampling by ESI-LRMS. Initial sample shows dominant mass ion at 1006.5 *m/z*. Later samples show near-statistical distributions of multiple adducts 971.5 *m/z* (10 %), 1006.5 *m/z* (40 %), 1040.5 *m/z* (75 %), 1078.4 *m/z* (100 %), 1112.4 *m/z* (55 %), 1148.3 *m/z* (10 %).

*Selected ^{1}H NMR data for in-situ generated **41**:* **^{1}H NMR** (300 MHz, CD_2Cl_2) δ 8.02 (t, $^3J_{HH}$ = 7.6, 1H, py), 6.87 (d, $^2J_{HH}$ = 15.6, 1H, pyC*H*$_2$), 6.76 (d, $^2J_{HH}$ = 15.6, 1H, pyC*H*$_2$), 5.34 (app. d, *J* = 15, 2H, 2xpyC*H*$_2$), 4.28 – 4.55 (m, 2H, *N*-CH_2), 3.64 – 3.91 (m, 2H, *N*-CH_2), 1.34 (s, 18H, C(C*H*$_3$)$_3$), 1.29 (s, 18H, C(C*H*$_3$)$_3$).

4.6.2 Crystallographic Data

Crystallographic data for **27**, **16**, **31**, **33** and **40** are summarised in **Table 4.3**. Data were collected on an Oxford Diffraction Gemini Ruby CCD disffractometer using graphite monochromated Mo Kα (λ = 0.71073 Å) (for **27**, **16**, **31** and **33**) or Cu Kα (λ = 1.54178 Å, for **40**) radiation and a low temperature device [150(2) K]. Data were collected and reduced using CrysAlisPro. All non-hydrogen atoms were refined anisotropically using SHELXL,[41] through the Olex2 interface.[42] Hydrogen atoms were placed in calculated positions using the riding model.

Table 4.3: *Crystallographic data for* ***27****,* ***16, 31, 33*** *and* ***40****.*

	27	**16**	**31**	**33**	**40**
ID code	0204abc16	0202abc16	0136abc14	0188abc15	0133abc14
Figure	**4.2**	**4.5**	**4.7**	**4.11**	**4.14**
Formula	$C_{49}H_{33}BF_{24}N_5Rh$	$C_{50}H_{33}BCl_6F_{24}N_5ORh$	$C_{70}H_{69}BCl_2F_{24}N_5Rh$	$C_{95}H_{105}BF_{24}N_5Rh$	$C_{69}H_{67}BCl_2F_{24}N_5Rh$
M	1261.52	1502.23	1620.92	1886.55	1606.89
Crystal system	triclinic	triclinic	monoclinic	monoclinic	monoclinic
Space group	P-1	P-1	C2	$P2_{1/n}$	$P2_{1/n}$
T **[K]**	150(2)	150(2)	150(2)	150(2)	150(2)
a **[Å]**	12.7811(2)	13.8858(3)	19.1587(2)	12.43136(18)	26.8979(4)
b **[Å]**	13.0076(2)	14.9383(4)	16.83656(19)	42.1247(5)	17.00649(19)
c **[Å]**	16.4419(4)	16.7603(4)	22.6457(2)	18.0976(3)	37.3088(5)
α **[°]**	95.0738(17)	110.475(2)	90	90	90
β **[°]**	97.8097(17)	104.695(2)	99.7709(3)	92.5387(13)	91.5792(14)
γ **[°]**	110.5406(17)	106.317(2)	90	90	90
V **[Å^3]**	2508.53(9)	2876.33(13)	7198.78(13)	9467.8(2)	17060.0(4)
Z **(*Z'*)**	2	2	4	4	8
Density [g cm^{-3}]	1.670	1.735	1.496	1.324	1.251
μ **(mm^{-1})**	0.472	0.697	0.419	0.274	2.996
ϑ **range [°]**	3.13 ≤ θ ≤ 26.4	2.93 ≤ θ ≤ 26.4	3.02 ≤ θ ≤ 27.1	2.92 ≤ θ ≤ 27.1	6.40 ≤ θ ≤ 66.6
Reflns collected	36873	55884	48024	120735	124572
R_{int}	0.0256	0.0394	0.0253	0.0606	0.0700
Completeness [%]	99.9	99.8	99.8	99.9	99.8
No. of data/restr/param	10248/540/835	11754/342/851	15805/428/1001	20847/1591/1379	30090/1383/1985
R_1 **[I > 2σ(I)]**	0.0357	0.0326	0.0340	0.0523	0.1047
wR_2 **[all data]**	0.0940	0.0802	0.0987	0.1392	0.3231
GoF	1.039	1.038	1.097	1.033	1.096
Largest diff. pk and hole [e Å^{-3}]	0.74/-0.47	0.66/-0.53	0.70/-0.61	0.65/-0.42	3.01/-0.71
Flack (*x*)	n/a	n/a	n/a	n/a	n/a

4.7 References

(1) Trost, B. M.; Chan, C.; Ruhter, G. *J. Am. Chem. Soc.* **1987**, *109*, 3486-3487.
(2) Chinchilla, R.; Nájera, C. *Chem. Rev.* **2013**, *114*, 1783-1826.
(3) Pell, C. J.; Ozerov, O. V. *ACS Catal.* **2014**, *4*, 3470-3480.
(4) Baidossi, W.; Goren, N.; Blum, J.; Schumann, H.; Hemling, H. *J. Mol. Catal.* **1993**, *85*, 153-162.
(5) Leroyer, L.; Maraval, V.; Chauvin, R. *Chem. Rev.* **2012**, *112*, 1310-1343.
(6) Yoshida, K.; Morimoto, I.; Mitsudo, K.; Tanaka, H. *Tetrahedron* **2008**, *64*, 5800-5807.
(7) Saito, S.; Yamamoto, Y. *Chem. Rev.* **2000**, *100*, 2901-2916.
(8) Liu, J.; Lam, J. W. Y.; Tang, B. Z. *Chem. Rev.* **2009**, *109*, 5799-5867.
(9) Jahier, C.; Zatolochnaya, O. V.; Zvyagintsev, N. V.; Ananikov, V. P.; Gevorgyan, V. *Org. Lett.* **2012**, *14*, 2846-2849.
(10) Weng, W.; Guo, C.; Celenligil-Cetin, R.; Foxman, B. M.; Ozerov, O. V. *Chem. Commun.* **2006**, 197-199.
(11) Kleinhans, G.; Guisado-Barrios, G.; Liles, D. C.; Bertrand, G.; Bezuidenhout, D. I. *Chem. Commun.* **2016**, *52*, 3504-3507.
(12) Platel, R. H.; Schafer, L. L. *Chem. Commun.* **2012**, *48*, 10609-10611.
(13) Schäfer, M.; Wolf, J.; Werner, H. *Organometallics* **2004**, *23*, 5713-5728.
(14) Lee, C.-C.; Lin, Y.-C.; Liu, Y.-H.; Wang, Y. *Organometallics* **2005**, *24*, 136-143.
(15) Schafer, M.; Wolf, J.; Werner, H. *Dalton Trans.* **2005**, 1468-1481.
(16) Ghosh, R.; Zhang, X.; Achord, P.; Emge, T. J.; Krogh-Jespersen, K.; Goldman, A. S. *J. Am. Chem. Soc.* **2007**, *129*, 853-866.
(17) Alós, J.; Bolaño, T.; Esteruelas, M. A.; Oliván, M.; Oñate, E.; Valencia, M. *Inorg. Chem.* **2014**, *53*, 1195-1209.
(18) Chen, X.; Xue, P.; Sung, H. H. Y.; Williams, I. D.; Peruzzini, M.; Bianchini, C.; Jia, G. *Organometallics* **2005**, *24*, 4330-4332.
(19) Komeyama, K.; Kawabata, T.; Takehira, K.; Takaki, K. *J. Org. Chem.* **2005**, *70*, 7260-7266.
(20) Fooladi, E.; Dalhus, B.; Tilset, M. *Dalton Trans.* **2004**, 3909-3917.
(21) Zenkina, O. V.; Keske, E. C.; Wang, R.; Crudden, C. M. *Organometallics* **2011**, *30*, 6423-6432.
(22) Di Giuseppe, A.; Castarlenas, R.; Pérez-Torrente, J. J.; Crucianelli, M.; Polo, V.; Sancho, R.; Lahoz, F. J.; Oro, L. A. *J. Am. Chem. Soc.* **2012**, *134*, 8171-8183.
(23) Dewar, M. J. S.; Ford, G. P. *J. Am. Chem. Soc.* **1979**, *101*, 783-791.
(24) Huang, Z.; Brookhart, M.; Goldman, A. S.; Kundu, S.; Ray, A.; Scott, S. L.; Vicente, B. C. *Adv. Synth. Catal.* **2009**, *351*, 188-206.
(25) Young, K. J. H.; Oxgaard, J.; Ess, D. H.; Meier, S. K.; Stewart, T.; Goddard, I. I. I. W. A.; Periana, R. A. *Chem. Commun.* **2009**, 3270-3272.
(26) Plikhta, A.; Pöthig, A.; Herdtweck, E.; Rieger, B. *Inorg. Chem.* **2015**, *54*, 9517-9528.
(27) Danopoulos, A. A.; Wright, J. A.; Motherwell, W. B. *Chem. Commun.* **2005**, 784-786.
(28) Danopoulus, A. A.; Pugh, D.; Wright, J. A. *Angew. Chem., Int. Ed.* **2008**, *47*, 9765-9767.
(29) Cao, P.; Cabrera, J.; Padilla, R.; Serra, D.; Rominger, F.; Limbach, M. *Organometallics* **2012**, *31*, 921-929.
(30) Serra, D.; Cao, P.; Cabrera, J.; Padilla, R.; Rominger, F.; Limbach, M. *Organometallics* **2011**, *30*, 1885-1895.
(31) Fulmer, G. R.; Miller, A. J. M.; Sherden, N. H.; Gottlieb, H. E.; Nudelman, A.; Stoltz, B. M.; Bercaw, J. E.; Goldberg, K. I. *Organometallics* **2010**, *29*, 2176-2179.
(32) Altaf, M.; Stoeckli-Evans, H. *Polyhedron* **2010**, *29*, 701-708.
(33) Dias, H. V. R.; Wu, J. *Eur. J. Inorg. Chem.* **2008**, *2008*, 509-522.
(34) Krossing, I.; Reisinger, A. *Angew. Chem. Int. Ed.* **2003**, *42*, 5725-5728.
(35) Dahlenburg, L.; Frosin, K. M.; Kerstan, S.; Werner, D. *J. Organomet. Chem.* **1991**, *407*, 115-124.

(36) Xie, F.; Qi, Z.; Yu, S.; Li, X. *J. Am. Chem. Soc.* **2014**, *136*, 4780-4787.
(37) Weding, N.; Jackstell, R.; Jiao, H.; Spannenberg, A.; Hapke, M. *Adv. Synth. Catal.* **2011**, *353*, 3423-3433.
(38) Taylor, R. T.; Stevenson, T. A. *Tetrahedron Lett.* **1988**, *29*, 2033-2036.
(39) Philp, D.; Gramlich, V.; Seiler, P.; Diederich, F. *J. Chem. Soc., Perkin Trans. 2* **1995**, 875-886.
(40) Chen, S.-Y.; Joullié, M. M. *Synth. Commun.* **1984**, *14*, 591-597.
(41) Sheldrick, G. *Acta Crystallogr. Sect. A* **2008**, *64*, 112-122.
(42) Dolomanov, O. V.; Bourhis, L. J.; Gildea, R. J.; Howard, J. A. K.; Puschmann, H. *J. Appl. Crystallogr.* **2009**, *42*, 339-341.

CHAPTER 5. SUMMARY OF FINDINGS

This thesis has described the preparation of d^8 transition metal complexes of bis(NHC)-pincer macrocycles, **2** and **11**, and subsequent study of their structural and chemical behaviour.

Firstly, study of palladium chlorides **3** enabled not only the establishment of an *in-situ* transmetallation procedure that proved applicable to generation of palladium, rhodium and nickel compounds, but also elucidation of the optimal ring size for such bis(NHC)-lutidine systems. Using the structural and spectral properties of **3**, and of palladium fluoride derivatives **4**, the dodecamethylene spaced macrocycle **2c** was found to comfortably encapsulate a metal and a small ancillary ligand (**Fig. 5.1**).

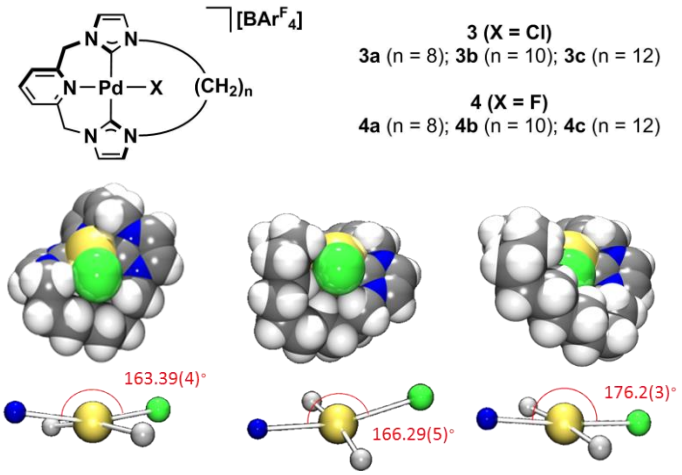

Fig. 5.1: *Spacefill and ball-and-stick representations showing varying degrees of distortion in the solid-state structures of* ***3a*** *(**left**),* ***3b*** *(**centre**) and* ***3c*** *(**right**).*

Building on these findings, rhodium carbonyl complexes of C^N^C-based **2c** and a C-N-C analogue **11** were synthesised *via* a template-based procedure from acyclic precursors. Resulting macrocycles **9** and **10**, respectively, were fully characterised in solution and in the solid-state, with both corroborating encapsulation of the carbonyl ligand within the cavity of each macrocycle. Dynamic behaviour of **9** was comprehensively interrogated and two reaction pathways – one thermal, the other induced by coordination of CO – substantiated using DFT calculations, analysis by VT NMR and IR spectroscopy, alongside synthesis of acyclic **16** and bis-carbonyl **18** as structural analogues (**Scheme 5.1**).

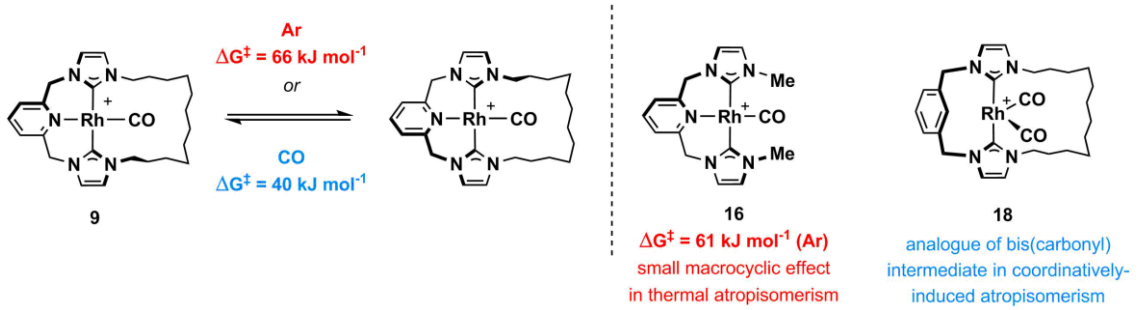

Scheme 5.1: *Atropisomerism of **9** and **16**, with structure of **18**. [BAr$^F_4$]$^-$ counter anions omitted for clarity.*

Interestingly, **10** demonstrates a Rh···Rh interaction in the solid state and more facile oxidative addition reactions, affording well-defined and stable rhodium(III) adducts. In contrast, **9**, with a significantly augmented steric profile, affords unstable products that must be instead characterised *in-situ*. The C^N^C pincer backbone of **9** can be deprotonated to afford highly reactive dearomatised complex **19** (**Scheme 5.2**). In the absence of such reactivity of the ligand, stable rhodium(III) derivatives of **10** are better suited to transmetallation reactions with organometallic reagents, *i.e.* the reaction of **21b** with phenylethynyl magnesium bromide to afford bis(alkynyl) **22**.

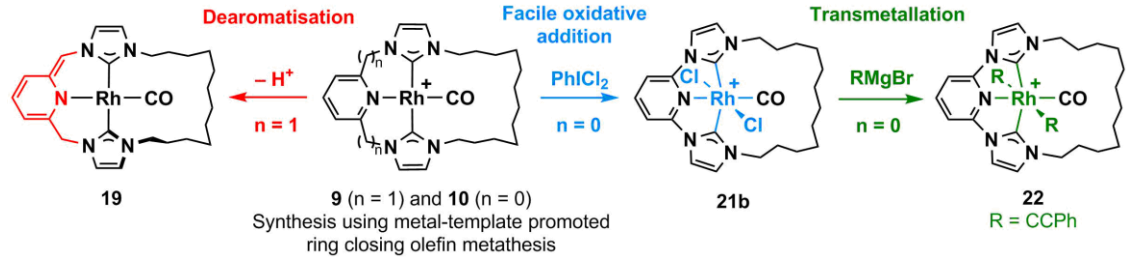

Scheme 5.2: *Reactions of **9** and **10**. [BAr$^F_4$]$^-$ counter anions omitted for clarity.*

Rhodium(I) carbonyl complexes **9** and **10** offer useful insights into the robust, but flexible, nature of the constituent macrocyclic ligands. However, the strong rhodium-carbonyl bond, which could not be readily cleaved in either system, precludes wider study of their application in organometallic and supramolecular chemistry. Instead, transmetallation methodology described herein was employed for the generation of labile rhodium ethylene complexes **27** and **28** – direct analogues of **16** and **9**, respectively. Reaction of acyclic **27** and macrocyclic **28** with terminal alkynes showcased the capacity of the macrocycle to exert kinetic and thermodynamic control in homo-coupling reactions (**Scheme 5.3**). Although **27** showed low catalytic activity, *E*-1,4-enynes were formed as the major products. In the case of **28**, these products were mechanically entrapped within the ligand themselves, allowing insights into the mechanism of this atom-efficient reaction. These include the identification of a vinyl-alkynyl intermediate (R = ^{t}Bu), and the reversible formation of a *gem*-1,3-enyne (R = 3,5-(^{t}Bu)$_2$C$_6$H$_3$).

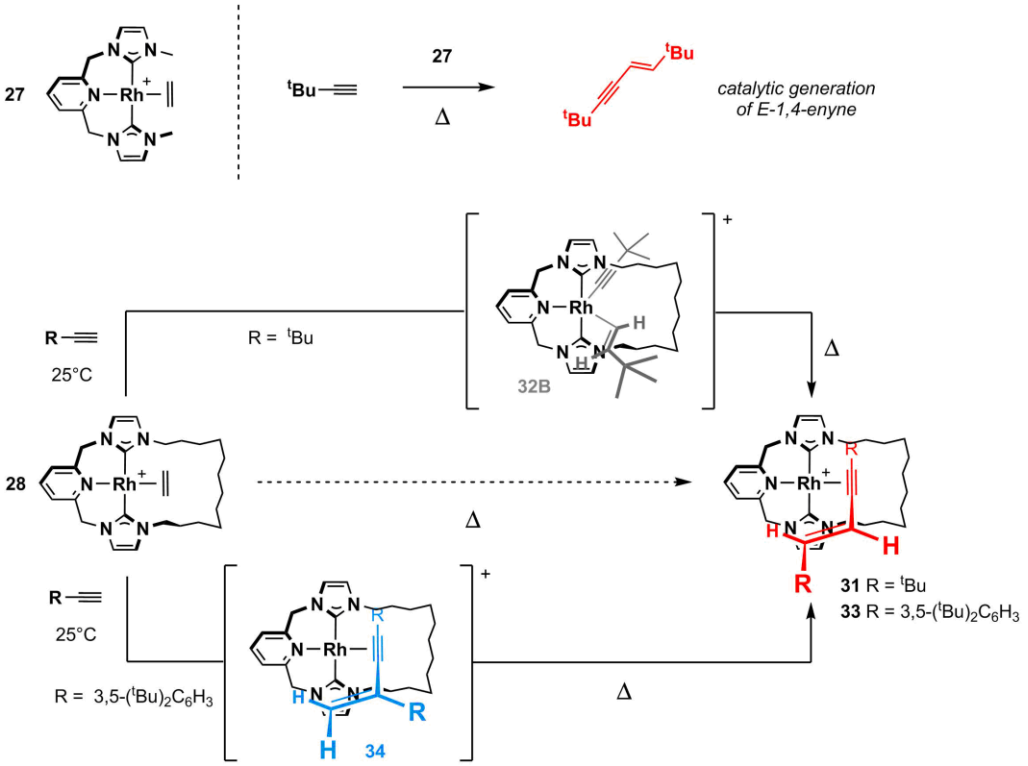

Scheme 5.3: *Reactions of **27** and **28** with terminal alkynes. $[BAr^F_4]^-$ counter anions omitted for clarity.*

Although **31** can be oxidised using $PhICl_2$, the mechanically entrapped enyne is inert to hydrogenation, even under forcing conditions. Hydrogenation, as a means to induce dissociation of the bound enyne, is a potential route to the generation of free-moving supramolecular architectures from **31** and **33** and may require modification of the macrocyclic ligand. A dependency on ring size was observed for the stability and solution dynamics of palladium halides **3** and **4**, and derivatives of **31** and **33** bearing larger macrocycles could potentially allow hydrogenation of the enyne. As demonstrated by the reactivity differences of **9** and **10**, alteration of the pincer backbone could augment the reactivity of the bound metal; for example, use of an anionic central donor group could enable more facile oxidative addition of H_2. Both of these directions are being explored in the Chaplin group.